The Single-Phase ProtoDUNE

Preliminary Technical Design Report

(For distribution to CERN SPSC)

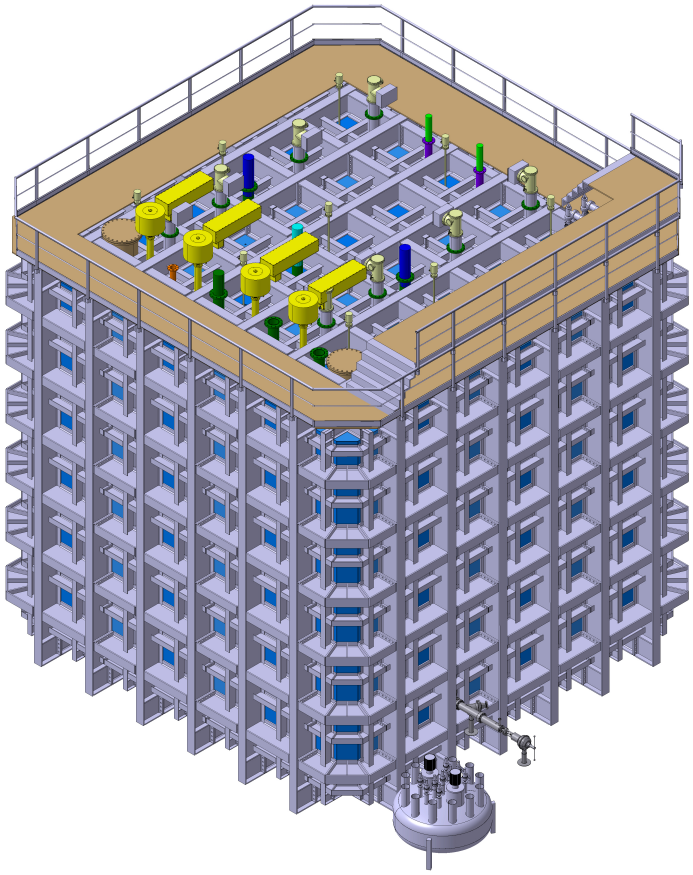

October 11, 2016

DEEP UNDERGROUND NEUTRINO EXPERIMENT

1

Contents

List of Figures

List of Tables

Todo list

FR4 definition ok?

Chapter 1

Introduction

1.1 ProtoDUNE-SP in the context of DUNE/LBNF

ProtoDUNE-SP is the single-phase DUNE Far Detector prototype that is under construction and will be operated at the CERN Neutrino Platform (NP) starting in 2018. It was proposed to the CERN SPSC in June 2015 (SPSC-P-351), and following positive recommendations by SPSC and the CERN Research Board in December 2015, was approved at CERN as experiment NP-04 (ProtoDUNE). The Fermilab Director and the CERN Director of Research and Scientific Computing signed a Memorandum of Understanding (MoU) for this experiment in December 2015 that is initially valid until December 2022, and may be extended by mutual agreement.

ProtoDUNE-SP, a crucial part of the DUNE effort towards the construction of the first DUNE 10-kt fiducial mass far detector module (17 kt total LAr mass), is a significant experiment in its own right. With a total liquid argon (LAr) mass of 0.77 kt, it represents the largest monolithic single-phase LArTPC detector to be built to date. It is housed in an extension to the EHN1 hall in the North Area, where the CERN NP is providing a new dedicated charged-particle test beamline. ProtoDUNE-SP aims to take its first beam data before the LHC long shutdown (LS2) at the end of 2018.

ProtoDUNE-SP prototypes the designs of most of the single-phase DUNE far detector module (DUNE-SP) components at a 1:1 scale, with an extrapolation of about 1:20 in total LAr mass. This is similar to the scaling factor adopted by ICARUS; its T600 detector, split into two half-modules of about 375 t total LAr mass each, was preceded by the 14-t "10-m^3" prototype.

The detector elements, consisting of the time projection chamber (TPC), the cold electronics (CE), and the photon detection system (PDS), are housed in a cryostat that contains the LAr target material. The cryostat, a free-standing steel-framed vessel with an insulated double membrane, is based on the technology used for liquefied natural gas (LNG) storage and transport. A cryogenics system maintains the LAr at a stable temperature of about 89 K and at the required purity level through a closed-loop process that recovers the evaporated argon, recondenses and filters it, and returns it to the cryostat.

The construction and operation of ProtoDUNE-SP will serve to validate the membrane cryostat technology and associated cryogenics, and the networking and computing infrastructure that will handle the data and simulated data sets. A charged-particle beam test will enable critical calibration measurements necessary for precise calorimetry. It will also enable the collection of invaluable data sets for optimizing the event reconstruction algorithms – i.e., for finding interaction vertices and for particle identification – and ultimately for quantifying and reducing systematic uncertainties for the DUNE far detector. These measurements are expected to significantly improve the physics reach of the DUNE experiment.

Given its technical challenges, its importance to the DUNE experiment and the timeframe in which it must operate, ProtoDUNE-SP has put in place a strong organizational structure incorporating contributions from a large number of DUNE collaboration institutes.

1.2 The ProtoDUNE-SP detector

detector

The ProtoDUNE-SP TPC, illustrated in Figure 1.1 comprises two drift volumes, defined by a central cathode plane that is flanked by two anode planes, each at a distance of 3.6 m, and a field cage (FC) that surrounds the entire active volume. The active volume is 6 m high, 7 m wide and 7.2 m deep (along the drift direction). Each anode plane is constructed of three adjacent Anode Plane Assemblies (APAs) that are each 6 m high by 2.3 m wide in the installed position. Each APA consists of a frame that holds three parallel planes of sense and shielding wires; the wires of each plane are oriented at different angles with respect to those on the other planes to enable 3D reconstruction. The wire pitch for all wire planes is 4.5 mm, and each APA holds a total of 2,560 wires.

The cathode plane, called the Cathode Plane Assembly (CPA) is an array of 18 (six wide by three high) CPA modules, which consist of flame-retardant FR4 frames, each 1.18 m wide and 2 m high, that hold thin panels with a resistive coating on both sides. The CPA is held at −180 kV providing the 500-V/cm drift field in the 3.6-m-deep drift regions. Uniformity of the electric field is guaranteed by the surrounding FC.

The CE, mounted onto the APA frame, and thus immersed in LAr, amplifies and continuously digitizes the induced signals on the sense wires at several MHz, and transmits these waveforms to the Data Acquisition system (DAQ). From the DAQ the data are transmitted through the buffer to disk, then to the central CERN Tier-0 Computing Center, and finally to other partner sites for processing and analysis.

The modular PDS is integrated into the APAs. Each PDS module (referred to as a PD) consists of a bar-shaped light guide and a wavelength-shifting layer (surface-coating or mounted radiator plate). The wavelength-shifting layer converts incoming VUV (128 nm) scintillation photons to longer-wavelength photons, in the visible blue range. Some of the converted photons are emitted into the bar, a fraction of which are then internally reflected to the bar's end where they are detected by silicon photomultipliers (SiPMs). Each APA frame is designed with ten bays into which PDs are inserted after the TPC wires have been strung. This allows for final assembly at

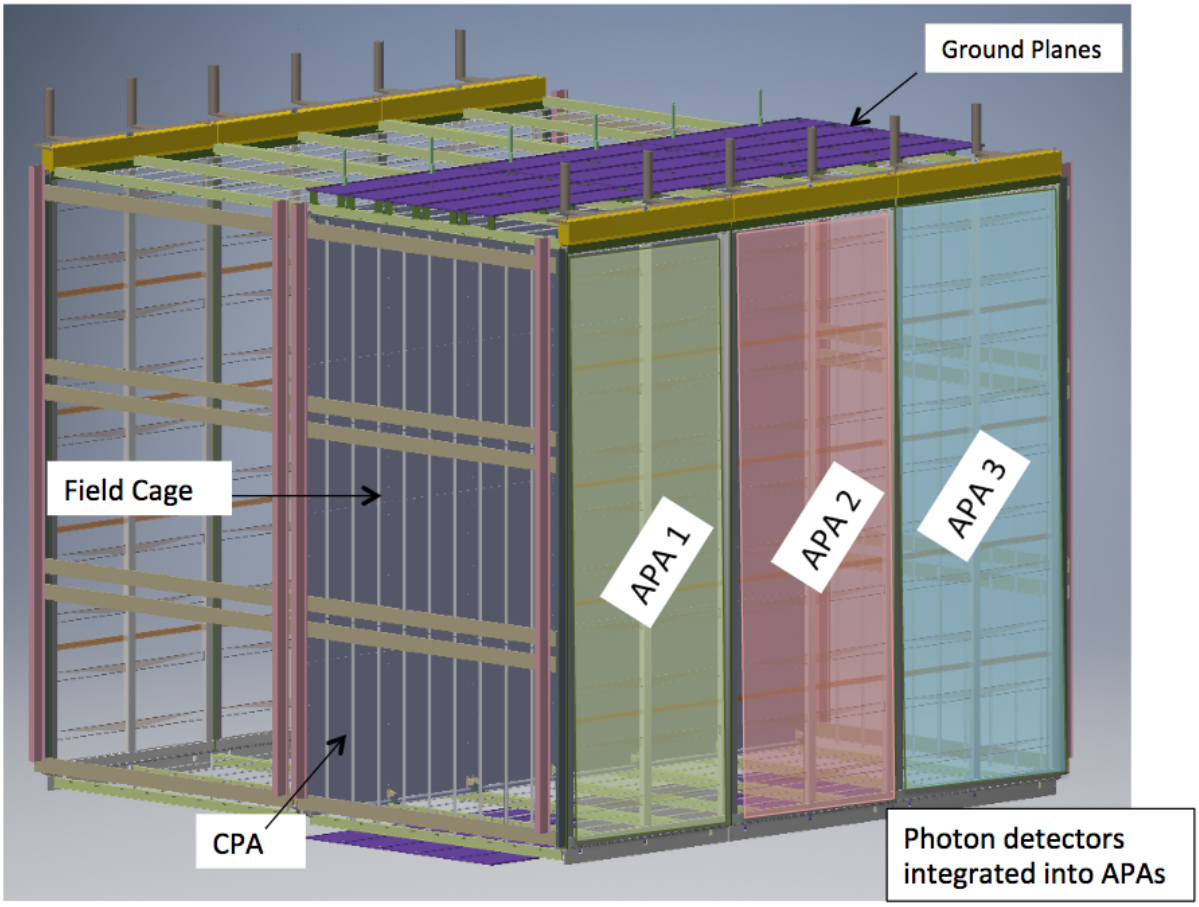

Figure 1.1: The major components of the ProtoDUNE-SP TPC. Note that the field cage shows a vertical stack of three FC assemblies; the design now calls for a stack of four. fig:prot

the integration area (in a clean room) at the CERN NP prior to installation inside the cryostat.

1.3 Goals of ProtoDUNE-SP

ro:goals

The ProtoDUNE-SP test program at CERN has two very clear primary goals. First, it will benchmark the principal technical solutions for the DUNE SP far detector components and, if they are found to be fully adequate, to endorse them. Operating the detector in real experimental conditions and for an extended period will allow for a full characterization of the components, including the membrane cryostat and the cooling and purification circuit, the APA design and the layout of its cold read-out electronics, the HV system, and the PDS and its warm read-out electronics. Secondly, ProtoDUNE-SP will perform the measurements needed to understand, and quantify to the extent possible, the systematic uncertainties that will affect the DUNE oscillation measurements. In many cases these measurements will produce physics results that are of interest to the wider community.

The construction and operation of ProtoDUNE-SP are thus indispensable steps toward the first DUNE Far Detector module, DUNE-SP. ProtoDUNE-SP will allow the collaboration to validate and benchmark the far detector engineering, to test and validate associated infrastructure requirements, and ultimately to extend the physics reach of the experiment.

1.3.1 Detector engineering validation

ProtoDUNE-SP is designed such that it will provide information on the actual far detector performance in as close as possible a configuration to the actual far detector layout, given the practical considerations imposed by time, space, and cost. To achieve this, the cold components are identical to the components proposed for the far detector, to the extent possible.

The APAs are full-scale pre-production modules for the far detector. The ground connections between the electronics, the APA mechanical structure, the photon detectors, and the detector support structure are the same as those proposed for DUNE-SP. ProtoDUNE-SP is instrumented with three APAs along each wall; this will test for cross talk between the middle APA and its neighbors. Whereas DUNE-SP is designed with a 12-m-high TPC, based on a two-APA-high layout, ProtoDUNE-SP TPC is one APA high, due to practical limitations. The collaboration will test the mechanical process of installing the two-APA detector configuration, along with the related cabling, separately.

The cold readout electronics design is based on the DUNE-SP cryogenic front-end pre-amp/shaper chip and ADC. The dedicated ASIC for serializing the data and providing a 1-GB/s link is not yet available, therefore an FPGA emulating its functionality is used; it is mounted on a dedicated mezzanine board. All the analog components, the conversion to digital, and the grounding/power distribution for the final electronics can be tested in this configuration.

ProtoDUNE-SP will be the largest experiment to date to take data with cold electronics, allowing high-statistics detailed studies of the performance. In the event further optimization of the ASICs is required based on the ProtoDUNE-SP findings, it can be implemented before the start of production in 2020. Since there is no charge amplification in the liquid, the electronics is required to be extremely sensitive. The grounding and shielding are therefore critical, and the designs are as similar as is practical to those of DUNE-SP. The building ground in ENH1, with the interconnected rebar in the concrete floor connected to the building ground bus, will provide a fairly good ground. The cryostat itself is isolated from the building ground, and all the mechanical/electrical connections have dielectric breaks. DUNE-SP, in contrast, will be installed a mile underground in a very dry mine, and better isolation from the environment is expected. ProtoDUNE-SP will test the ground isolation and shielding under conservative conditions.

The FC and cathode planes are full-scale prototypes, with the same maximum drift distance and corresponding high voltage. This allows ProtoDUNE-SP to use the same HV feedthrough and drift-field configuration as is planned for DUNE-SP. The cryostat dimensions are selected to be the same for both ProtoDUNEs to leverage the same cryostat and cryogenics system designs. In order to fit the ProtoDUNE-SP TPC in the cryostat, the wall-to-cathode plane distance is slightly smaller than in DUNE-SP, making this setup a conservative test of the HV design. Testing the TPC components under the most likely operating conditions for DUNE-SP is extremely important, as this is the first test of the updated LArTPC design, which incorporates a resistive cathode and FC construction with metal profiles and fiberglass I-beam support.

ProtoDUNE-SP also offers a unique platform to validate and possibly optimize the cryogenics design for DUNE-SP. All cryostat penetrations are designed with gas purge to prevent contaminates from migrating from warm surfaces to the ullage volume, and the the liquid and gas flows inside the cryostat are being modeled. This is expected to provide an excellent test bed to validate the cryogenics design for DUNE-SP.

ProtoDUNE-SP will prototype the tooling and procedures for transporting APAs and transferring them to a suspended rail system. Similarly, the assembly and transport processes of the CPAs and top/bottom FC assemblies are being developed. Due to space constraints inside the cryostat, the rail structure on which the detector is hung will most likely be different for DUNE-SP. Despite these differences, the experience gained in installing the ProtoDUNE-SP detector will be invaluable in planning the DUNE-SP installation.

Integration of the test beam with ProtoDUNE-SP is quite different from the neutrino beam integration planned for DUNE-SP. To minimize the material interactions of the particle beam in the ProtoDUNE-SP cryostat upstream of the TPC, a volume of LAr along the beam path (between the cryostat membrane and the FC) is displaced, and replaced by a less dense volume of dry nitrogen gas. This requires a penetration into one of the FC assemblies to install a beam plug. To ensure that the displacement plug does not compromise the ProtoDUNE-SP operation, a dedicated HV test at Fermilab is planned that will test the final beam plug in the exact field configuration planned for ProtoDUNE-SP.

1.3.2 Physics

The use of the CERN charged-particle beams of known particle type and incident energy provide the means to achieve a better understanding of the interaction processes occuring within a argon target and help to optimize event reconstruction techniques, particle identification algortihms, and calorimetric energy measurements. The beam measurements will also provide a calibration data set for tuning the Monte Carlo simulations and a reference data set for the DUNE experiment.

Pion and proton beams in an energy range from about one to a few GeV will be used primarily to study hadronic interaction mechanisms and secondary particle production. At higher energies, these beams will be used to study shower reconstruction and energy calibration. Electrons will be used to benchmark and tune electron/photon separation algorithms, to study electromagnetic cascade processes and to calibrate electromagnetic showers at higher energies. Charged kaons produced in the tertiary beamline are rare but are copiously produced by the pion beam interactions inside the detector. These will be extremely useful for characterizing kaon identification efficiency for proton decay sensitivity studies. Samples of stopping muons with Michel electrons from muon decay (or without them, in the case of negative muon capture) will be used for energy calibrations in the low-energy range of the SN neutrino events and for the development of charge-sign determination methods.

A cumulative ProtoDUNE-SP test-beam run period of 16 weeks is assumed, but it depends on the extent of beamline sharing with other users at EHN1. The run will take place prior to the long shutdown of the LHC in late 2018 (LS2).

ProtoDUNE-SP will acquire cosmic data during periods with no beam. A dedicated external trigger system consisting of arrays of scintillator paddles, suitably positioned and arranged in *coincidence* trigger logic, will select specific classes of cosmic muon events. Dedicated runs, e.g., runs looking for long muon tracks crossing the entire detector at large zenith angles, allow for an overall test of the detector performance and the DAQ. Runs looking for muons stopping inside the LAr volume and the accumulation of accurate Michel electron spectra may be useful for energy calibration purposes in the low-energy range.

It is important to note that ProtoDUNE-SP offers much beyond calibration and detector performance characterization. The LArTPC simultaneously features precise 3D tracking and accurate measurement of energy deposited. Its large active volume allows for good containment of the hadronic and electromagnetic interaction products in the few GeV range. These capabilities have never before been combined in one detector. The unprecedented event reconstruction capability combined with the exposure of the detector's large active volume to the CERN charged-particle beams open the way to a truly rich program of new physics investigations into particle interaction processes.

Hadronic (π, K and p) interactions on an Ar target around one GeV produce low-multiplicity final states rather than "hadron showers," and similarily 1-GeV electrons (with critical energy $\simeq$ 30 MeV in Ar) produce low-populated cascades, with only a few tens of secondary energetic electrons (positrons). "TPC/imaging-aided calorimetric measurements" will allow investigations of energy deposition mechanisms in this energy range where the standard hadronic and electromagnetic

shower concepts and features are either not well defined or cannot be applied. The calorimetric measurement of the total energy deposited can, in fact, be accomplished, by detecting and summing over the energy deposited by each individual secondary particle/track thanks to the imaging capabilities of the LArTPC. In particular, the determination of the electromagnetic content in hadron-initiated cascades, π^0 multiplicity, and the energy fraction carried as a function of primary hadron incident energy will be of interest.

1.4 Run plan

:runplan

May need some intro/transition content here since this section was just moved in from a different part of the document

Beam simulations show that the hadron rates at energies below 1 GeV/c are low. Moreover, low-energy beams are more subject to degradation by materials in the beamline. The optimization of the run plan factors in the beam composition and particle rates of the H4 beamline, and also particle interaction topologies in the ProtoDUNE-SP detector. Full simulations of particle transport in the ProtoDUNE-SP detector, including the beam window, have been performed.

At a beam momentum of 1 GeV/c, 35% of protons are stopped before reaching the active TPC region, while the percentage reduces to 0.5% at 2 GeV/c. The kinetic energy distributions of protons and pions at the entrance point of the TPC for different beam momenta are shown in Figure 1.2. The fraction of stopping π's for one π produced at the secondary target is 3% at $p = 0.4$ GeV/c and decreases to 1.3% at $p = 0.7$ GeV/c. The long distance (37 m) between the secondary target and the front of the LAr cryostat has a significant impact on the pion and kaon rates in the TPC. Due to pion lifetime, many of the low-energy pions produced at the secondary target decay in the beam pipe before reaching the cryostat. The situation is even more significant for kaons; most kaons below 2 Gev/c do not make it to the cryostat. Consequently the H4 beamline will not be operated much below 1 GeV/c in the hadron mode. For electrons, the beam momentum should go as low as possible to study the topology of very low-energy electron-initiated showers.

fig:pandpint

To formulate a preliminary run plan, the hadron beam spectrum and rates are assumed as given in Tables 5.2 and 5.3. For the purpose of estimating the sample composition and beam time request, the following assumptions are used:

tab:beamparticlerates

- Trigger rate = 25 Hz
- Two 4.8 sec spills per SPS Super Cycle
- SPS Super Cycle = 48 sec
- 10^6 (10^4) secondary particles on target per spill for hadron (electron) beam
- Particle ID trigger for electrons from 0.5 to 7 GeV/c

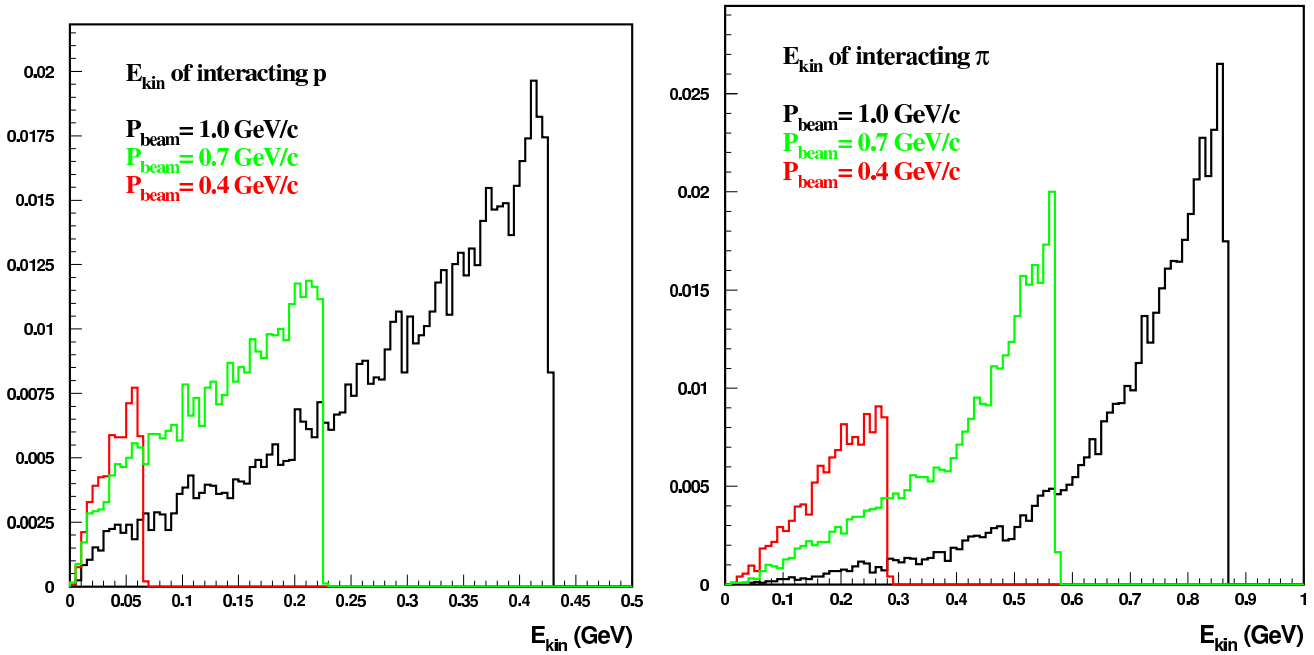

Figure 1.2: Kinetic energy of particles at the point of interaction in the ProtoDUNE-SP active volume, for different beam momenta. Histograms are normalized to one particle injected in the beamline acceptance. Simulations include the beam window materials, beams are considered as monochromatic and parallel. Left: protons, Right: pions.

fig:pand

- Trigger rate for electron in hadron beam is prescaled to 0.5 Hz
- Data collection efficiency = 50%

It is planned to run the H4 beamline in two modes: the first configuration is optimized for the production of hadrons and the second configuration is optimized for the production of high-purity electrons. Even in the hadron mode, the beam is still dominated by electrons, especially for low beam momenta. However, the electrons in the hadron beam are not particularly "clean" due to the amount of materials in the beamline from the particle identification (PID) instrumentations. The proposal is to heavily prescale the electron events using PID (e.g., Threshold Cherenkov counters) trigger while running in hadron mode. The PID systems that contribute significantly to the material budget will be removed when the beamline is reconfigured for electron beam. Various run plan scenarios are under investigation. One of the scenarios is shown in Tables 1.1 and 1.2. Similar values are expected for the negative beam sample.

tab:HadRunPlan tab:ElecRunPlan

Based on the information available, the total estimated beam time needed to carry out the physics program in this proposal, with the assumptions stated earlier, is on the order of 16 weeks.

Table 1.1: A preliminary run plan for ProtoDUNE-S P hadron beam. The expected sample (positive beam) as a function of momentum is shown.

P (GeV/c)	# of Spills	# of e^+	# of K^+	# of μ^+	# of p	# of π^+	Total # of Events	Beam Time (days)
1	70K	84K	≈ 0	70K	689K	625K	1.5M	19.4 days
2	16K	19K	9K	36K	336K	572K	1.0M	4.4 days
3	13K	16K	26K	17K	181K	540K	780K	3.6 days
4	11K	13K	19K	16K	107K	510K	660K	3.1 days
5	11K	13K	29K	13K	96K	510K	660K	3.1 days
6	11K	13K	36K	12K	94K	510K	660K	3.1 days
7	11K	13K	42K	8K	87K	510K	660K	3.1 days
Total	143K	171K	161K	172K	1.6M	3.8M	5.9M	39.7 days

dRunPlan

Table 1.2: A preliminary run plan for ProtoDUNE-SP electron beam. The expected sample for positive beam configuration is shown.

Momentum Bins (GeV/c)	# of Spills per Bin	# e^+ per Bin	Beam Time per Bin (days)
0.5, 06, 0.7, 0.8, 0.9, 1, 2, 3, 4, 5, 6, 7	5000	300K	1.4

cRunPlan

Chapter 2

Detector components

2.1 Overview of detector components

The elements composing the detector, listed in Section 1.2, include the time projection chamber (TPC), the cold electronics (CE), and the photon detection system (PDS). The TPC components, e.g., anode planes, a cathode plane and a field cage, are designed in a modular way. The six APAs are arranged into two APA planes, each consisting of three side-by-side APAs. Between them, a central cathode plane, composed of 18 CPA modules, splits the TPC volume into two electron-drift regions, one on each side of the cathode plane. A field cage (FC) completely surrounds the four open sides of the two drift regions to ensure that the electric field within is uniform and unaffected by the presence of the cryostat walls and other nearby conductive structures. The sections in this chapter describe the components individually.

Figure 1.1 illustrates how these components fit together. The FC is shown in Figure 2.1.

Table 2.1 lists the principal detection elements of ProtoDUNE-SP along with their approximate dimensions and their quantities.

Table 2.1: TPC detection components, dimensions and quantities

Detection Element	Approx Dimensions	Quantity
APA	6 m H by 2.4 m W	3 per anode plane, 6 total
CPA module	2 m H by 1.2 m W	3 per CPA column, 18 total in cathode plane
Top FC module	2.4 m W by 3.6 m along drift	3 per top FC assembly, 6 total
Bottom FC module	2.4 m W by 3.6 m along drift	3 per bottom FC assembly, 6 total
End-wall FC module	1.5 m H by 3.6 m along drift	4 per end-wall assembly (vertical drift volume edge), 16 total
PD module	2.2 m $\times$ 86 mm $\times$ 6 mm	10 per APA, 60 total

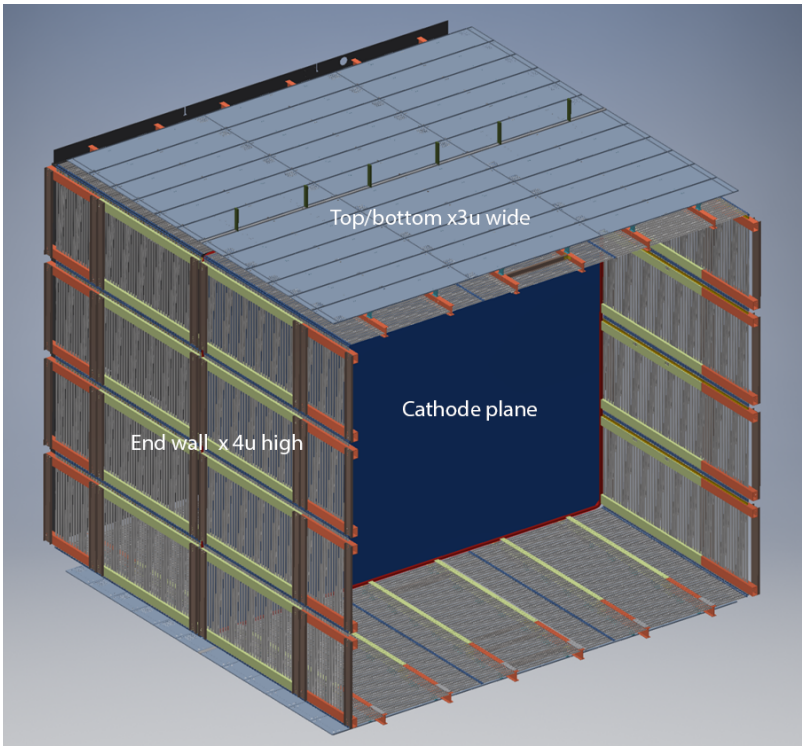

Figure 2.1: A view of the TPC field cage and the central cathode plane (CPA). The APA that would be positioned at the open end of the FC, and thus obscure the CPA, is not shown. fig:fc-c

2.2 Anode Plane Assemblies (APA)

2.2.1 Scope and requirements

Anode Plane Assemblies (APAs) are the detector elements utilized to sense ionization created by charged particles traversing the liquid argon volume inside the single-phase TPC. The scope of the APAs includes:

- framework of lightweight, rectangular stainless steel tubing;
- a mesh layer attached directly to both sides of the APA frame;
- layers of sense and shielding wires wrapped at varying angles relative to each other;
- stacked head electronics boards, which are wire boards for anchoring the wires at the top (head) of the APA;
- capacitive-resistive (CR) boards that link the wire boards to the CE;
- side and foot boards along the other three edges of the APA with notches and pins to hold the wires in place;

- modular boxes to hold the CE;
- comb wire supports, mounted on cross braces distributed along the length of the APA, to prevent wire deflection; and
- pin/slot pairs on the side edges of adjacent APAs to maintain coplanarity.

The initial physics performance requirements that drive the design of the APA are listed in Table 2.2. These are chosen to enable high-efficiency reconstruction throughout the entire active volume of the LArTPC.

Table 2.2: Preliminary physics requirements that motivate APA design parameters.

Requirement	Value
MIP Identification	100% efficiency
High efficiency for charge reconstruction	>90% for >100 MeV
Vertex Resolution (x,y,z)	(1.5 cm, 1.5 cm, 1.5 cm)
Particle Identification	
Muon Momentum Resolution	<18% for non-contained <5% for contained
Muon Angular Resolution	<1°
Stopping Hadrons Energy Resolution	1-5%
Hadron Angular Resolution	<10°
Shower identification	
Electron efficiency	>90%
Photon mis-identification	<1%
Electron Angular Resolution	<1°
Electron Energy Scale Uncertainty	<5%

The ability to identify minimum-ionizing particles (MIPs) is a function of several detector parameters, including argon purity, drift distance, diffusion, wire pitch, and Equivalent Noise Charge (ENC). It is required that MIPs originating anywhere inside the active volume of the detector be reconstructed with 100% efficiency. The choice of wire pitch (i.e., ∼5 mm), combined with the design values of the other high-level parameters, listed in Table 2.3, is expected to enable this efficiency.

The fine wire spacing of the APA enables excellent precision in identifying the location of any vertices in an event (e.g., the primary vertex in a neutrino interaction, or gamma conversion points in a π^0 decay), which has a direct impact on reconstruction efficiency. It is required to reach a vertex resolution of ∼1.5 cm along each coordinate direction. In practice, the resolution on the drift-coordinate (x) of a vertex or hit will be better than that on its location in the y-z plane, due to the combination of drift-velocity and electronics sampling-rate uncertainties.

2.2.2 APA design overview

An APA is constructed from a framework of lightweight, rectangular stainless steel tubing, with a fine mesh covering the rectangular area within the frame, on both sides, that defines a uniform ground across the frame. Along the length of the frame and around it, over the mesh layer, layers of sense and shielding wires are strung or wrapped at varying angles relative to each other, as illustrated in Figure 2.2. The wires are terminated on boards that anchor them and also provide the connections to the cold electronics. The APAs are 2.3 m wide, 6.3 m high, and 12 cm thick. The size of the APAs is chosen for fabrication purposes, compatibility with over-the-road shipping, and for eventual transport to the 4850 level at SURF and installation into the membrane cryostat of a detector module. Sufficient shock absorption and clearances are taken into account at each stage. The dimensions are also chosen such that an integral number of electronic readout channels and boards fill in the full area of the APA. The modularity of the APAs allows them to be built and tested at off-site production facilities, decoupling their manufacturing time from the construction of the membrane cryostat. As mentioned above, the principal design parameters are listed in Table 2.3.

Table 2.3: APA Design Parameters.

Parameter	Value
Active Height	5.920 m
Active Width	2.295 m
Wire Pitch (U,V)	4.67 mm
Wire Pitch (X,G)	4.79 mm
Wire Position Tolerance	0.5 mm
Wire Plane Spacing	5 mm
Wire Angle (w.r.t. vertical) (U,V)	35.7°
Wire Angle (w.r.t. vertical) (X,G)	0°
Number Wires / APA	960 (X), 960 (G), 800 (U), 800 (V)
Number Electronic Channels / APA	2560
Wire Tension	5.0 N
Wire Material	Beryllium Copper
Wire Diameter	150 μm
Wire Resistivity	7.68 $\mu\Omega$-cm @ 20° C
Wire Resistance/m	4.4 Ω/m @ 20° C
Frame Planarity	5 mm
Photon Detector Slots	10

Starting from the outermost wire layer, there is first a shielding (grid) plane, followed by two induction planes, and finally the collection plane. All wire layers span the entire height of the APA frame. The layout of the wire layers is illustrated in Figure 2.2.

The angle of the induction planes in the APA ($\pm$35.7°) is chosen such that each induction wire only crosses a given collection wire one time, reducing the ambiguities that the reconstruction must address. The design angle of the induction wires, coupled with their pitch, was also chosen

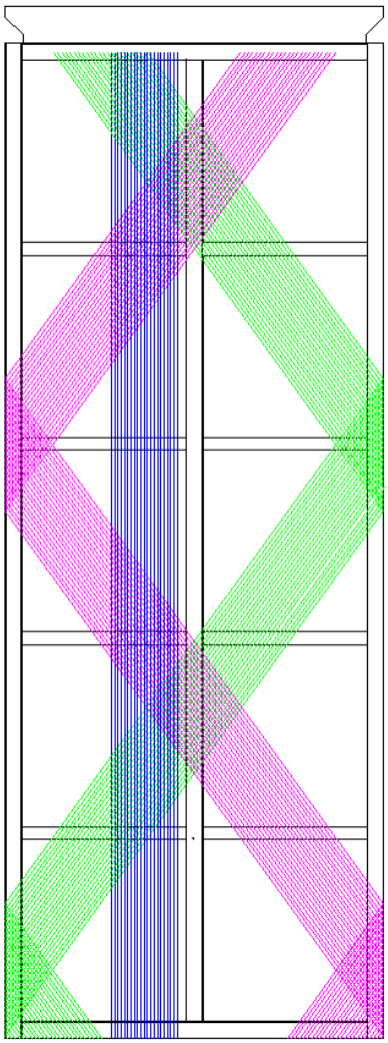

Figure 2.2: Sketch of a ProtoDUNE-SP APA. This shows only portions of each of the three wire layers, U (green), V (magenta), the induction layers; and X (blue), the collection layer, to accentuate their angular relationships to the frame and to each other. The induction layers are connected electrically across both sides of the APA. The grid layer (G) wires (not shown), run vertically, parallel to the X layer wires; separate sets of G and X wires are strung on the two sides of the APA. The mesh is not shown. fig:tpc_

such that an integer multiple of electronics boards reads out one APA.

The wires of the grid (shielding) layer, G, are not connected to the electronic readout; the wires run parallel to the long edge of the APA frame; there are separate sets of G wires on the two sides of the APA. The two planes of induction wires (U and V) wrap in a helical fashion around the long edge of the APA, continuously around both sides of the APA. The collection plane wires (X) run vertically, parallel to G. The ordering of the layers, from the outside in, is G-U-V-X, followed by the mesh.

The operating voltages of the APA layers are listed in Table 2.4. When operated at these voltages, the drifting ionization follows trajectories around the grid and induction wires, ultimately terminating on a collection plane wire; i.e., the grid and induction layers are completely transparent to drifting ionization, and the collection plane is completely opaque. The grid layer is present for pulse-shaping purposes, effectively shielding the first induction plane from the drifting charge and removing the long leading edge from the signals on that layer; again, it is not connected to the electronics readout. The mesh layer serves to shield the sense planes from pickup from the Photon Detection System and from "ghost" tracks that would otherwise be visible when ionizing particles have a trajectory that passes through the collection plane.

Table 2.4: Baseline bias voltages for APA wire layers

Anode Plane	Bias Voltage
Grid (G)	-665 V
Induction (U)	-370 V
Induction (V)	0 V
Collection (X)	820 V
Mesh (M)	0 V

The wrapped style allows the APA plane to fully cover the active area of the LArTPC, minimizing the amount of dead space between the APAs that would otherwise be occupied by electronics and associated cabling.

In the current design of the DUNE-SP far detector module, a central row of APAs is flanked by drift-fields, requiring sensitivity on both sides. The wrapped APAs allow the induction plane wires to sense drifting ionization originating from either side of the APA. This double-sided feature is not strictly necessary for the ProtoDUNE-SP arrangement, which has APAs located against the cryostat walls and a drift field on one side only, but it is compatible with this setup as the grid layer facing the wall effectively blocks any ionization generated outside the TPC from drifting in to the wires on that side of the APA.

The choices of wire tension and wire placement accuracy are made to ensure proper operation of the LArTPC at voltage, and to provide the precision necessary for reconstruction. The tension of 5 N, when combined with the intermediate support combs (described in Section 2.2.5) ensure that the wires are held taught in place with no sag. Wire sag can impact the precision of reconstruction, as well as the transparency of the TPC. The tension of 5 N is low enough that when the wires are cooled, which increases their tension due to thermal contraction, they will stay safely below the break load of the beryllium copper wire, as described in Section 2.2.3. To further mitigate wire

breakage and its impact on detector performance, each wire in the APA is anchored twice on both ends, with both solder and epoxy.

2.2.3 Wire properties

pa_wires

Beryllium copper (CuBe) wire is known for its high durability and yield strength. It is composed of ∼98% copper, 1.9% beryllium, and a negligible amount of other elements. The APA wire has a diameter of 150μm (.006 in), and is strung in varying lengths across the APA frame. Three key properties for its usage in the APA are: low resistivity, high tensile or yield strength, and coefficient of thermal expansion suitable for use with the APA's stainless steel frame.

Tensile strength of the wire describes the wire-breaking stress (see Table 2.5). The yield strength is the stress at which the wire starts to take a permanent (inelastic) deformation, and is the important limit stress for this case, though most specifications give tensile strength. Fortunately, for the CuBe alloys of interest, the two are fairly close to each other. Based on the tensile strength of wire purchased from Little Falls Alloy (over 1,380 MPa or 200,000 psi), the yield strength is greater than 1,100 MPa. Given that the stress while in use is around 280 MPa, this leaves a comfortable margin.

The coefficient of thermal expansion (CTE) describes how material expands and contracts with changes in temperature. The CTEs of CuBe alloy and 304 stainless steel are very similar. Integrated down to 87 K, they are 2.7e-3 for stainless and 2.9e-3 for CuBe [1]. Since the wire contracts slightly more than the frame during cool-down the wire tension increases. If it starts at 5 N, the tension rises to about 5.5 N when everything is cool.

The change in wire tension during cool-down could also be a concern. In the worst case, the wire cools quickly to 87 K before any significant cooling of the frame – a realistic case because of the differing thicknesses. In the limiting case, with complete contraction of the wire and none in the frame, the tension would be expected to reach ∼11.7 N. This is still well under the ∼20 N yield tension. In practice, the cooling will be done gradually to avoid this tension spike as well as other thermal shock to the APA.

Table 2.5: Tensile strength and coefficient of thermal expansion (CTE) of beryllium copper (CuBe) wire.

Parameter	Value
Tensile Strength (from property sheets) (psi)	208,274
Tensile Strength (from actual wire) (psi)	212,530
CTE of CuBe, integrated to 87 K (m/m)	2.9e-3
CTE of 304 stainless steel, integrated to 87 K (m/m)	2.7e-3

tab:wire

2.2.4 APA frame and mesh

The stainless steel frame of the APA (Figure 2.3) is 6.06 m long, not counting electronics and mounting hardware, and 2.30 m wide. It is 76.2 mm thick, made from imperial size 3-in × 4-in × 0.120-in wall rectangular tubing. The cross pieces have a cross-sectional area of 2 in × 3 in, and are connected to edge pieces using joints, as in Figure 2.4. It is mounted in the cryostat with its long axis vertical; multiple APAs are mounted edge-to-edge to form a continuous plane. An electron deflection technique is used to ensure that electrons drawn towards a joint between two APAs will be deflected to one or the other, and not lost.

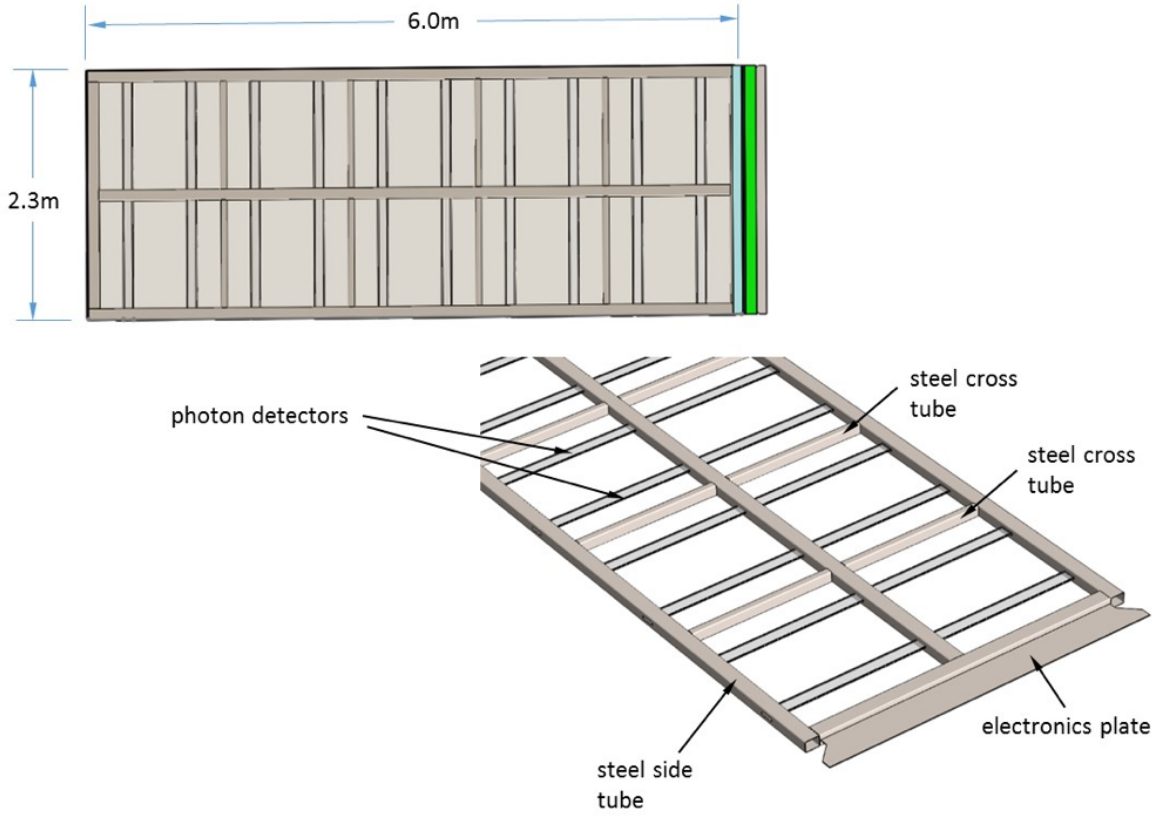

Figure 2.3: An APA showing overall dimensions and main components.

A fine mesh screen is glued directly to the steel frame surface, over the frame on both sides. It creates a uniform ground layer beneath the wire planes.

The mesh is clamped around the perimeter of the opening and then pulled tight (by opening and closing clamps as needed during the process). When the mesh is taut, a 25-mm-wide strip is masked off around the opening and glue is applied through the mesh to attach it to the steel. Although measurements have shown that this gives good electrical contact between the mesh and the frame, a deliberate electrical connection is also made. Figure 2.5 depicts the mesh application setup for a full-size ProtoDUNE-SP APA.

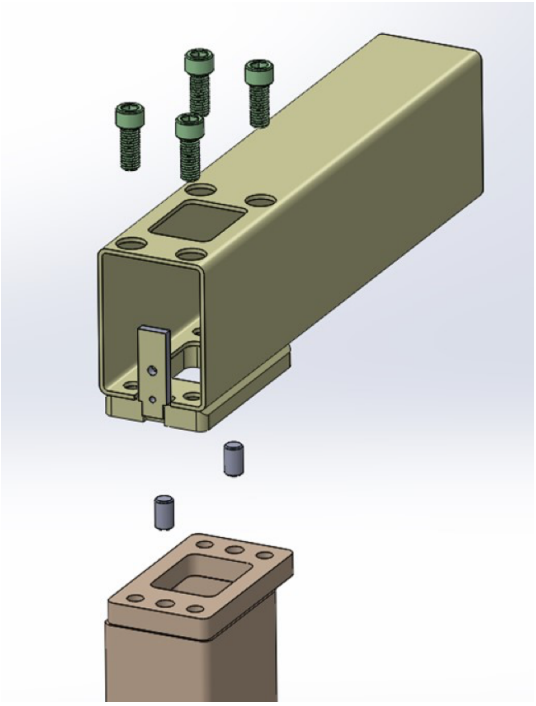

Figure 2.4: A model of the bolted joint. The holes on the top of the tube are for access to tighten the screws. The heads actually tighten against the lower hole, inside the tube. fig:tpc_

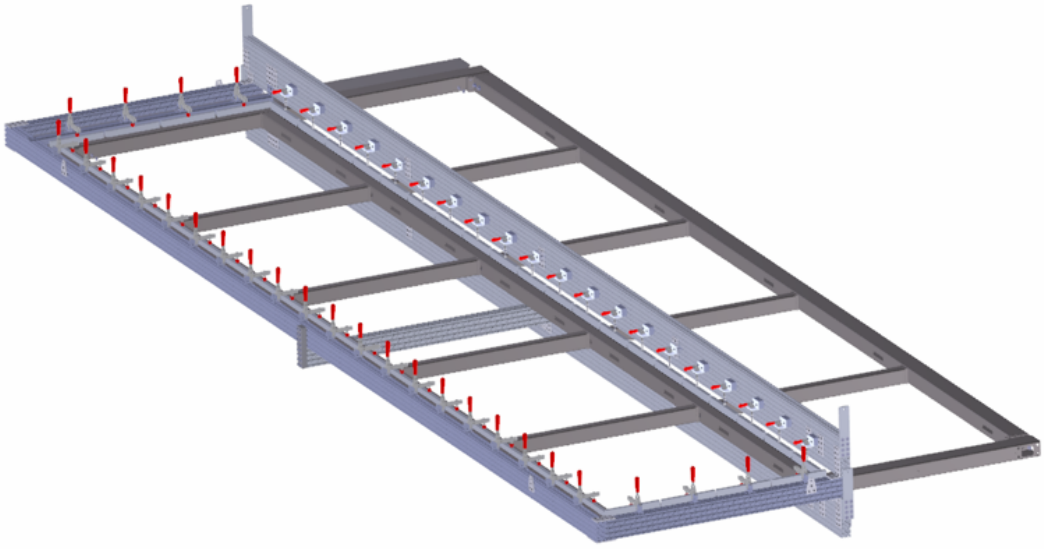

Figure 2.5: The mesh clamping jig for the full size APA. fig:tpc_

2.2.5 Anchoring elements and wire boards

Head electronics boards

At the head end of the APA, stacks of electronics boards (referred to as "wire boards") are arrayed to anchor the wires. They also provide the connection between the wires and the cold electronics.

All APA wires are terminated on the wire boards, which are stacked along the electronics end of the APA frame; see Figure 2.6. Attachment of the wire boards begins with the X plane (innermost). After the X-plane wires are strung top to bottom along each side of the APA frame, they are soldered and epoxied to their wire boards and trimmed. The remaining wire board layers are attached as each layer is wound. The main CR boards (capacitive-resistive), which provide DC bias and AC coupling to the wires, are attached to the bottom of the wire board stack. They are described in Section 2.2.5.

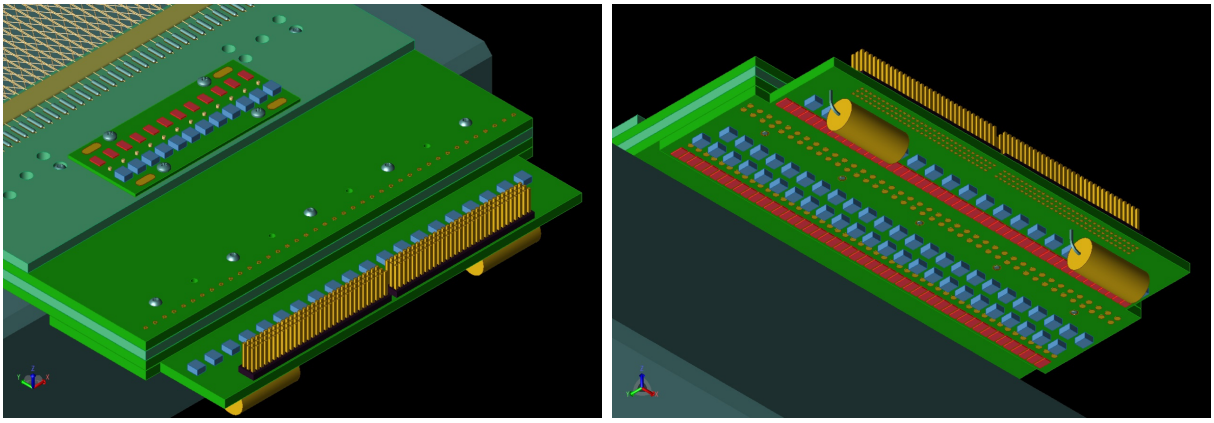

Figure 2.6: Left: View of the APA wire board stack, as seen from the top/side. The wire board layers can be seen at the bottom-left of the illustration, X on the bottom (it doesn't go all the way back, but extends farther forward and has the main CR board attached), followed by U, V, then G (which doesn't go all the way forward, and has its own CR board attached). Right: the same stack viewed from below.

figure 2.6 needs labeling

The outermost G-plane wire boards connect adjacent groups of four wires together, and bias each group through an R-C filter whose components are placed on special CR boards that are attached after the wire plane is strung. The X, U and V layers of wires are connected to the CE (housed in boxes mounted on the APA) either directly or through DC-blocking capacitors. The X and U planes have wires individually biased through 50-MΩ resistors. Electronic components for the X- and U-plane wires are located on a common CR board.

Mill-Max pins and sockets provide electrical connections between circuit boards within a stack. They are pressed into the circuit boards and are not repairable if damaged. To minimize the possibility of damaged pins, the boards are designed so that the first wire board attached to the frame has only sockets. All boards attached subsequently contain pins that plug into previously mounted boards. This process eliminates exposure of any pins to possible damage during winding,

soldering, or trimming processes.

Ten stacks of wire boards are installed across the width of each side along the head of the APA. The X-layer board in each stack has room for 48 wires, the V layer has 40 wires, the U layer 40 wires and the G layer 48 wires. Each board stack, therefore, has 176 wires but only only 128 signal channels since the G wires are not read out. With a total of 20 stacks per APA, this results in 2,560 signal channels per APA and a total of 3520 wires starting at the top of the APA and ending at the bottom. There is a total of ∼23.4 km of wire on the two surfaces of each APA. Many of the capacitors and resistors that in principle could be on these wire boards are instead placed on the attached CR boards to improve their accessibility in case of component failure. Figure 2.7 depicts the connections between the different elements of the APA electrical circuit.

fig:tpc_apa_electroni

this figure could use some labelling

At the head end of the APA, the wire-plane spacing is set by the thickness of these wire boards. The first layer's wires solder to the surface of the first board, the second layer's wires to the surface of the second board, and so on. For installation, temporary toothed-edge boards beyond these wire boards align and hold the wires until they are soldered to pads on the wire boards. After soldering, the extra wire is snipped off.

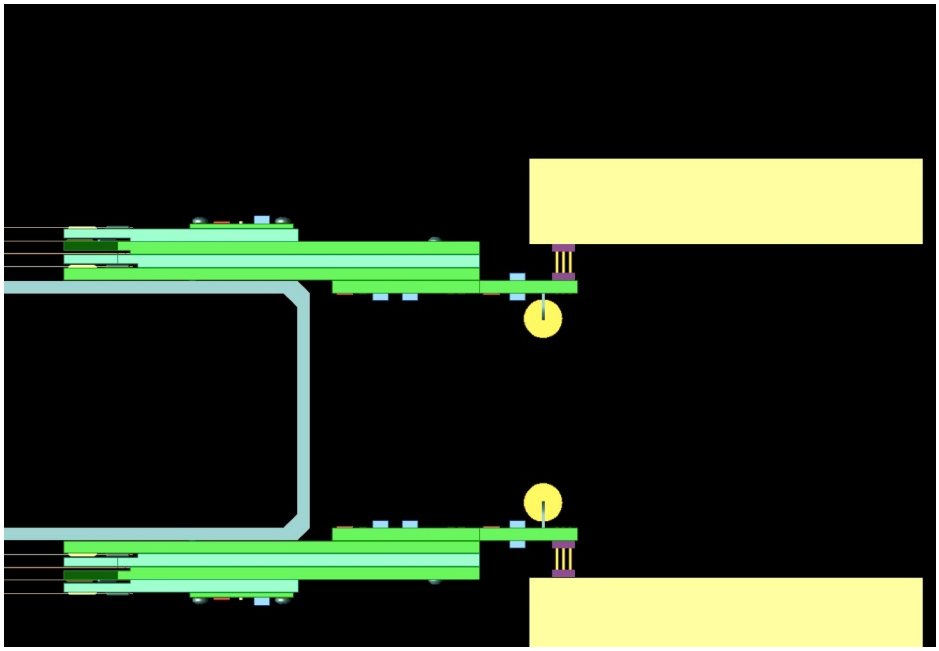

Figure 2.7: Diagram of the connection between the APA wires, viewed from the APA edge. The set of wire boards within a stack can be seen on both sides of the APA, with the CR board extending further to the right, providing a connection to the cold electronics, which are housed in the boxes at the far right of the figure

fig:tpc_

CR boards

The CR boards carry a bias resistor and a DC-blocking capacitor for each wire in the X and U planes. These boards are attached to the board stacks after fabrication of all wire planes. Electrical connections to the board stack are made though Mil-Max pins that plug into the wire boards. Connections from the CR boards to the CE are made through a pair of 96-pin Samtec connectors.

Surface-mount bias resistors on the CR boards have resistance of 50 MΩ are constructed with a thick film on a ceramic substrate. Rated for 2.0-kV operation, the resistors measure 0.12 × 0.24 inches. Other ratings include operation from −55 to +155 C, 5% tolerance, and 100-ppm/C temperature coefficient. Performance of these resistors at LAr temperature is verified through additional bench testing.

The selected DC-blocking capacitors have capacitance of 3.9 nF and are rated for 2.0-kV operation. Measuring 0.22 × 0.25 inches across and 0.10 inches high, the capacitors feature flexible terminals to comply with PC board expansion and contraction. They are designed to withstand 1,000 thermal cycles between the extremes of the operating temperature range. Tolerance is also 5%.

Eric has question mark on the temp range

In addition to the bias and DC-blocking capacitors for all X- and V-plane wires, the CR board includes two R-C filters for the bias voltages. The resistors are of the same type used for wire biasing except with a resistance of 2 MΩ. Capacitors are 47 nF at 2 kV. Very few choices exist for surface-mount capacitors of this type, and they are exceptionally large. Polyester or Polypropylene film capacitors that are known to perform well at cryogenic temperatures are used.

Side and foot boards

The boards along the sides and foot of the APA have notches, pins and other location features to hold the wires in the correct position as they wrap around the edge from one side of the APA to the other.

G10 circuit board material is ideal for these side and foot boards due to its physical properties alone, but it has an additional advantage: a number of hole or slot features in the edge boards provide access to the underlying frame. In order that these openings are not covered by wires, the sections of wire that would go over the openings are replaced by traces on the boards. After the wires are wrapped, the wires over the opening are soldered to pads at the ends of the traces, and the section of wire between the pads is snipped out (Figure 2.8). These traces are easily and economically added to the boards by the many commercial fabricators who make circuit boards.

The placement of the angled wires are fixed by pins as shown in the right-hand picture of Figure 2.9. The wires make a partial wrap around the pin as they change direction from the face of the APA to the edge. The X- and G-plane wires aren't pulled to the side so they can't be pulled against a

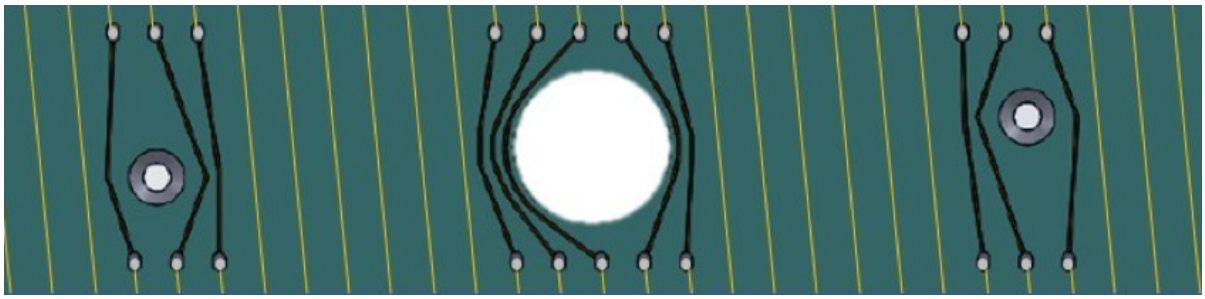

Figure 2.8: Model of board with wires showing how traces connect wires around openings in the side boards. The wires are wound straight over the openings, then soldered to pads at the ends of the traces. After soldering the sections between the pads are trimmed away. fig:tpc_

Figure 2.9: Boards with injection molded tooth strips glued on. The left shows an end board with teeth for fixing the position of the longitudinal wires. The teeth there form small notches. The right is a side board for fixing the position of the angled wires where the wires are angled around a pin. fig:tpc_

pin. Their positions are fixed by teeth with slots, as shown in the left-hand picture in Figure 2.9.

The polymer used for the strips is Vectra e130i (a trade name for 30% glass filled liquid crystal polymer or LCP). It retains its strength at cryogenic temperature and has a CTE similar enough to G10 that differential expansion/contraction is not a problem.

Glue and solder

The ends of the wires are soldered to pads on the edge of the wire boards. Solder provides both an electrical connection and a physical anchor to the wires. As an additional physical anchor, roughly 10 mm of the wires are glued near the solder pads. For example, in Figure 2.9, in addition to soldering the wires on the pads shown in the left-hand photograph, an epoxy bead is applied on the wires in the area between the solder pads and the injection-molded tooth strips.

Gray epoxy 2216 by 3M is used for the glue. It is strong, widely used (therefore much data is available), and it retains good properties at cryogenic temperatures. A 62% tin, 36% lead and 2% silver solder was chosen. A eutectic mix (63/37) is the best of the straight tin/lead solders but the 2% added silver gives better creep resistance.

Comb wire supports on inner frame members

Some wire segments are quite long; for instance, the X- and G-plane wires extend from one end of the APA to the other without going around a side – a length of 6 m. Even the diagonal wires across the middle of the APA are 3.9 m long. To prevent deflection from gravity, electrostatic forces, or liquid drag from moving argon, the wires are supported at regular locations along the length of the APA. This is done with *combs* mounted on each of the four cross braces that are regularly spaced along the length of the APA. This keeps the longest unsupported wire length under 1.6 m.

The nominal wire tension is 5 N but even the 1.6-m-long wires could fall to 3 N of tension before the wire, held horizontally, would deviate 150 microns – one wire diameter. During operation the wires are either vertical or 35.7° from vertical, so the actual deviation would be less.

The combs are made from 0.5-mm-thick G10 with slots cut into it. The comb for the lowest layer is glued to a base strip that is glued to the frame. After each layer is wound, another comb strip is glued to the tips of the teeth of the previous one to position the wires in the next layer. Each successive comb holds the previous layer of wires in the bottom of its slots (Figure 2.10).

Periodic holes along the length of the strip allow the use of pins to accurately position each successive strip with respect to the previous one. A series of jigs is used to create and install these combs. One jig aligns the first strip to the base strip during gluing. Another jig locates this assembly on the frame as it is glued in place. A third jig locates each successive comb using these holes (labeled registration holes in Figure 2.10).

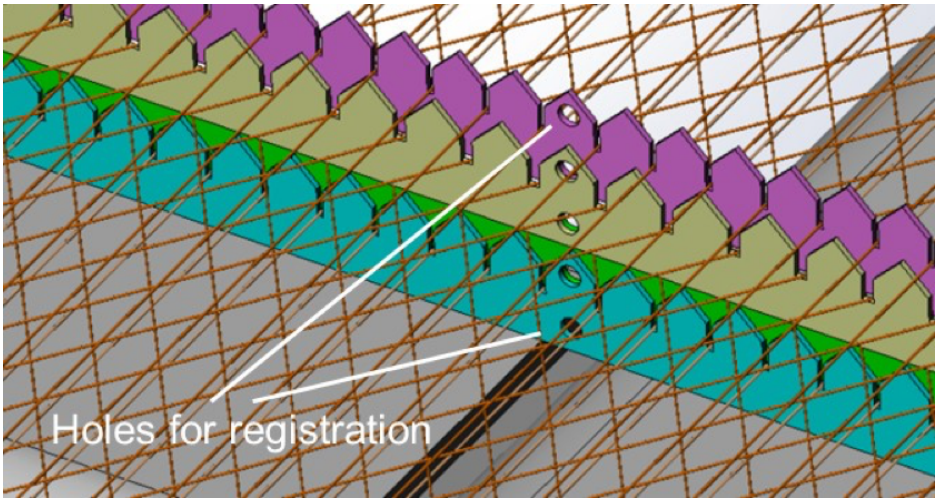

Figure 2.10: A model of the combs showing how they stack. After winding a layer, the comb for the next layer is put in place. Each comb hold the wires from the previous layer in its slots.

The wire openings in the comb stack are small enough that the wires are accurately positioned at the combs, and therefore the gluing of wires into the combs is not required.

2.2.6 Interconnection features

CE boxes

Pins extending outward from the CR boards provide connections from the APA to the modularly designed CE, and the CE modules are housed in small boxes that provide shielding. The CE boxes are illustrated in Figure 2.11. Each board stack has one CE box installed near it that holds the CE module for the stack.

Putting the electronics in small boxes simplifies installation and replacement, and also helps with the dissipation

getting rid of

of argon gas generated by the warm electronic components. The CE modules are mounted in such a way that any of them can be removed from a single side of the APA after APA installation.

Adjacent APAs

A constraint is needed between adjacent APAs to keep them co-planar. It is also important that this constraint not apply a vertical load to adjacent APAs. The constraint takes the form of a pair of protruding pins on one edge of the APA (one high and one low) and a pair of matching slots

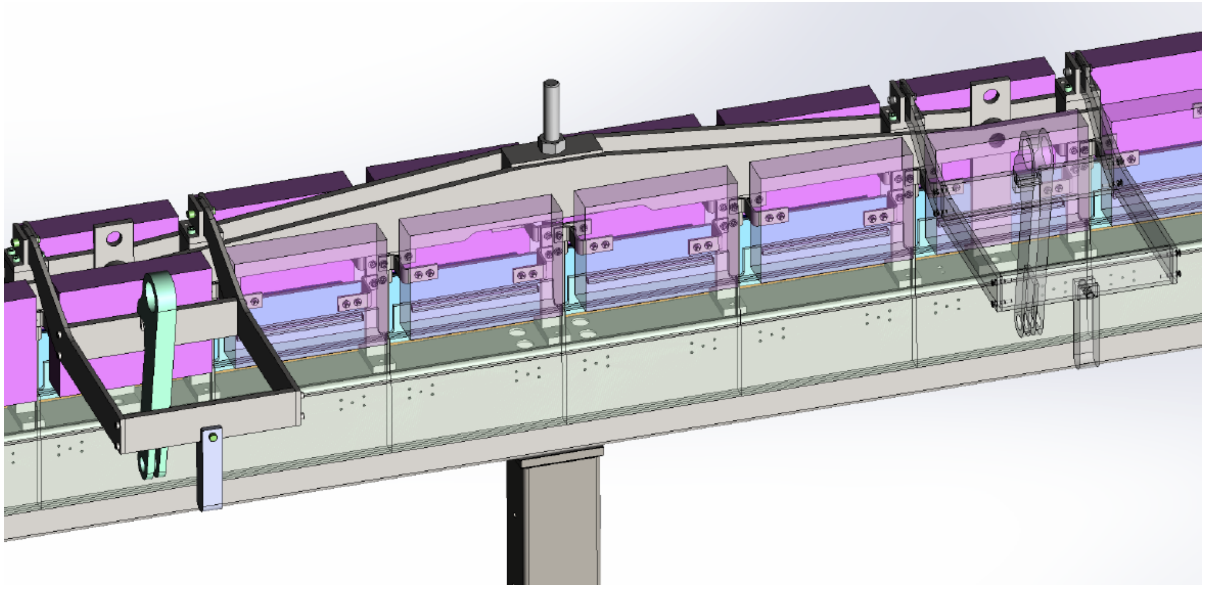

Figure 2.11: Solid model of modular CE boxes.

fig:tpc_

on the edge of the adjacent APA to engage the pins (Figure fig:tpc_apa_pinslotdrawing 2.12). The pins have steel cores for strength.

Electronics noise concerns have made it desirable to isolate APAs from each other. Therefore, the alignment pins have G10 sleeves covering their steel cores at places where they come into contact with the frame of the adjacent APA.

2.3 Cathode Plane Assembly (CPA)

sec:cpa

2.3.1 Scope and requirements

The cathode plane, also called the cathode plane assembly, or CPA, is located in the middle of the TPC, dividing the detector into two equal-distance drift volumes. The cathode plane's 7 m × 6 m area is made up of six *CPA columns*, each of which is constructed of three vertically stacked *CPA modules*. The CPA therefore consists of 18 CPA modules.

The scope of the CPA includes:

- 18 CPA modules, each with a frame and resistive cathode panel,
- HV bus connecting the CPA columns and modules, and
- HV cup for receiving input from the power supply.

The CPA plane is required to:

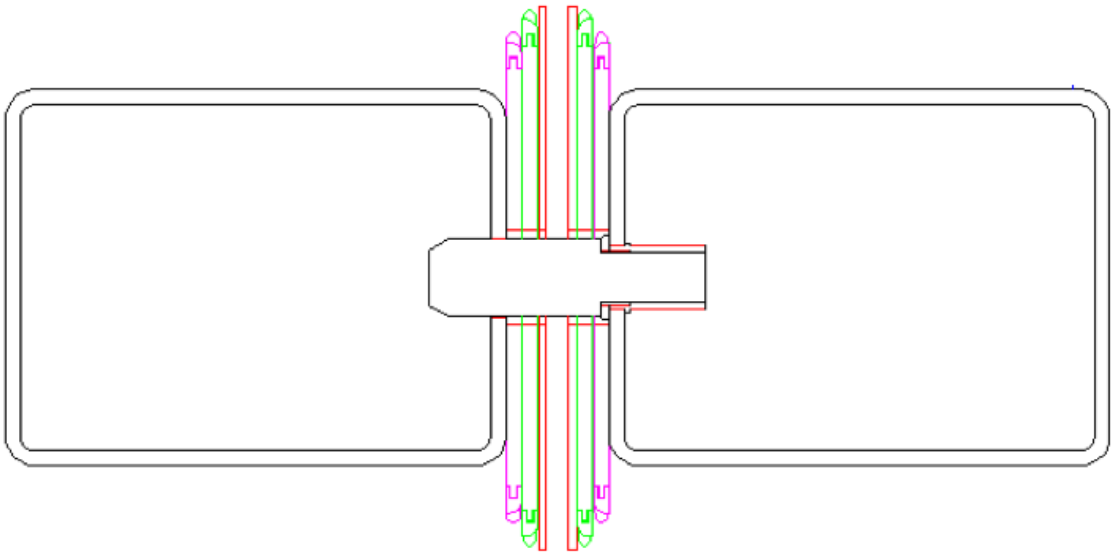

Figure 2.12: The pin/slot constraint. The pin screws into an insert in the outside frame member of one APA and engages a slot in the outside frame member of the adjacent APA.

fig:tpc_

- provide equipotential surfaces at −180kV nominal bias voltage,
- maintain a flatness better than 1 cm when submerged in the liquid argon,
- be constructed of materials with comparable CTEs to that of stainless steel,
- limit the electric field exposed to LAr to under 30 kV/cm
- prevent damage to the TPC, including its readout electronics, in case of a HV discharge anywhere on the cathode,
- provide constant bias voltage and current to all attached field cage (FC) resistor divider chains,
- support the full weight of the four connected top/bottom FC modules plus a person on the bottom FC during installation,
- accommodate cryostat roof movement between warm and LAr-filled states,
- be constructed in a modular form that can be easily installed in the cryostat,
- accommodate Photon Detection System (PDS) calibration features, and
- avoid any trapped volume of LAr.

2.3.2 Design considerations

For the DUNE-SP far detector, the cathode planes are planned to be 12 m tall by nearly 60 m long. When biased to the nominal voltage of −180 kV, each of these cathode planes stores more than 100 J of energy. If this energy were to be released suddenly and completely in a high-voltage discharge event, it could greatly affect the integrity of the detector elements, including the sensitive front-end electronics. Study has shown [2] that a cathode plane made of interconnected metallic electrodes would present significant risk to the front-end ASICs based on the potential charge injection through the capacitive coupling between the cathode and the anode wires originating from such an event.

To address this issue, the entire cathode plane is made out of highly resistive material such that it has a very long discharge time constant. In the event of HV breakdown at a given location on the cathode plane, the sudden change in voltage is restricted to a relatively localized area on the CPA module in question. The rest of the CPA maintains its original bias voltage, and gradually discharges to ground through the large resistivity of the cathode material. This greatly reduces the instantaneous charge injection to the front-end electronics.

2.3.3 CPA design

CPA modules

The cathode plane design chosen for the ProtoDUNE-SP TPC is an array of 18 moderately sized modules constructed from strong 6-cm-thick FR4 (the fire-retardant version of G10) frames. The frames hold 3-mm-thick FR4 panels laminated on both sides with a commercial resistive Kapton film. Each CPA module is 1.16 m wide and 2 m high, and they stack to form six CPA columns of height 6 m. The six-column-wide CPA has the same dimensions as each of the two APA planes, with a width of about 7 m.

The surface of the frame facing the APAs is covered by a set of resistive FR4 strips with a different bias voltage, set such that the frame itself causes no distortion in the drift field beyond the resistive surfaces.

Each CPA column is suspended under the cathode support rail by a single insulating FR4 bar. On the top and bottom edges of a CPA, two hinges support the partial weight of the top and bottom field cage modules. Adjacent CPAs are aligned through pin-and-slot connections to maintain co-planarity while allowing minor relative vertical shift due to cryostat roof movement.

The electrical connectivity of the resistive panels within a CPA column is maintained by several tabs through the edge frames. There is no direct electrical connection across the CPA columns. Instead, the voltage is passed from one column to another through embedded cables in the CPA panels referred to collectively as the HV bus. Redundant connections in the HV bus between CPA columns are used to ensure reliability. The HV bus also provides a low-resistance path for the voltage needed to operate the FC resistive divider chains. The required connections to the FC

modules are made at the edges of the cathode plane. Along the perimeter of the CPA, the HV bus cables are hidden between the field-shaping strip overhang and the main cathode resistive sheet. The cables must be capable of withstanding the full cathode bias voltage to prevent direct arcing to (and as a result, the recharging of) a CPA panel that discharges to ground.

The outer edges of the cathode plane facing the cryostat wall are populated with the same metal profiles, with insulating polyethylene caps, as used in the field cage. This eliminates the need for a special design of the most crucial regions of the cathode plane: the edges of the CPA now look just like a continuation of the FC. Since these profiles are the only objects facing grounded surfaces, they are the most likely candidates to have HV discharges to ground. To limit peak current flow, these edge profiles are resistively connected to the main cathode panels through their laminated resistive surfaces. The resistive surface concept is illustrated in Figure 2.13.

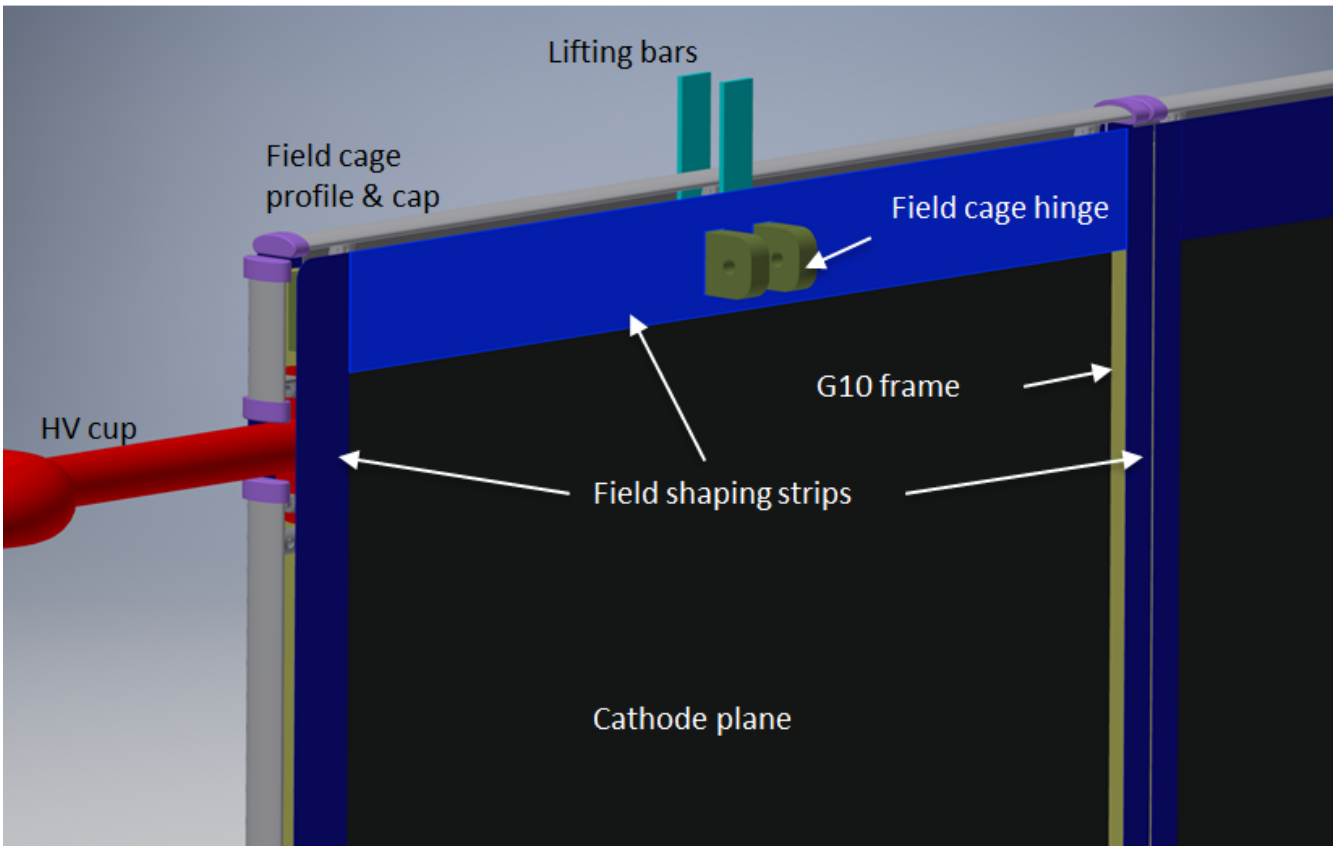

Figure 2.13: The resistive surface CPA concept showing a 3D model of a corner of the cathode with major components.

The CPA is connected to the HV feedthrough through a receptacle, called the *HV cup*, at the back end of the cryostat (with respect to the beam entrance) and biased at −180 kV. It provides this voltage and the required current to all the FC modules (top, bottom and end walls) through electrical interconnects (Section 2.4). The CPA is suspended by insulating bars from the CPA installation rail. It also mechanically supports six pairs of top/bottom FC modules.

The main criteria for the selection of Kapton as the resistive material to be used to coat the CPA module panels are:

- surface resistivity range,
- compatibility with cryogenic temperatures,
- robustness to HV discharges,
- material ageing,
- radio-purity,
- ability to coat a large surface area, and
- flatness, per the cathode flatness requirement.

Figures 2.14 and 2.15 show the basic geometry of the cathode plane. Figure 2.15a shows the block at the top of a CPA that is secured to the top cross bar and extends to the top supporting I-beam. This block must support the weight of four half FCs (4 × 220 lbs) and the weight of the CPA itself (160 lbs) for a total weight of 1,041 lbs. Figure 2.16 shows how the FC is attached to the assembled cathode plane.

Deformation and stress due to pressure from circulating LAr

Calculations indicate that a uniform 2-Pa pressure applied to the resistive panels during cooldown will result in 0.090 inch deflections of the panel at its center. The entire TPC (i.e., the CPA/FC/APA assembly) will displace 8.8 mm laterally as a result of the net force from this pressure.

Thermal considerations

When the CPA modules are cooled, their width will shrink by 0.9 mm. The supporting stainless steel beam will shrink by 1.6 mm over the width of the CPA. If the CPA supports are rigidly attached to the supporting stainless steel beam, then an interference of 0.7 mm (the difference) will occur. To prevent this interference and ensure contact between CPAs after cooldown, an initial gap of 0.7 mm between CPAs is required.

The steel beam between the CPA and APA will shrink by 5.2 mm relative to the field cage length when cooled to LAr temperature. The joint between the FC and the CPA is designed to accommodate this shrinkage.

2.3.4 Mechanical and electrical interconnections between modules

Three modules are stacked vertically to form the 6-m height of a CPA. The frames of these modules are bolted together using tongue-and-groove connections at the ends. The resistive cathode sheets and the field-shaping strips are connected using a few metallic buttons to ensure redundant electrical contact between the CPAs.

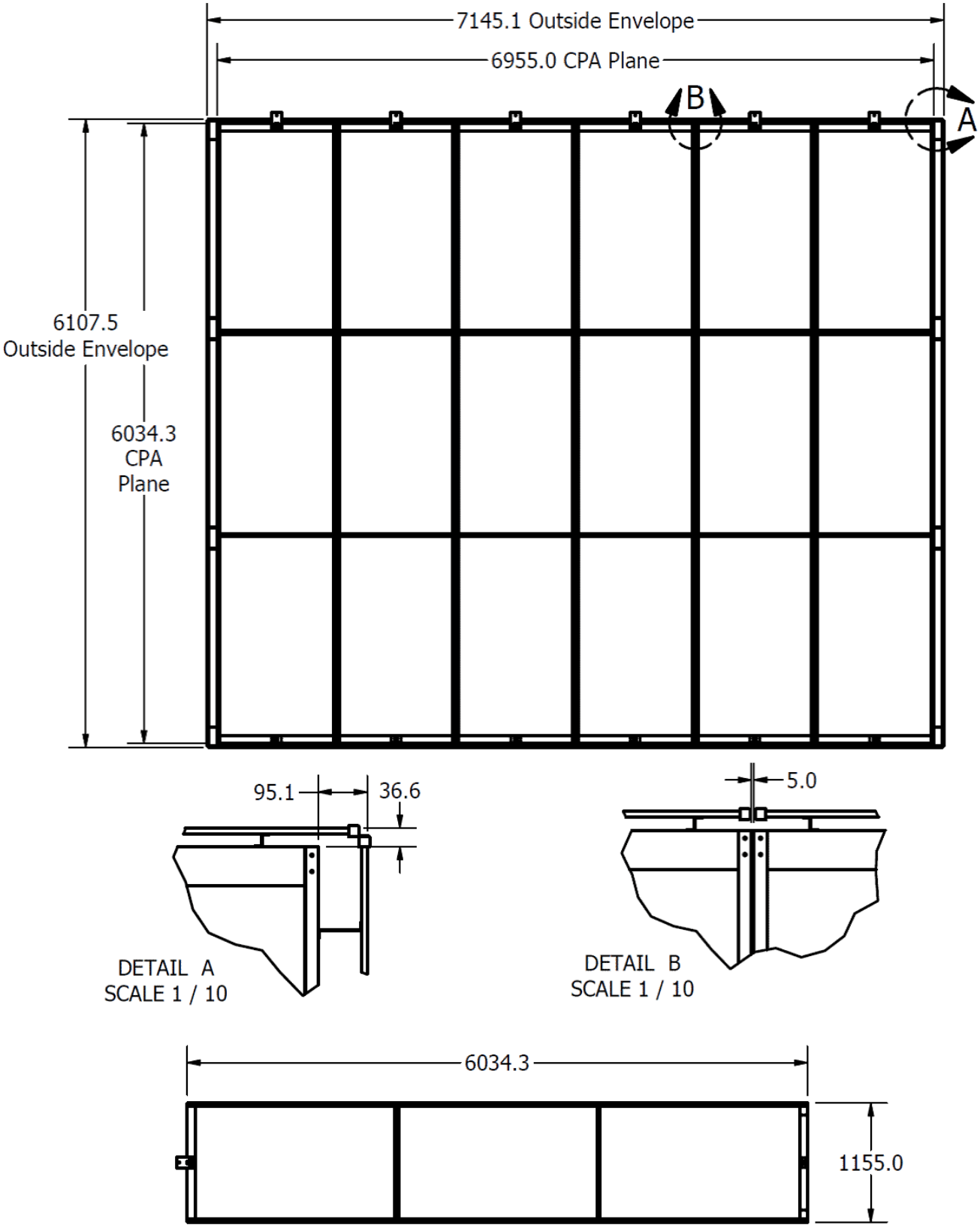

Figure 2.14: Basic geometry of the CPA array, close ups and a CPA column (on its side)

fig:cpa-

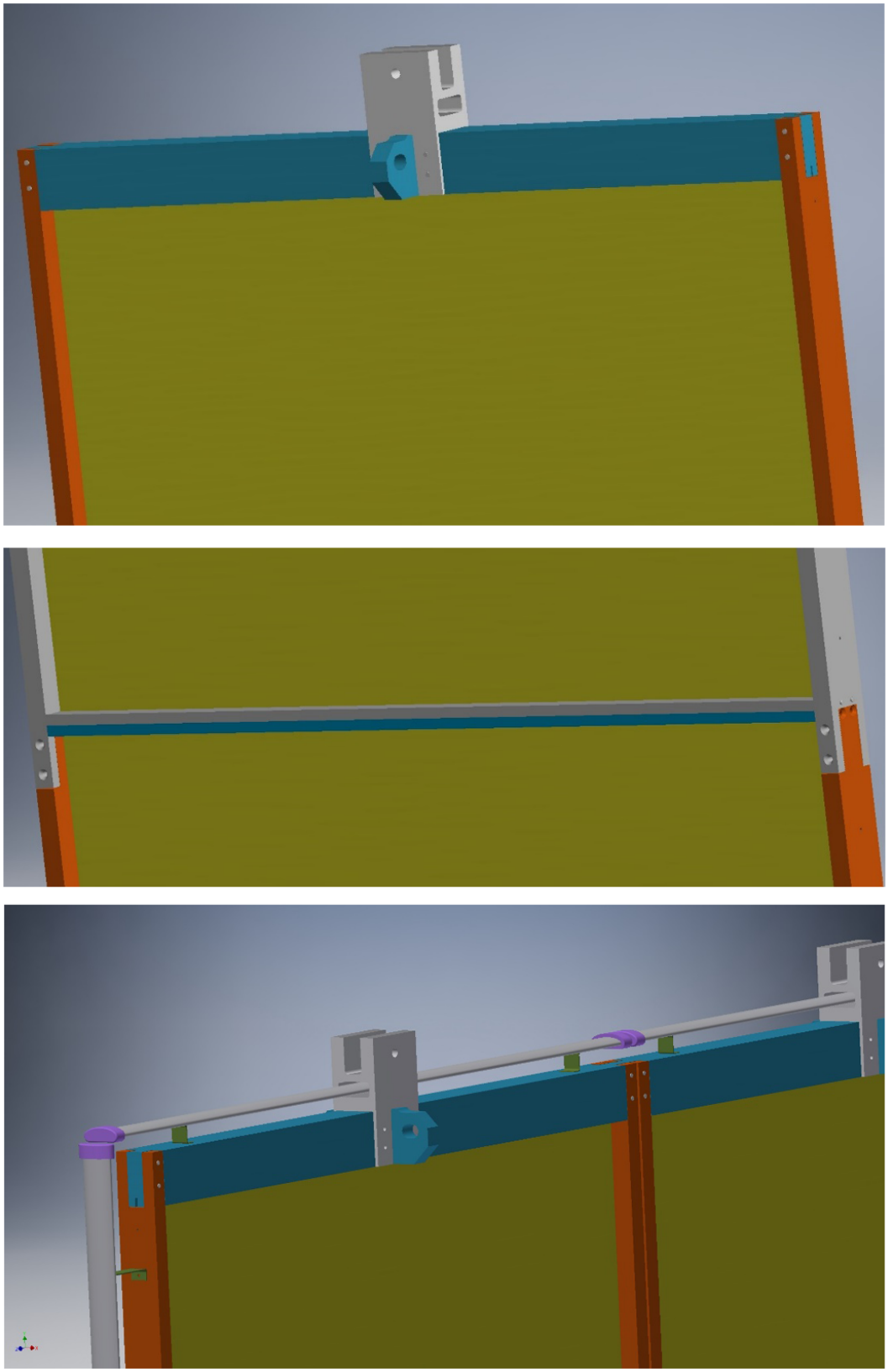

Figure 2.15: Views of various parts of a CPA. Top: the block at the top of a CPA. Middle: hardware connecting two vertically stacked CPA modules. Bottom: connection between two adjacent CPA columns.

fig:cpa-

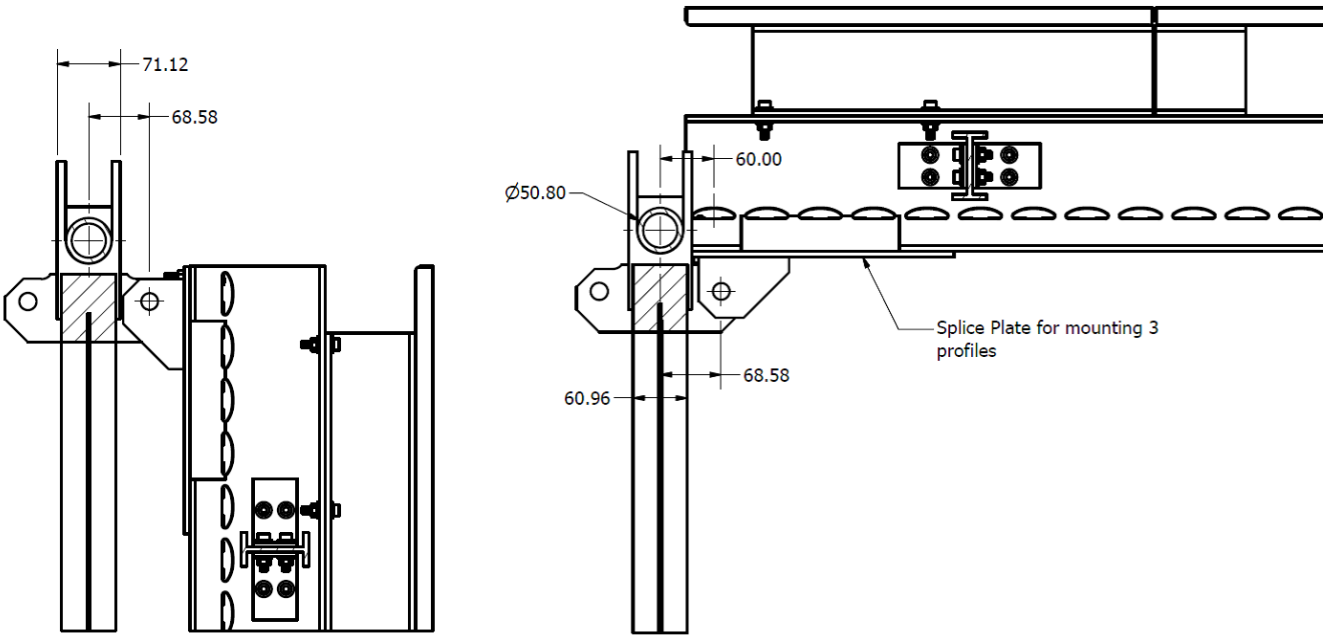

Figure 2.16: The top field cage modules are hung vertically with the CPAs when moved into the cryostat, then rotated to horizontal to attach to the APA.

are the “buttons” called something else in the figures?

Each CPA is suspended from the cathode rail using a central lifting bar. Due to the roof movement between the warm and cold phases of the cryostat as it is cooled, each CPA is expected to move ∼2 mm relative to its neighbors. Several pin-and-slot connections are implemented at the long edges of the CPA columns to ensure the co-planarity of the modules while allowing for a small vertical displacement.

The HV bus provides the high voltage to the FC circuits and CPA modules with a voltage drop much less than 0.1% of the default voltage. The location of the bus with respect to the CPA frame is shown in Figure 2.17. The field-shaping electrodes on the faces of the CPA module frames are part of the FC circuit, described in Section 2.4. FC electrodes on the outer edges of the CPA are held at the cathode potential to provide field uniformity and to protect the HV bus from discharge.

2.4 Field Cage (FC)

2.4.1 Scope and requirements

In the TPC, each pair of facing cathode and anode planes form an electron-drift region. A field cage (FC) must completely surround the four open sides of this region to provide the necessary boundary conditions to ensure a uniform electric field within, unaffected by the presence of the

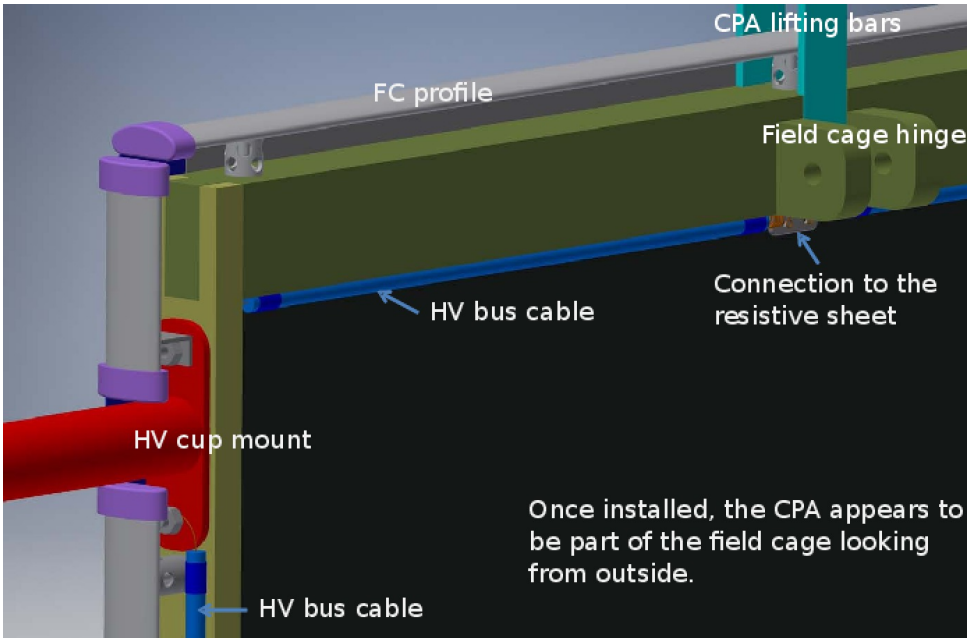

Figure 2.17: A perspective view of CPA frame showing the location of the HV bus cable and attachments to the HV cup and resistive cathode, with CPA frame electrodes omitted to make HV bus visible. fig:HVbu

cryostat walls. The scope of the FC includes:

- six top FC assemblies;
- six bottom FC assemblies; and
- four end-wall panels, each of which consist of four (side) assemblies.

Each assembly is made up of

- parallel metallic profiles;
- a resistive divider chain that interconnects the parallel metal profiles to provide voltage step-down;
- FR4 I-beams that form a support structure for the top and bottom assemblies; and
- ground planes (GP) for the top and bottom assemblies, six GP panels per FC module.

In addition, the FC assemblies include FR4 pieces to make the mechanical connections to the CPA and APAs. One end-wall assembly is specially configured to accommodate the cylindrical beam plug, which displaces the LAr in the region where the beam enters the cryostat.

The FC is required to:

- provide the nominal drift field of 500 V/cm;

- withstand −180 kV near the cathode;
- define the drift distance between the APAs and CPAs to <1 cm;
- limit the electric field in the LAr volume to under 30 kV/cm;
- miminize the peak energy transfer in case of a HV discharge anywhere on the field cage or cathode;
- provide redundancy in the resistor divider chain;
- maintain the divider current much greater than the ionization current in the TPC drift cell, yet less than the power supply current limit when all dividers are connected in parallel;
- be modular in form such that they can be easily installed in the cryostat;
- provide support for the beam plug;
- support a 200-lb. person standing on the support beam of the bottom FC module; and
- prevent any trapped volume of liquid.

2.4.2 Mechanical design

The FC has six top and six bottom FC assemblies, arranged in sets of three along each horizontal boundary of the two drift regions. It has four end-wall panels (each made up of four end-wall assemblies), one covering each vertical boundary of the two drift regions, shown in Figures 2.1 and 2.18. Each endwall panel consists of four assemblies in "landscape" orientation, stacked vertically. FC assemblies are constructed from pultruded G10 I-beams and box beams that support extruded field-shaping aluminum profiles. The support structure for each of the top and bottom FC assemblies consists of two main I-beams that are 3.6 m long, and three cross I-beams that brace the main I-beams for structural stability. The main I-beams have cutouts to hold the field-shaping profiles.

Aside from the profiles themselves, the nuts and bolts holding them, and the ground plane panels, all FC components are made of insulating material. The material selected for these structural components is fiberglass-reinforced plastic (FRP), which prevents binding when the structure is at cryogenic temperatures. The ground plane panels are made of stainless steel.

The inward-facing side of the ground planes are approximately 20 cm away from the top of the field-shaping profiles, mounted at this fixed distance by standoffs. Figure 2.19 shows a set of ground planes situated over the I-beams and cross beams attached to a FC assembly.

The parallel metal profiles in each FC assembly are interconnected by a resistive divider chain, and supported by the FRP beams that span the drift distance. Between adjacent field cage assemblies,

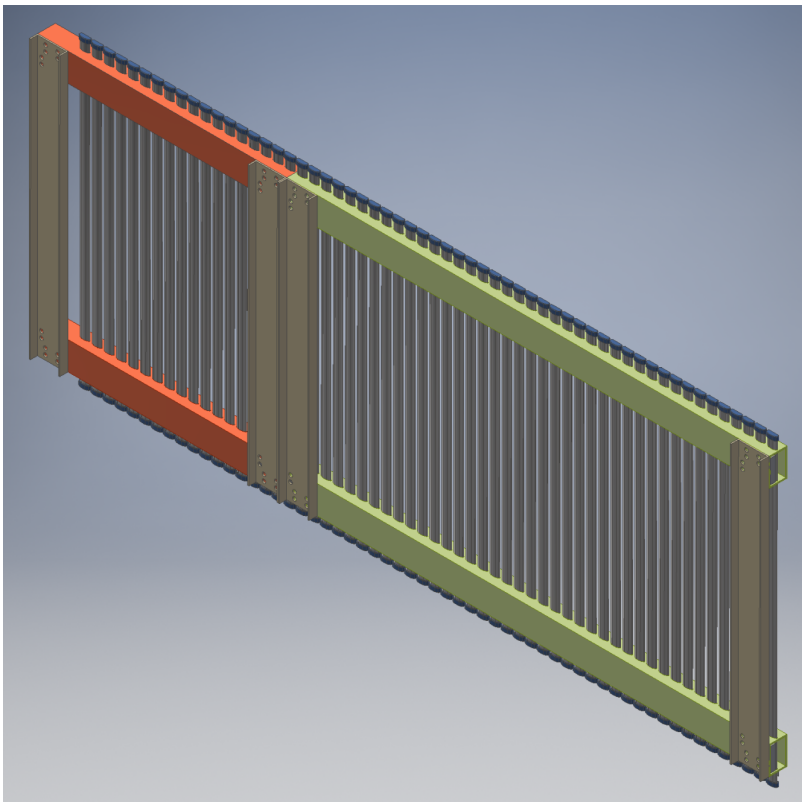

Figure 2.18: A view of an end-wall field cage assembly. An end-wall panel consists of a stack of four of these assemblies (each in landscape orientation). fig:fc-e

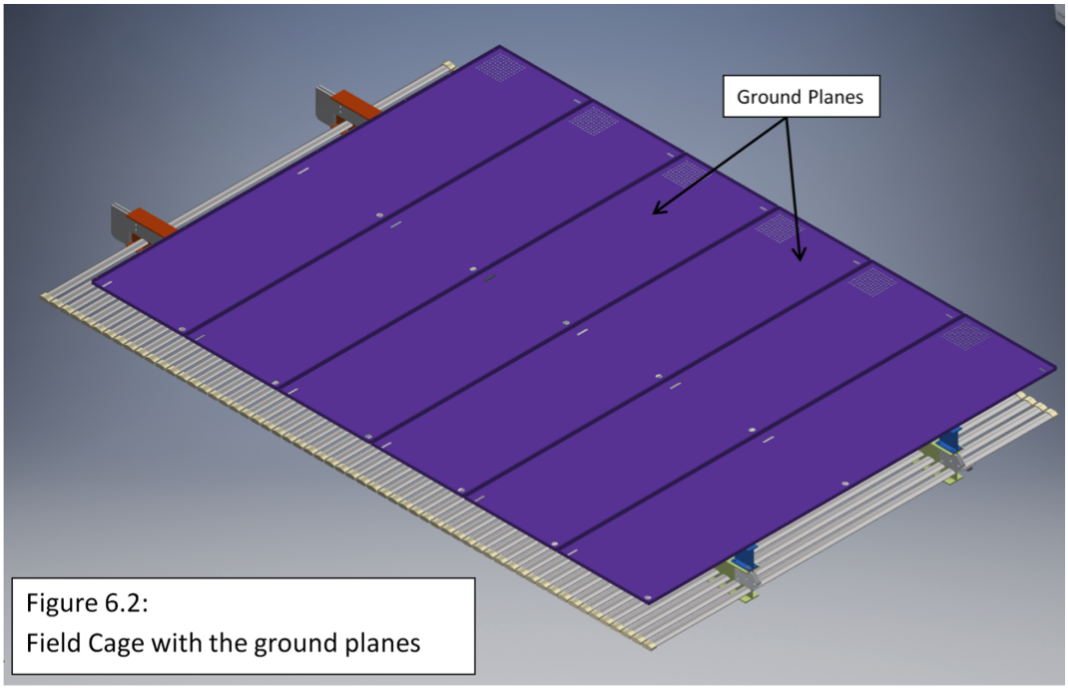

Figure 2.19: The field cage with ground planes fig:fc-w

however, the metal profiles are neither mechanically nor electrically connected. Gaps between assemblies that range from a few millimeters to a few centimeters are designed into the TPC assembly to ensure sufficient clearance for the installation. The electrical isolation between the field cage modules minimizes the peak energy dump in case of a HV discharge.

2.4.3 Electrical design

Given a large standoff distance between the FC and the grounded cryostat wall, it is relatively easy to design a FC that meets the 30-kV/cm electric field limit with 180-kV bias. However, as this distance is reduced to increase the active detector volume, the design becomes more challenging. Optimizing the active detector volume requires the use of electrodes with low profiles, rounded edges, no trapped volumes, and low cost. Fortunately, several commercially available roll-formed metal profiles were studied and appear to meet these requirements.

fig:fc-schematic

Figure 2.20 is a schematic of the electrical design of the CPA and a top/bottom field cage module pair.

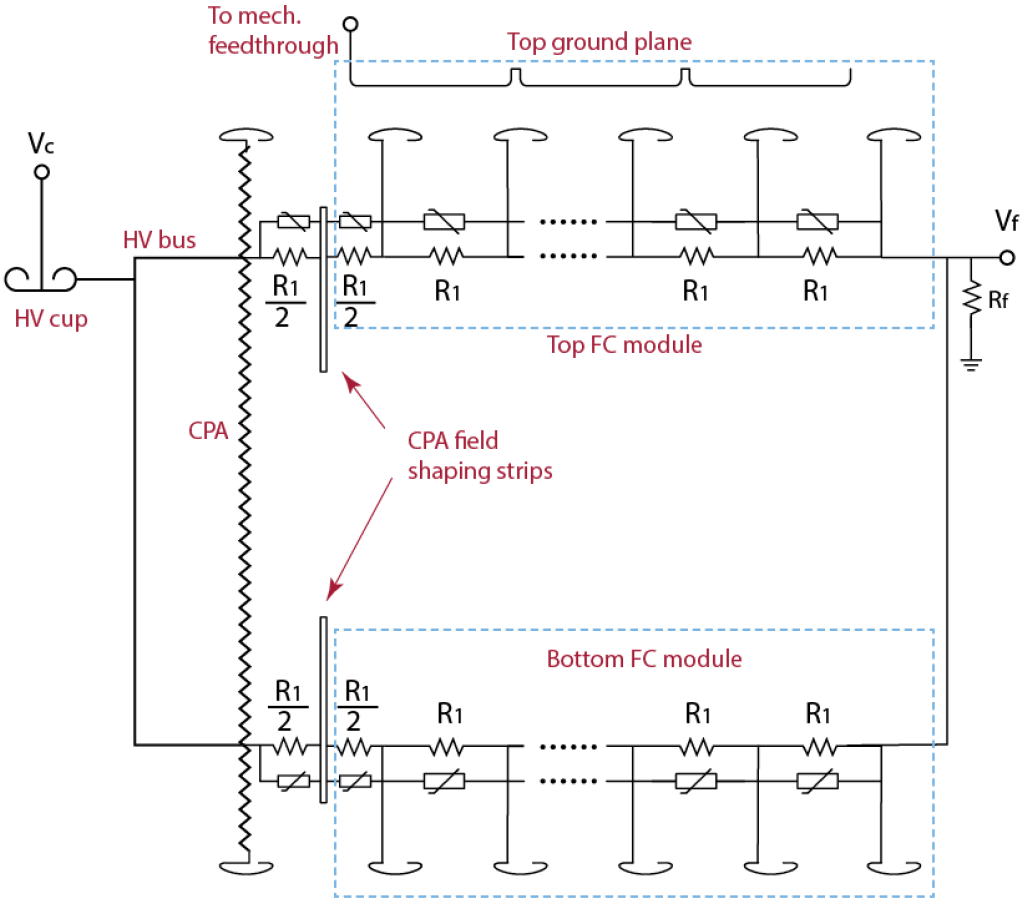

Figure 2.20: A schematic diagram of the CPA and a top/bottom field cage module pair

fig:fc-s

2.4.4 Top/bottom FC assemblies and GP modules

In order to confine the electric field in the active LAr region, a grounded metallic plane is installed between the upper FC assemblies and the liquid-gas interface, and also between the lower FC assemblies and the bottom of the cryostat. Each of the six top FC assemblies has six ground plane (GP) panels attached to it, aligned along their long (2.3-m) dimension. The GPs are connected to the FC I-beam with additional G10 support pieces that are also used to connect adjoining GP panels. Figure 2.21 shows the frame of a top/bottom FC assembly and Figure 2.22 shows a 3D model of a fully assembled FC module with attached GP panels.

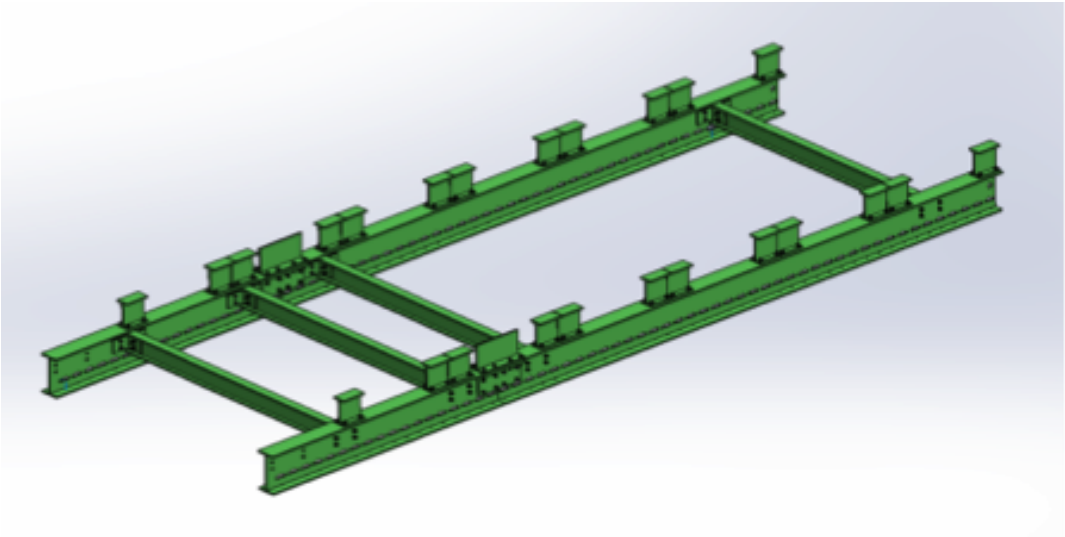

Figure 2.21: A top/bottom FC assembly with the frame

The electrical connections between consecutive panels are to be made with either metallic screws (using holes on the planes edges) or looser connections, e.g., copper strips, that better adapt to the shrinking of the structure during cooldown. The GP panels are connected directly to the detector ground, referenced from the top of the cryostat.

In addition to the six primary GP panels attached to the the top FC modules,

- Smaller panels are to be connected to the modules on one side of the CPA so that, once in position, they cover the CPA frame. Their dimensions are still to be defined, depending on the final design of the CPA hanging scheme. These pieces will also connect to the top FC modules covering the opposite drift region, once in their final position.

- An additional set of small panels is installed on the outer top FC modules of the FC to extend the GP coverage over the end-wall FC assemblies to further constrain the electric field in these regions. A FEA shows that the optimized overhang distance is 20 cm, provided that the surface of the LAr is 40 mm above the GP. In this configuration, the maximal residual field is of the order of 13 kV/cm, with no greater than 1 kV/cm fields in the gass ullage at the top of the cryostat.

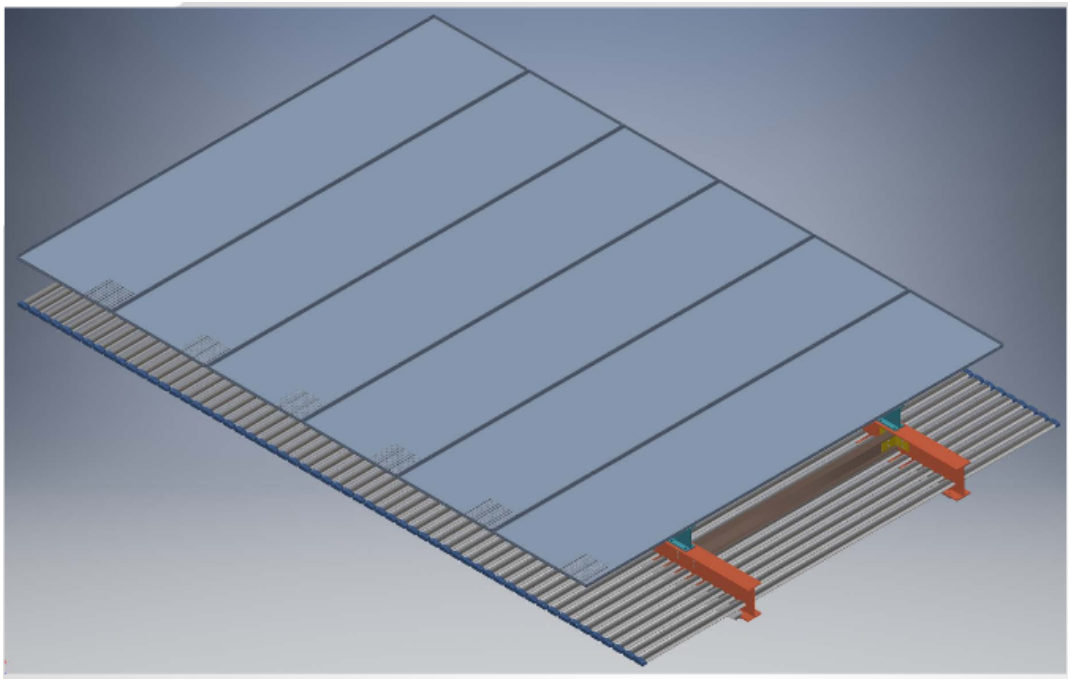

Figure 2.22: 3D model of one fully assembled FC+GP module

fig:fc_f

2.4.5 Interfaces to other TPC components

FC to CPA

On the top and bottom of the TPC, hinges connect each FC module to two CPA columns. These hinges allow the FC modules to be pre-attached to the CPAs during installation, preventing accidental damage to the APA wire planes when FC modules are raised and connected to the APAs.

The end-wall FC assemblies are hung from the CPA and APA support rails. There is no strong mechanical coupling between the end-wall FC assemblies and the CPAs or APAs. However, the end-wall FC module resistive divider chains do have an electrical connection to the HV bus on the CPA plane.

FC to APA

The I-beams of the top/bottom FC modules are designed to be latched onto mating brackets on the APAs. In addition to the mechanical connection, the ground side of the divider chain must be connected to the APA's frame ground. There is also an electrical connection between the FC module resistor divider chains, and ground is referenced from the APA frame.

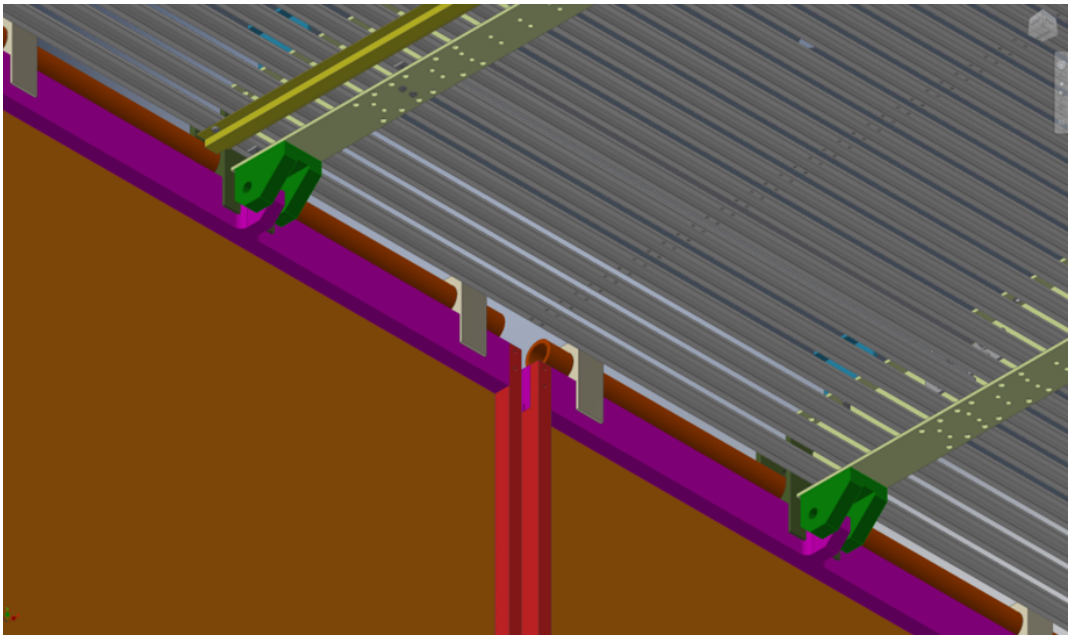

Figure 2.23: A top field cage module (grey) connected to two CPA modules (brown) fig:cpa-

FC to beam plug

The LAr-displacement beam plug, a cylindrical glass-fiber composite pressure vessel, about 50 cm in length and 22 cm in diameter, is filled with nitrogen gas via a stainless steel line that extends to the top of the cryostat. It is illustrated in Figure 2.24. A pressure relief valve (or burst disk) is installed on the nitrogen fill line on the top of the cryostat (externally) to ensure the pressure inside the beam plug does not exceed the safety level of 25 psi. A component-level view of the beam plug is shown in Figure 2.25. The beam plug is secured to the FC support structure as described in Section 2.4.5. The front portion of the beam plug extends 5 cm into the active region of the TPC through an opening in the FC. The FC support is designed with sufficient strength and stiffness to support the weight of the beam plug before filling, while it is suspended in air. When the cryostat is filled with LAr, the beam plug is roughly neutrally buoyant. The total internal volume of the beam plug is about 16 liters.

The requirements on the acceptable leak rate is between 7.8×10^{-5} scc/s and 15.6×10^{-5} scc/s. This is very conservative and is roughly equivalent to leaking 15% of the nitrogen in the beam plug over the course of a year. In the worst-case scenario in which all the nitrogen in the beam plug leaks into the LAr cryostat, the increase in concentration is about 0.1 ppm, which is still a factor of 10 below the maximum acceptable level, as specified by light detection requirements.

need some reference with details for this requirement

At nominal operation, the voltage difference across the beam plug (between the first and the last grading ring) is 165 kV.

To minimize risk of electrical discharges, the beam plug is divided into sections, each of which is

bonded to stainless steel conductive grading rings. The seven grading rings are connected in series with two parallel paths of resistor chains. The ring closest to the FC is electrically connected to one of the FC profiles. The ring nearest the cryostat wall is grounded to the cryostat inner membrane via a short grounding cable. The maximum total power dissipated by the resistor chain is about 0.6 W.

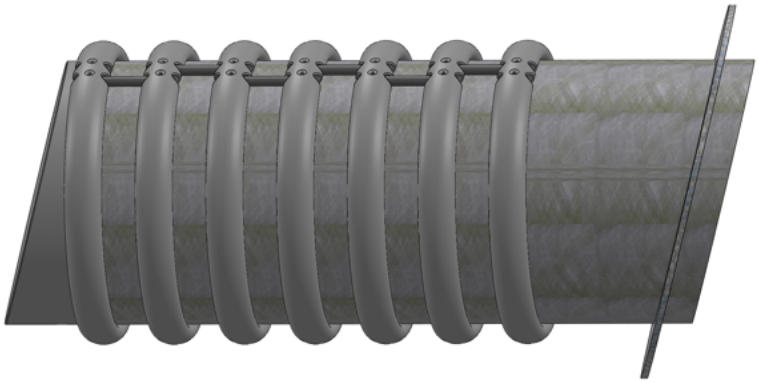

Figure 2.24: The beam plug is a composite pressure vessel filled with dry nitrogen gas. The vessel is about 50 cm in length and about 22 cm in diameter. The pressure vessel is divided into sections with each section bonded to a stainless steel grading ring. The grading rings are connected by two parallel paths of resistor chain.

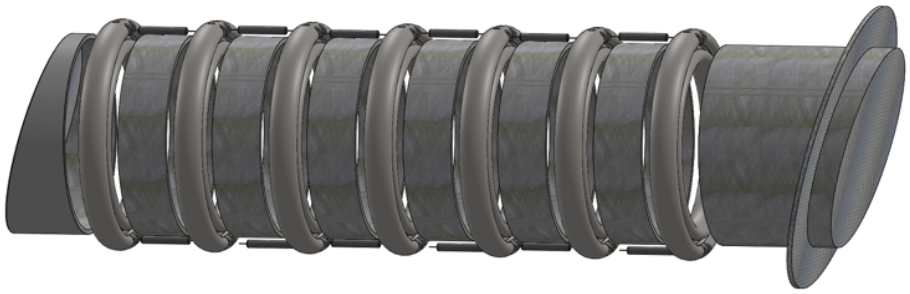

Figure 2.25: Component-level view of the beam plug showing alternating electrode and composite ring structure.

The metal electrode rings are spaced at regular intervals and interspersed with composite tube sections. The shape of the rings has been designed to minimize high electric field corners. The results of the field calculations are shown in Figures 2.26 and 2.27. The average field in the vicinity of the beam plug is about 4.4 kV/cm. The maximum field of 15.7 kV/cm is on the electrode ring surface. In all regions the field is well below the 30-kV/cm limit.

citation to doc describing limit would be good

The beam plug is mounted onto one of the field cage support structures as shown in Figures 2.28 and 2.29.

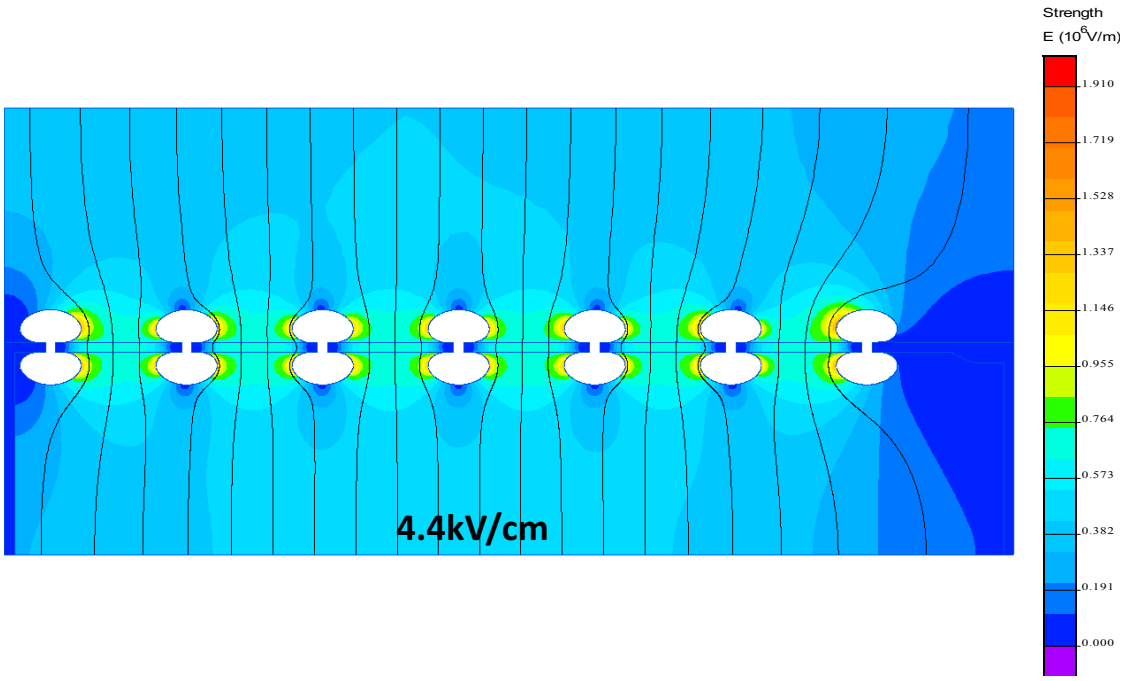

Figure 2.26: Electric field calculation of the electrode ring design. The average field in the beam plug region is about 4.4 kV/cm. The maximum field of 15.7 kV/cm is on the electrode ring surface. fig:beam

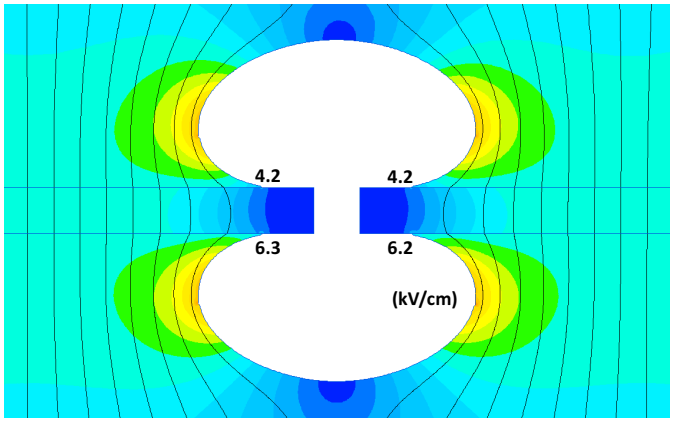

Figure 2.27: Electric field calculation near the vicinity of the electrode. The shape of the ring minimizes the high field region near the joints between the electrode, LAr, and composite shell. The field is well below the 30-kV/cm limit in all regions. fig:beam

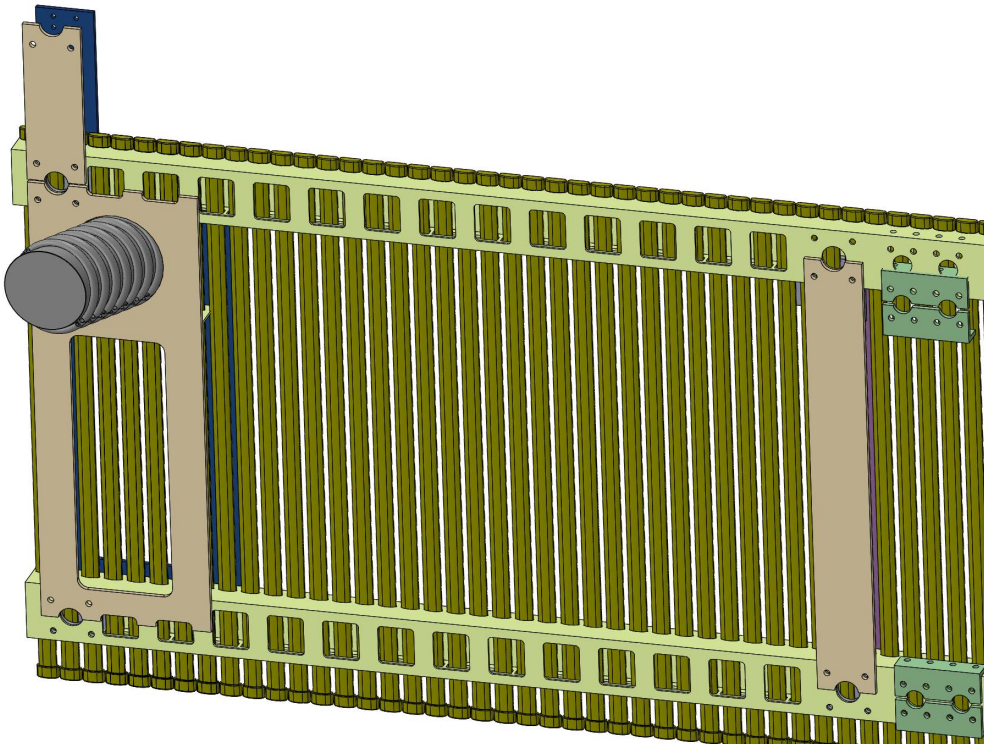

Figure 2.28: Beam plug to field cage interface. fig:beam

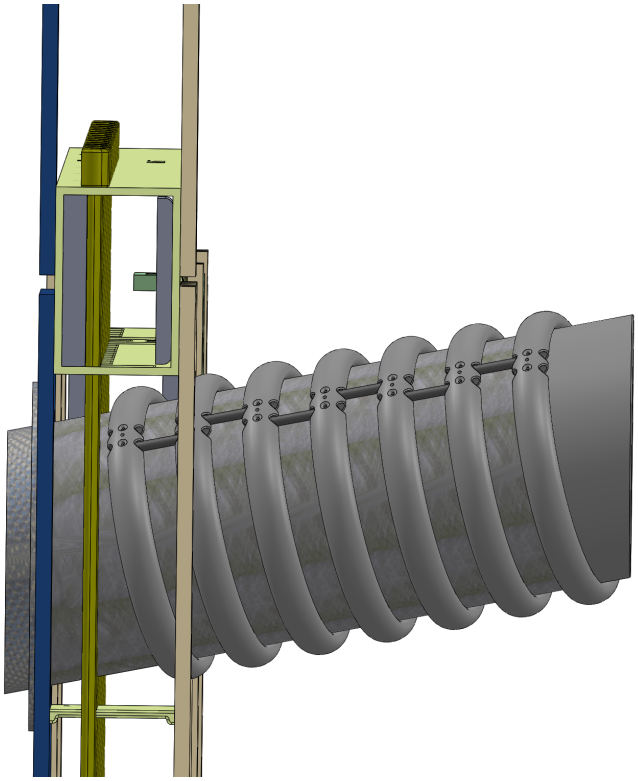

Figure 2.29: Cutaway sideview of the beam plug to field cage interface. fig:beam

2.5 TPC high-voltage (HV) components

2.5.1 Scope and requirements

The TPC high voltage (HV) components include the HV power supply, cables, filter circuit, HV feedthrough, and monitoring for currents and voltages (both steady state and transient).

A schematic of the complete TPC HV circuit is shown in Figure 2.30. fig:TPCHVcircuit

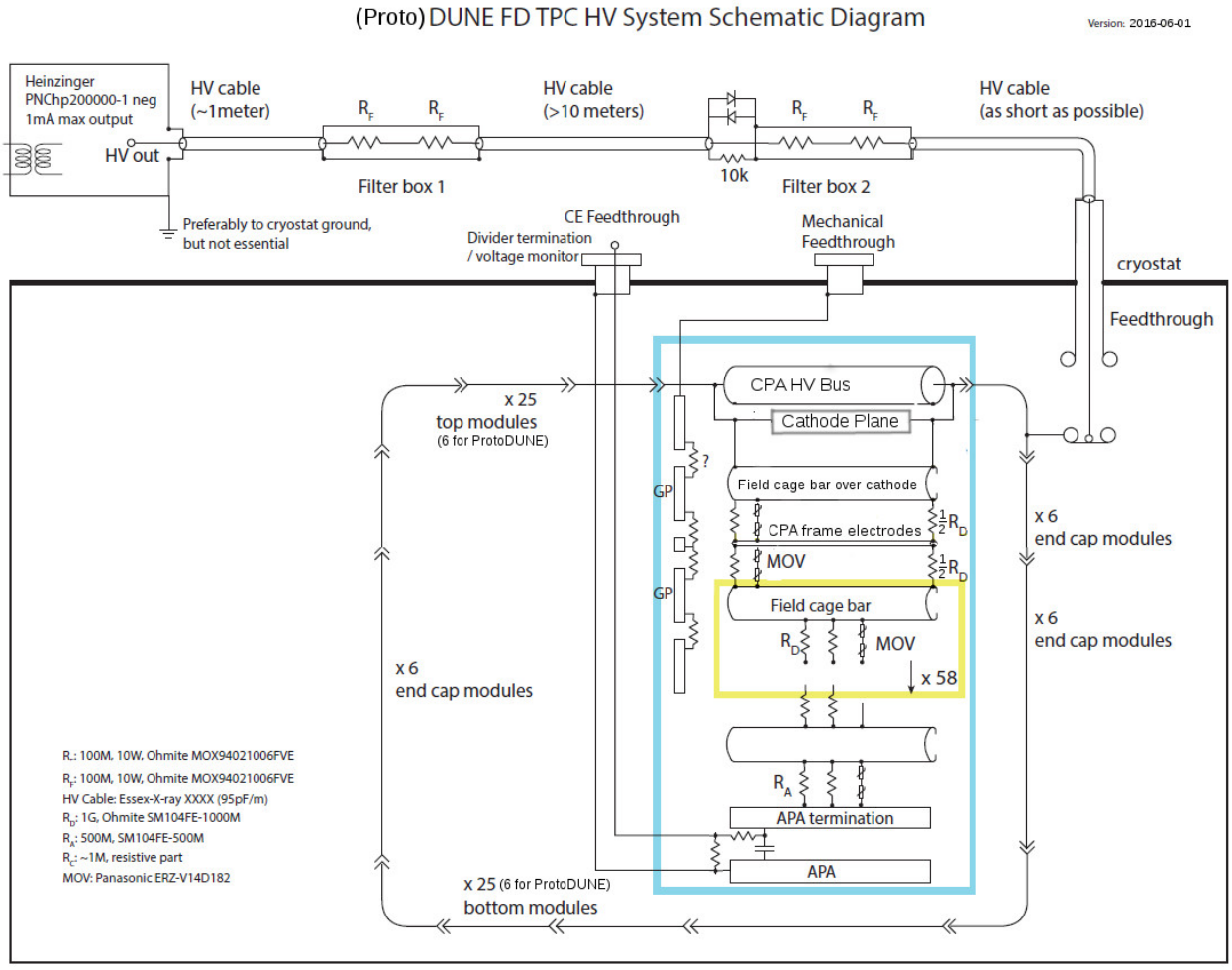

Figure 2.30: A schematic of the TPC high voltage circuit. fig:TPCH

The cathode plane is biased at −180 kV to provide the required 500 V/cm drift field. It is powered by a dedicated HV power supply through an RC filter and HV feedthrough. The power supply for the cathode plane must be able to provide −200 kV. The output voltage ripple must not introduce more than 10% of the equivalent thermal noise from the front-end electronics. The power supply must be programmable to shut down its output at a certain current limit. During power cycling, both controlled and uncontrolled, the voltage ramp rate at the feedthrough must be limited to prevent damage to the in-vessel electronics from excess charge injection. The HV feedthrough

must be able to withstand −250 kV in its center conductors in a 1 atm argon gas environment when terminated in liquid argon.

2.5.2 HV feedthrough design, power supply and cabling

The design of the HV feedthrough as well as the procurement of the HV power supply, cables, and possibly filter circuits, are activities being jointly pursued by the ProtoDUNE-SP and ProtoDUNE-DP efforts. In particular:

- The Heinzinger 300-kV power supply (residual ripple less than 10^{-5}) and cable specified for ProtoDUNE-DP are well suited for ProtoDUNE-SP, which operates at a lower HV setting.
- The present ProtoDUNE-DP HV feedthrough design is adaptable to ProtoDUNE-SP without any major modification in its dimensions or mechanical features.
- The filtering scheme and the monitoring system required for ProtoDUNE-SP is more demanding than that for ProtoDUNE-DP, due to its more sensitive front-end electronics, and can be used for both detectors.
- Common spare components are also being utilized.

The design of the 300-kV feedthrough is based on the very successful construction technique adopted for the ICARUS HV feedthrough, which was operated at 75 kV without interruption for more than three years without any failure. The feedthrough was also successfully operated for several days as a test after the run at 150 kV. The design is based on a coaxial geometry, with an inner conductor (HV) and an outer conductor (ground) insulated by ultra-high-molecular-weight polyethylene (UHMW PE) as shown in Figure 2.31.

The outer conductor, made of a stainless-steel tube, surrounds the insulator, extending down through the cryostat into the LAr. In this geometry, the electric field is confined within regions occupied by high-dielectric-strength media (UHMW PE and LAr). The inner conductor is made of a thin-walled stainless steel tube to minimize the heat input and to avoid the creation of argon gas bubbles around the lower end of the feedthrough. A contact, welded at the upper end for the connection to the HV cable, and a round-shaped elastic contact for the connection to the cathode, screwed at the lower end, completes the inner electrode. Special care has been taken in the assembly to ensure complete filling of the space between the inner and outer conductors with the PE dielectric, and to guarantee leak-tightness at ultra-high vacuum levels.

2.5.3 HV monitoring

HV-circuit monitoring devices include a toroid transformer to detect spikes and noise in the current draw, and a monitoring point at the end of the field cage resistor chain, which also provides a means to control field-shaping around the edge of the APA.

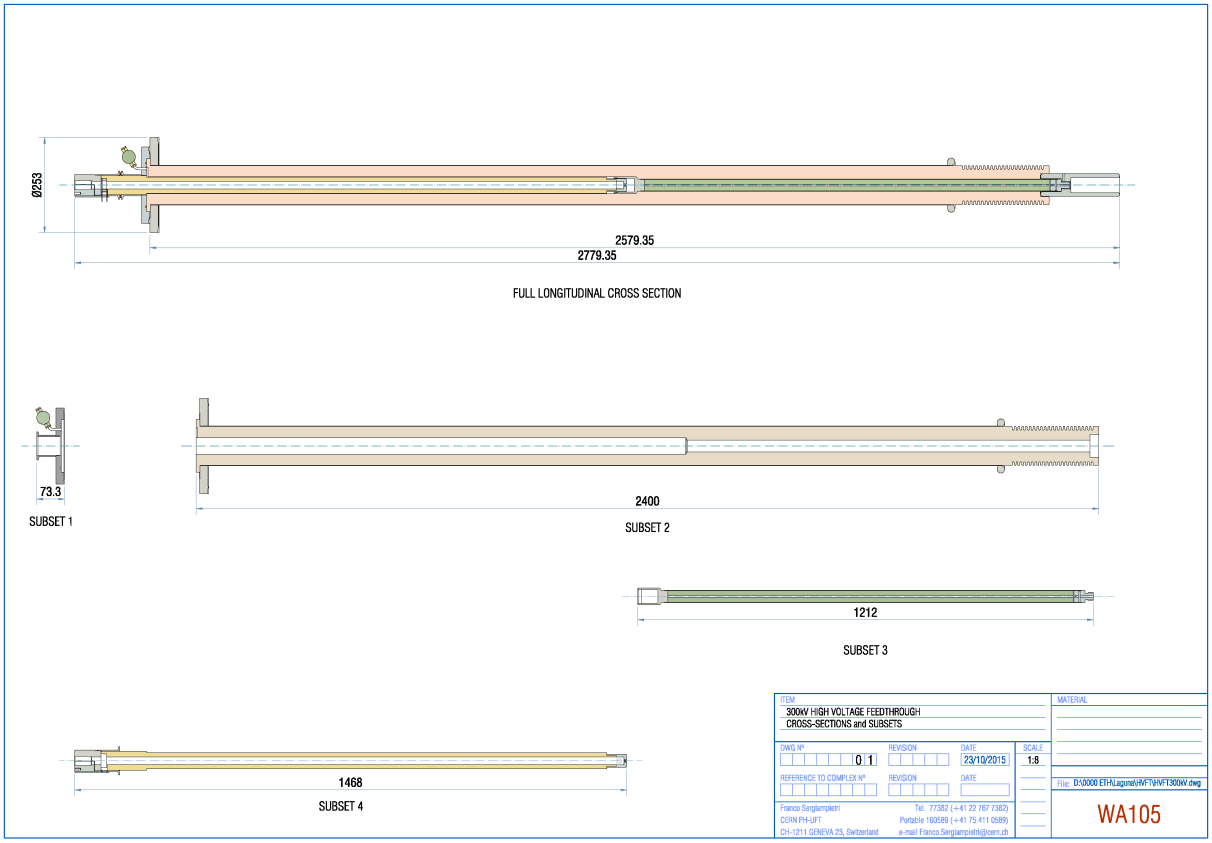

Figure 2.31: Preliminary design of the HV feedthrough.

fig:hv-f

2.6 TPC Front-end Electronics

ch:ce

2.6.1 Scope and requirements

ce_intro

The DUNE single-phase TPC read-out electronics are referred to as the "Cold Electronics" (CE) because they reside in LAr, mounted directly on the APA, as shown in Figure 2.32, thus reducing channel capacitance and noise by minimizing the length of the connection between an anode wire and its corresponding electronics input.

fig:tpcce_FEMBonAPA

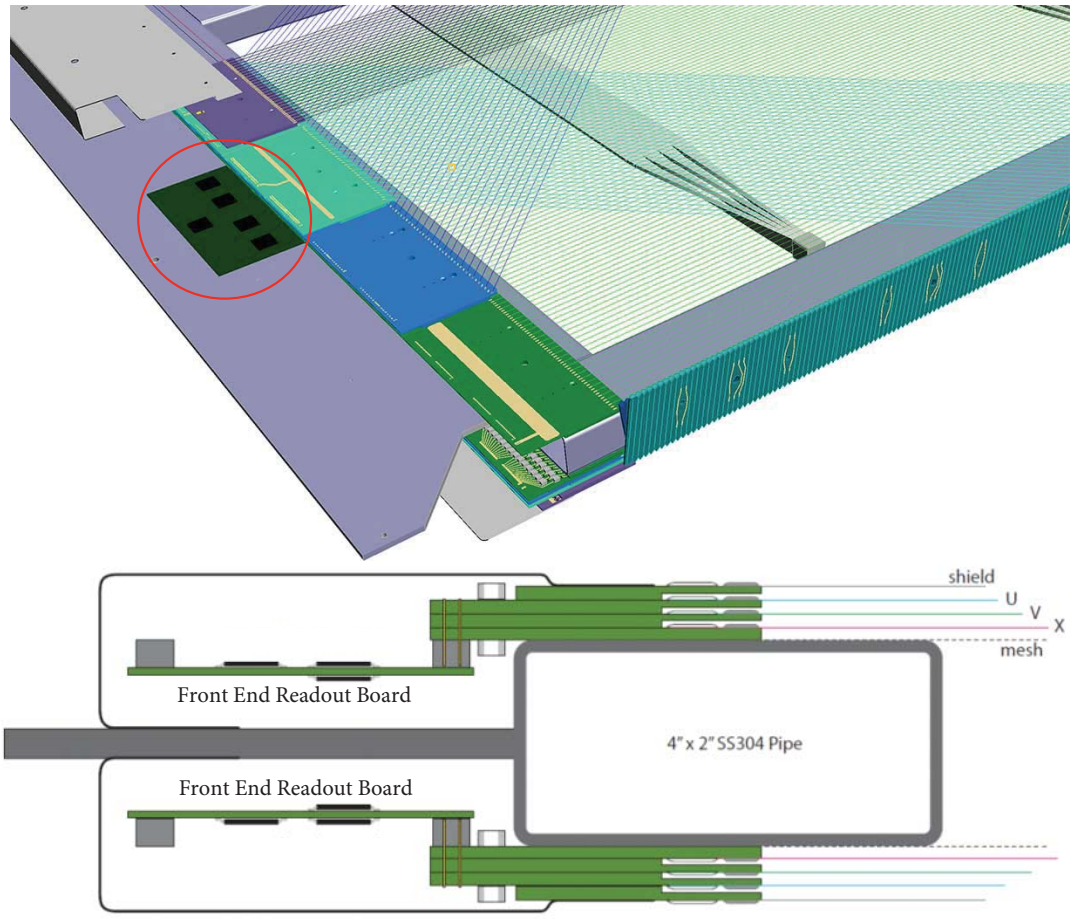

Figure 2.32: The front-end electronics as mounted on an APA. Top: The front-end electronics is shown in the red circle. Bottom: Cross section view showing the layered wire boards. Mounting hardware between the front-end electronics and the APA is not shown.

fig:tpcc

The CE signal processing is implemented in ASIC chips using CMOS technology, which has been demonstrated to perform well at cryogenic temperatures, and includes amplification, shaping, digitization, buffering, and multiplexing (MUX) of the signals. The CE is continuously read out, resulting in a digitized ADC sample from each APA channel (wire) up to every 500 ns (2-MHz maximum sampling rate).

The 2,560 channels from each APA are read out by 20 Front-End Motherboards (FEMBs), each providing digitized wire read-out from 128 channels. One cable bundle connects each FEMB to

the outside of the cryostat via a feedthrough (a *CE feedthrough*) in the signal cable flange at the top of the cryostat, where a single flange services each APA, as shown in Figure 2.33. Each cable bundle contains wires for low-voltage (LV) power, high-speed data readout, and clock/digital-control signal distribution. Eight separate cables carry the TPC wire-bias voltages from the signal flange to the APA wire-bias boards, as shown schematically in Figure 2.34.

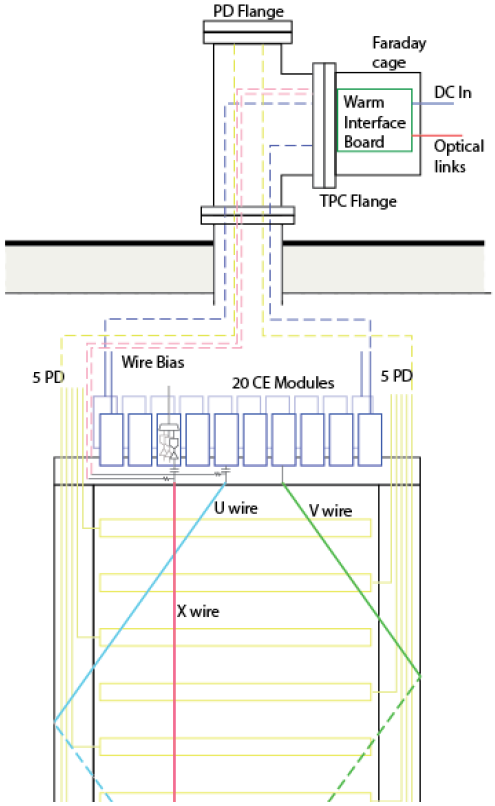

Figure 2.33: Connections between the signal flange and APA.

The components of the CE system are the

- Front-end mother boards (FEMBs), which house the cold ASICs and are installed on the APAs;
- Cables for the data, clock/control signals, LV power, and wire-bias voltages between the APA and the signal flanges (cold cables);
- Signal flanges with a CE feedthrough to pass the data, clock/control signals, LV power, and APA wire-bias voltages between the inside and outside of the cryostat;
- Warm electronics crates (WECs) that are mounted on the signal flanges and contain the warm interface boards (WIBs) and Power and timing cards (PTCs) for further processing and distribution of the signals entering/exiting the cryostat;
- Fiber cables for transmitting data and clock/control signals between the WECs and the data acquisition (DAQ) and slow control systems;

- Cables for LV power and wire-bias voltages between the signal flange and external power supplies (warm cables); and

- LV power supplies for the CE and bias-voltage power supplies for the APAs.

The electrical cables for each APA enter the cryostat through a single signal flange, creating an integrated unit that provides local diagnostics for noise and validation testing, and follows the grounding guidelines in Section 2.6.2. The components, the quantity of each required for ProtoDUNE-SP, and the number of channels that each component has, are listed in Table 2.6.

Table 2.6: Electronics components and quantities

Element	Quantity	Channels per element
TPC	1	15,360
APA	6	2,560
Front-End Mother Board (FEMB)	120, 20 per APA	128
FE ASIC chip	120 × 8, 8 per FEMB	16
ADC ASIC chip	120 × 8, 8 per FEMB	16
FEMB FPGA	120, 1 per FEMB	128
Cold cable bundles	120, 1 per FEMB	128
Signal flange	6, 1 per APA	128 × 20 (i.e., 2,560)
CE feedthrough	6, 1 per APA	128 × 20
Warm interface boards (WIB)	30, 5 per APA	(128 × 20) /5 (i.e., 512)
Warm electronics crates (WEC)	6, 1 per APA	128 × 20
Power and timing cards (PTC)	6, 1 per APA	128 × 20
Passive backplane (PTB)	6, 1 per APA	128 × 20
MPOD LV power supplies	6, 1 per APA	128 × 20
MPOD wire-bias power supplies	6, 1 per APA	128 × 20
MPOD power supply chassis	2, 1 per 3 APAs	15,360 /2

check Table 2.6 ; there are some missing numbers

The most significant requirements for the CE are listed here. The CE shall:

- Provide the means to read out the TPC wires and transmit their data in a useful format to the DAQ.

- Operate for the life of the facility without significant loss of function.

- Record the channel waveforms continuously without dead time.

- Be constructed only from materials that are compatible with high-purity LAr.

- Provide sufficient precision and range in the digitization to:

  - Discriminate electrons from photon conversions;
  - Optimize the reconstruction of high- and low-energy tracks from accelerator-neutrino interactions;
  - Distinguish a Minimum Ionizing Particle (MIP) from noise with a signal-to-noise ratio $> 9{:}1$;
  - Measure ionization up to 15 times that of a MIP particle, so that stopping kaons from proton decay can be identified.
- Ensure that all power supplies have:
  - Local monitoring and control;
  - Remote monitoring and control through DAQ; and
  - Over-current and over-voltage protection circuits.
- Ensure that the CE feedthroughs are able to withstand twice their nominal operating voltages with a maximum specified leakage current in 1-atm argon gas.

2.6.2 Grounding and shielding

To avoid structural ground loops, the APA frames described in Section 2.2.4 are insulated from each other. Each frame is electrically connected to the cryostat at a single point on the CE feedthrough board in the signal flange where the cables exit the cryostat. Mechanical suspension of the APAs is accomplished using insulated supports.

The analog portion of the FEMB contains eight front-end (FE) ASICs configured as 16-channel digitizing charge amplifiers. Input amplifiers on the ASICs have their ground terminals connected to the APA frame. All power-return leads and cable shields are connected to both the ground plane of the FEMB and to the signal flange.

Filtering circuits for the APA wire-bias voltages are locally referenced to the ground plane of the FEMBs through low-impedance electrical connections. This approach ensures a ground-return path in close proximity to the bias-voltage and signal paths. The close proximity of the current paths minimizes the size of potential loops to further suppress noise pickup.

Photon detector signals, described in Section 2.7, are carried directly on shielded, twisted-pair cables to the signal flange. The cable shields are connected to the cryostat at a second feedthrough, the PDS feedthrough, and to the PCB shield layer on the photon detectors. There is no electrical connection between the cable shields and the APA frame except at the signal flange.

2.6.3 Distribution of APA wire-bias voltages

Each side of an APA includes four wire layers as described in Section 2.2.2. The innermost X-plane layer of wires is nominally biased at +820 Volts, with each wire AC coupled to one of the 128 charge amplifier circuits on the FEMB. The V-plane wire layer is effectively biased at zero volts, with each wire directly connected to one of the charge amplifier circuits. The U-plane wire layer is nominally biased at −370 Volts with each wire AC-coupled to one of the 128 charge amplifier circuits. The outermost G-plane wire layer, which has no connection to the charge amplifier circuits, is biased at −665 Volts.

Electrons passing through the wire grid must drift unimpeded until they reach the X-plane collection layer. The nominal bias voltages are predicted to result in this electrically transparent configuration.

As described in Section 2.2.5 the filtering of wire-bias voltages and AC coupling of wire signals passing onto the charge amplifier circuits is done on Capacitance-Resistance (CR) boards that plug inbetween the APA wire-board stacks and FEMBs. Each CR board includes single R-C filters for the X- and U-plane wire-bias voltages. In addition, each board has 48 pairs of bias resistors and AC coupling capacitors for X-plane wires, and 40 pairs for the U-plane wires. The coupling capacitors block DC while passing AC signals to the CE motherboards.

Separate CR boards include a single R-C filter for the G-plane wires and 12 pairs of bias resistors and coupling capacitors. Groups of four wires are tied together to share single bias resistors and filter capacitors. These CR boards do not connect to the charge amplifier circuits on the FEMB.

The amplifier circuits have input impedance of 50 Ω using 22-nF coupling capacitors. Clamping diodes limit the input voltage received at the amplifier circuits to between zero and +1.8 Volts.

Coupling capacitors for the X-plane and U-plane wires are required to block DC bias voltages. However they also impact the efficiency of the detector circuits. The sense wires are expected to have 200 pF of capacitance to the APA frame. Induced or collected charges are effectively divided between the wire capacitance and the coupling capacitor. To achieve a charge-calibration accuracy of 0.5 percent or better, the coupling capacitors must be 4.7 nF at ten percent tolerance, or 2.2 nF at five percent tolerance. Voltage ratings should be at least 1.5 times the expected operating voltages.

Bias resistance values should be at least 20 MΩ to maintain negligible noise contributions. A target value of 50 MΩ is desired. The higher value helps to achieve a longer time constant for the high-pass coupling networks. Time constants should be at least 25 times the electron drift time so that the undershoot in the digitized waveform is small and easily correctable. However, leakage currents can develop on PC boards that are exposed to high voltages over extended periods. If the bias resistors are much greater than 50 MΩ, leakage currents may affect the bias voltages applied to the wires.

The bias-voltage filters are R-C low-pass networks. Resistance values should be much smaller than the bias resistances to control crosstalk between wires and limit the voltage drop if any of the wires

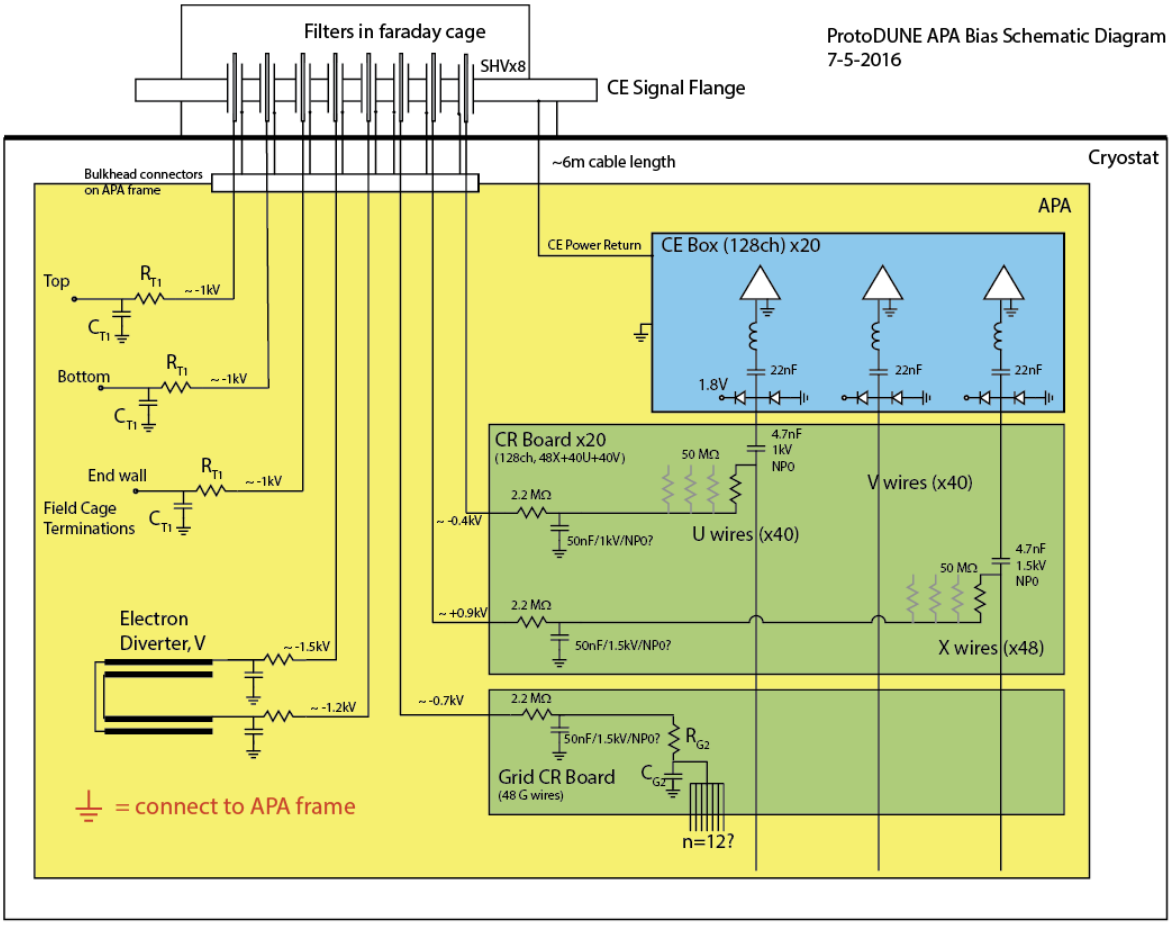

Figure 2.34: APA wire bias schematic diagram, including the Capacitance-Resistance (CR) board. fig:tpc

becomes shorted to the APA frame. A value around 2.2 MΩ is desired. Smaller values may be considered although a larger filter capacitor would be required to maintain a given level of noise reduction. A target value of 47 nF has been established for the filter capacitors.

For the grid-plane bias filters, component values are less critical. If possible they will be identical to those used for the bias resistors and coupling capacitors (50 MΩ and 2.2 to 4.7 nF).

2.6.4 Front-End Mother Board

The main component of the CE architecture, illustrated in Figure 2.38, is the 128-channel FEMB, which itself consists of an analog motherboard and an attached FPGA mezzanine card for processing the digital outputs. Each APA is instrumented with 20 FEMBs, for a total of 2,560 channels per APA. The FEMBs plug directly into the APA CR boards, making the connections from the U- and V-plane induction wires and X-plane collection wires to the charge amplifier circuits as short as possible.

The analog mother board is instrumented with eight 16-channel FE ASICs, eight 16-channel ADC ASICs, LV power regulators, and input-signal protection circuits. The 16-channel FE ASIC provides amplification and pulse shaping. The 16-channel ADC ASIC comprises 12-bit digitizers performant at speeds up to 2 MS/s, local buffering, and an 8:1 MUX stage with two pairs of serial readout lines in parallel.

(Figure 2.39). Each FE ASIC channel has a charge amplifier circuit with a gain selectable from one of 4.7, 7.8, 14 and 25 mV/fC (full scale charge of 55, 100, 180 and 300 fC), a high-order anti-aliasing filter with adjustable time constant (peaking time 0.5, 1, 2, and 3 μs), an option to enable AC coupling, and a baseline adjustment for operation with either the collecting (200 mV) or the non-collecting (900 mV) wires. Shared among the 16 channels in the FE ASIC are the bias circuits, programming registers, a temperature monitor, an analog buffer for signal monitoring, and the digital interface. The estimated power dissipation of FE ASIC is about 6 mW per channel at 1.8 V supply.

The FE ASIC layout is shown in Figure 2.37. The ASIC was implemented using the commercial CMOS process (0.18 μm and 1.8 V), which is expected to be available for at least another 10 years. The charge amplifier input MOSFET is a p-channel biased at 2 mA with a L/W (channel length/width) ratio of 0.27 μm / 10 μm, followed by dual cascade stages. The charge amplification and shaping filter have digitally programmable gain and peaking time (as specified in Section 2.6.4). Each channel also implements a high-performance output driver, which can be used to drive a long cable, but is disabled when interfaced to an ADC ASIC to reduce the power consumption. The ASIC integrates a band-gap reference (BGR) to generate all the internal bias voltages and currents. This guarantees a high stability of the operating point over a wide range of temperatures, including cryogenic. The ASIC is packaged in a commercial, fully encapsulated plastic QFP 80 package.

Prototypes have been evaluated and characterized at RT (300 K) and LN2 (77 K) temperature. During testing the circuits have been cycled multiple times between the two temperatures and

operated without any change in performance. Figure 2.35 shows the measured pulse response, both as a function of temperature and the programmable settings of the chip. These results are in close agreement with simulations and indicate that both the analog and the digital circuits and interface operate as expected in a cryogenic environment.

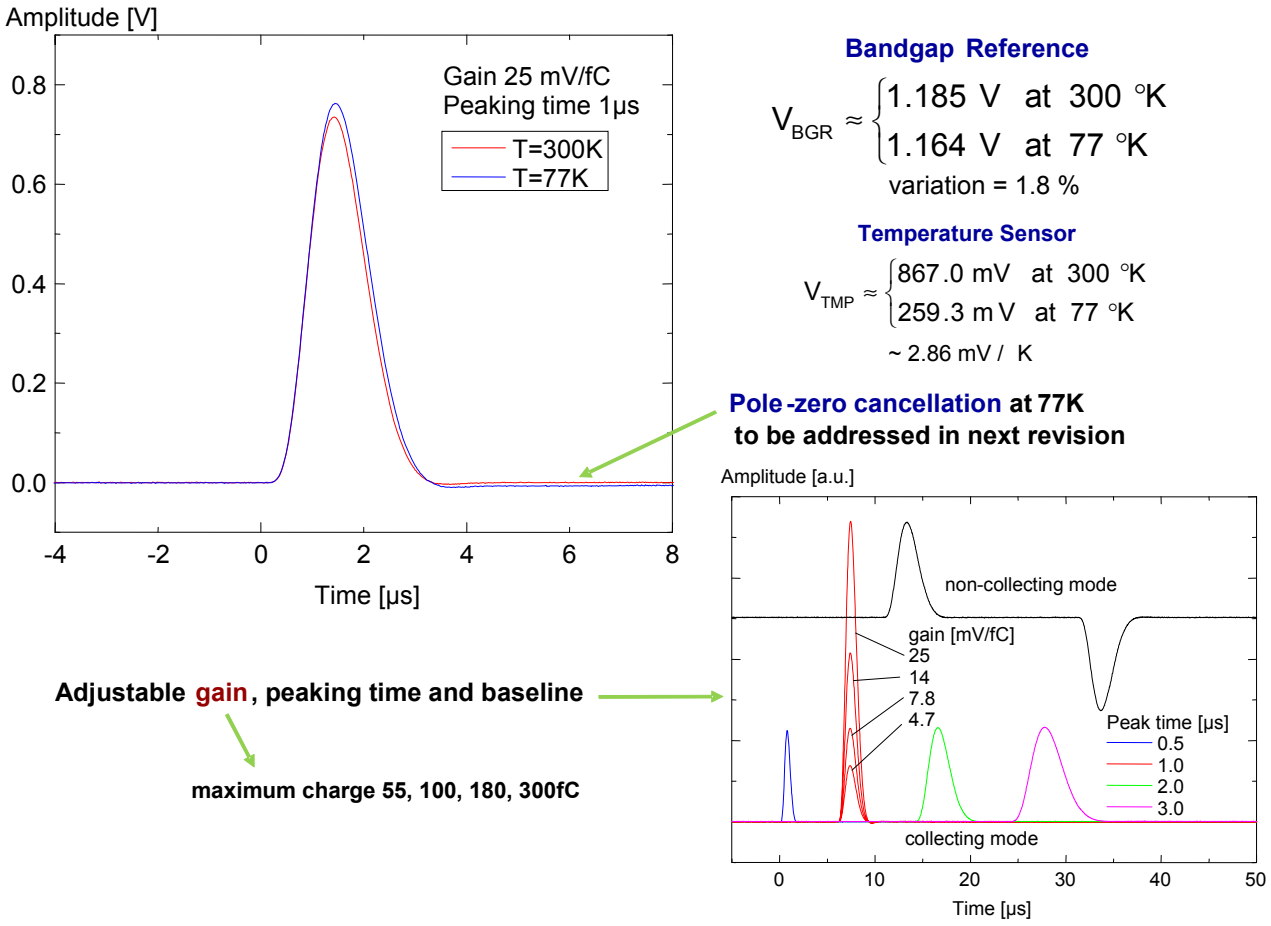

Figure 2.35: Measured pulse response with details on gain, peaking time and baseline adjustments

Figure 2.36 shows the measured Equivalent Noise Charge (ENC) versus filter-time constant (peaking time) for two different gains, where ENC is the value of charge (in electrons) injected across the detector capacitance that would produce at the output of the shaping amplifier a signal whose amplitude equals the output R.M.S. noise. These measurments were made with prototype FEMBs at both RT and submerged in LN2 with a wire-simulating input capacitance of $C_f = 150$ pF. In LN2, for peaking times >1 μs, less than 600 e^- was measured. For comparison, a MIP travelling perpendicularly to the wire plane in the direction of wire spacing is expected to deposit $\sim$ 10,000 e^- on the collection wires, for a worst-case S:N$\sim$16:1.

Each channel is equipped with an injection capacitor which can be used for test and calibration and can be enabled or disabled through a dedicated register. The injection capacitance has been measured using a calibrated external capacitor. The measurements show that the calibration capacitance is extremely stable, changing from 184 fF at RT to 183 fF at 77 K. This result and the

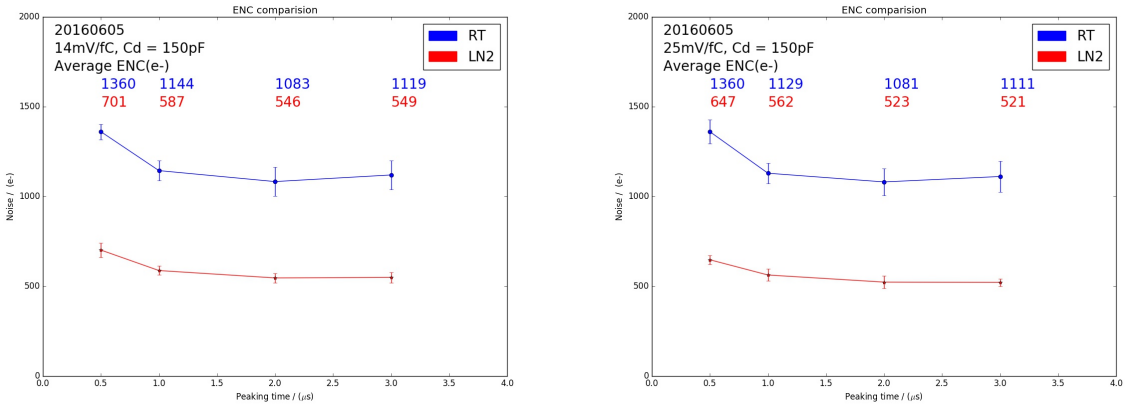

Figure 2.36: Measured ENC vs filter time constant from the latest prototype version of the FEMB for two different gains, 14 mV/fC and 25 mV/fC. RT = room temperature and LN2 = liquid nitrogen

fig:tpcc

measured stability of the peaking time demonstrate the high stability of the passive components as a function of temperature. Channel-to-channel and chip-to-chip variation in the calibration capacitor are typically less than 1%.

The ADC ASIC design is also implementd using the CMOS process (0.18 μm and 1.8V). The layout of the ADC ASIC is shown in Figure 2.37. The ADC ASIC is a complex design with 320,000 transistors, while the FE ASIC has 16,000. The transistor design work has been done following the rules for long cryo-lifetime. Shared among the 16 channels in the ADC ASIC are the bias circuits, programming registers, an 8:1 MUX, and the digital interface. The estimated power dissipation of FE ASIC is below 5 mW per channel at 1.8 V supply.

fig:tpcce ADC ASIC

The ADC ASIC has an input buffer with offset compensation to match the output of the FE ASIC. The input buffer first samples the input signal (with a range of 0.2 V to 1.6 V), then provides a current output after compensating for offset voltage error. This current output is then supplied to the ADC which converts the input to digital in two phases. The MSB (Most Significant Bit) 6 bits are first determined followed by the LSB (Least Significant Bit) 6 bits. After the conversion the thermometer code is converted to binary and latched. The output of ADC channel 16 can be monitored externally. The data from the 16 ADCs are transferred in parallel to the FIFO block. The built-in FIFO is 32 bits wide and 192 bits long, and has full and empty indicator flags, needed for interfacing to the FPGA. The ADC along with the input buffers are biased internally using a bias generator and a bandgap voltage reference. The bandgap voltage (VBGR) can be monitored and/or controlled externally. It can be put in the low-power sleep mode, and woken up in less than 1 μs.

Prototypes have been evaluated and characterized at RT (300 K) and LN2 (77 K) temperature. During these tests the circuits have been temperature-cycled multiple times. The effective resolution with reference to the input referred noise is ~11.6 bits at both 300 K and 77 K. The differential non-linearity (DNL) is less than 4 LSBs for 99% of ADC bins at both 300 K and 77 K.

The ADC outputs are passed to the FPGA mezzanine board for transmission to the warm electronics located on the outside of the signal flange. The FPGA has four 4:1 MUX circuits that

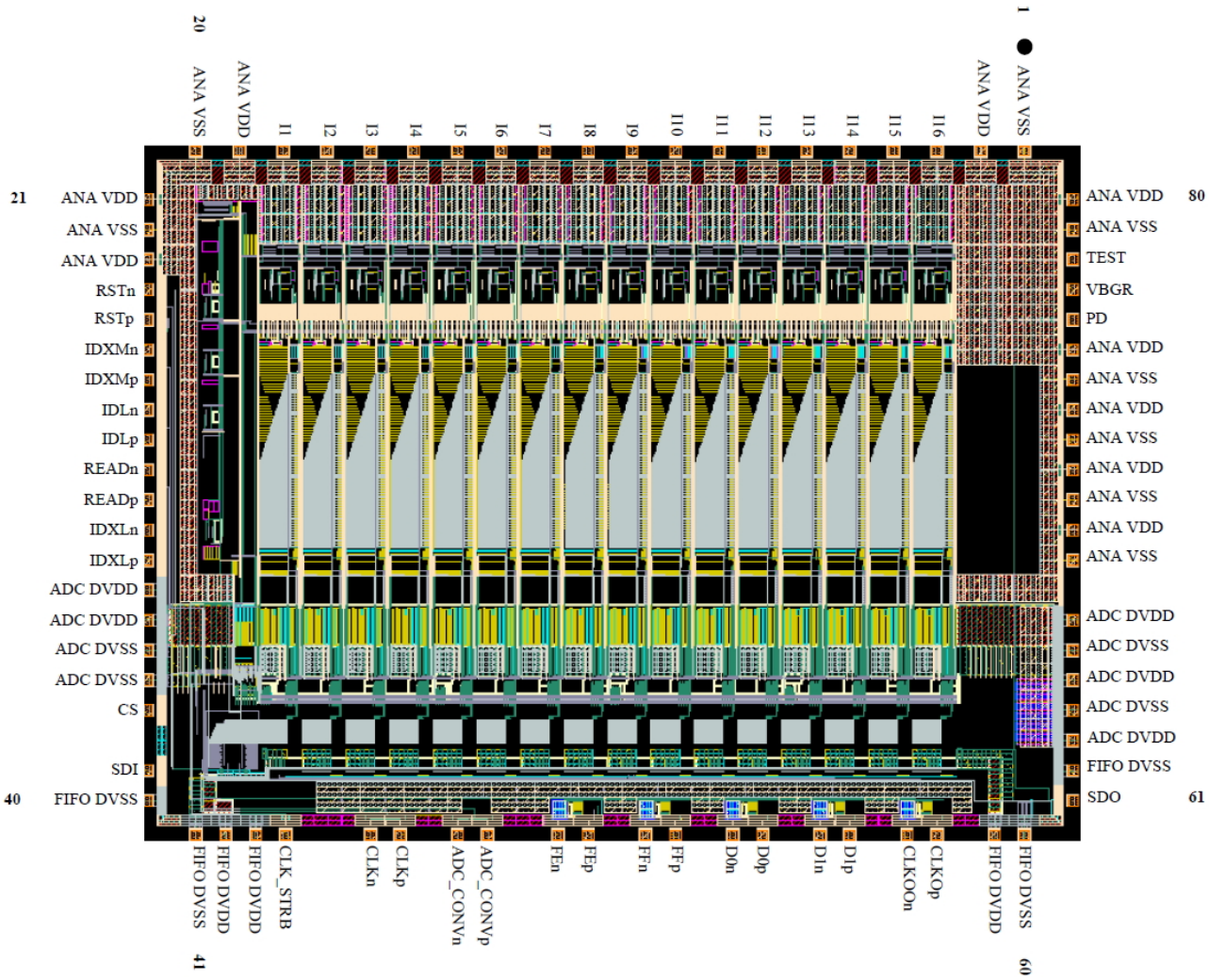

Figure 2.37: The layout of the 16-channel ADC ASIC

fig:tpcc

combine the 16 serial lines from the eight ADC channels into four serial lines of 32 channels each, and four ∼1.2 Gigabit-per-second (Gbps) serial drivers that drive the data in each line over cold cables to the WIBs.

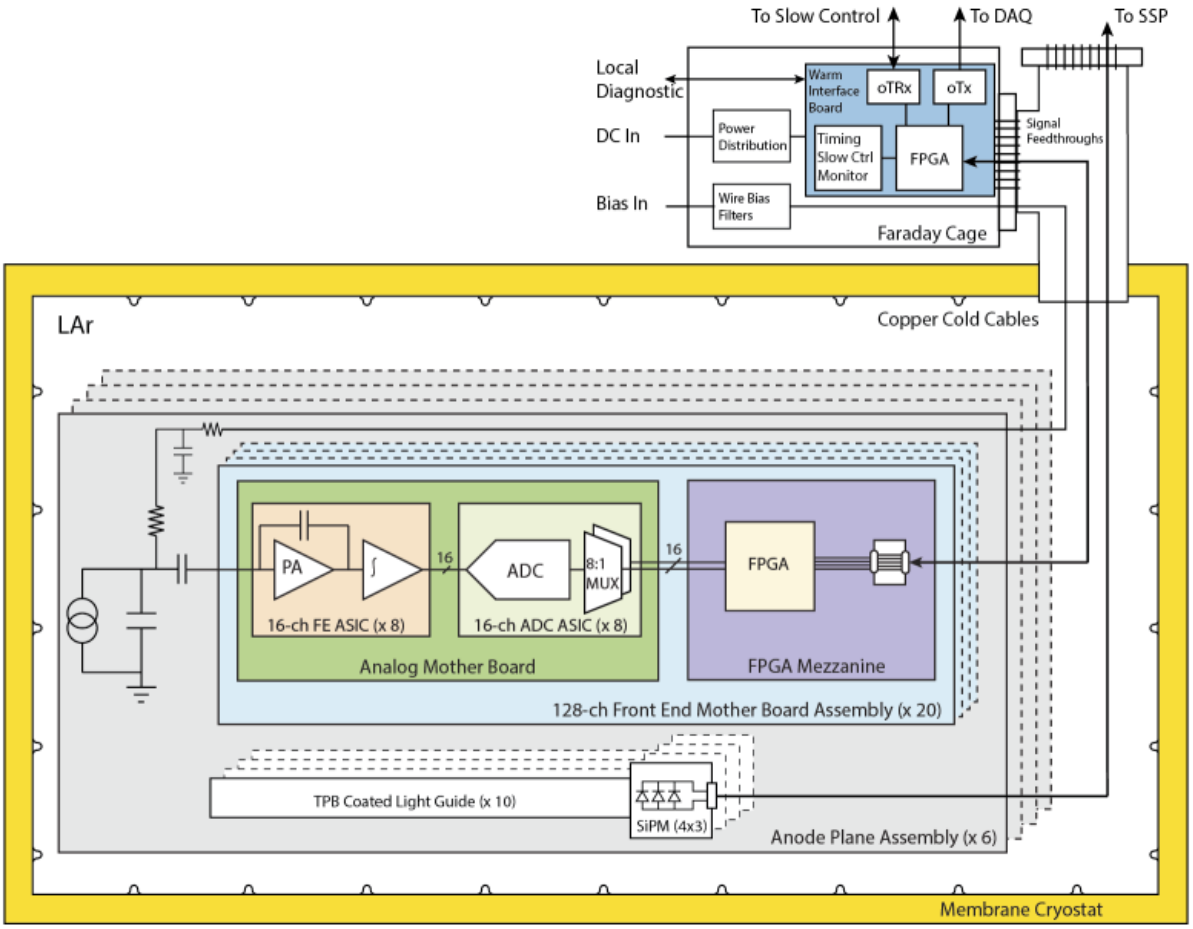

Figure 2.38: The CE Architecture. The basic unit is the 128-channel FEMB.

The data are passed through the signal flange to the WIBs on copper cables utilizing LV differential signaling (LVDS). On the WIBs, the data is further MUXed by 4:1 and transmitted over optical fibers to the DAQ system described in Section 2.9.9.

The FPGA on the mezzanine card is also responsible for communicating with the DAQ and timing systems and providing the clock and control signals required by the FE and ADC ASICs.

Each FEMB is enclosed in a Faraday box to provide shielding from noise. As shown in Figure 2.40, the Faraday box is designed to make the electrical connection between the FEMB and the APA frame. Mounting hardware inside the Faraday box connects the ground plane of the FEMB to the box casing. The box casing is electrically connected to the APA frame via twisted conducting wire (not shown in Figure 2.40). This is the only point of contact between the FEMB and APA, except for the input amplifier circuits connected to the CR board, which also terminate to ground at the APA frame, as shown in Figure 2.34.

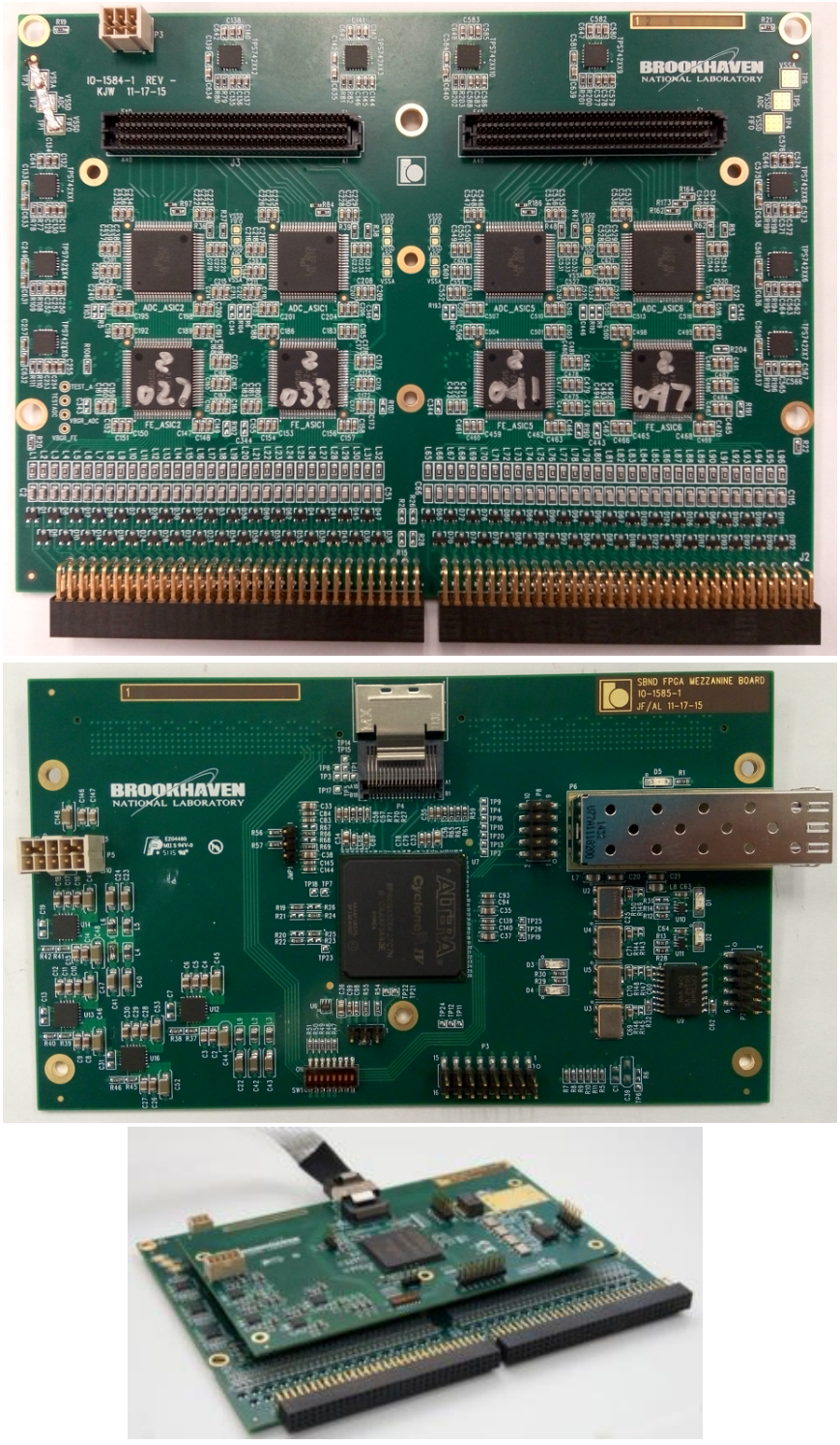

Figure 2.39: The Front End Mother Board (FEMB), as used in the early set of tests. **Top:** The analog mother board, showing four ADC ASICs and four FE ASICs surface mounted. The other side of the board has another four ADC and FE ASICs. Except for anticipated small modifications, this board is essentially the final version. **Middle:** The FPGA mezzanine, used in place of the digital ASIC mezzanine for the early set of tests. **Bottom:** The complete FEMB assembly as used in the early set of tests. The cable shown in the high-speed data, clock, and control cable. fig:tpcc

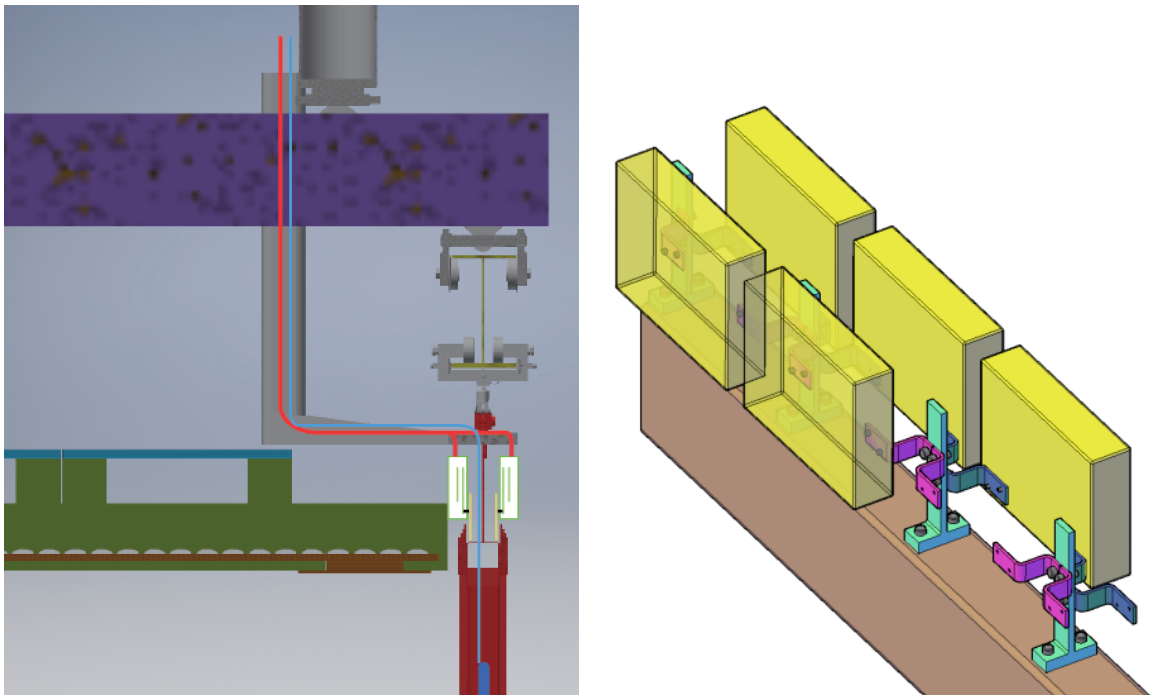

Figure 2.40: Faraday box for the FEMB.

2.6.5 CE feedthroughs and cold cables

All cold cables originating from inside the cryostat connect to the outside warm electronics through PCB board feedthroughs installed in the signal flanges that are distributed along the cryostat roof (Figure 2.41). The TPC data rate per APA, with an overall 32:1 MUX and 80 ∼1 Gbps data channels per APA, is sufficiently low that the signals can be driven over copper LVDS tansmission lines. Additional LVDS transmission lines are available for the distribution of clock signals and control information, which are transmitted at a lower bit rate. Optical fiber is employed externally from the WIBs on the signal flange to the DAQ and slow control systems.

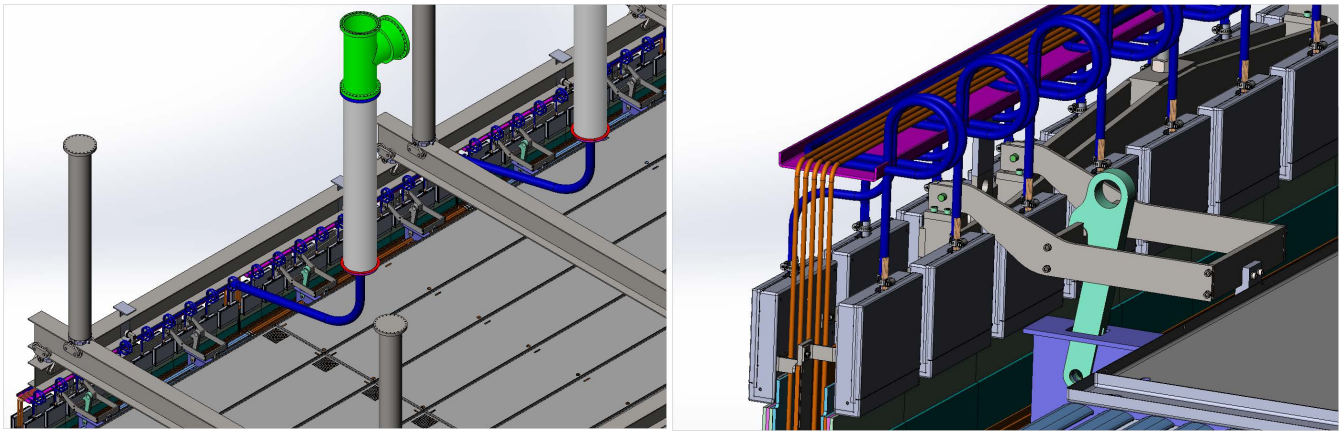

Figure 2.41: The CE feedthrough configuration and internal cable routing. The left panel shows a cutaway view of the cryostat. The right panel shows more detail at the Faraday boxes.

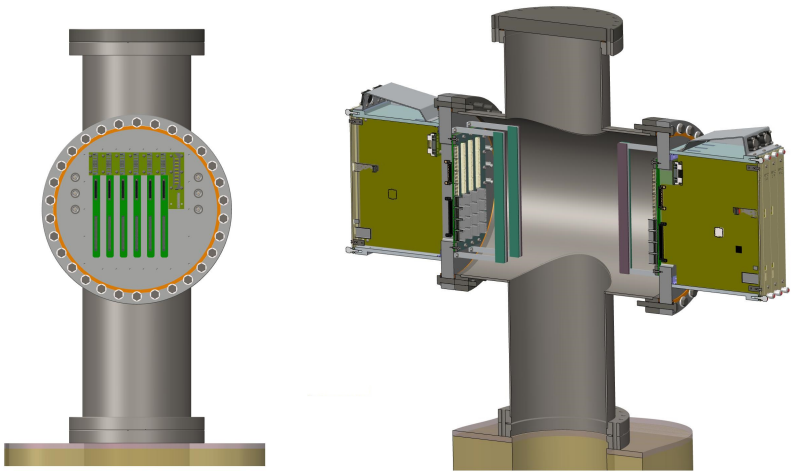

Figure 2.42: TPC CE feedthrough. The WIBs are seen edge-on in the left panel, and in an oblique side-view in the right panel, which also shows the warm crate for a DUNE module in a cutaway view (for ProtoDUNE-SP, there is a crate only on one side). fig:tpcc

The current design of the signal flange includes a T-shaped pipe, separate PCB feedthroughs for the CE and PDS cables, and an attached crate for the TPC warm electronics, as shown in fig:tpcce_signal_FT Figure 2.42. The wire-bias voltage cables connect to standard SHV (safe high voltage) connectors machined directly into the CE feedthrough, ensuring no electrical connection between the wire-bias voltages and other signals passing through the signal flange. Each CE feedthrough serves the bias/power/digital IO needs of one APA, as shown in Figure 2.43. fig:tpcce_cable_routing

A program for minimizing potential contamination of the LAr from the cable plant contained within the ullage (the warmer gas phase at the top of the cryostat) is being carefully followed.

Data/control cable bundles are used to send system clock and control signals from the signal flange to the FEMB, stream the ∼1 Gbps high-speed data from the FEMB to the signal flange, and provide backup JTAG programming to the cold FPGA, in case the power-up programming from the onboard EEPROM fails. As described in Section 2.6.1, each FEMB connects to a signal subsec:ce_intro flange via one data cable bundle, leading to 20 bundles between one APA and one flange. Each data bundle contains 12 low-skew copper twin-axial cables with a drain wire, to transmit the following differential signals:

- 4×1.2 Gbps high-speed data
- One 50 MHz system clock
- One 2 MHz CONVERT clock
- 2 I2C control and configure
- 4 single-ended JTAG programming for the FPGA

The selected cables are Samtec 26 AWG twin-axial bundles with Samtec HSEC08 connectors to

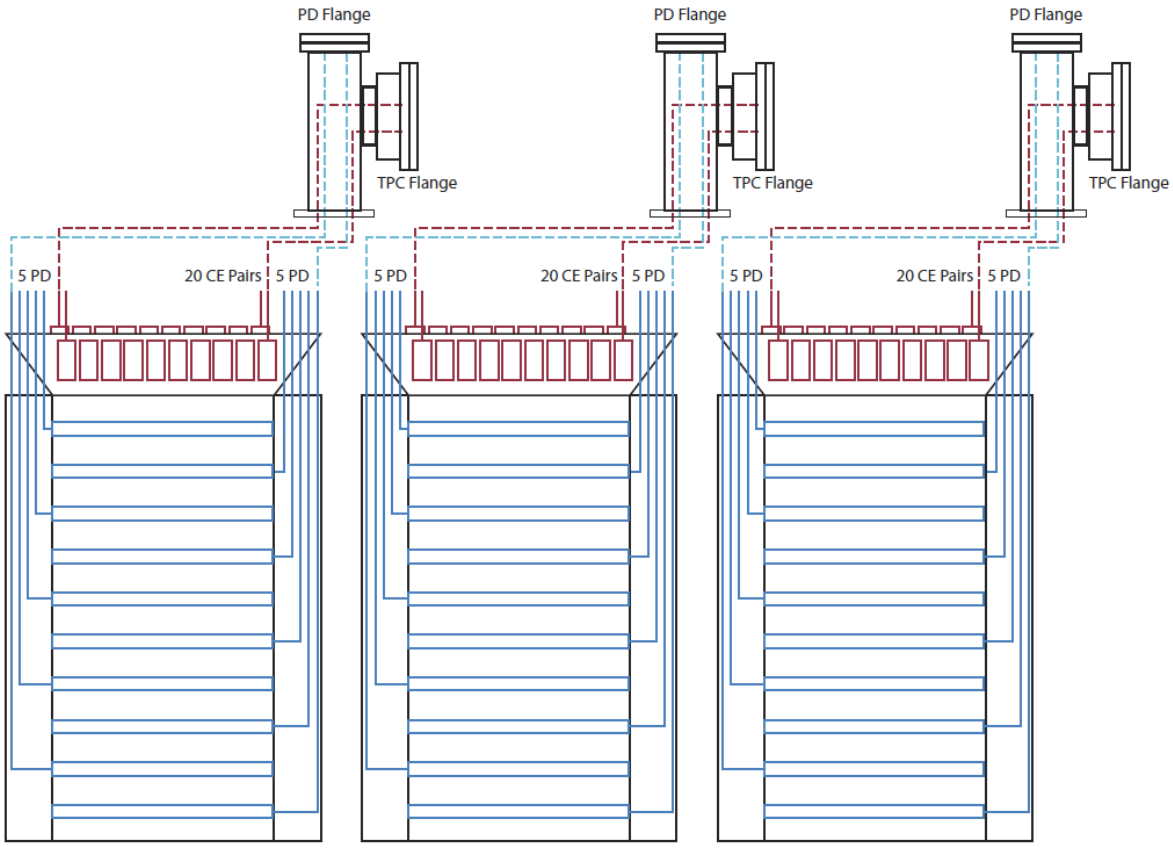

Figure 2.43: TPC cable routing scheme for three APA section.

fig:tpcc

both the FEMB mezzanine board and the signal flange. The HSEC08 connectors lock into place with tabs on each side of the connector. A sample of the Samtec cable with THV outer jacket has passed outgassing tests in the LAr Materials Test Stand at Fermilab.

The Samtec 26 AWG cable has been tested and demonstrated to have low enough dispersion such that both the LVDS 50 MHz system clock and ∼1 Gbps high-speed data can be recovered over 25 meters of RT cable, significantly longer than the required seven meters needed to run cables between the FEMBs and signal flanges.

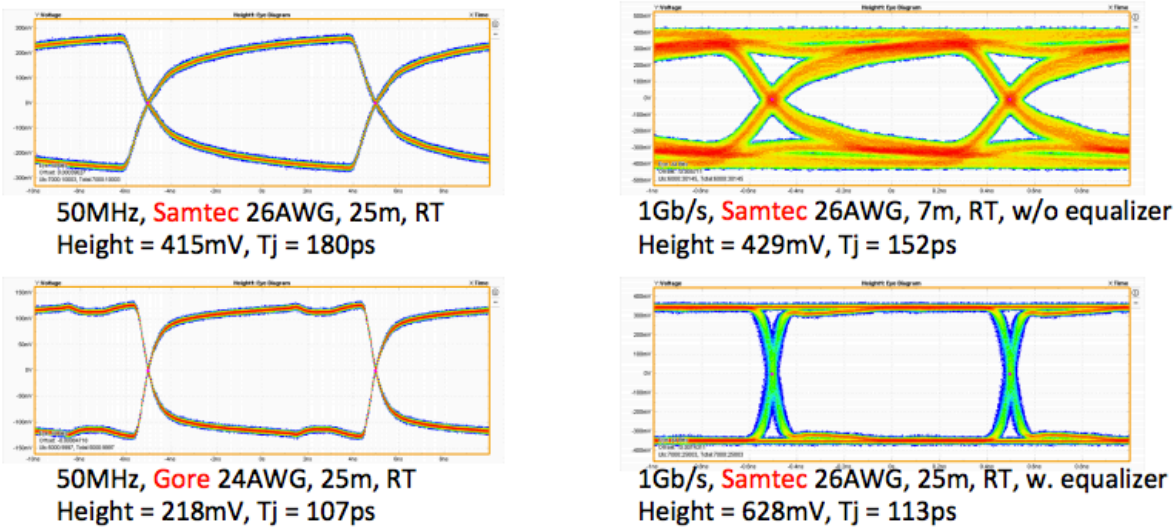

Figure 2.44: Eye diagrams from cable validation testing. **Top Left:** 50 MHz system clock over 25 m RT (RT) Samtec 26AWG cable. For comparison, **Bottom Left** shows the same clock over the heavier, prohibitively expensive Gore 24AWG cable. **Top Right:** 1 Gbps data over 7 m (ProtoDUNE length) RT Samtec 26AWG cable without active recovery by equalizers. **Bottom Right** 1 Gbps data over 25 m (DUNE length) RT Samtec 26AWG cable with active recovery.

fig:tpcc

fig:tpcce_samtec_results

Figure 2.44 shows results from the cable validation testing. The eye diagrams show the edges of the differential signals after LVDS transmission over the specified cable types and lengths. The height of eye diagram shows the size of the recovered signal in mV and the slope of the rising and falling edges are jitter in picoseconds (ps). An eye diagram is sufficient to show that the edges of the differential signals can be recovered, but not enough to demonstrate the bit error rate (BER). However, the Samtec 26 AWG cable has also passed a BER test, transmitting 10^{13} bits without error.

LV power is passed from the signal flange to the FEMB by bundles of 16 Samtec 20 AWG twisted-pair wires, as shown in Figure 2.43. One IPD1 connector attaches all 16 wires at the signal flange, and two IPD1 connectors are attached to the FEMB (one to the analog motherboard and one to the FPGA mezzanine). In total, 20 wire bundles bring LV power to the FEMBs associated with one APA.

fig:tpcce_cable_routing

Eight of the 16 wires are power feeds, as described in Figure 2.45. The other eight wires are attached to the grounds of the input amplifier circuits, as described in Section 2.6.3. For a single FEMB, the resistance is < 30 mΩ at RT or < 10 mΩ at LAr temperature. Each APA has a copper

fig:tpcce_lv_req

subsec:ce_wire_bias

cross-section of approximately 80 mm^2, with a resistance < 1.5 mΩ at RT or < 0.5 mΩ at LAr temperature.

FEMB 7m Cable	Net Name	# of Wires	R_RT [Ω]	R_LAr [Ω]	XSection [mm^2]
Analog Mother Board	FE-ANA-IN	3	0.078	0.025	1.554
	REGR_BIAS	1	0.233	0.074	0.518
FPGA Mezzanine	P1.5V	1	0.233	0.074	0.518
	P2.8V	1	0.233	0.074	0.518
	P3.6V	1	0.233	0.074	0.518
	BIAS	1	0.233	0.074	0.518
Summary		8	0.029	0.009	4.144

Figure 2.45: Samtec LV power feed wire specifications.

The wire-bias voltage cables are required to deliver voltages up to a few thousand Volts and currents up to a few milliAmps.

The bias voltages are applied to the X-, V-, and G-plane wire layers, three field cage terminations, and an electron diverter, as shown in Figure 2.34. The voltages are supplied through eight SHV connectors mounted on the signal flange. RG-316 coaxial cables carry the voltages from the signal flange to a patch panel PCB which includes noise filtering mounted on the top end of the APA.

From there, wire-bias voltages are carried by single wires to various points on the APA frame, including the CR boards, a small PCB mounted on or near the patch panel that houses a noise filter and termination circuits for the field cage voltages, and a small mounted board near the electron diverter that also houses wire-bias voltage filters.

2.6.6 Warm interface electronics

The warm interface electronics are housed in warm electronics crates (WECs) attached directly to the signal flange. The WEC shown in Figure 2.46 contains one Power and Timing Card (PTC), up to five Warm Interface Boards (WIBs) and a passive backplane (PTB), which fans out signals and LV power from the PTC to the WIBs.

The WIB is the interface between the DAQ system and up to four FEMBs. It receives the system clock and control signals from the timing system and provides for processing and fan-out of those signals to the four FEMBs. The WIB also receives the high-speed data signals from the four FEMBs and transmits them to the DAQ system over optical fibers. The WIBs are attached directly to the TPC CE feedthrough on the signal flange. The feedthrough board is a PCB with connectors to the cold signal and LV power cables fitted between the compression plate on the cold side, and sockets for the WIB on the warm side. Cable strain relief for the cold cables is supported from the back end of the feedthrough.

The PTC provides a bidirectional fiber interface to the timing system. The clock and data streams are separately fanned-out to the five WIBs as shown in Figure 2.47. The PTC fans the clocks out

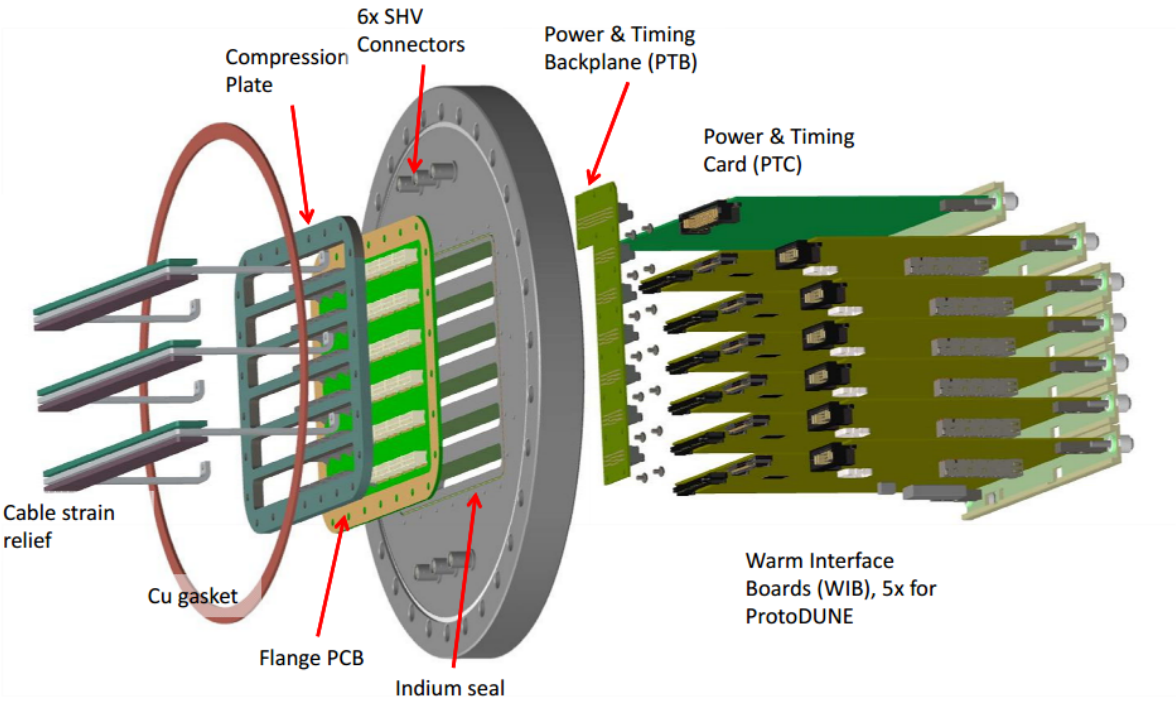

Figure 2.46: Exploded view of the signal flange for SBND (ProtoDUNE-SP has five WIBs). fig:tpc

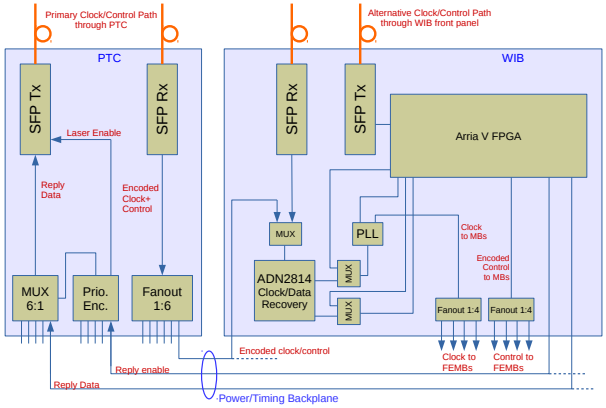

Figure 2.47: Power and Timing Card (PTC) and timing distribution to the WIB and FEMBs. fig:tpc

to the WIB over the PTB, which is a passive backplane attached directly to the PTC and WIBs. The received clock on the WIB is separated into clock and data using a clock/data separator.

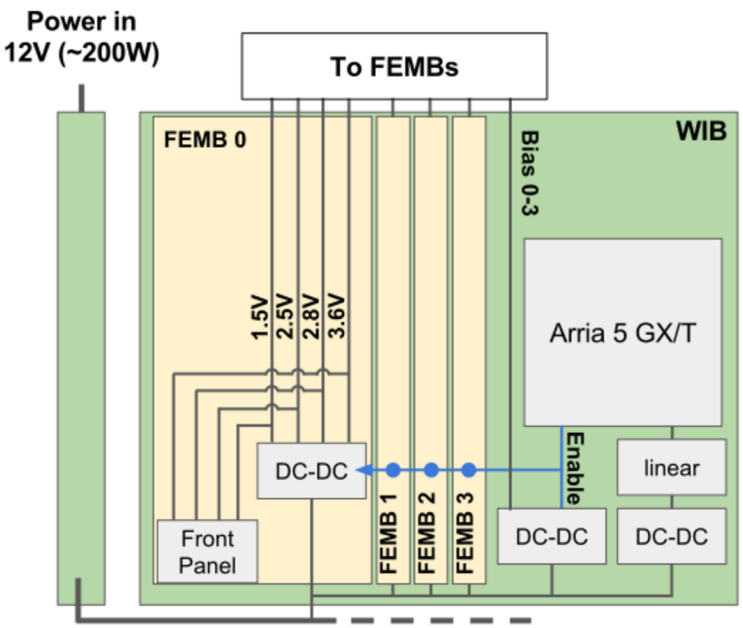

Figure 2.48: LV power distribution to the WIB and FEMBs. 200 W is for a fully-loaded crate with the majority of the power dissipated by the 20 cold FEMBs in the LAr.

The PTC also receives LV power for all cold electronics connected through the signal flange, approximately 200 W at 12 V for a fully-loaded flange (five WIB + 20 FEMB). The LV power is then fanned out on the PTB to each WIB, which provides the necessary DC/DC conversions and fans the LV power out to each of the cold FEMBs supplied by that WIB, as shown in Figure 2.48. The majority of the 200W drawn by a full flange is dissipated in the LAr by the cold FEMB.

Each WIB contains a unique IP address for its UDP slow control interface. The IP address for the WIB is derived from a crate and slot address: the crate address is generated on the PTC board via dipswitches and the slot address is generated by the PTB slot, numbered from one to five. Note that the WIBs also have front-panel connectors for receiving LV power; these can be used in place of the LV power inputs on the PTB generated by the PTC.

The WIB is also capable of receiving the encoded system timing signals over bi-directional optical fibers on the front panel, and processing these using either the on-board FPGA or clock synthesizer chip to provide the 50 MHz clock required by the cold electronics.

The FPGA on the WIB is an Altera Arria V GT variant, which requires a 125 MHz clock for its state machine that is provided by an on-board crystal oscillator. The GT variant of the Arria V transceivers can drive the high-speed data to the DAQ system up to 10.3125 Gbps per link, implying that all data from two FEMB (2×5 Gbps) could be transmitted on a single link. However, it is planned to use a QSPF socket on the WIB to deliver ∼5 Gbps on four optical fibers (one fiber per FEMB) to two RCEs.

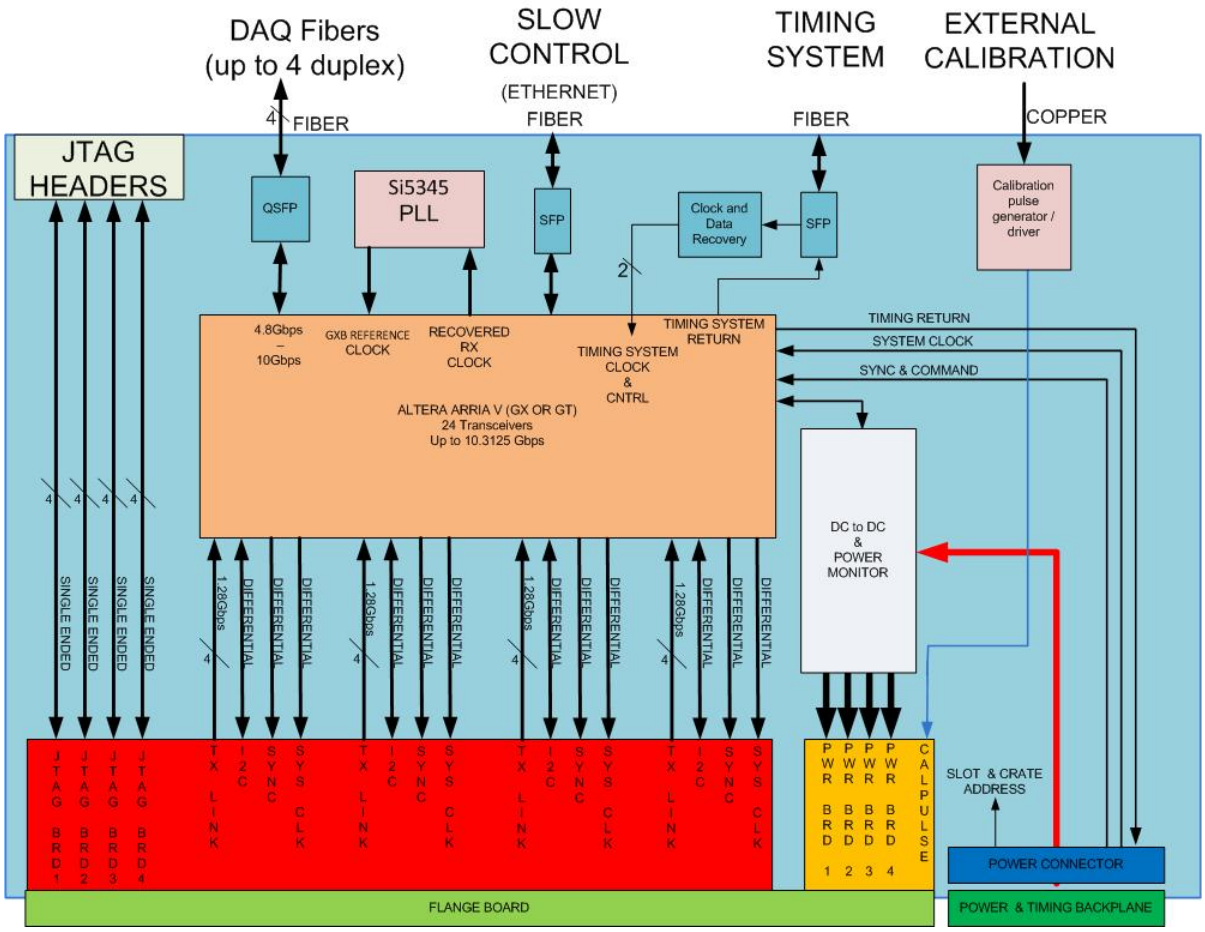

Figure 2.49: Warm interface board (WIB). Note that front panel inputs include a LEMO connector and alternate inputs for LV power.

fig:tpc

write out

The FPGA has an additional Gbps Ethernet transceiver I/O based on the 125 MHz clock, which provides real-time digital data readout to the slow control system.

2.6.7 External Power and Cables

The LV power to the FEMB and WIB is supplied by Weiner MPOD power supplies.

define MPOD

The CE power-per-channel is about 25 mW in the LAr. Including power for the WIB, a fully loaded WIB (one WIB plus four FEMBs) requires 12V and draws approximately 3.3 Amps. Therefore, the full electronics for one APA (five WIBs + 20 FEMBs) requires 12 V and draws approximately 16 Amps, for a total power of almost 200 W, as described in Section 2.6.6.

Each MPOD LV power unit has two DSUB37 connectors, each with four channels of LV output, including negative and positive sense wires. Each channel has three pins of negative output and three pins of positive output. Five of the eight channels provide the 12 V/3.3 A to each WIB via the PTC, and one channel provides LV power to the PTC itself, with two of the eight channels unused.

Each MPOD wire-bias voltage unit supplies the wire-bias voltages to eight SHV connectors at the signal flange. One MPOD chassis contains three LV and three wire-bias units, and can supply all the LV and wire-bias power to three APAs worth of cold electronics. Therefore, a total of two MPOD chassis are required for the detector.

The LV power cable uses DSUB37 connectors. The bottom of the fuse PCB at the MPOD end of the cable is shown in Figure 2.50. Each of the three output pins on each channel are tied together in parallel going to one wire large enough to carry the full supply voltage. Fuses can optionally be populated on each output pin as shown in Figure 2.50; however, if fusing is not selected, the pins will be connected with 0 Ω resistors. This fusing would serve as a final protection. The primary protection would come from the Over Current protection on the MPOD, which is set above the 3.3 A required by each WIB, but below the combined fuse value.

The five separate 12 V/3.3 A channels to the WIBs are delivered to the PTC using two normal DSUB37 connectors to attach the LV power cable. The fusing for the sense wires is implemented on the PTC.

Each APA requires three wire-bias voltage connections at +820V, −370V, and −665V, as described in Section 2.6.3. The current on each of these supplies is expected to be zero at normal operation. However the ripple voltage on the supply must be carefully controlled to avoid noise injection into the front-end electronics.

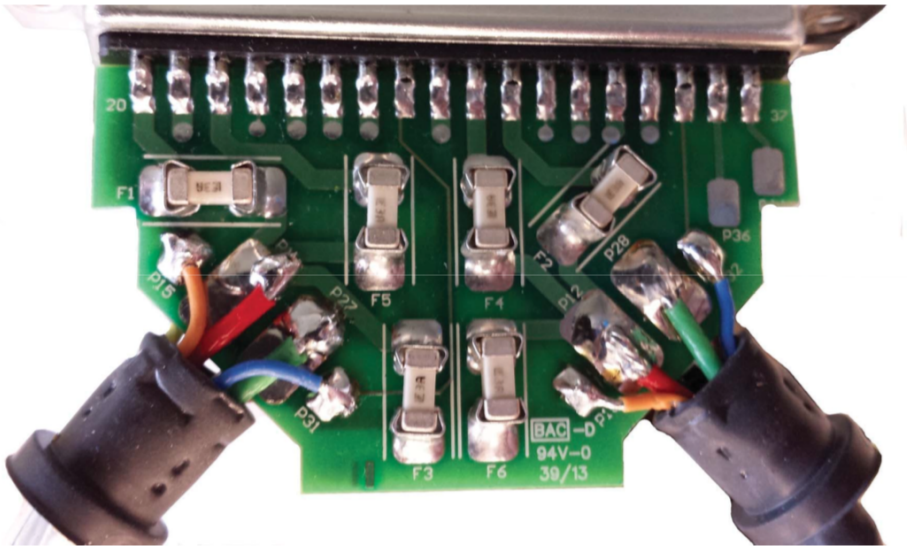

Figure 2.50: Bottom of the fuse PCB at the MPOD end of the cable.

RG-58 coaxial cables connect the wire bias voltages from the MPOD to the standard SHV connectors machined directly into the CE feedthrough, so there is no electrical connection between the LV power and data connectors and wire-bias voltages. The length of the cables from the Weiner MPODs to the signal flanges is estimated to be 18 meters.

Optical fibers provide the connections between the WECs, which act as Faraday-shielded boxes, to the DAQ and slow control systems. Each WIB uses QSFP sockets for four pairs of fiber, implying a total of 120 optical data fibers for the 30 WIB boards in the system. The optical fibers from the signal flanges to the DAQ room are estimated to be 30−40 m in length.

Duplex LC optical fiber is under consideration for transmitting the one GIG-E connection from each WIB to the slow control system. The WIB reports the current draw from each FEMB to the slow control system, while the current draw for each WIB is monitored at the MPOD itself.

2.7 Photon Detection System (PDS)

LAr is an excellent scintillating medium and the photon detection system (PDS) is used to obtain additional event information from the photons produced by particles traversing the detector. With an average energy of 19.5 eV needed to produce a photon (at zero field), a typical particle depositing 1 MeV in LAr generates 40,000 photons with a wavelength of 128 nm. In higher electric fields this number is reduced, but at 500 V/cm the yield is still ∼20,000 photons per MeV. Roughly 1/4 of the photons are promptly emitted with a lifetime of about 6 ns, while the rest are produced with a lifetime of 1100–1600 ns. Prompt and delayed photons are detected in precisely the same way by the photon detection system. LAr is highly transparent to the 128-nm VUV photons with a Rayleigh scattering length of (66 ± 3) cm

Missing this citation in common/pdune-tdr-citedb.bib"

and absorption length of >200 cm; assuming a LN_2 content of less than 20 ppm. The relatively large light output makes the scintillation process an excellent candidate for determining the t_0 for non-beam related events. Detection of the scintillation light can also be helpful in performing background rejection and triggering on non-beam events.

2.7.1 Scope and requirements

The photon detector system (PDS) includes the following components:

- Light collection system including wavelength shifter and light guides
- Light sensors: Silicon photo-multipliers (SiPMs)
- Readout electronics
- Monitoring system
- Related infrastructure (frames, mounting boards, etc.).

The primary requirement is the detection of light from proton decay candidates (as well as beam neutrino events) with high efficiency to enable 3D spatial localization of candidate events. The assumed light yield necessary for meeting this requirement is 0.1 pe/MeV for a particle track near the cathode plane (the farthest possible location from the PDS) after the application of all relevant detection efficiencies. In DUNE, the TPC provides supernova neutrino detection, while the detection of light from supernova neutrino interactions localize the events and disentangles them from background noise in the TPC. The photon system provides the t_0 of events relative to TPC timing with a resolution better than 1 μs (providing position resolution along the drift direction on the order of a couple of mm). Measurements will determine the absolute light yield by measuring light from beam particles and cosmic ray muons tracked in the TPC or identified by external muon trigger counters.

Figure 2.51 shows the layout for the photon detector system described in this section.

2.7.2 Photon detector modules

Two different styles of PDS modules are planned to be installed in the detector. The two designs test similar light-collection strategies, which differ primarily in the number of times the LAr scintillation light is shifted.

The first design, shown schematically in Figure 2.51. is based on wavelength-shifting radiator plates

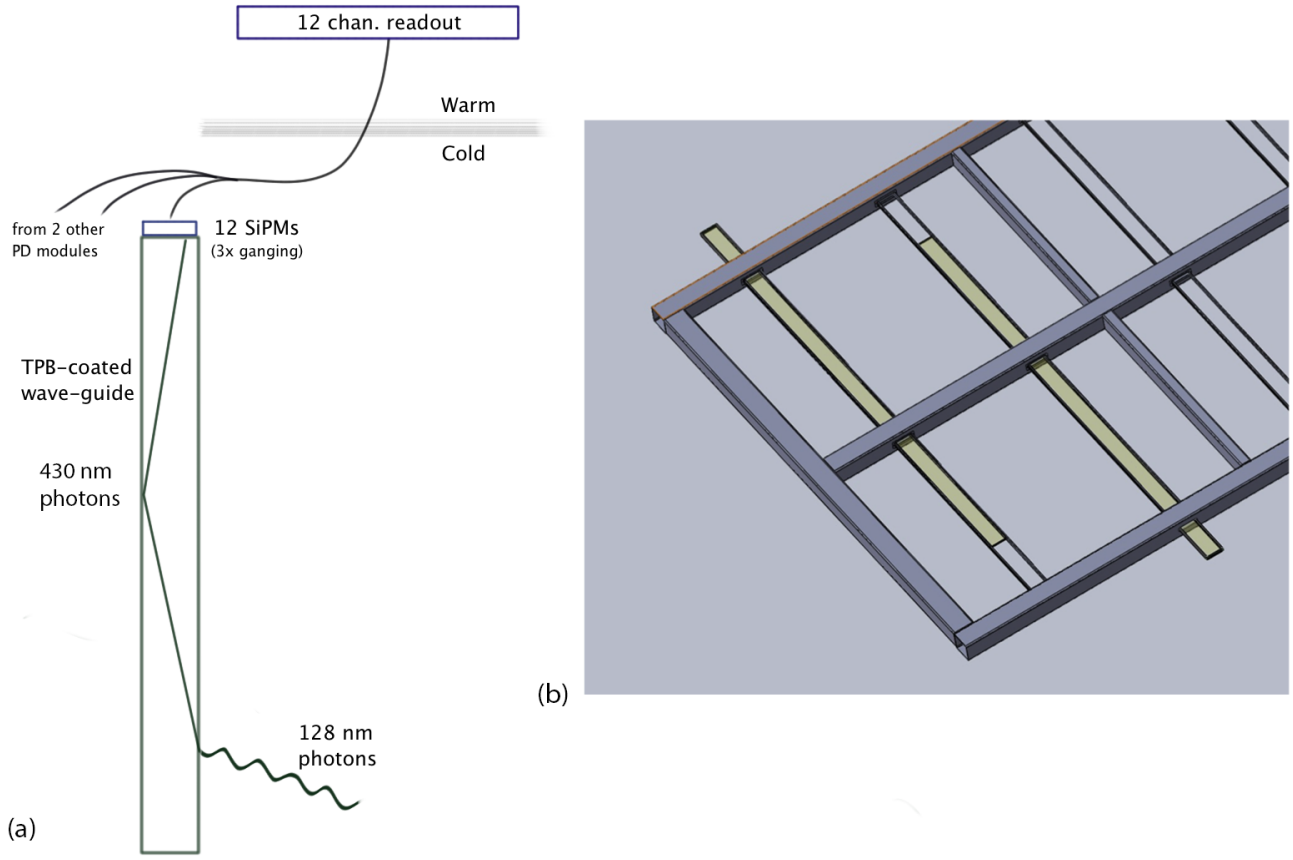

Figure 2.51: Overview of the PDS system showing a cartoon schematic (a) of a single PDS module in the LAr and the channel ganging scheme used to reduce the number of readout channels. Panel (b) shows how each PDS module is inserted into an APA frame. Ten photon detectors (PDs) are inserted into an APA frame. fig:PD_c

mounted to wavelength-shifting light guides. The plates are coated with tetraphenyl-butadiene (TPB) to produce blue ($430nm$) light from the 128-nm VUV scintillation light. This blue light is absorbed by the commercially produced wavelength shifting (WLS) polystyrene bar with Y-11 fluor, producing green light, which is transmitted through the light guide to the photosensor mounted at its end. The radiator plates are held captive in mounting blocks that are glued to the WLS bar at regular intervals as shown in Figure 2.52.

fig:PD_radiator_mount

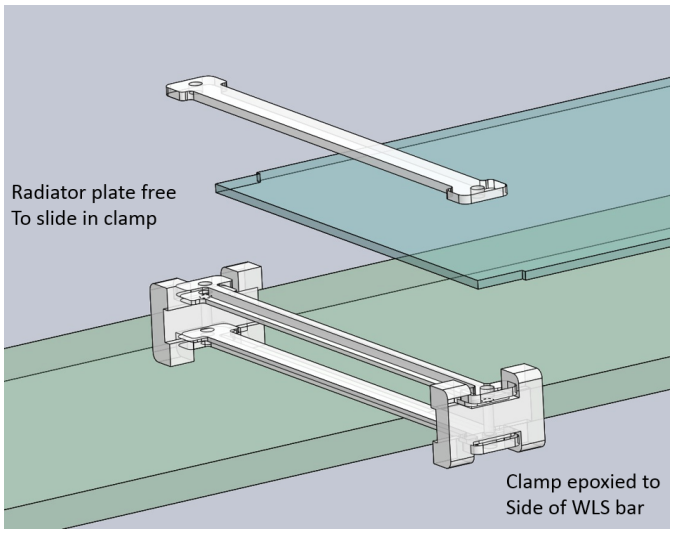

Figure 2.52: Mounting of the radiator plates to the WLS bar for the reference design scheme

fig:PD_r

The second design uses the same mounting, but with no radiator plates installed. Instead, an acrylic light-guide bar is dip-coated with a solution of TPB, solvents, and a surfactant to produce a wavelength-shifting layer on the outside surface of the bar. The 128-nm VUV scintillation light is shifted to blue light within the surface coating and transmitted directly through the lightguide to the photosensor. Because the design uses only one wavelength shifting step, potential efficiency increases are possible.

2.7.3 Sensors

The planned photodetector is a SiPM, model SensL C-Series 6 mm^2 (MicroFB-60035-SMT). This model of SiPM has a detection efficiency of 41%; the quoted detection efficiency incorporates Quantum Efficiency (QE) and the effective area coverage accounting for dead space between pixels. At LAr temperature (89 K) the dark rate is of order 10 Hz (0.5 p.e. threshold), and after-pulsing has not been observed. An on-going testing program is in place to ensure that the SiPMs can reliably survive the stresses associated with any thermal cycling in LAr and long-term operation at LAr temperature.

All photodetectors are subjected to testing to determine forward and reverse bias I-V curves, breakdown voltage, dark current and dark count rate, photodetector gain, crosstalk estimation, response, and bias dependence of parameters.

Each SiPM is tested before mounting on the readout boards to determine if the part meets the

specifications in a warm test. After mounting to the readout board all items are tested both warm and cold (cyrogenic temperature) to determine the operating characteristics.

In addition to these tests, the photodetectors are tested for their response to light signals from an LED of appropriate wavelength. These tests will be sensitive enough to determine if one of the three SiPM elements operating in parallel is not functioning.

2.7.4 Mechanical design and installation

The PDS is configured as a set of *modules* that are mounted on the APA frames. A PDS module is the combination of one light guide (also called a "bar" due to its shape) and 12 SiPMs, as shown in Figure 2.51 (a). The APA frames hold ten PDS modules, approximately 2.2-m long, 86-mm wide and 6-mm thick, equally spaced along the full length of the APA frame, as shown in Figure 2.51 (b). The light guides are inserted into the APA frame on rails gliding on their radiator plate mounting blocks, as shown in Figure 2.53 (right).

fig:PD_overview
fig:PD_overview
fig:PD_mounting_inslide

check if right figure ref

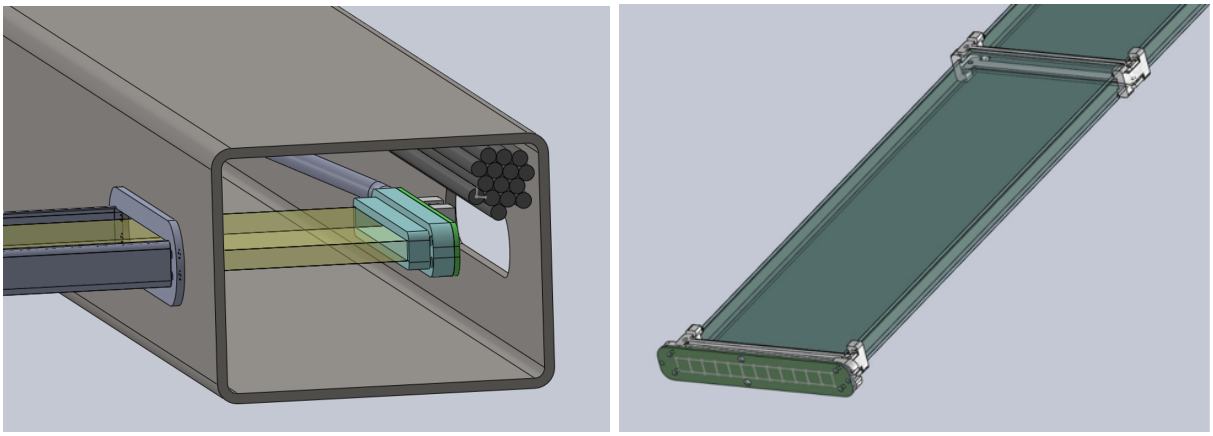

Figure 2.53: (left) Rendering of the installation of a PDS module into an APA frame, shown just before it comes to rest on the inside face of the APA tube. (right) Rendering of the the SiPM mounting board installed on the end of the PDS module before insertion.

fig:PD_m

The mounting system has been tested using a prototype PDS module as shown in Figure 2.54.

fig:PD_flat_instal

Each photon detector has a single SiPM mounting board with 12 surface-mount SiPMs mounted on its face as shown in Figure 2.55 (left). Four groups of 3 SiPM elements go to single channels of the readout electronics in order to reduce the overall system cost. The board is held close to the bar, without touching, using four screws that go into tapped holes on the end mounting block that is glued to the bar. The mounting block assembly is shown in Figure 2.53 (right) The circuit board also has holes at each end for mounting to the APA frame.

fig:PD_SiPM_PCB_front
fig:PD_mounting_inslide

The cabling plan for the system has one cable with four shielded twisted pairs connected to each SiPM mounting board via the surface mount RJ-45 connector shown mounted on the back of the

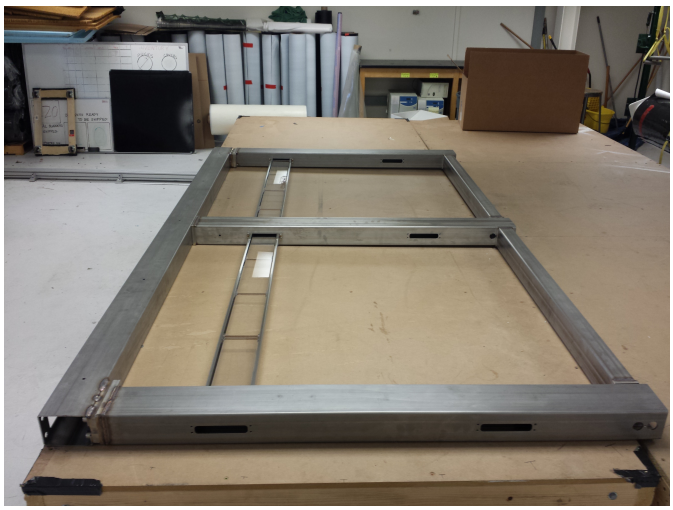

Figure 2.54: Photograph of the installation test of a mock PDS module in a 1/5 section of an APA frame. fig:PD_f

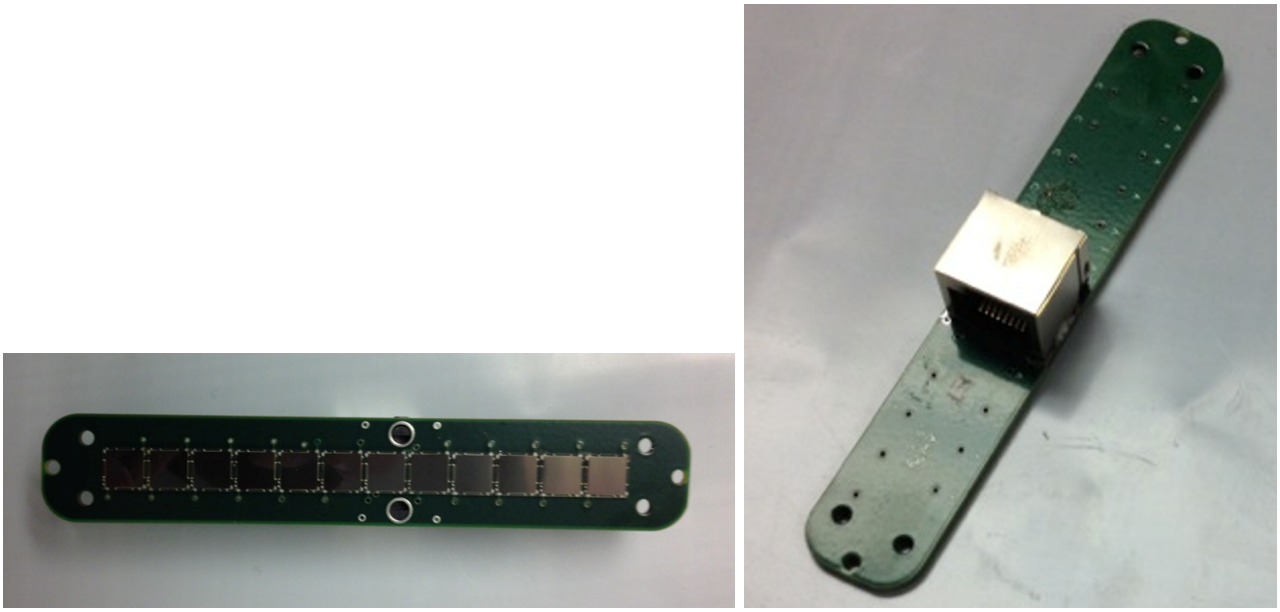

Figure 2.55: Photograph of a SiPM mounting board with the full complement of 12 SiPMs installed on the board (left), and with the RJ-45 connector for the cable (right). fig:PD_S

readout PCB in Figure 2.55 (right). The cables run through the APA tubing to the top of the APA frame as seen in Figure 2.56. The cable bundles are installed and connected after the PD has been installed into the slot.

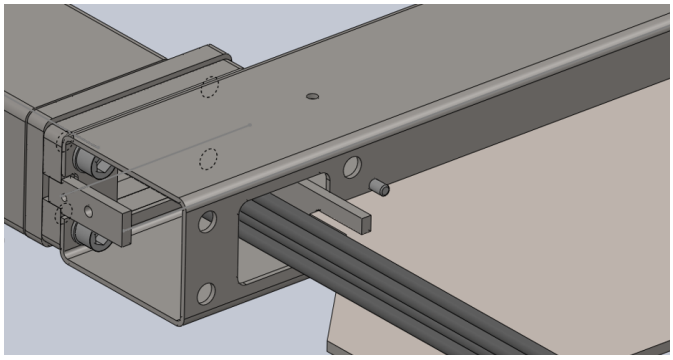

Figure 2.56: Diagram showing the routing of the PDS cables through the APA frame.

2.7.5 Alternative photo detector under development

While a sufficient number of the two types of PDS modules are being produced to fully outfit the detector, it is possible that a few of the 60 APA slots will be used to house experimental photon detectors. One type of detector that is being developed in an attempt to increase the light detection eficiency is referred to as the ARAPUCA design.

The ARAPUCA design is based on a new technology that allows for the collection of photons in a 5×5-cm^2 window with detection efficiencies at the level of several percent. The trapped light is detected by two SIPMs (SensL 60035 - 6×6 mm^2 active area each). The basic concept behind the ARAPUCA design is to trap photons inside a teflon box, of dimensions of $5\times5\times1$ cm^3, with highly reflective internal surfaces, such that the detection efficiency of the trapped photons remains high even with limited sensor coverage on these internal surfaces [3].

Photon trapping is achieved by using a wavelength-shifting technique coupled with the technology of the dichroic shortpass optical filters. The latter are multilayer acrylic films with the property of being highly transparent to photons with a wavelength below a tunable cut-off while being almost perfectly reflective to photons with wavelength above the cut-off. A dichroic shortpass filter deposited with two different wavelength shifters (one on each side) is the core of the device. In particular, it serves as the acceptance window for the ARAPUCA device. The rest of the device is a flattened box with highly reflective internal surfaces (PTFE, 3M-VIKUITI ESR, ...), closed on the top by the dichroic filter deposited with the two shifters. A fraction of the internal surface of the box is occupied by the active photo-sensors (Silicon Photomultipliers, or SiPMs) that detect the trapped photons.

It is envisioned that several of these devices could be installed on the detecotr to directly compare their performances with those of the other PDS modules. A mechanical solution has been developed such that 16 of the ARAPUCA devices can be installed on the same mounting structure used for the other PDS modules as shown in Figure 2.57.

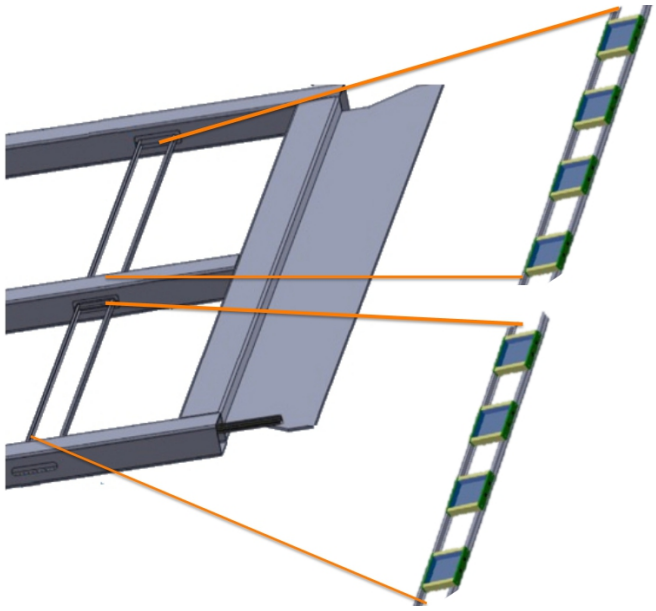

Figure 2.57: One ARAPUCA array of eight devices installed in a APA frame in place of a scintillating bar.

The readout scheme foresees the ganging of the SiPMs from two ARAPUCA devices (four sensors total). The 16 devices on one mounting structure then have a total of four readout channels, which can take advantage of the same cabling and readout scheme used for the other PDS modules.

2.7.6 Photon detector UV-light monitoring system

A UV-light-based monitoring system is used to monitor the relative performance and time resolution of the system. The system uses external UV LEDs (245-280 nm) as light sources in the VUV wavelength range, which are coupled to quartz fibers to transmit light from outside the detector volume to desired locations on the CPA plane. Light diffusers located on the CPA surface uniformly illuminate the APA area containing the PDS. The UV light system is used in association with cosmic ray muon tracks and Michel electrons as means of calibration. The UV light essentially mimics physics, although at a different wavelength starting from the wavelength-shifter conversion, light guide propagation, photo-sensor detection and the front-end electronics readout.

The external UV-light monitoring system is designed with the following goals:

- No active components within PD/APA;
- Provide uniform illumination over the APA surfaces;

In terms of technical requirements the system needs to:

- provide light levels down to a single p.e. for individual photon-detector channels,

- provide higher light levels to test linearity of the PDS,
- provide variable pulse width to test the time resolution of the photon detector response, and

Figure 2.58 illustrates the system design schematically. The system consists of a 1U rack mount Light Calibration Module (LCM) sitting outside the cryostat. The LCM generates light pulses that propagate through a quartz fiber-optic cable to diffusers at the CPA to distribute the light uniformly across the photon detectors mounted within the APA. Five light diffusers on the CPA plane are used: one in the center and four diffusers close to the CPA corners.

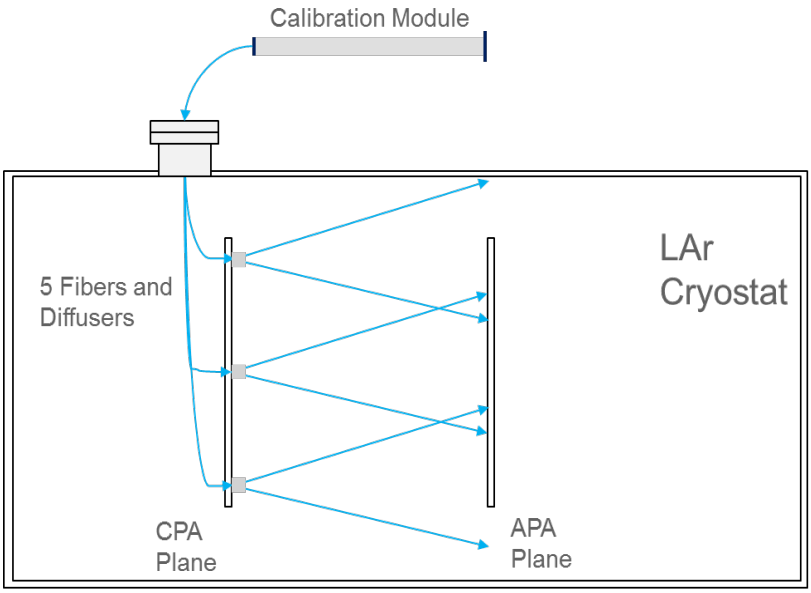

Figure 2.58: Concept of the UV-light monitoring system for the photon detector in liquid argon.

The LCM utilizes the logic and timing control of the photon-detector readout electronics (*SSP*) unit, described in Section 2.8. A single SSP board was repackaged into a deeper rack mount chassis that accommodates a new internal LED Pulser Module (LPM) and an additional bulk power supply. The LPM utilizes five digital outputs from the SSP board to control the LPM pulse and its duration. These outputs are derived from the charge injection control logic within the SSP's FPGA. The even-channel SiPM bias Digital to Analog Converters (DACs) are used to control the LPM pulse amplitude. The adjacent odd channels are used to read out a reference photodiode used for pulse-by-pulse monitoring of the LED light output. The output of the monitoring diode is available for normalizing the response of the SiPMs in the detector to the monitoring pulse.

The controlled source of light in this monitoring system is used to perform time offset and time resolution measurements. Many effects contribute to a finite time resolution, including the relative time offset of photon-detector channels, scintillation time constants, photon conversion with wavelength shifter, photon propagation through photon-detector paddle, SiPM jitter, and the resolution of the readout electronics. Most of these effects are constant and can be individually measured on the bench. The UV light monitoring system monitors overall stability of the photon detector in

both time and amplitude.

2.8 PDS electronics

Scintillation light from LAr comes from two different excited states with lifetimes of about 6 ns and 1.6 μs. Only a limited amount of light is collected, so the electronics are designed to collect the light from both excited states. A summary of the general requirements for the system, including initial requirements from a physics performance perspective, are given in Table 2.7.

Table 2.7: Physics requirements for the PDS electronics

Performance Parameter	Target
Time Resolution	Better than 30 ns wrt event time zero ("t0")
Charge Resolution	0.25% photo-electron equivalent
Dynamic Range	$\sim$ x10 better than detector (1000:1)
Linearity	Sufficient to resolve 1 photo-electron signals
Multi-Hit Capability	Sufficient to measure Triplet (late) Photons
Dead Time	Live up to 2 drift times either side of beam spill
Bias Control	0.1 V resolution up to 30 V per channel
Calibration	On-board Charge Injection
Timing	Events time-stamped using NOνA Timing or equivalent syst.

There are no PDS front-end electronics in the LAr cold volume. The un-amplified signals from the SiPMs are transmitted directly to outside the cryostat for processing and digitization, with the advantage that the infrastructure required for inside the cryostat is reduced (power, data cables, precision clocks, data protocols, etc.). A custom module, called the SiPM Signal Processor (SSP), receives the SiPM signals outside the cryostat.

An SSP consists of 12 readout channels packaged in a self-contained 1U module. Each channel contains a fully-differential voltage amplifier and a 14-bit, 150 MSPS analog-to-digital converter (ADC) that digitizes the waveforms received from the SiPMs. The front-end amplifier is configured as fully-differential with high common-mode rejection, and receives the SiPM signals into a termination resistor that matches the characteristic impedance of the signal cable. Currently there is no shaping of the signal, since the SiPM response is slow enough relative to the speed of the digitization to obtain several digitized samples of the leading edge of the pulse for the determination of signal timing.

The digitized data is stored in pipelines in the SSP, for up to $\sim$ 13 μs. The processing is pipelined, and performed by a Xilinx Artix-7 Field-Programmable Gate Array (FPGA). The FPGA implements an independent Data Processor (DP) for each channel. The processing incorporates a leading edge discriminator for detecting events and a constant fraction discriminator (CFD) for sub clock timing resolution. Because the FPGA is programmable and accessible, it is possible to explore different data processing algorithms and techniques, and even customize the readout for

a given type of event (supernova for example.) A picture of the module is shown in Fig. 2.59. A block diagram of the system is shown in Fig. 2.60.

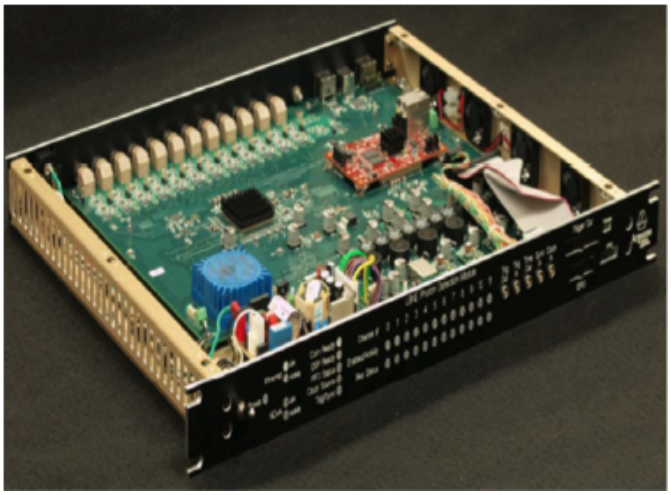

Figure 2.59: Picture of SSP module.

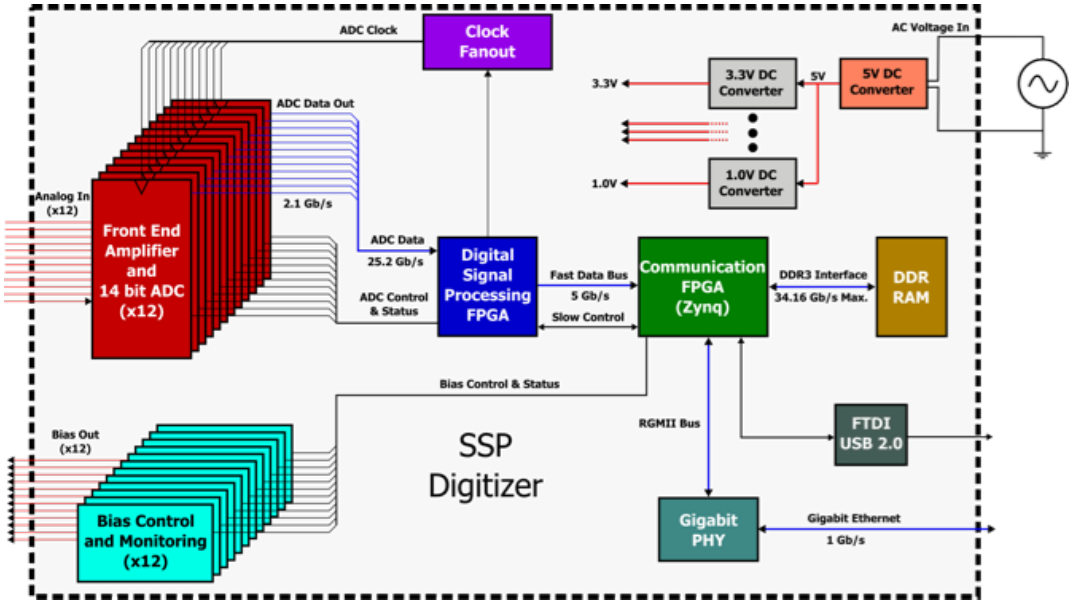

Figure 2.60: Block diagram of the SSP Module.

In the simplest mode of operation, the module performs waveform capture, using either an internal or external trigger. Up to 2046 waveform samples may be read out for each event. When waveform readouts overlap the device can be configured to offset, truncate or completely suppress the overlapping waveform. Pile-up events can also be suppressed.

In order for the events measured in the photon detector to be matched up with the corresponding events in the TPC, the front-end electronics attaches a timestamp to the data as it is acquired. The timestamp is unique, and has a correspondence with the timestamps in the TPC electronics processing. The timestamp in the SSP is applied to the event data as it is digitized. In the case where zero-suppression and data sparsification are used, the timestamp on accepted data remains intact. To achieve this, the TPC and PD electronics must be synchronized, including timestamp

counter resets, based on a known and stable calibration for the timing resolution of the ADC conversion between the two systems.

A Xilinx Zynq FPGA, onboard the MicroZed system-on-module, handles the slow control and event data transfer. The SSP has two parallel communication interfaces; USB 2.0 and 10/100/1000 Ethernet. The 1 Gb/s Ethernet supports full TCP/IP protocol. The module includes a separate 12-bit high-voltage DAC for each channel to provide up to 30 V of bias to each SiPM. The module also feature charge injection for performing diagnostics and linearity monitoring, and also voltage monitoring.

In tests to date, the SSP is capable of measuring single photo-electron signals coming from the SiPMs over a cable length of 30 meters when the SiPMs are operated at LAr temperatures. The timing resolution of the signals has been measured to be better than 3 ns. The full-differential signal processing in the front-end circuitry is important in achieving this result.

As noted previously, three PDS SiPM signals are ganged together into a single readout channel. A multi-conductor cable with four twisted pairs is used to read out PDS modules, each of which incorporates 12 SiPMs.

2.9 Data Acquisition (DAQ)

sec:daq

2.9.1 Scope and requirements

The data acquisition (DAQ) system is shown in Figure 2.61 along with its interfaces to the cold electronics, beam instrumentation, and online computing systems.

fig:daq-overview

Figure 2.61 requires significant zooming to read. Need a simpler diagram initially to show the major pieces, and only the DAQ pieces. Also some descriptive text; relate the physical components to data rates and such.

List components: timing, trigger, throttle systems, FPGA-based master, etc.

The physics requirements of ProtoDUNE-SP are the primary drivers of the DAQ system requirements. The front-end electronics and assumed bandwidth and storage requirements from the online and offline computing systems impose additional constraints.

The run plan (see Section 1.4) calls for about 25 M analyzable beam events to be collected in the first run of ProtoDUNE-SP. Data sets may be enhanced in desirable particle types and energies with dedicated triggers (such as PID) from the beam instrumentation. The latter is described in Section 5.3.

sec:runplan

sec:beaminstruments

Parameters of the data collection plan are listed in Table 2.8. The lossless compression factor cited in the table is based on the assumption that the signal-to-noise level is similar to or better than

tab:goldi

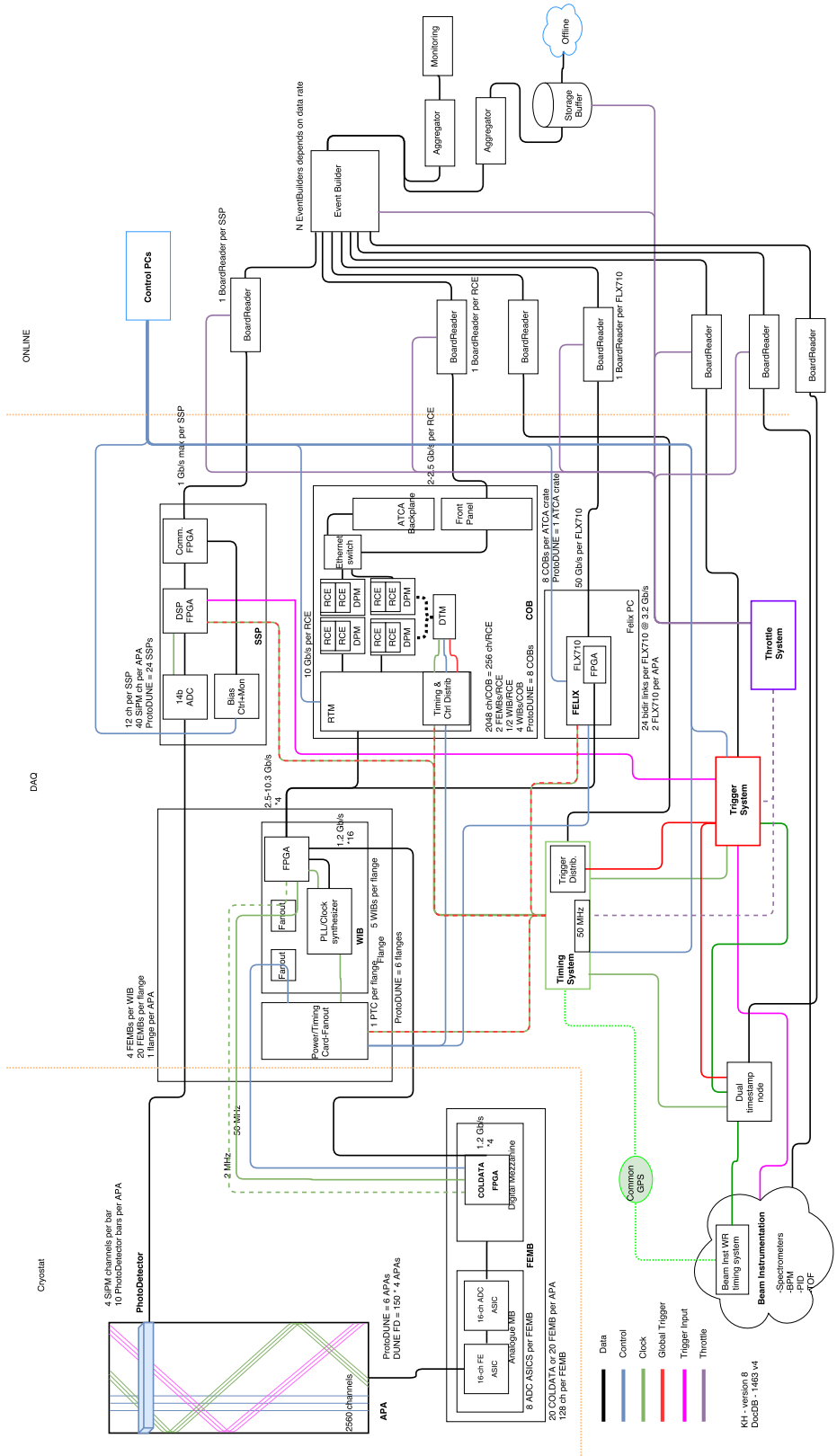

Figure 2.61: Detailed overview of the DAQ system, its interconnections, data flow, timing and control signals, and the interfaces to the electronics and online computing systems

fig:daq-

that achieved by MicroBooNE.

needs citation

Table 2.8: Parameters defining data rate and volume in the "most likely" scenario v5 [4]. The buffer depth includes both the in-spill and out-of-spill data.

Parameter	Value
Trigger rate	25 Hz
Spill duration	4.8 s
SPS Cycle	22.5 s
Readout time window	5 ms
# of APAs to be read out	6
Single readout size (per trigger)	230.4 MB
Lossless compression factor	4
Instantaneous data rate (in-spill)	1440 MB s^{-1}
Average data rate	576 MB s^{-1}
3-Day buffer depth	300 TB

The baseline trigger rate during the SPS spill is taken to be 25 Hz. Cosmic data are also acquired at an appropriate rate such that bandwidth and processing priority are given to beam data. The data rate from the electronics is dominated by the TPC data. However, the photon detection system (PDS) can produce a signifcant amount of calibration data (where full waveforms are extracted), during commissioning and special runs (up to 24 Gb/s maximum).

The TPC data are sent via the Warm Interface Boards (WIB) on the cryostat flanges for the six APAs, un-triggered at a total rate of 480 Gb/s. The PDS is estimated to send data at a total rate of 1.2 Gb/s from the 24 SSPs (detailed further in Section 2.9.6). The maximum bandwidth from the ProtoDUNE-SP online system to CERN IT (and hence, the offline world), is 20 Gb/s at a maximum. Therefore, the DAQ system must reduce the data by a significant fraction before they are sent offline. This is achieved by a combination of data compression and triggering.

2.9.2 Timing, trigger and beam interface

The timing and trigger are two distinct subsystems. The timing system provides the distribution for the trigger signals over the same fabric as the clock and calibration signals.

Timing

The timing system is required to provide a stable and phase-aligned master clock to all DAQ components; synchronize external signals into the ProtoDUNE-SP clock domain and time-stamp them; distribute synchronization, trigger and calibration commands to the DAQ system; and

conduct continuous checks of its own function. In addition, the timing system acts as a data source, providing a record of triggers received, distributed, or throttled. The system is designed to meet the full eventual requirements of the DUNE experiment, but needs only a subset of that functionality for ProtoDUNE-SP. For instance, absolute time-stamping with respect to an external GPS reference is not required.

An FPGA-based master unit receives a high-quality clock signal (from a quartz crystal oscillator or external source) and external signals from the trigger system and SPS accelerator. It interfaces to the ProtoDUNE-SP control and DAQ via a gigabit Ethernet interface. The master unit multiplexes synchronization and trigger commands, along with arbitrary command sequences requested by software, into a single encoded data stream, which is broadcast to all timing endpoints, and decoded into separate clock and data signals. A uniform phase-aligned cycle counter, updating at the ProtoDUNE-SP system frequency of 50 MHz, is maintained at all endpoints, allowing commands to take effect simultaneously at all endpoints regardless of cable lengths or other phase delays.

The timing signal is broadcast via multi-mode optical fiber (for medium-distance connection to the WIB crates on the detector) and LVDS signals are sent over twisted-pair cable (for short-distance connection to RCEs, SSPs and FELIX modules). Optical signals are fanned out and recombined using commercial 32:1 passive splitters, and active optical–LVDS converter boards further split the signals for local distribution to endpoints.

Endpoints decode the timing signal into separate clock and data signals using a commercial clock-data recovery ASIC [5], which in turn feeds a low-bandwidth phase-locked loop (PLL) in order to remove any remaining jitter in the clock and provide phase adjustment. The data stream employs 8b/10b encoding, ensuring sufficient transitions in the timing signal for clock recovery and correct operation of optical links, and uses scrambling of idle patterns to minimize electromagnetic interference (EMI). A common firmware block is used to decode the timing protocol, which is incorporated into the overall firmware design of the receiving FPGA in each DAQ component.

Trigger

The baseline trigger solution for ProtoDUNE-SP is the Central Trigger Board (CTB). The triggers expected for the CTB are a beam minimum bias trigger, an electron beam trigger, and, if possible, a π/K/p will also be added. The CTB provides a means to select the most interesting physics events during the beam spill and suppress inter-spill background events (or events so busy to prohibit accurate reconstruction). The final trigger selection will be driven by ProtoDUNE's physics goals. The CTB is designed to receive triggers from various subsystems (Photon Detection System, Beam Instrumentation, SPS spill signal, veto signals, etc.). Up to 100 input channels are provided. It combines these into a global trigger based on a configurable input mask (or more sophisticated algorithm, if desired). It provides functionality to globally time-stamp triggers, keep event counts, and provide artDAQ-compatible (see Section 2.9.7) header information with trigger type and error conditions. Internally generated triggers and calibration pulses allow for testing the board itself and the end-points receiving the trigger signals.

The CTB is based on the MicroZed development board [6], which comprises a Xilinx Zynq-

7000 System-on-Chip (SoC), 1-GB DDR3 RAM, Gigabit Ethernet, and 115 I/O ports. The Programmable Logic of the Zynq-7000 is used to perform fast triggering operations, whilst the Processing System is used to interface to the readout and controls systems.

Configuration and operation is performed using an XML file which is sent to the CTB. This allows for fast reconfiguration of the CTB without the need for new firmwares. The file is used to both configure the board and send start/stop/reset, etc., commands from the run control. The trigger output format consists of a trigger type (physics/calibration/random), a time-stamp, the trigger word, counter information and the values of the inputs causing the triggers. The trigger system uses the timing system clock and global triggers are distributed via the timing system.

Beam Interface

The beam instrumentation is described in Section 5.3. The beam instrumentation DAQ and the DAQ for ProtoDUNE-SP have separate timing systems. A common GPS clock is used to keep both systems synchronized relative to each other. A common endpoint receives time stamps from both WhiteRabbit (for the beam instrumentation) and the ProtoDUNE-SP timing system, which are used to create a matching table from the two systems. Data from the beam instrumentation are acquired continuously via a separate DAQ path. Triggered data for ProtoDUNE-SP includes TPC, PDS, and beam instrumentation data, as well as the timestamps and trigger information associated with each.

2.9.3 TPC data readout

The readout of the TPC wires, prior to being received by PCs in the back-end DAQ, consists of CE on the APAs inside the cryostat and the warm electronics outside the cryostat on the flange. CE data are received on the WIBs which are housed in the WECs, situated on the top of the flanges.

Each WIB receives the data from four FEBs over sixteen 1.25-Gbps data lines, and multiplexes these data to four 5-Gbps (or two 10 Gbps) lines that are sent over optical fibers to the DAQ.

Two systems are used to receive data from the WIBs. The default system is based on Reconfigurable Computing Elements (RCE) and a proposed alternative system is based on the Front-End-Link-EXchange (FELIX) technology.

2.9.4 RCE-based readout

The data from the WIB are received by processing units called RCEs (Reconfigurable Cluster Element), [7] which are housed in industry-standard ATCA shelves on COB (cluster-on-board) motherboards that are designed at SLAC for a wide range of applications. The RCE is a SoC

from the Xilinx Zynq family and contains a full Linux processor system on the chip accompanied by 1 GByte of DRAM. The primary processing functions of the RCEs are compression (and/or zero-suppression) and buffering of the raw data and then sending data to the back-end upon the receipt of an external trigger. Each COB carries eight RCEs, all connected to each other via an on-board 10-Gbps Ethernet switch, which also sends data out of the COB to the back-end DAQ PCs.

The interface with the WIB is provided via the ATCA compliant rear-board, the RTM (Rear Transition Module). This application-specific board uses a set of QSFP transceivers to receive the data from the WIB and an SFP+ (small form-factor pluggable) optical interface for communication with the timing and trigger distribution system.

As the multiplexed data from the WIB come into the RCE FPGA fabric, it is de-multiplexed and buffered into per-channel, fixed-time-length chunks (for instance 512- or 1024-ticks). These chunks are compressed and written to the DRAM where the RCE processor waits for a trigger (also handled by the FPGA) to arrive. Upon a trigger, the processor sends data for a fixed window in time, including pre- and post-trigger time chunks for all channels, to the back-end PCs.

For ProtoDUNE-SP, 256 wires worth of data (2 FEBs) are sent to each RCE. Given that there are 120 FEBs in ProtoDUNE-SP, 60 RCEs are needed to readout the full detector. These fit into eight COBs which in turn reside in a single 14-slot ATCA shelf.

2.9.5 FELIX-based readout

The FELIX is a PCIe card receiving data on point-to-point links from the detector electronics and routing those through a switched network to computers. The aim is to reduce to a minimum any specific hardware developments and to fully rely on commercial networks and servers to perform the DAQ tasks. For ProtoDUNE-SP, data from five WIBs (20 FEBs) are read out over ten 9.6-Gbps links into two FELIX cards. Grouping time slices around a trigger signal, as well as data compression, is dealt with in software. Similar to the RCE-based readout, the FELIX generates artDAQ fragments to be sent to the event builder.

2.9.6 PDS and beam instrumentation data readout

-readout

A combination of externally triggered events and self-triggered events make up the PDS data. The external triggers come from the beam instrumentation via the trigger system at 25 Hz. This amounts to 118 Mb/s. The self-triggered data are induced by cosmic rays. A cosmic rate of 10 kHz is assumed, totalling 1106 Mb/s. The combined rate comes to ≈1.2 Gb/s. An alternative scheme with just self-triggered header-only data with a resultant rate of ≈1.1 Gb/s is considered for implementation if the former proves difficult.

2.9.7 Event-building software

Developed within the Fermilab Scientific Computing Division and already used for the 35-t prototype, *artDAQ* provides data transfer, event building, and event analysis functionality. This latter feature includes built-in support for the *art* event analysis framework, also developed at Fermilab [8], allowing experiments to run art modules for real-time filtering, compression, disk-writing and online monitoring. As art is also used for offline analysis, a major advantage of artDAQ is that it allows developers to easily switch between developing online and offline software.

ArtDAQ provides three types of processes, each of which fulfills a specific role. In the order of upstream-to-downstream, these are boardreader processes, eventbuilder processes, and aggregator processes. A given boardreader process is intended to be associated with a particular geographical region of the detector, and provides hooks (in the form of C++ base classes) for an experiment's developers to embed experiment-specific code (called "fragment generators"), designed both to upload configuration values to hardware and to read out the hardware. For ProtoDUNE-SP, the full DAQ consists of 87+ boardreaders, in charge of the 60 RCEs, 24 SSPs, the timing system, the Penn Trigger Board, and at least one for the beam instrumentation. For testing purposes, fragment generators can perform useful functions such as providing a "playback" mechanism," and modeling sudden or unexpected data flow events.

Downstream of the boardreader processes are the eventbuilder processes. An eventbuilder receives data from every boardreader (a chunk of data from one boardreader corresponding to an event is referred to as a "fragment"), and assembles the fragments for a given event into a raw, complete data event. Optionally, filtering via art modules can be performed at this stage.

The most downstream process type is the aggregator. Traditionally in artDAQ-based DAQ systems, there are two aggregators, one in charge of writing data to disk and reporting aggregate statistics (e.g., MB/sec), and one in which experiments can run art analysis modules for real-time online monitoring. For ProtoDUNE-SP this model will change as artDAQ becomes more flexible and throughput capability increases. The functionality of aggregators may be replicated in eventbuilders. While this solution reduces the number of interprocess connections in the DAQ software, the number of processes assembling raw events is the same as the number of processes writing to disk.

For the 35-t prototype, artDAQ processes were controlled by a program called *DAQInterface*. DAQInterface takes charge of launching the artDAQ processes, checking for error states, and shutting down processes in an orderly fashion as needed, to avoid improperly closed output files, zombie processes, etc. For ProtoDUNE-SP, some of the functionality of DAQInterface (e.g., querying status) is shifting to JCOP (Joint Controls Project); DAQInterface code is reused as appropriate/possible, to minimize duplication of effort.

2.9.8 Control, configuration and operational monitoring

The artDAQ software used for all applications dealing with the movement, processing and storage of data is interfaced with software of the Joint Controls Project (JCOP) for the purpose of control, configuration and operational monitoring. JCOP provides a toolkit to implement run control (finite state machine (FSM), distribution of commands, error propagation and handling) as well as graphics tools that allow for the implementation of user interfaces and monitoring dashboards.

In order to minimize the software development needs, the same FSM as defined by artDAQ is implemented and commands are sent to the applications using the already supported XML-RPC protocol. Monitoring data are pushed into the JCOP framework by implementing the appropriate artDAQ monitoring plugin. Log and error messages will be most probably collected and processed using an implementation of the ELK (elastic search, logstash, kibana [9]) stack. The internal configuration of DAQ applications are carried out using the mechanisms provided by artDAQ. The overall system is modeled and configured using the JCOP paradigm (data points).

2.9.9 Interface of the DAQ to the online storage

The software framework for interfacing with the electronics, building events, writing data files, and providing an interface to online monitoring of data as they are acquired is *artdaq* [10].

Computers running BoardReader processes read out the RCEs and SSPs and transmit data to a set of computers running EventBuilder processes. These computers and a pair of 10 Gbit/sec NIC provide the CPU and networking needed to build events, collect basic metadata, and send the data to storage and online monitoring. The Event Builders assemble data fragments into self-consistent events and perform basic data integrity checks before writing records out.

define NIC

Table 2.8 indicates a nominal trigger rate of 25 Hz for the mid-range scenario. Data are assumed to be collected based on prompt trigger signals generated by the beamline instrumentation in order to purify samples of desired particles.

Current estimates put the PDS data at approximately 10% of the TPC data rate. Beam instrumentation data are expected to be lower still. Although adding to the total data rate only slightly, adequate resources must be provisioned in order to acquire and store the data from these systems.

The network speed of all computers in the DAQ chain is anticipated to be 20 Gbits/sec. Computers running nearline processing of subsets of the data, which are generally CPU-bound, may be connected with 1 GBit/sec links.

Given that each RCE reads out 256 channels of the TPC, 60 RCEs need to be active. For the PDS, 24 SSPs are used. At least two computers running BoardReader processes are therefore used to read out the RCEs and transmit the data to the EventBuilder processes.

The online buffer layer consists of ∼300 TB of storage, which is connected directly to the Event Builders. The baseline storage option consists of two SAS arrays DAS with > 40Gbit/s bandwidth, redundant paths, controllers, and power supplies. A backup option for storage is an XRootD cluster [11] taking data directly from the Event Builders over the network.

After the data are written to disk by artDAQ, the data handling system creates metadata files, optionally runs nearline monitoring jobs, and transfers the data from EHN1 to the CERN Computing Center [12]. The *Fermi File Transfer Service* (F-FTS) software developed and maintained at Fermilab is the central element of the data flow management at this level.

2.9.10 Data-quality monitoring

In addition to the monitoring of the operations of the DAQ system, the quality of the data taken by the detectors has to be constantly monitored. This assurance is provided by the online and nearline monitoring systems. This subsection describes the baseline monitoring frameworks for ProtoDUNE-SP. The final implementation is subject to change, but will likely be similarly linked to artDAQ and LArSoft as described here.

Online monitoring

The online monitoring framework runs as a DAQ process and therefore is able to provide data quality assurance in real-time. ArtDAQ splits the data into distinct physics and monitoring streams via its aggregator processes. The data rate to the monitoring is tunable such that the monitoring can digest the data in a timely fashion. The software framework used for online monitoring consists of an `art::Analyzer` module which interfaces with the artDAQ framework and owns instances of further classes, each designed to handle different aspects of the monitoring.

The DataReformatters restructure the data to allow for efficient subsequent analysis and provide a standard interface to the methods, which look through the events. These reformatted objects are passed to MonitoringData, which owns all of the data products (`TTree`s, `TH1`s, `TGraph`s, etc.) output from the monitoring software and provides methods for filling them when required. Finally, the online event displays are contained within the monitoring framework using the EventDisplay class.

The output is then saved in a common area for offline access and for syncing with a web server. This is hosted at CERN and allows for remote monitoring of the experiment.

Nearline monitoring

The nearline monitoring is designed to provide complimentary information to that given by the online system. It runs separately as a series of automated shell scripts and provides feedback on

a slower timescale than the online monitoring, thus allowing for a broader view of the quality of data over time. It also utilizes offline software (LArSoft) to provide, for example, reconstruction, facilitating a more complete monitoring of much more complex information.

Once an output data file has been closed by the DAQ, it can be processed by the nearline system. A LArSoft job is initially run over the events to perform reconstruction and extract information from the data. The output of this, along with the output of other runs, is then analyzed by a separate automated job, to form the high-level view of the data for monitoring.
Similarly to the online framework, an interface for this system with the web allows for remote access of the information.

2.10 Cryostat and feedthroughs

2.10.1 Scope and requirements

This may need some massaging to put 'scope and req' at the beginning of this section

The cryostat consists of a steel warm outer structure, layers of insulation and an inner cold membrane. The outer structure (shown in Figure 2.62), which provides the mechanical support for the membrane and its insulation, consists of vertical beams that alternate with a web of metal frames. It is constructed to withstand the hydrostatic pressure of the liquid argon, the pressure of the gas volumes and satisfies the external constraints. In particular, this structure is to be constructed in EHN1 without any mechanical attachment to the floor or the building side walls.

what are the ext constraints? Also, the text on the figure is too small; is it intended to indicate what each color is? Can you clarify and make sure each part/color is labeled?

Inside the steel structure, a 10-mm thick skin of stainless steel plates are welded to provide a gas barrier to the outside. The top of the cryostat is accessible for installation of the detector elements, the electrical/signal feedthrough, the detector supports and other cryogenics services. The dimensions are dictated by the required active volume of LAr, constraints on the distances from the active volume to the cryostat inner walls and cryostat material thicknesses. The inner cryostat dimensions are: width = 8.548 m, length = 8.548 mm and height = 7.900 m. The dimensions ensure that all crossing penetrations are arranged as requested and that there is enough space for maintenance.

A secondary membrane is located within the insulation layer. The cold vessel is based on the GTT membrane technology [13]. Thermal requirements call for a thickness of 800 mm, including the insulation, and the primary and secondary membranes. These two membranes provide a first and second level of containment. There is no requirement at this point for additional containment at the level of the warm steel structure. The SS skin of 10-mm thickness between the warm structure and the insulation provides an effective gas enclosure, which allows control of the argon atmosphere

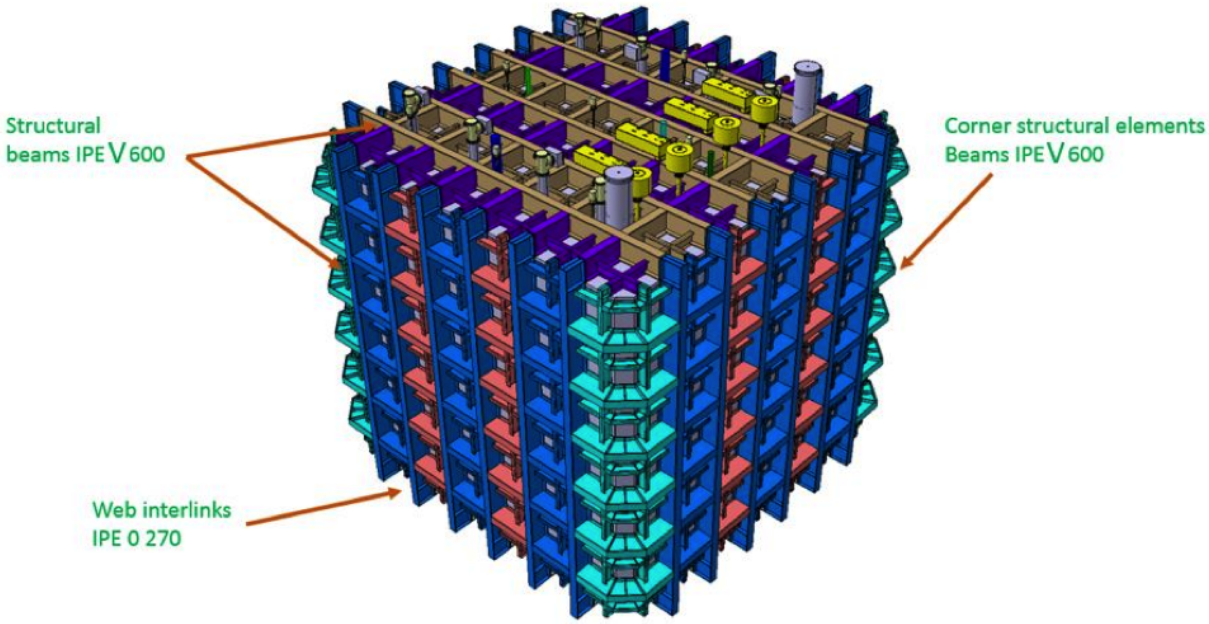

Figure 2.62: Warm vessel layout showing the various major components

fig:warm

inside the insulation volume. All necessary information can be found in [14]. The 3D detailed CAD model is visible in [15].

Prior to installation of the GTT insulation and inner membranes, the gas tightness of the SS 10-mm membrane will be measured and verified by CERN using dye penetrant analysis, local vacuum-bag techniques, and He leak detection at the level of the natural He present in the atmosphere ($\sim 2-3\times10^{-6} mbar/l/sec$). A report will be presented to GTT.

2.10.2 Storage characteristics

The cryostat is required to store LAr at a temperature between 86.7 K and 87.7 K with a pressure inside the tank of 950 < P < 1100 mbar. The thermal fluxes must be tightly controlled, i.e., they will be kept under 5 W/m2 on the inner membrane that is in contact with liquid, in order to prevent boiling of the LAr.

The storage parameters of the cryostat are as follows:

- The inner dimensions are 7900 mm high × 8548 mm length × 8548 mm wide. This corresponds to a total volume of ∼580 m^3.
- Tank liquid capacity (assuming a ∼4% ullage): ∼ 557 m^3
- Residual Heat Input (RHI): 5-6 W/m^2

- Insulation weight: 90 kg/m^3
- Insulation thickness (all included): 0.8 m
- Design pressure: Max 1350 mBar / Min 950 mBar. The 1350 mBar is for an accident condition during the cryogenics operation.
- Operating temperature: 86K-89 K

Figure 2.63 shows a side cross section of the cryostat with the inner dimensions of the cryostat, the thickness of the insulation and the overall outer dimensions of the warm structure.

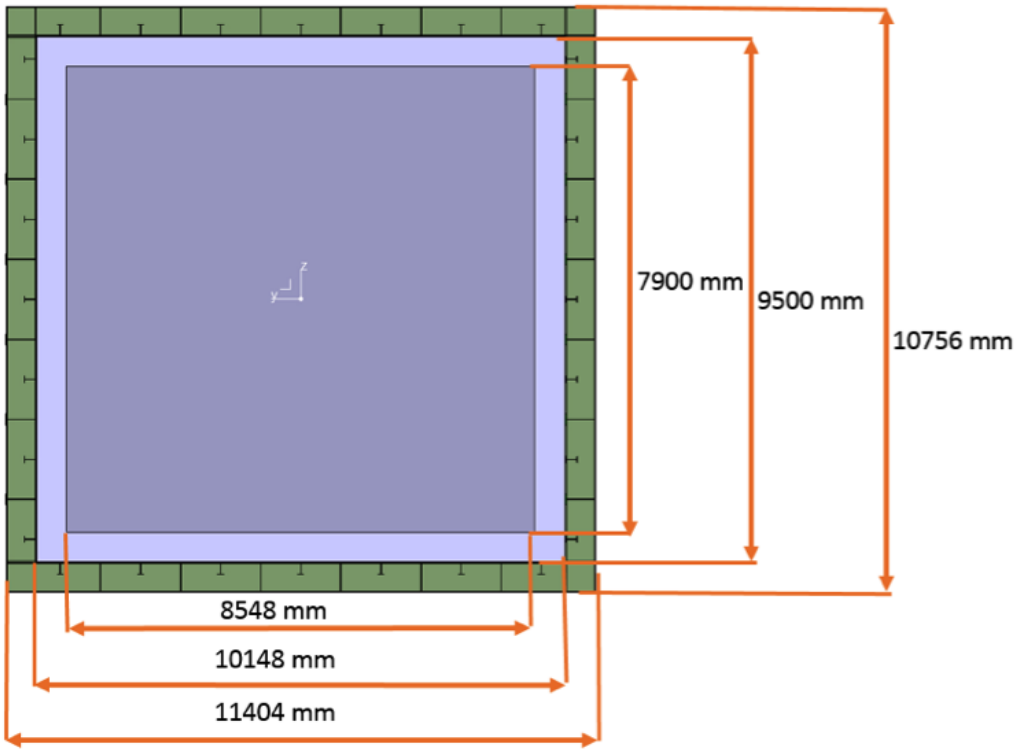

Figure 2.63: Cryostat overall dimensions

2.10.3 Cold GTT vessel

The GTT cold vessel is installed inside the warm support structure, which includes the stainless steel gas enclosure membrane. The cold vessel consists of a thermal insulation, a primary corrugated stainless steel membrane, as well as a secondary thin membrane, to provide primary and secondary liquid containment. A cross sectional view of the insulation and membrane layers is shown in Figure 2.64.

The primary membrane is made of corrugated stainless steel 304 L and is 1.2 mm in thickness.

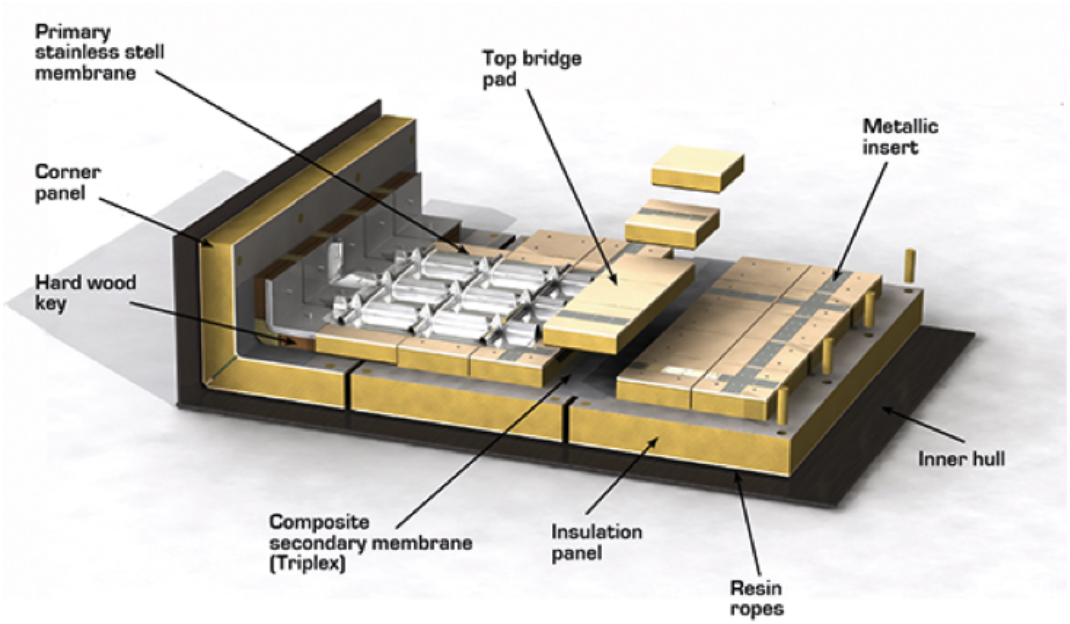

Figure 2.64: Cross section of insulation layers on membranes

fig:xsec

The standard size of the sheets is 3 m × 1 m. The secondary membrane is made of Triplex. This is a composite laminated material of a thin sheet of aluminium between two layers of glass cloth and resin. It is positioned inside the prefabricated insulation panels between two of the insulation layers. The insulation is made from reinforced polyurethane foam. The insulation panels are bonded to the inner 10 mm skin using resin ropes. The insulation layers are instrumented with gas inlets, outlets, temperature and pressure sensors.

2.10.4 Temporary Construction Opening (TCO)

A dedicated access window is necessary to install the ProtoDUNE-SP detector. This is referred to as the temporary construction opening (TCO) and shown in Figure 2.65. This means that no insulation of membrane can be installed at the beginning in this location. Once the detector installation has progressed as far as possible and all of the large TPC components are inside the cryostat, the TCO will be closed. The 10-mm SS skin, insulation and cold membranes are installed and welded in place.

fig:front-tco-np04

2.10.5 LAr pump penetration

To keep the high level of purity required, LAr is extracted from a point as low as possible in the cryostat and pushed by cryo-pumps to the external filtering system through the liquid recirculation circuit. A special penetration is thus required on one side wall of the cryostat to connect through a dedicated system of safety valves to the liquid argon pumps. This penetration requires a local modification of the insulation panels and the SS primary membrane, and consists of a crossing

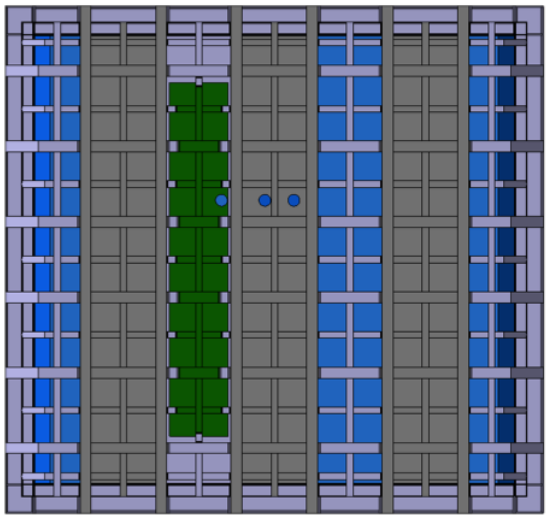

Figure 2.65: Front view of the cryostat with the TCO for the NP04 cryostat shown in green. fig:fron

tube with a diameter of 168 mm for the insulation and the membrane, and a larger-diameter hole at the stainless steel plate.

2.10.6 Beam window penetration

amwindow

Once constructed, the ProtoDUNE-SP detector will be exposed to the charged particle beam from the SPS accelerator. To minimize energy loss and multiple scattering of the beam particles in the dead material of the cryostat and its insulation, a beam window is inserted at the primary beam position as defined in Section 5.1. sec:beamrequirements

The vacuum pipe of the beamline has an external diameter of 219 mm. The beam window is being designed with a dimension of 250 mm in diameter to allow for alignment tolerances. The direction of the beam window follows the one of the beam. The outer portion of the beam window penetration is a vacuum pipe that extends from the H4 beamline (see Section 5.2) through the outer insulation layer and ends at the secondary membrane. A safety valve at the cryostat entrance ensures fast segmentation of the vacuum in case of accident. The portion of the foam insulation between the secondary and the primary membrane is replaced with a lower density foam (9 kg/m^3). To maintain structural integrity, the plywood supporting the primary membrane in the vicinity of the beam window penetration is replaced with a Nomex honeycomb plate sandwiched between thin G10 or Carbon layers. Nomex is a polymer material with high thermal resistance and Nomex sandwiches are well known for their structural resistance, and have already been used at cryogenic temperatures in the ATLAS detector. In this design, both the primary and secondary stainless steel membranes remain intact. Care has been taken to position the beam window exit on the interior of the cryostat to match a flat section of the corrugated primary SS membrane. Thermal and stress analyses are being conducted in collaboration with GTT. These will influence the detailed design sec:h4beamline

of the first segment of the beam window. The total amount of material in this design, including the primary membrane, and assuming a 0.3 mm G10 thickness on both sides of the Nomex sandwich and a 0.3-mm-thick steel beam window, is equivalent to 10% of a radiation length.

2.10.7 Roof signal, services and supports penetrations

The penetrations through the cryostat have been arranged by position and diameter. Most of the penetrations are placed on the ceiling of the cryostat. They have been differentiated into two main groups according to their function and the thermal stresses they will be submitted to. The classification determines whether penetrations can be used to support the weight of the detector or not. The penetrations on the roof of the NP04 cryostat are detailed in Table 2.9. A 3D CAD model to identify all positions can be found at [16] and in an associated drawing [17].

Table 2.9: Cryostat penetrations in roof and on side.

Component	Quantity	Value
West TPC translation suspension:	crossing tube diameter	200 mm
Center TPC translation suspension:	crossing tube diameter	200 mm
East TPC translation suspension:	crossing tube diameter	200 mm
Signal cable chimney FTs:	crossing tube diameter	250 mm
Spare on Signal cable row FTs:	crossing tube diameter	250 mm
Laser FTs:	crossing tube diameter	160 mm
Calibration Fiber CPA FT:	crossing tube diameter	250 mm
Spare on CPA line FTs:	crossing tube diameter	150 mm
HV FT:	crossing tube diameter	250 mm
Manhole:	crossing tube diameter	710 mm
Angled beam windows – west side:	crossing tube diameter	250 mm
	Vertical: 11.342°	
	Horizontal: 11.844°	
TCO - side:	1200mm × 7300mm	
Cryogenic pipes - roof:		
	crossing tube diameter	250 mm
	crossing tube diameter	304 mm
	crossing tube diameter	152 mm
	crossing tube diameter	125 mm
	crossing tube diameter	250 mm
Cryogenic pipes – north side:	crossing tube diameter	168 mm

2.10.8 Detector Support Structure (DSS)

Prior to the installation of the TPC, the detector support structure DSS is installed inside the cryostat. The DSS is shown in Figure 2.66. It is positioned near the ceiling and is supported by nine penetrations through the cold side of the membrane extending up to the warm structure of the cryostat. The warm structure of the cryostat supports all of the loads from the detector. The DSS consists of two layers of I beams. The top (yellow) layer is oriented in the y direction and designated as the Y beams and the bottom (purple) layer is oriented in the x direction and designated as the X beams.
The Y beams are fixed in the y direction at the center support point, but free to move during the cool down at the two outer points. The ends of the Y beams are expected to shrink ∼10 mm towards the center during cooldown to LAr temperature.

The X beams are used for the direct support and positioning of the TPC components. Only three X beams are shown in Figure 2.66, but there are two additional inbetween the ones shown. The full set of beams is shown in Figure 2.67 along with the naming convention for the X beams. X beam A supports the row of APAs near the Saleve side of the cryostat. X beam B is used for the installation and support of the end wall FC in the Saleve drift of the cryostat. X beam C supports the row of CPAs. X beam D is used for the installation and support of the end wall FC in the Jura drift. X beam E supports the row of APAs near the Jura side of the cryostat.

The X beams have the ability to translate on rolling trolleys in the Y direction in order to move the TPC components from the TCO entrance to their correct position in Y inside the cryostat. They are fixed in the X direction to the Y beams at the beam side of the cryostat. The reason to fix the X beams on the beam side is to limit the movement of the beam side of the TPC with respect to the membrane wall since the beam plug is mounted at this side of the TPC.

Figure 2.66: Detector support system

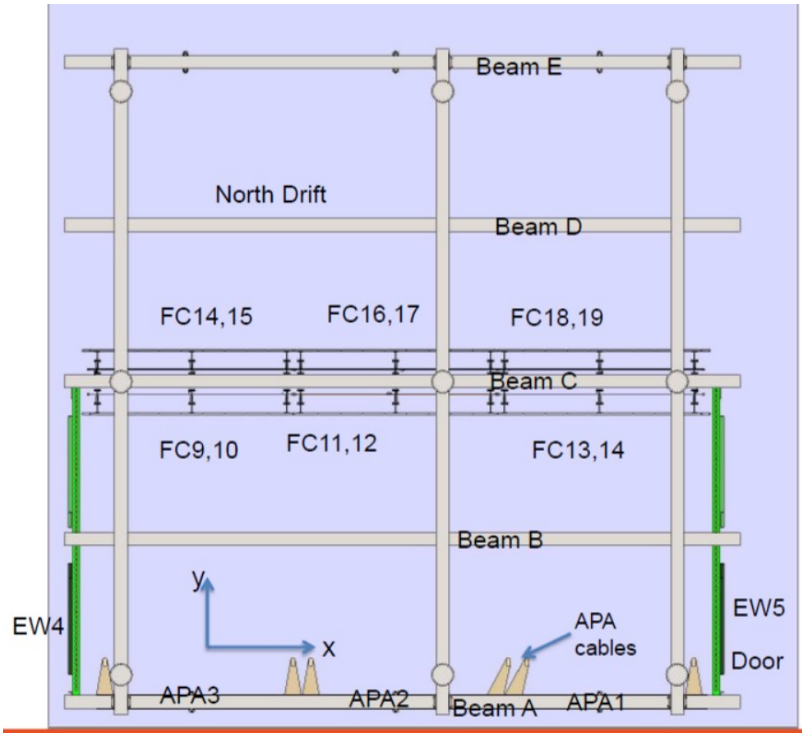

Figure 2.67: DSS showing full set of beams

fig:dss-

2.11 Installation

2.11.1 Anode Plane Assemblies (APAs)

The APAs will be delivered to EHN1 in containers as shipped from the production sites. These containers will be opened inside EHN1 and special lifting fixtures will be attached to each end of the APA. The APA will be positioned and attached to two conveyances installed in EHN1. Both conveyances will be used to lift the APA from the container, oriented as shown in Figure 2.68 (right), and then rotate it 90° from that orientation, as in the left portion of the figure.

fig:apa-tooling

Once the APA is removed from the container and properly oriented, the lifting strap and fixtures will be removed from the lower edge of the APA, the roof hatch on the material SAS for the clean room will be opened, and the APA will be lowered through the hatch. The APA will then be transferred to a rolling trolley attached to a series of rails, and moved into the clean room via these rails. These spaces and rails are described in more detail in Chapter 4.

ch:spacereq

Once in the clean room, the APA will go through a series of acceptance tests for both electrical integrity and wire tension. It will also be inspected for broken wires or any other damage that could have resulted from shipment.

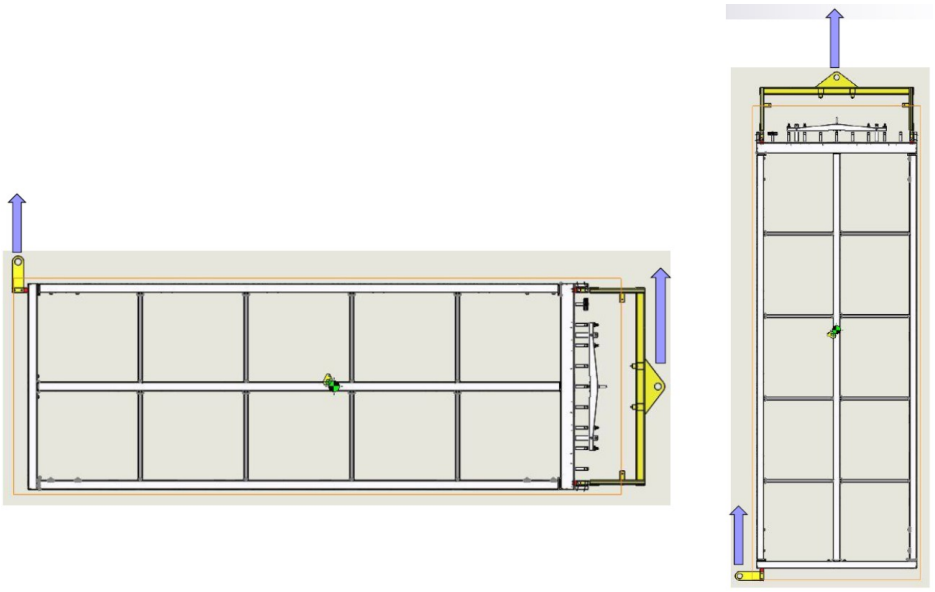

Figure 2.68: The APA with the lifting tooling attached. The right image shows the orientation of the APA as delivered, the left shows the orientation when it is lowered into the material SAS. fig:apa-

2.11.2 Photon Detection System (PDS)

After this testing is complete, the APA is integrated with the PDS. There are ten PDs per APA, inserted into alternating sides of the APA frame, five from each direction. This is shown in Figure 2.69. Once a PD is inserted, it is attached mechanically to the APA frame with fasteners, a single electronics cable is attached, and strain is relieved. Each PD is tested immediately after installation to ensure proper operation and to verify the cable readout.

fig:pds-install

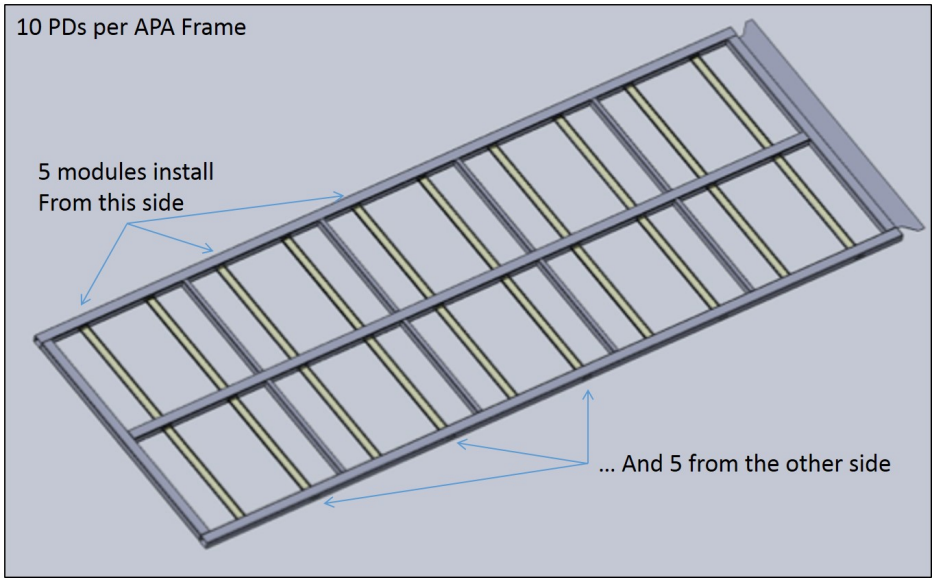

Figure 2.69: PDS installation fig:pds-

2.11.3 Cold Electronics (CE)

Once the PD installation is complete 20 CE units are installed at the top of the APA frame. Each CE unit consists of an electronics enclosure that contains the TPC read-out electronics inside. Each unit also includes a bundle of cables that connect the electronics to the outside of the cryostat via the flange on the feedthrough port. The location of the CE units on the APA is shown in Figure 2.70. These units will be connected via matching electrical connectors on the FEMB and the CR board mounted on the APA. There will also be mechanical fasteners to hold the enclosure to brackets supported by the APA frame.

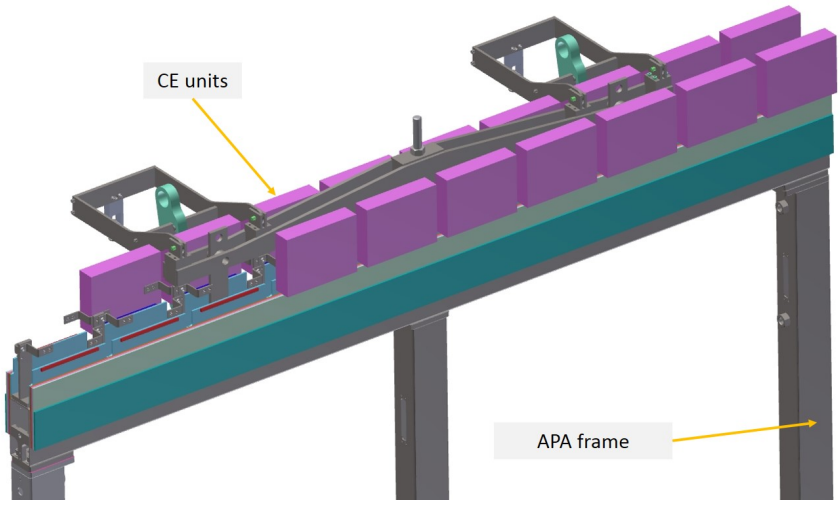

Figure 2.70: CE installation

After the APA has been fully integrated with the PDS and CE, it will be moved via the rails in the clean room to the integrated cold test stand. This test stand, shown in Figure 2.71, is a large insulated box that is light-tight for PD testing and has a Faraday shield for CE testing. At the top of the box is a crossing tube, similar to those in the cryostat, with a ConFlat fitting that accepts the warm-cold interface flange for the PD and CE cable connections. To prepare for the series of warm electronics tests, the PD and CE cables will be routed and connected to their flanges, the APA will be moved inside the test stand box, and the end cap that completes the Faraday cage will be installed closing the box.

A first set of tests at room temperature will be performed. Once the warm tests are complete, the inner volume of the box will be purged with dry gas and the volume will be slowly cooled, using cold nitrogen gas, to a temperature of approximately 100 °K. The rate of cooldown must be less than 10 °K/hr, the same foreseen for the cryostat cooldown. The cooldown system is designed to maintain the inner volume near 100 °K for approximately 48 hours. A full set of tests at a temperature close to operation LAr temperature will be performed for detectors functionality (APA and PD) and electronic noise assessment. After the cold test procedure is complete and the detector slowly warmed up back to room temperature, the box is opened, cables are disconnected and secured and the APA is extracted from the box on the rail system in the clean room.

The APA is now ready to be moved into the cryostat through the TCO and transferred onto the

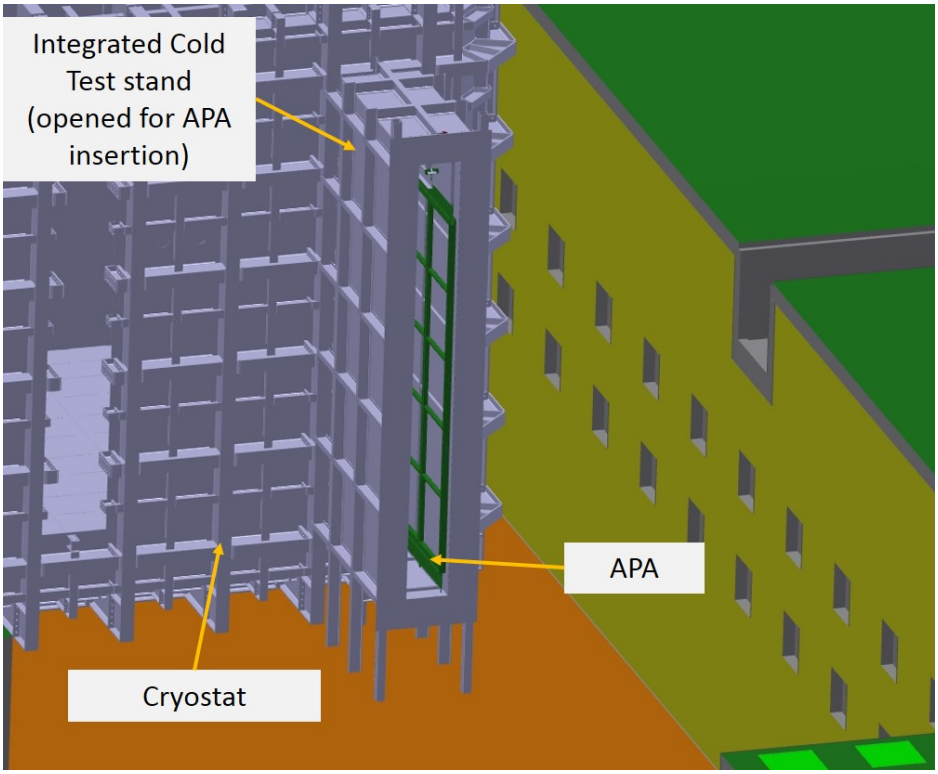

Figure 2.71: A model of the integrated cold test stand in the ProtoDUNE-SP clean room in EHN1. fig:cold

appropriate rail in the detector support system. The two anode planes of the TPC (Saleve side and Jura side) will then be assembled inside the cryostat, each one out three fully tested APAs mechanically linked together. Signal cables from the TPC read-out electronics boards and from the PD modules are routed up to the feedthrough flanges on the cryostat top side. The cables from each of the CE and PDs on the APA are then routed and connected to the final flanges on the cryostat.

2.11.4 Cathode Plane Assemblies (CPAs)

Individual CPA modules will be delivered to EHN1 in containers as shipped from the production sites. Each CPA module weights roughly 24 kg and will be lifted out of the shipping crate by hand. Three CPA modules will be placed on a flat surface and screwed/pinned together to form a CPA column. The crane then will be attached at the top end of the CPA column with appropriate lifting straps and shackles. The assembled CPA column will be lifted to the vertical position. Once the successive CPA column is formed, it is brought together with the previous one within 1 mm along their (vertical) length. This alignment is provided by two pins located on the side of the CPA that will fit into a vertical slot on the side of the next CPA. Six CPAs columns locked together will eventually form the cathode plane and moved inside the cryostat through the TCO and positioned parallel to the APA plane at the design drift distance.

FLC: it would be desirable to have a picture of the CPA here

2.11.5 Field Cage (FC)

Three basic elements comprise the FC: the top, bottom and end-wall FC assemblies. The top and bottom FC assemblies are basically mirror assemblies that are hinged from the top and bottom of the CPAs. Figure 2.72 (left) shows a top/bottom FC assembly. The ground plane covers one side of the field shaping profiles. The right-hand image in the figure shows a top and bottom FC attached only to one side of the CPA. These will be attached to both sides for the ProtoDUNE-SP installation.

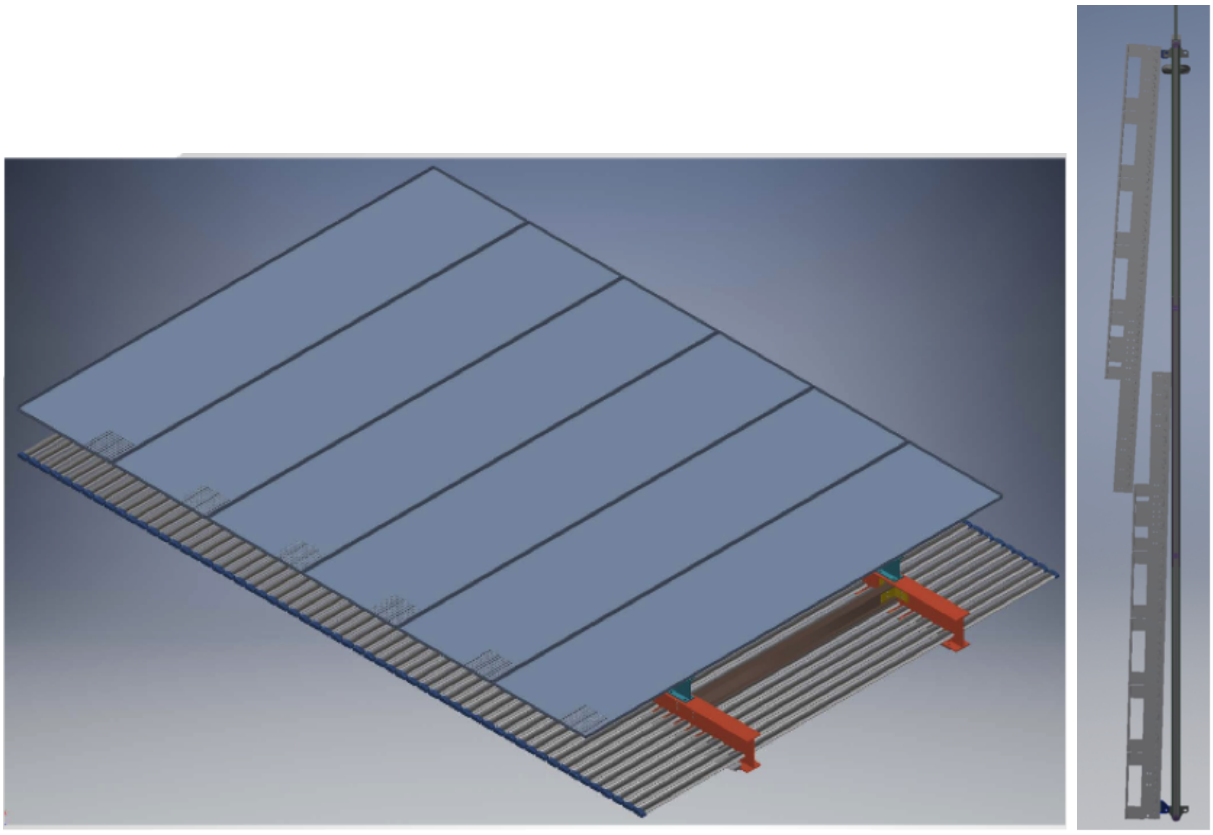

Figure 2.72: Top/bottom FC assembly

The end-wall FC assembly is constructed from four stacked end-wall FC modules. Figure 2.73 shows one of the end-wall FC modules. Four of these modules will be stacked and connected together to build the end-wall. The stacking will be done by the overhead hoist near the TCO in the clean room. Once the end wall is complete, it will be moved into the cryostat on the rails in the clean room and positioned on the appropriate beam in the DSS. The end-wall is supported by a spreader bar that is in turn supported from the beam. The spreader can swivel about the support point; this is necessary for positioning the end-wall with respect to the APA and CPA.

Figure 2.73: FC end wall panel

Jack needs to remake the fc end wall panel picture

The sequence of installation for the FC components is as follows:

- After the first row of APAs is installed and translated to the Salève side of the cryostat, the two end-walls for the Salève drift will be constructed and moved inside the cryostat supported by X beam B.

  shown in some figure?

- As the CPAs are constructed outside the cryostat, both the top and bottom FC assemblies are attached on both sides, top and bottom. This combination of FC and CPA is then moved into the cryostat and supported by X beam C.

  shown in some figure?

  This is done three times to get all into position.

- After the second row of APAs is installed and translated to the Jura side of the cryostat, the two end-walls for the Jura drift are constructed and moved inside the cryostat supported by X beam D.

  again, figure?

2.12 Cryogenics and LAr purification systems

yo-purif

2.12.1 Overview, Overall planning and ES&H

The scope of the ProtoDUNE Cryogenics includes the design, procurement, fabrication, testing, delivery, installation oversight and acceptance tests of a comprehensive cryogenic system that meets the performance requirements for purging, cooling down and filling the cryostat, acquiring and maintaining the LAr temperature within ± 1 K around nominal temperature (88.3 K), purifying the Liquid Argon (LAr) outside the cryostats, and re-condensing and purifying the boil-off Gaseous Argon (GAr).

The reference-design for the ProtoDUNE cryogenics infrastructure includes the External, Proximity and Internal Cryogenics.

The *External Cryogenics* includes the systems used for the storage and eventual production of the cryogens needed for the operation of the cryogenic system (liquid ntrogen, LN2, for cooling; LAr for the cryostat) and GAr generated from the cryogenic storage tanks. In particular, it encompasses:

- The receiving facilities for LAr and LN2 tanker trucks;

- The cryogenics transfer lines to deliver LAr and LN2 to the Proximity Cryogenics (in the vicinity of the cryostat);

- The ambient vaporizer and transfer lines to deliver GAr to the cryostat for the piston purge and the GAr make-up; and
- The regeneration system for the LAr purification (with GAr and GAr/H2 cylinders).

The *Proximity Cryogenics* takes the cryogens from the External Cryogenics and delivers them to the Internal Cryogenics under the required pressure, temperature, purity and mass flow rate. It encompasses:

- The condenser (with heat exchanger) to re-condense the boil-off GAr;
- The LAr purification system with inline purity monitor;
- The LAr recirculation pumps;
- The LAr Phase separator to feed the cryostat;
- The LN2 Phase separator to feed the condenser;
- The GAr purification system;
- The cryostat-purge equipment; and
- The condenser LAr pump.

The *Internal Cryogenics* includes all the cryogenic equipment located inside the cryostat. It encompasses:

- The cryostat/detector cool down manifolds
- The LAr distribution manifold
- The GAr purge distribution manifold.

The equipment described in this chapter will be used for the cool-down, filling, operation, purification, emptying and warm-up of the ProtoDUNE Single Phase cryostat. These operations are described in greater detail in Section 2.12.3.

The development of the ProtoDUNE cryogenics is part of a common effort between CERN and Fermilab which includes the cryogenics for the ProtoDUNE Single Phase and Dual Phase detectors at CERN, and the Short Baseline Neutrino Near Detector (SBND) and Far Detector (SBN-FD) at Fermilab.

The cryogenic systems for all four projects are developed jointly with a standard approach to minimize the duplication of work, benefit of existing knowledge (at Fermilab and CERN), and also prototype for the Long Baseline Neutrino Facility (LBNF)/Deep Underground Neutrino Experiment (DUNE) project. The systems build on the successful experience of the Liquid Argon Purity

Demonstrator (LAPD), 35-t prototype, and MicroBooNE at Fermilab, and the development of the WA105 1×1×3 Dual Phase prototype at CERN and CERN's experience in the design and operation of large-volume noble liquid detectors.

During all phases, CERN codes and standards will guide the design, procurement and installation phases of the ProtoDUNE Single Phase cryogenics. The planned work process will provide for reviews throughout all phases of the project to guarantee stringent adherence to the safety and scientific requirements.

The project requirements for the ProtoDUNE cryogenics system are identical to those of the DUNE Far Detector cryogenics. The current list of requirements is available at [18]. DUNE_FD_cryogenics_req

A selection of the most relevant requirements is presented here:

- Cryo-se-4: The system shall allow recirculation and purification of the liquid argon inventory to achieve the needed LAr purity to meet the scientific requirement (less than 10 day/volume change based on ICARUS experience).

- Cryo-se-6: The purification system shall be capable of removing contaminants form the LAr prior to filling and shall maintain purity during operation.

- LArFD-L2-se-44: Electron lifetime greater than 3 ms (maximum drift time at nominal field is 2.25 ms).

- Cryo-se-5: The system shall provide an argon gas boil off and reliquefaction system.

- Cryo-se-16: The cryogenics system shall not allow sources of argon gas reliquefaction inside the cryostat, e.g. uninsulated pipes carrying liquid argon.

- Cryo-se-25: The cryostat and cryogenic systems shall be designed for using the piston-purge technique (introducing heavy gas at the bottom and taking out exhaust from the top) for removing initial electronegative impurities.

- Cryo-se-8: The cryogenics system shall not introduce unwanted noise into the electronics.

- Cryo-se-10: The cryogenics system shall provide a stable environment in the cryostat for the detector.

- Cryo-se-28:The cryogenics system shall be designed in accordance with the cryostat to maintain a single phase in the entire liquid argon volume at a stable temperature. The chosen temperature is 88.3 K ± 1 K.

2.12.2 Cryogenics Layout

The Process Flow Diagram (PFD) of the ProtoDUNE cryogenic system is shown in Figure 2.74. The External Cryogenics located outside of the EHN1 building, is shared with the Dual Phase prototype, which is located in the same experimental hall, few tens of meters away.

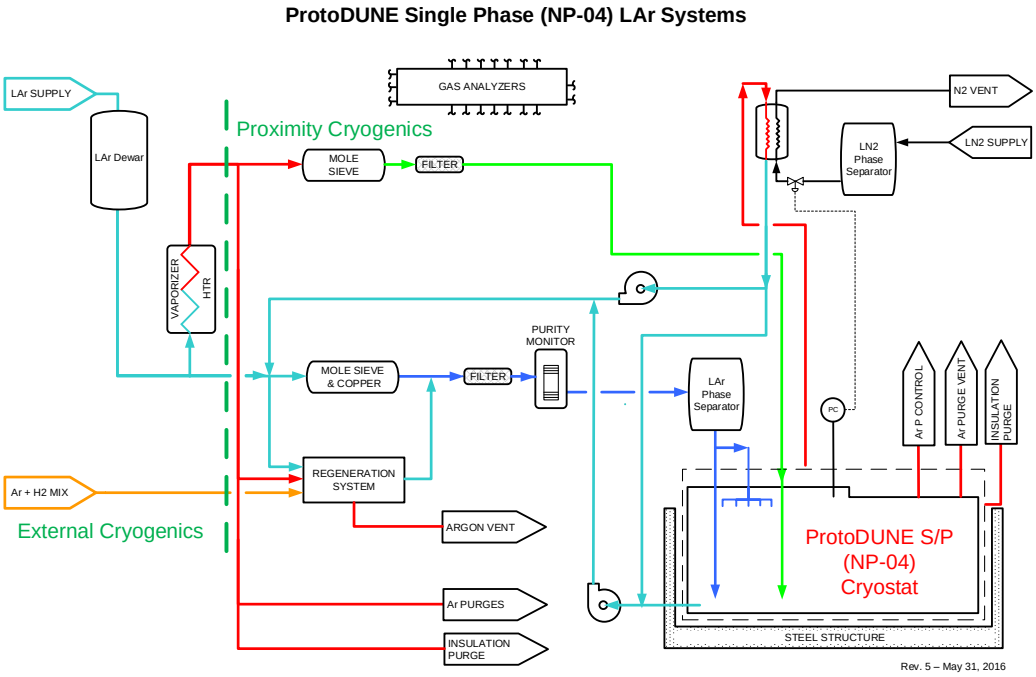

Figure 2.74: Process Flow Diagram

The system has the following functions:

- It provides the GAr for the piston purge phase and the GAr make-up.
- It provides the LAr to the cryostat.
- It provides the LN2 to the condenser.
- It provides the cooling power by means of evaporation of liquid nitrogen and condensation of GAr, to the liquid argon cryostat, for its cool-down, normal operation and warm-up phases.
- It provides the capability to purify the cryostat liquid argon volume to a level of parts per trillion (ppt) Oxygen equivalent contamination; the purification process uses mole-sieve and active copper.
- It provides the capability to purify the re-condensed boil off before reintroducing it inside the cryostat.
- It provides means to cool down the cryostat and the detector following the requirements.

- It distributes the LAr and GAr inside the cryostat to meet the requirements.

fig:3d-view-cryo-installation
Figure 2.75 shows a 3D view of the cryogenic installation as currently designed. The red and green lines entering from the bottom of the figure are the LN2 and LAr supply lines, respectively, from the external cryogenics.

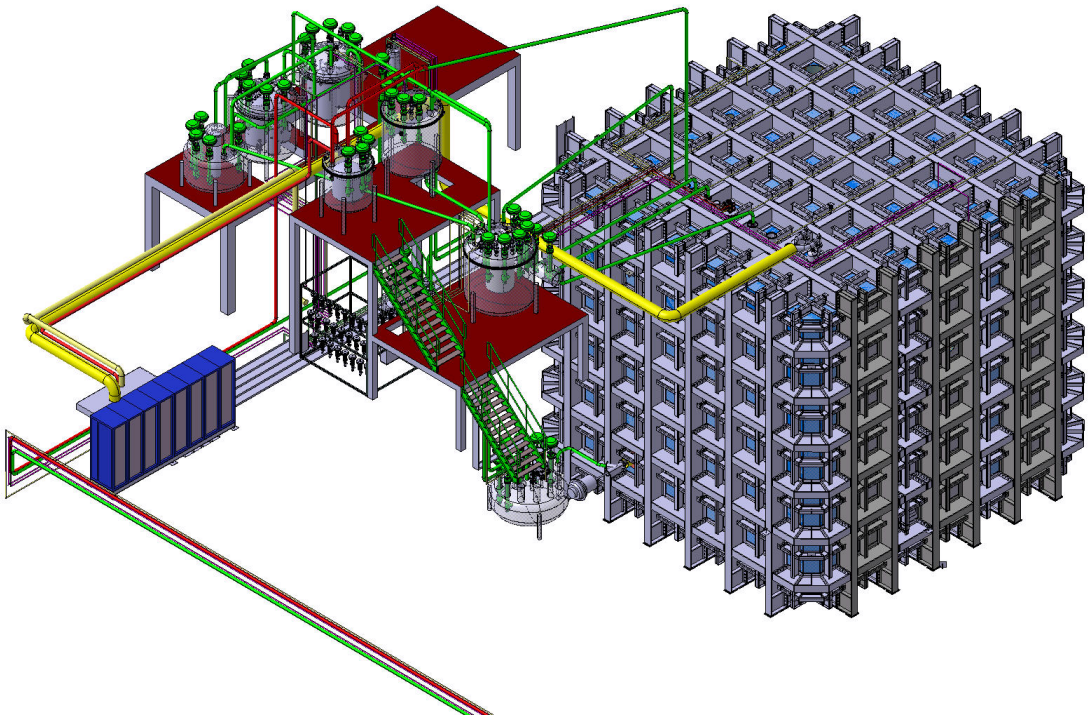

Figure 2.75: 3D model of the installation

fig:3d-v

fig:int-cryogenics-detail
Figure 2.76 shows a 3D view of a detail of the internal cryogenics: the cryostat and detector cool down manifolds at the top of the cryostat.

There is a common receiving facility for NP-02 and NP-04 located outside the building, from which Argon and Nitrogen lines take LAr, GAr, and LN2 to the respective installations.

A 50 m^3 (69 tons of LAr capacity) vertical dewar will allow for receipt of LAr deliveries for the initial filling period. This liquid argon dewar serves also as a buffer volume to accept liquid argon during the fill period. An analyzer rack with instruments to check water, nitrogen, and oxygen content of the delivered LAr batches will also be located in the vicinity. A 55-kW vaporizer is used to vaporize the liquid argon from the storage dewar prior to delivery to the GAr pipes.

The cryostat will have its own argon condenser (16 kW of cooling power), argon-purifying equipment and overpressure protection system. The full power of the argon condenser is used during the initial cool down phase only, which is expected to take two to three weeks.

A 50 m^3 vertical dewar (40-t LN2 capacity) will allow for receipt of LN2 deliveries and storage of LN2 for cool down and normal operations. LN2 is flown into the heat exchanger of a condenser

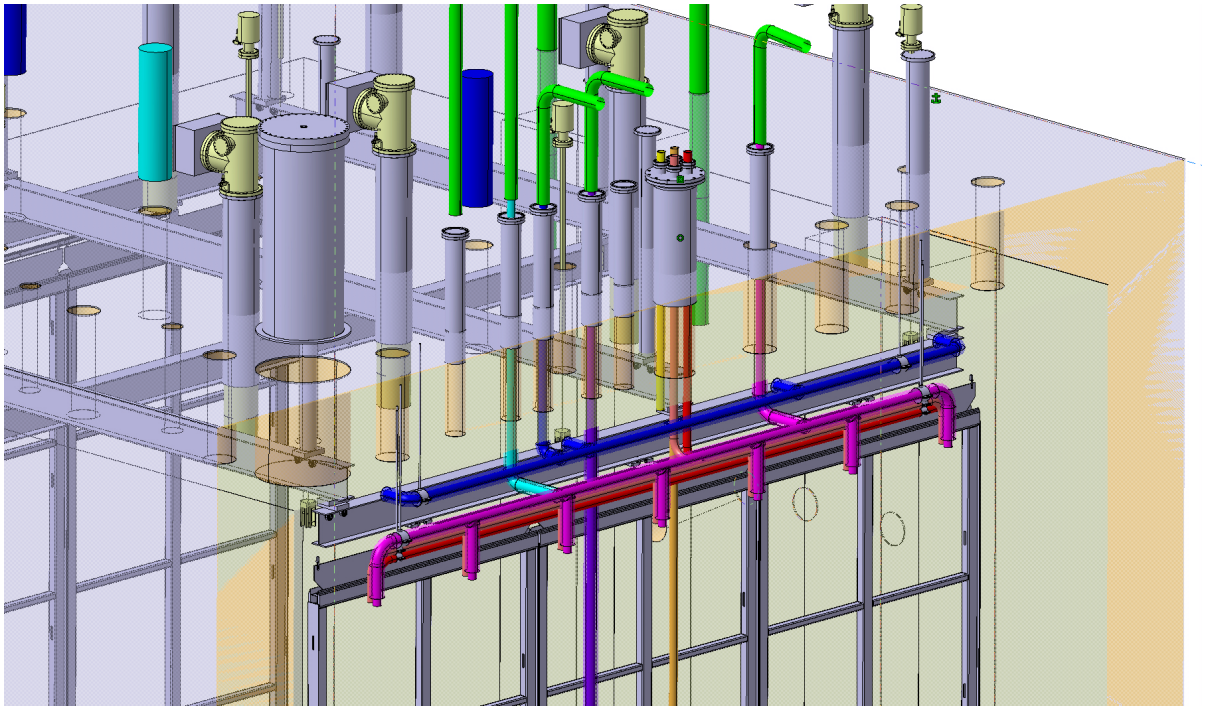

Figure 2.76: Detail of the internal cryogenics

fig:int-

located in close proximity of the cryostat to recondense the boil-off GAr coming from the cryostat itself.

Two LAr recirculation pumps are placed outside of the membrane cryostat to circulate liquid from the bottom of the tank through the purifier and then back to the tank to ensure the needed LAr purity. The purification filters are located in the vicinity of the cryostat. The filters contain dual media, a molecular sieve for removal of water and a copper coated catalyst media for oxygen removal. There is one gas filter that is used during the purge in closed loop phase and two liquid filters used during the filling and normal operations to continuously purify the bulk of the LAr inside the cryostat. Associated with the filters, there will be regeneration equipment such as heaters and a Ar/H2 mix. Before the Ar is returned to the cryostat, the LAr flows into a phase separator: the liquid is taken from the bottom and delivered to the cryostat, while the gas is returned to the condenser.

2.12.3 Modes of operation

op-modes

The major functions of the cryogenics system servicing the cryostat are to supply cryogens for cool down and fill, and to provide gas argon filtration and condensing, liquid argon filtration and circulation. The methods presented in this section are motivated by experience from the cryogenic systems of other LAr Time Projection Chamber (TPC) experiments, such as ICARUS, LAPD, the 35 ton detector and MicroBooNE.

Cryostat piston purge After the cryostat construction and following the installation of all scientific equipment, the cryostat will be cleaned and purged in preparation for cool down and filling. Construction procedures leading up to this point will ensure that the completed cryostat does not contain debris and is free of all loose material that may contaminate the LAr.

Purge in open loop Argon piping will be isolated, evacuated to less than 0.1 mbar absolute pressure and backfilled with high-purity argon gas. This cycle will be repeated several times to reduce contamination levels in the piping to the ppm level. The reference-design choice for removing air from the membrane cryostat will be to flow/piston-purge argon, introducing the heavier argon gas at the bottom of the tank and removing the exhaust at the top. The exhaust will be taken from the main GAr outlet, but also from all the side ports located on each penetration through the roof to ensure that all volumes (especially trapped volumes) are properly purged.

The flow velocity of the advancing GAr will be set to 1.2 m/hour. This is twice the diffusion rate of the air downward into the advancing argon so that the advancing pure argon-gas wave front will displace the air rather than just dilute it. A 2D ANSYS model of the purge process shows that after about 13 hours of purge time and 2 volume changes, the air concentration will be reduced to less than 1%. At 44 hours of elapsed time and seven volume changes, the purge process is complete with residual air reduced to a few ppm. This simulation includes a representation of the perforated field cage at the top and bottom of the detector and heat sources due to the readout electronics.

The Computational Fluid Dynamics (CFD) model of the purge process has been verified in multiple arrangements: (1) in an instrumented 1 m-diameter by 2 m-tall cylinder, (2) in LAPD, a 3 m-diameter by 3 m-tall cylindrical tank where gas-sampling measurements were at varying heights and times during the purge process, and (3) within the 35 ton membrane cryostat, the prototype vessel built at FNAL in 2013. The results of these tests are available in [19] and [20]. Once the residual air inside the tank is at the the ppm level, the process continues in the closed loop configuration.

Purge in closed loop Water and oxygen will continue to be removed from the system for several days following the initial purge. During this step the GAr is no longer exhausted but recirculated through the GAr purifier and sent back to the bottom of the cryostat. The cryostat contains a relatively large amount of FR4 circuit-board material and a smaller inventory of plastic-jacketed power and signal cables. These somewhat porous materials may contain as much as 0.5% water by weight. Water-vapor outgassing from these materials will be entrained in the gas flow exiting the top of the cryostat and will be removed from the gas stream by filters. Adsorbed water will also be removed from the metallic inner surfaces of the cryostat and piping system. Water deep within porous materials will remain; this is not a problem since the water diffusion rate in FR4 at room temperature is already quite low (0.3 $(\mu\text{m})^2/\text{s}$) and the FR4 assemblies are relatively thick (1 cm).
This process reduces the oxygen and water contamination inside the cryostat to sub-ppm levels, at which point the cool down may commence.

Cool-down Purified LAr will be mixed with GAr and distributed by a set of dedicated sprayers near the top of the cryostat and on the side of the TPC to cool down the cryostat and the detector in a controlled way. The sprayers deliver a mix of LAr and GAr in atomized form that is moved inside the cryostat by another set of sprayers flowing GAr only. Part of the boil-off gas is re-condensed inside the condenser and it then flows back as liquid to feed the LAr sprayers. The balance is vented during the process. Simulations have shown that this cool-down method can maintain the cool down requirements of the detector, as listed in Table 2.10 , and those of the cryostat, which are less stringent. The required cooling rate is determined by the maximum stress that detector components can tolerate. For example, the 150 μm APA wires will cool much more rapidly than the APA frames. A temperature-monitoring system (provided by the detector) will be used to control the temperature difference across the cryostat and the detector.

Filling Once the cryostat and the TPC are cold, LAr is introduced in the cryostat through the cryostat filling pipework. Argon is transferred directly from the LAr storage tank after passing thorough the LAr filtration system for purification. The filling process will take place over three to four weeks if two trucks per day are delivered; if only one truck per day is delivered, it will take twice as long.

Steady state operations During steady state operations :

- LAr is continuously circulated and purified by means of an external LAr pump (two are installed for redundancy, but only one is in use at a time).
- Boil-off GAr is re-condensed in a condenser situated outside the cryostat and purified before being reintroduced as LAr. The re-condensed LAr is sent to the LAr filtration system by means of a dedicated LAr pump and mixed in line with the bulk of the liquid coming from the cryostat. Alternatively, it is possible to send it to the inlet of the main LAr circulation pumps and from there as a single LAr stream to the filtration system.

Emptying At the end of operations (or if/when maintenance on the tank is needed) the tank is emptied and the LAr removed. The LAr is returned to the storage tank outside the building and from there unloaded back to LAr tankers.

Parameters Table 2.10 presents a list of relevant parameters for the installation. The filling flow rate of 18 l/min (0.42 kg/s) is an estimate. The actual value might be limited by the pressure inside the LAr storage dewar. We are also assuming that we are able to receive 2 trucks/day of LAr, which will need to be confirmed by the suppliers.

Table 2.10: List of engineering parameters for cryogenics installation

Mode	Parameter	Value	Notes
Piston purge	GAr flow rate	88 m3/hr	From 1.2 m/hr
Cooldown	Maximum cool-down rate TPC	40 K/hr	T sensors on the detector responsibility of detector
Cooldown	Maximum delta T between any two points in the detector	50K	T sensors on the detector responsibility of detector
Filling (*)	LAr filling flow rate	18 l/min (0.42 kg/s)	Assuming 2 trucks/day
Normal ops	Cryostat static heat leak	3.0 kW	GAr boil-off (18 g/s)
Normal ops	Other heat loads (estimate)	5.0 kW	Total estimate is ∼8 kW
Normal ops	LAr circulation (5 days turnover)	72 l/min (1.67 kg/s)	72 l/min (1.67 kg/s)
Emptying	Nominal flow rate emptying	72 l/min (1.67 kg/s)	
All	Condenser size	16 kW	

l-params

2.12.4 Features

This section briefly describes the main features of the various parts of the cryogenic system.

External Cryogenics The external cryogenics comprises the Liquid Argon and Liquid Nitrogen receiving facilities, the LAr/GAr and LN2 distribution systems, the Argon/Hydrogen mixture to regenerate the LAr/GAr purification filters and the mechanical filters on the LAr filling line.

The cryostat will hold an inventory of 760 ton of liquid argon. The standard grade specification for argon is a minimum purity of 99.995%, allowing a maximum concentration of 5.0 ppm for O2 and 10.5 ppm for H2O.

This implies that N2 is at the level of 30-35 ppm - way too bad for the Scintillation Light .. practically unacceptable, as it would imply a loss of 70% of the light due to N2 quenching.

This is designated as Grade 4.5 in the gas-supply industry. Requiring higher-purity product might increase the cost and push out the schedule. Suppliers may also decide not to quote for such an amount of a higher purity fluid. Therefore, standard product will be procured.

Facilities are required for the offloading of LN2 and LAr road tankers. Vehicle access and hard-surfaced driving areas are being constructed adjacent to the LN2/LAr dewars and the LAr/LN2-supply pipes. A LAr storage dewar will hold the contents of a road tanker in order to minimize off-loading time. Road tankers will connect to a manifold and will use their on-board pumps to transfer the LAr to the storage dewar. The LAr will be stored and transported as a liquid inside the cryostat during the filling process. A battery of fourteen (14) 12-bottle racks containing 1.5% Hydrogen (by volume) and a balance of Argon will be stored outside the building as well. They will be used to regenerate the LAr and GAr purification filters as needed. One 1-micron mechanical filter is located on the LAr feed line. It prevents dirt and impurities from the LAr supply to enter

the purification system and the cryostat.

Proximity Cryogenics The Proximity Cryogenics comprises the argon condenser, the purification system for the LAr and GAr, the LAr circulation pumps, and the LAr/LN2 phase separators:

Argon reliquefaction and pressure control The high-purity liquid argon stored in the cryostat will continuously evaporate due to the unavoidable heat ingress. The argon vapor (boil-off gas) will be recovered, chilled against a stream of liquid nitrogen, condensed and returned to the cryostat. A closed system is required in order to prevent the loss of the high-purity argon. The re-condensed boil-off can be returned to the cryostat in three ways:

1. With a small LAr pump that sends it into the main LAr circulation stream (normal mode).

2. Directly to the condenser (emergency mode, when we cannot go through the purification system).

3. To the inlet of the main LAr circulation pumps (when the small LAr pump needs maintenance, to guarantee a continuous purification of the boil-off GAr).

During normal operation the expected heat ingress of approximately 8 kW to the argon system will result in an evaporation rate of 30 g/s and expanding in volume by a factor of 200 when it changes from the liquid to vapor phase. This increase in volume within a closed system will, in the absence of a pressure-control system, raise the internal pressure.

Argon vapor will also be removed from the top of the cryostat through the chimneys that contain the cryogenic feedthroughs. As the vapor rises, it cools the cables and feedthrough, thereby minimizing the outgassing. The exiting gaseous argon will be directed to the same condenser as above, in which it is chilled against a stream of liquid nitrogen and condensed back to a liquid. As the argon vapor cools, its volume reduces and, in the absence of pressure control, further gas would be drawn into the heat exchanger, developing a thermal siphon. Therefore, a pressure-control valve on the boil-off gas lines will control the flow to the condenser to maintain the pressure within the cryostat at 0.113 MPa $\pm$ 0.003 MPa. The liquid nitrogen stream (that provides the coolant for the condenser) will be supplied from the LN2 phase separator, which is fed by the LN2 storage dewar located outside of the building. After the heat exchanger the returning N2 vapor is exhausted outside the building. The estimated heat loads to the argon system are listed in Table 2.11.

Table 2.11: Estimated heat loads within the cryostat

Item	Heat Load (kW)
Insulation Heat Loss	3.0
All other contributions (Recirculation pumps, pipes, filters, electronics, etc.)	5.0
Total	8.0

Argon purification The cryostat is designed with one penetration below the liquid level for external pumps used to transfer LAr from it to the purification system. The pumps are inserted into a valve box that is an integral part of the proximity cryogenics. The pump suction must be located at a minimum distance (normally about 1.5 to 2.0 m) below the lowest liquid level at which they are to pump in order to prevent cavitation and vapor-entrapment. There are two pumps for continuous operation during maintenance, but only one is expected to be in service at any moment in time.

The liquid-argon volume will turn over every 5.5 days, which corresponds to 1.67 kg/s (72 l/min) of flow rate. As a point of comparison, ICARUS T600 has a maximum turn-over rate of eight to ten days.

The multiple-pump arrangement provides a high level of redundancy, which will extend the maintenance-free operating period of the cryostat.

The liquid purification system, located nearby the cryostat, consists of two sets of three filter vessels containing molecular-sieve (1) and copper media (2) filters. They have been arranged in this configuration to reduce the size of the valve box containing them. Each molecular-sieve filter is 0.4 m in diameter by 0.9 m tall and contains 80 kg of media. Each copper filter is 0.6 m in diameter by 1.3 m tall and contains 298 kg of media. The filters are sized to provide effective media usage at low pressure drop over the expected range of flow rates. They are used during the filling and normal operations.

The gas purification system, located nearby the cryostat as well, is used to purify the GAr for the purge in close loop process. It consists of one filter vessel containing molecular-sieve and copper media filters in the same vessel. The mol sieve part measures 0.3 m in diameter by 0.1 m tall and contains 5 kg of media. The copper part measures 0.3 m in diameter by 0.6 m tall and contains 34 kg of media.

During the filling the LAr will flow through the liquid filtration, then the LAr phase separator and into the cryostat.

After the filling is completed, the cryostat liquid argon inventory is continuously circulated through one set of liquid purification filters for oxygen and water in order to quickly reduce and maintain the impurity concentration at the level of < 100 ppt oxygen equivalent, matching the required electron lifetime of the TPC detector. A dedicated special device, originally developed by ICARUS (usually indicated as “Purity Monitor"), for the measurement of the impurity concentration in liquid argon will be located immediately downstream the filtration system, providing information about the quality of the liquid and correspondingly about the actual level of impurity removal efficiency of the filter. After the filter the ultrapure argon is returned back to the cryostat via the LAr phase separator. Purity monitors will also be resident inside the cryostat, measuring the electron lifetime at different depths of the LAr volume. The purity monitors (provided by the ProtoDUNE-SP collaboration) are described in greater detail in Section 2.13.1.

The filter material, composed by molecular sieve pellets to remove water and by alumina porous granules covered by highly active metallic copper for catalytic removal of O_2 by Cu oxidization, is subject to saturation when the trapped/reacted impurity budget exceeds the removal capacity

of the filter material. When this occurs (signaled by the fast drop of LAr purity level detected by the external purity monitor) the liquid argon flow is switched to the back-up, ready-for-use filter and the saturated one is regenerated in-situ.

The filter regeneration process is done in subsequent steps. The saturated filter is first warmed up with heated argon gas to an elevated temperature driving into the gas the water captured by the molecular sieve media. A gas mixture of 1.5% hydrogen (reducing agent) with a balance of argon (inert carrier) at high temperature (500 K) is then used for the reduction of the copper oxide back to metallic copper. Water produced by the reduction process is vented out with the gas flow. The regenerated filter is finally cooled down and ready to be switched into service.

Internal Cryogenics Internal piping is positioned inside the cryostat to support the air purge and cool-down processes, but also the LAr distribution during filling and normal operations. During air purge argon gas is injected at the bottom of the cryostat and distributed through a set of pipes that pushes the air up and forces it out from the roof. The flow nozzles will be directed downward and to the side so that the injection velocity will not cause local vertical gas plumes or turbulent mixing but rather will spread across the bottom of the tank and produce a stable, upwardly advancing argon wave front. The vertical velocity of 1.2 m/hr for the gas purge includes a contingency for some level of turbulent mixing. In addition to the main vent, all nozzles and dead-end (stagnant) volumes located at the top of the cryostat will have gas-exhaust lines for the initial purge and for continuous sweep-purge of those volumes during normal operations. The sweep-purge during the initial stage of purging will be vented outside of the building, whereas the sweep-purge during normal operations will be re-condensed and recirculated as liquid.

The cool-down of the cryostat and detector is performed through a set of manifolds flowing LAr (one) and GAr (two). The LAr manifold and a GAr manifold are joined together and terminate with a set of sprayers that deliver a mist of LAr and GAr. This mist is circulated within the cryostat by a jet of GAr coming from the other manifold, which also terminates with sprayers. These manifolds are located on the Jura side and are off to the side of the TPC so as not to flow LAr and GAr directly over the detector itself. The chosen sprayers guarantee a flat profile of the fluid (LAr and GAr) coming out.

During filling and normal operations, the LAr-supply pipework distributes the LAr at the bottom of the cryostat. The outlets are at the end of the pipes, as far away as possible from the side penetration from which the LAr is sent to the purification system.

2.12.5 Cryostat pressure control

The pressure inside the cryostat is maintained within a very narrow range by a set of active controls. There are pressure control valves that can increase or decrease the cooling power in the condenser by controlling the amount of LN2 flowing to the heat exchanger and being vented. Other pressure control valves can be used to vent GAr to atmosphere and/or introduce clean GAr from the storage, as needed. The system is always in place, from the initial purge to the emptying of the cryostat at the end of operations.

Normal Operations The pressure-control valves are sized and set to control the internal cryostat pressure under normal operating conditions to the nominal design pressure of 0.113 MPa. Fluctuations within the range 0.105 MPa (80 mBarg) to 0.120 MPa (230 mBarg) will be allowed. Excursions of a few percent (exact values to be determined) above or below these levels will set off warnings to alert the operator to intervene. Further excursion may result in automatic (executive) actions. These actions may include stopping the LAr circulation pumps (to reduce the heat ingress to the cryostat), increasing the argon flow rate through the condenser, increasing the LN2 flow through the heat exchanger inside the condenser, powering down heat sources within the cryostat (e.g., detector electronics), venting some of the GAr to reduce the pressure in a controlled way. Eventually, if the pressure continues to rise, it will trigger the Pressure Safety Valves (PSVs) to operate.

If the pressure decreases, we can introduce fresh GAr in the cryostat through the GAr make-up line, a dedicated GAr feed line that takes argon directly from the outside supply. If the pressure continues to decline, it will trigger the Vacuum Safety Valves (VSVs) to operate. Table 2.12 summarizes the cryostat pressures during normal operation.

Table 2.12: Cryostat pressures during normal operations

Cryostat part	Pressure
Vessel ullage pressurization	0.100 MPa (30 mBarg)
Pressure regulation	0.110 MPa (140 mBarg)
Vessel ullage depressurization	0.125 MPa (280 mBarg)
Relief valve set pressure	0.135 MPa (380 mBarg)
Warm structure design working pressure	0.135 MPa (380 mBarg)

The ability of the control system to maintain a set pressure is dependent on the size of pressure upsets (due to changes in flow, heat load, temperature, atmospheric pressure, etc.) and the volume of gas in the system. The reference design has 0.4 m of gas at the top of the cryostat. This is 5% of the total argon volume and is the typical vapor fraction used for cryogenic storage vessels. Reaction times to changes in the heat load are slow and are typically on the order of an hour.

Overpressure control In addition to the normal-operation pressure-control system, it is planned to provide a cryostat overpressure-protection system. This must be a high-integrity, automatic, failsafe system capable of preventing catastrophic structural failure of the cryostat in the case of excessive internal pressure.

The key active components of the planned system are Pressure Safety Valves (PSVs) located on the roof of the cryostat that will monitor the differential pressure between the inside and the outside of the cryostat and open rapidly when the differential pressure exceeds a preset value. A pressure-sensing line is used to trigger a pilot valve which in turn opens the PSV. The PSVs are self-contained devices provided specially for tank protection; they are not normally part of the control system.

The installation of the PSVs will ensure that each valve can periodically be isolated and tested for correct operation. The valves must be removable from service for maintenance or replacement

without impacting the overall containment envelope of the cryostat or the integrity of the over-pressure protection system. This normally requires the inclusion of isolation valves upstream and downstream of the pressure-relief valves and at least one spare installed relief valve (n+1 provision) or the use of a diverter valve that allows one valve to be always connected to the cryostat.
When the valves open, argon is released, the pressure within the cryostat falls and argon gas discharges into the argon vent riser. The valves are designed to close when the pressure returns below the preset level.

Vacuum-relief system The cryostat vacuum-relief system is a high-integrity, automatic, failsafe system designed to prevent catastrophic structural failure of the cryostat due to low internal pressure. The vacuum-relief system protects the primary membrane tank. Activation of this system is a non-routine operation and is not anticipated to occur during the life of the cryostat.

Potential causes of reduced pressure in the cryostat include operation of discharge pumps while the liquid-return inlet valves are shut, gaseous argon condensing in the condenser (a thermo-siphon effect) or a failure of the vent system when draining the cryostat. Vacuum-relief valves are provided on LNG storage tanks to protect the structure from these types of events.

The key active components of this additional protection system are Vacuum Safety Valves (VSVs) located on the roof of the cryostat that will monitor the differential pressure between the inside and the outside of the cryostat and open when the differential pressure exceeds a preset value, allowing air to enter the cryostat to restore a safe pressure. A combo PSV-VSV may be used instead of two separate devices, one for overpressure and one for vacuum.

2.13 Detector monitoring and slow control

wcontrol

The scope of the ProtoDUNE-SP detector control system (DCS) includes the design, procurement, fabrication, testing, and delivery of a comprehensive detector monitoring, control and safety system.

The responsibility for the system is split between ProtoDUNE-SP and CERN:

- The ProtoDUNE-SP collaboration is responsible for all the devices that will be installed and cabled inside the cryostat, the sensors needed to monitor the cryostat and its content, and the specifications for the system.

- CERN is responsible for the implementation of the control system elements outside the cryostat (hardware, firmware and software), including the high-voltage and low-voltage power supplies necessary for the detector operation.

This section describes the main requirements, constraints and assumptions of the control system, and its general structure and components.

2.13.1 Monitoring devices and sensors

A number of devices and sensors will be located inside the cryostat for either periodic or continuous monitoring of the LAr as well as the GAr in the ullage, and for the monitoring of the detector functionality.

A short section on requirements here would be useful

Purity Monitors

Three purity monitors (PrM) with sensitivity in the ppt range will be used for the direct determination of the impurity content of the LAr inside the ProtoDUNE-SP cryostat. These PrMs have been generously provided by ICARUS [**?**]

Can't find citation in bib file

after being decommissioned from the T600. The design has been replicated for MicroBooNE and other R&D test experiments at FNAL. Inside the ProtoDUNE-SP the monitors are arranged in a single vertical string located behind the APA planes on the Jura side (see Figure 4.2). The string hangs from the large blanking flange on the manhole, and ports with ConFlat sealing on the blanking flange will be made available for HV/Signal/OptFiber feedthroughs. The string is about 7 m long, with the three PrMs strung at different heights: one near the LAr surface, one at mid-height, and one at the very bottom near the LAr-return manifold, for monitoring the purity of the LAr entering the cryostat after the filtration process.

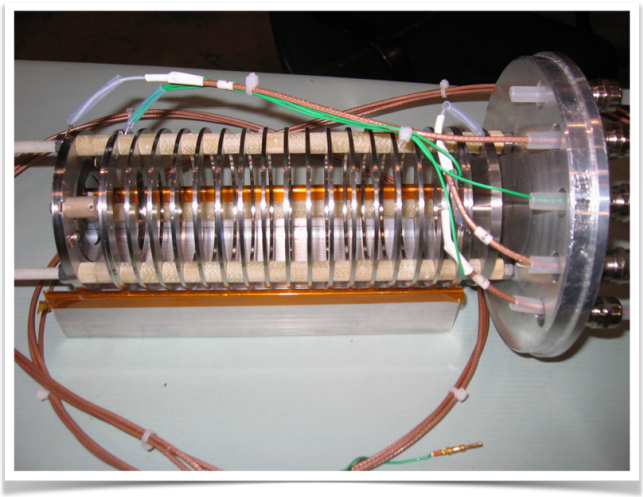

Figure 2.77: Picture of a purity monitor from the ICARUS T600, now available for installation in the ProtoDUNE-SP detector

Figure 2.77 was not referenced; I added one. It's pretty, but not very informative. It could use more description like "the 16(?) divisions in the device are the whatever, and the connection on the right is ..." Or we could take it out.

The three PrMs, one of which is pictured in Figure 2.77, are currently being refurbished with new gold photocathode and new quartz fiber. The drift length (25 cm) is the same for all them. Using parts of another (available) PrM to extend the drift length of one of the three (e.g., to 40 cm) for more precise measurements of the longer $e-$ lifetimes is currently under consideration. The mechanical structure of the string, the anchorage to the manhole flange at the top end, and the fastening of the string at the bottom are still under study. An additional PrM at the bottom on the opposite side of the cryostat would be useful for monitoring variations in the quality of the LAr at that level, and providing information for the fluid-dynamics computation inside the cryostat.

Vertical Temperature Gradient Monitor

Precise monitoring of the temperature gradient as a function of LAr depth is an important input for fluid dynamics modeling and simulations. The installation of a set of devices with precision better than 50 mK along the entire height of the LAr volume has recently been included in the internal instrumentation plan for this purpose. Commercial calibrated resistance temperature detectors (RTDs – Pt100 or Pt1000) with 15-mK precision at LAr temperature are well suited to this application, however the temperature probe wiring and signal transport outside the cryostat require extreme care in order to maintain the intrinsic precision of the probe.

The design for this device consists of a series of 25 Pt100 probes positioned at ∼30 cm intervals along a ∼7.5-m-long rigid string hanging behind the APA plane from an available port at the top of the cryostat. A special multi-pin FT is mounted on the flange for the signal extraction and readout from a temperature controller. Again, the mechanical structure, including the cable routing up to the multi-pin FT, is still subject to a detailed engineering study. A number of RTDs will also be positioned on the APAs and on the cryostat walls at different heights to monitor the temperature during the cooling process.

Webcams

Based on a system developed by ETH Zurich for WA105, six commercial webcams, sealed inside a specially developed metal case with a ConFlat optical window to allow operation at cryogenic temperatures, are located inside the cryostat. They are positioned at strategic points allowing inspection of the interior during filling and commissioning, and detection (and recording) of possible sparks in locations exposed to high electric field intensity.

Level Meters

Reliable LAr level determination is required in the ±20 cm around the nominal LAr surface level. Commercially available liquid-level sensors provide high-reliability monitoring. These are available in multiple technologies, including solid-state electro-optical, conductive, capacitive and piezo-resonant. Although the technology choice has not been made, designated ports on the top of the cryostat are available for this instrumentation. In the absence of these devices, the vertical temperature gradient device will provide a coarse level reading during filling, and some information about the steady-state LAr level will be available from the differential pressure transducer.

Pressure Sensors

Precise measurement of pressure in the GAr ullage is necessary. A number of pressure sensors, including a differential pressure transducer, are planned, and designated ports on the top of the cryostat are available for this instrumentation.

2.13.2 Slow Control System

The design of the ProtoDUNE-SP safety and control system is largely based on the experience gained in collaboration with ETH Zurich during the pilot WA105 project at CERN. The components of this system and their functions are as follows:

- The Process Control System (PCS) reads temperature sensors including the Vertical T Gradient monitor, pressure sensors and the purity monitors inside the cryostat and the trace analyzers (O_2, N_2, H_2O) in the external recirculation line.
- The Detector Control System (DCS) monitors and controls the low voltage (LV) and high voltage (HV) from the power supplies.
- The Detector Safety System (DSS) performs temperature surveys and monitors interlocks.

The system provides a graphical user interface to visualize the trends of monitored values and any alarm conditions. A web interface allowsfor remote monitoring.

The physical interface of the control system is located at the level of the outer flanges on the cryostat.

Where is this shown?

CERN EP/DT-DI will take care of connecting the control system to the flanges and interfacing to the cryogenics control infrastructure for information and signal exchange. The ProtoDUNE-SP experiment is responsible for all sensors, power distribution, etc., inside the cryostat, as well as for

defining the system specifications, I/O parameters and control and safety logic.

The supervisory control of the system and data acquisition (SCADA) is being developed, tested and provided by CERN EP/DT-DI.

Figure 2.78 shows the general architecture of the control and safety system for ProtoDUNE-SP, including the PCS, the DCS and the DSS.

The control system is composed of:

- a chassis for electrical distribution (380 Vac, 220 Vac, 24 Vdc redundant);
- two chassis for the PCS, composed of an FPGA, signal conditioners, interface, and cabling;
- one chassis for the DCS, composed of an interface for LV/HV monitoring & control;
- a chassis for the DSS, composed of an FPGA and relays for the safety of the experiment;
- a chassis for a PC data acquisition & supervision (PVSS SCADA Supervisor), composed of a computer with a display monitor, a switch and a server;
- four chassis for the remote I/O to capture signals close to the detector and to avoid multi-cabling structure; and
- one chassis for the HV, controlled by the slow-control system.

All these elements will be mounted in 19-in. racks.

The supervisory software is based on the JCOP framework, an integrated set of software tools originally developed for the control of the LHC experiments at CERN and now used in several more experiments at CERN. Besides providing a supervisory control and data acquisition system, the framework offers many tools for the implementation of finite state machines, archival of data, as well as graphical interfaces as web dashboards.

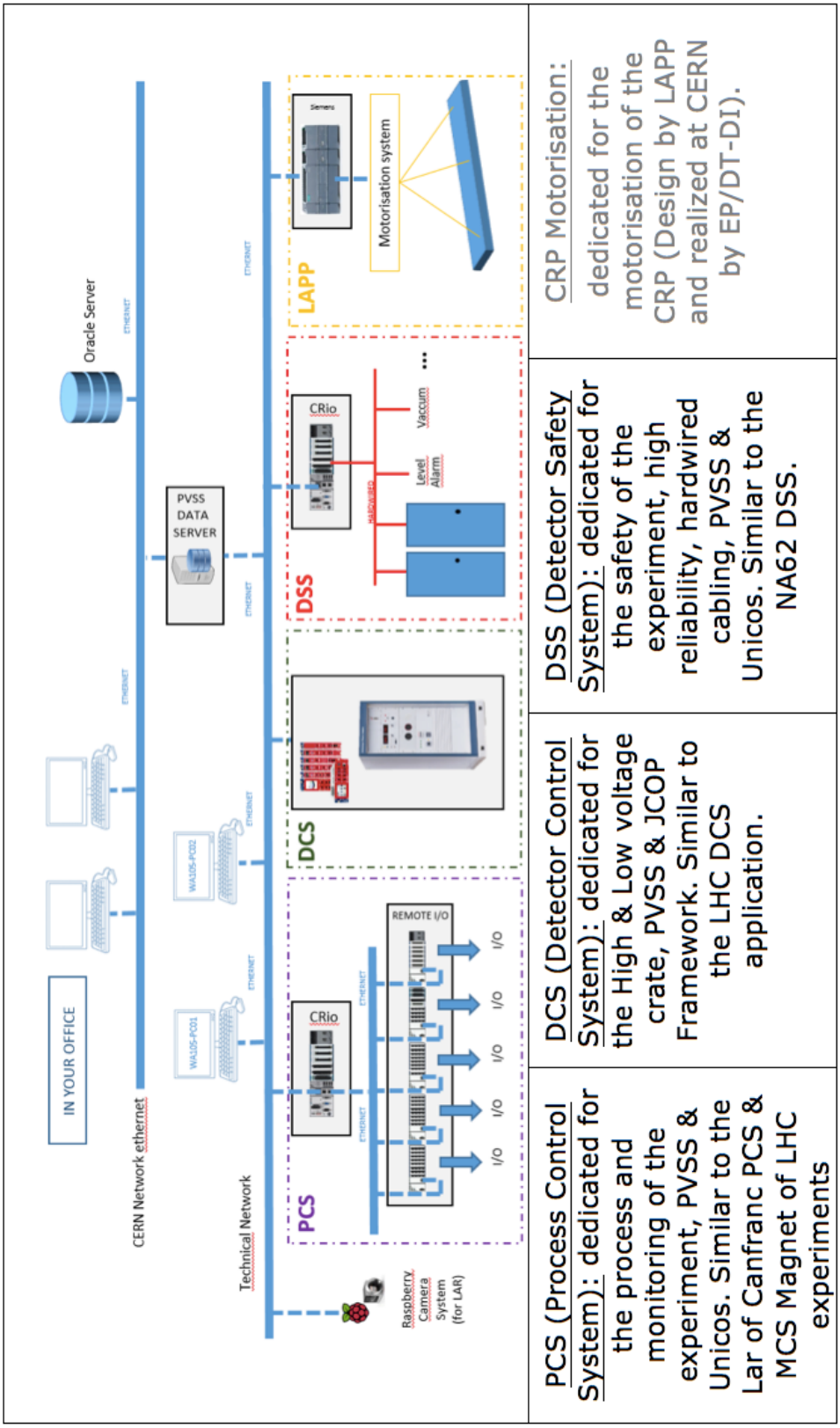

Figure 2.78: Proposed architecture and technical solution of the control and safety system. fig:dcsd

Chapter 3

Software and Computing

3.1 Overview

This chapter outlines the technical design of the offline computing system and introduces the software that will be used to simulate and reconstruct ProtoDUNE-SP data.

The data rate and the total data volume are the main factors influencing the design choices and scale of the offline computing system. The system provides resources necessary for data distribution, processing, and analysis on the grid[21].

The planned data processing steps include calibration, reconstruction, ntuplizing and user analysis. Multiple passes through this chain will be required for final results, as calibrations, algorithms, and ntuple definitions are expected to evolve.

A fraction of the data will be subject to *prompt processing*, which performs partial reconstruction of the data for QA/QC purposes with a short turnaround time (see 3.3.2). A metadata and file catalog system is necessary for managing the data.

3.2 Data storage and management system

3.2.1 Data characteristics

The characteristics of the raw ProtoDUNE-SP data are defined by the properties of the TPC:

- the multiple wire planes, the fine wire pitch, and the resulting high channel count;
- high digitization frequency (which is essential to ensure a precise position measurement along

the drift direction); and

- relatively slow drift velocity of electrons in LAr, which requires a readout window of the order of milliseconds to collect the ionization in the LAr volume stemming from the event of interest and overlapping cosmic rays.

Triggered readouts of the detector (events), contain a large amount of raw data, impacting the bandwidth and storage requirements. The run plan, described in Section 1.4, determines the total number of events, and thus helps define the design requirements for the data storage and management system.

The *"ProtoDUNE-SP Data Scenarios"* spreadsheet [4] describes a few possible running conditions. It includes estimates for their resulting data volumes and rates, and interpretations of these estimates in terms of network and disk bandwidth. The set of conditions labeled as "Central" represents the most likely scenario and is matched to the run plan. Estimates are also provided for data taken out of the spills in order to measure the contributions from cosmic rays. Table 2.8 summarizes these estimates.

Based on the estimated event size quoted in Table 2.8, the anticipated total raw data volume to be taken during the planned SPS run is 3 PB.

3.2.2 Raw data flow

A conceptual diagram of the raw data flow is presented in Figure 3.1. It shows the general logic of the data flow and does not rely on assumptions of specific technical implementations. It also reflects the central role of CERN EOS in the raw data management scheme, which is motivated by the experience and architecture of the LHC experiments.

what's EOS?

EOS serves as the staging area from which the data are committed to CASTOR (a hierarchical storage management system developed at CERN) and from which data are transmitted to a number of endpoints including principal data centers such as Fermilab and others. It is also used to provide input to QA and other express processing streams at CERN (Section 3.3.2).

3.3 Offline data processing

The data to be processed by the offline system can be classified as follows:

- A variety of calibration data derived from experimental data, including dedicated calibration runs where necessary, and/or subsamples of data collected specifically for calibration purposes during normal running conditions;

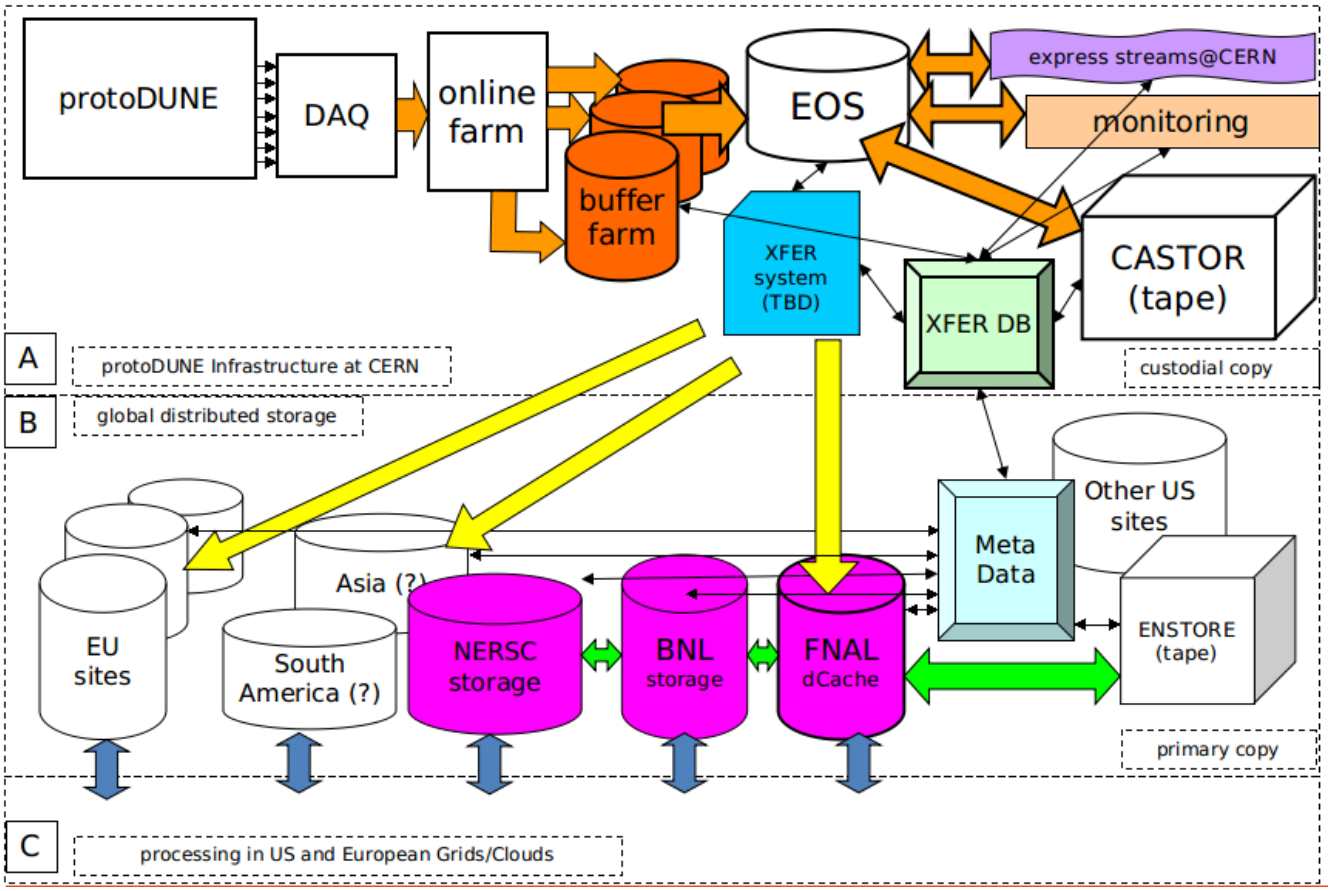

Figure 3.1: Conceptual diagram of the flow of raw data in ProtoDUNE-SP

- Processed experimental data, which may exist in several parallel branches corresponding to different reconstruction algorithms being applied, with the purpose of evaluating the performance of the different algorithms;

- Monte Carlo (MC) data, which contain multiple event samples to cover various event types and other conditions during data-taking; and

- Data derived from MC events, and produced with a variety of tracking and pattern recognition algorithms in order to create a basis for the detector characterization.

3.3.1 Production processing

The production processing has more than one processing step, thus creating derived data and multiplying the data volume. The volume of the derived data is assumed to be smaller than that for the raw data. Given the anticipated raw data volume, the plan is to provision ∼10 PB of tape storage to keep the raw and processed data. This includes two copies of the raw data at 3 pb each, two passes of derived data at 1 PB each, and 2 PB of simulation samples. One copy of the raw data may be included as part of the output of the reconstruction, for convenience in comparing raw and reconstructed data objects while also serving the purpose of providing a backup copy of

the raw data.

For efficient processing, disk storage is necessary to provide access to the data stored on tape. Extrapolating from experience running MC for previous DUNE MC campaigns, it is estimated that a few hundred TB of continuously available disk space is needed for samples that are repeatedly accessed, as well as ntuples for user analysis. The offline system takes advantage of the shared dCache resource

dcache reference needed

at Fermilab in order to provide efficient access to the data stored on tape.

3.3.2 Prompt processing

In the present context, *prompt processing* refers to a number of fast signal-processing and reconstruction processes (also called "express stream") that process a fraction of the raw data. Its main purpose is to aid in QA of the data and produce quick calibrations that may be necessary for detailed monitoring of the detector. For example, calculating the frequency spectra of noise and monitoring its level, evolution and other characteristics is an important aspect of ensuring the stability of the readout chain.

A limited number of metrics are calculated in order to make the process as quick as possible, enabling the operators to take action should the QA process indicate a potential problem in the detector or the data.

Processing roughly 1% of the data stream collected by the detector is predicted to be enough to meet the most important goals of prompt processing. The general strategy is to locate some of the prompt processing capability at CERN, at a scale adequate for the mid-range data-taking scenario, such as presented in Table 2.8. An estimated 300 cores are needed to cope with processing at that rate.

3.4 The LArSoft framework for simulation and reconstruction

cross check with description in DAQ section; there is some tolerable (?) overlap

LArSoft [22] is a suite of tools for simulating and reconstructing data collected from LArTPC detectors. It is built on the *art* [23] event-processing framework. The main features of the *art* framework are its configurability by human-readable and editable control files (that use the Fermilab Hierarchical Control Language (*FHiCL*)), and the scheduling of program module execution. The modules are of five types: event sources, filters, data-product producers, analyzers, and output. Common utilities that can be accessed by any program module at any time are called *services*.

The *art* framework defines the input/output structure of ROOT-formatted files using TTrees to store the data, metadata, and provenance information. The provenance information consists of the contents of the FHiCL documents used to steer the processing of the job that created the output file, and those of input files and parents.

The *art* framework's division of the simulation and reconstruction jobs into modular pieces allows multiple developers to contribute to an effort, and to test their ideas in isolation before integrating them into a larger system. Because the data read in from an event is placed in read-only memory, analyzers can program with confidence that upstream algorithms cannot alter the data, but must produce additional data products which can later be processed or written out.

The LArSoft suite provides the interface to the event generators and GEANT-4 [**?**] geant4

need citation in bib file

for simulation of the passage of particles through the detector, the details of which are described sec:larsoftsim in Section 3.5, and event reconstruction, the details of which are presented in Section 3.6. sec:larsoftreco

The *art* framework and LArSoft source code are publicly available, and pre-built versions are scisoft-web provided [24] for supported versions of Linux and Mac OS X. Tools for compiling the framework and applications are also provided, along with all of the required dependencies, including the gnu C++ compiler. The versions of the software and its dependencies are managed by the UNIX Product Support (UPS) system, which allows easy version selection, setup and configuration of the LArSoft environment on computers with previous versions already installed, such as those at Fermilab.

LArSoft is under rapid development by both the core LArSoft team and by contributors from participating experiments: ArgoNeuT, LArIAT, MicroBooNE, SBND, and DUNE. Within DUNE, the LArTPC near-detector option, both ProtoDUNE detectors, and the Far Detector are clients and contributors of LArSoft.

3.5 Event simulation

rsoftsim

Two kinds of events must be simulated in the ProtoDUNE-SP detector geometry: beam events and cosmic-ray events. Beam events are generated using a dedicated particle gun generator that has as input parameterizations of the flux and the beam profile parameters. The upstream beam instrumentation devices – wire chambers, Cherenkov counters, and time-of-flight-counters – are fully simulated as described in Section 5.3. Cosmic-ray events are simulated either with the sec:beaminstruments CRY, cry2 CRY [25, 26] event generator or CORSIKA [27]. Neutrino scattering events are simulated using Heck:1998vt GENIE [28]. While neutrino scattering events will be very rare in the detector, the extrapolation Andreopoulos:2009rq of the performance of the detector to the FD will require simulating neutrino scattering events. A dedicated generator in LArSoft simulates radionuclide decay products which can be overlaid on other events.

The detector geometry is coded in GDML files [29] that are generated by the GeGeDe [30] geometry system. These files contain the locations, sizes, shapes, and material content of the detector components, the active liquid argon volume, and the surrounding materials, such as the field cage, the beam windows, the cryostat the supporting structure, and the experimental hall. These external features will impact the distributions of cosmic-ray particles impinging on the active detector. The channels and volumes are numbered and named in the GDML files, with conventions followed by the LArSoft simulation code.

The active volume of the detector is divided into cubes 300 μm on a side, called *voxels*. GEANT4 tracks particles through the argon. Each step ends on a voxel boundary, allowing the simulation of small-scale physics processes such as delta-ray emission and showering at a level of detail smaller than the intrinsic resolution of the detector. While GEANT4 calculates the energy deposited by each particle for each step, the simulation of ionization and scintillation photon emission is performed using one of two algorithms in LArSoft: a dedicated parameterization that depends on the electric field in the liquid argon and the ionization density [31], or NEST [32], which is tuned to previous noble-liquid experimental results and introduces an anti-correlation between the photon yield and the ionization electron yield for each step.

An alternate simulation based on FLUKA [33, 34, 35] is being interfaced into LArSoft. FLUKA provides a MC simulation of neutrino-nucleus interactions as well as detailed modeling of particles traversing the detector, configurably replacing the functionality of both GENIE and GEANT in the simulation. The availability of alternatives allows for better flexibility in tuning the models to the data, as well as a basis of estimating systematic uncertainty.

The average specific energy loss for a minimum-ionizing particle (MIP) is approximately 2.12 MeV/cm. The W-value for ionization is 23.6 eV per electron-ion pair, and the W-value for scintillation is 19.5 eV per photon, resulting in tens of thousands of drifting electrons and photons per cm of charged-particle track in the detector. It is impractical to simulate the paths of each of these electrons and photons using GEANT4, and therefore computational techniques are incorporated into LArSoft to achieve a high simulation speed while preserving accuracy. The electrons are propagated by LArSoft-specific tools, including a tool that integrates over the distributions created by longitudinal and transverse diffusion, and a geometry tool that indicates the wire locations that record charge, assuming uniform wire spacing.

The effect of charge loss due to attachment of electrons to impurities (i.e., the effect of the electron lifetime), is implemented in this step. Effects due to space charge are simulated using a smoothly parameterized map of distortions in the apparent position components (x, y, z) of the charge deposits as functions of the true position. This map can be made using SPaCE [36], a program that traces particle trajectories in LAr based on the electric field calculated using Poisson's equation, a given space-charge density map, and the boundary conditions provided by the cathodes, anodes, and field cages. It is anticipated that the space-charge distortions in ProtoDUNE-SP may be as large as 20 cm [36].

Photon propagation is simulated using a library that contains the probabilities of observing a photon emitted at a particular point in space by a particular photon detector. Here, the space is divided into cubical voxels 6 cm on a side, and the library is indexed by photon detector element.

The simulated arrival times and charge amounts on each wire, and of each set of photons arriving at each photon detector, along with the identity of the particles generating them, are stored in the simulation output file for use in determining the performance of the downstream reconstruction algorithms. These charge depositions and photons are inputs to the detector response functions – the field response and the electronics response are convoluted with the true arrival times to make simulated waveforms. The detector field response functions are simulated using GARFIELD [37], but they will be validated with real data, as the simulation contains oversimplifications, such as inadequate modeling of induction signals.

The electronics gain is applied so that the simulated signals match the expected responses. Simulated noise is then added, and the result is quantized to reproduce the behavior of a 12-bit ADC, including realistic pedestals and saturation. A similar process is followed to simulate the response of the photon detectors, given the arrival times of the photons. Functionality exists within LArSoft to overlay MC-simulated particles with raw digits in the data in order to simulate pileup of cosmics and other beam interaction particles. The simulated raw digits are then written to compressed ROOT files for further analysis.

3.6 Event reconstruction algorithms and performance

3.6.1 Reconstruction

The interpretation of the data from LArTPC detectors has proven challenging, largely due to the wealth of information provided in each event by the detector, but also due to the high rate of multiple scattering and particle interactions, as well as the projection of 3D information onto a discretized 2D space of readout ADC counts on wires as functions of time. The flexibility of the *art*/LArSoft framework allows for multiple approaches for reconstructing and analyzing the data, and for the use of different approaches depending on the targeted physics deliverable.

For current large LArTPC detectors, noise filtering is applied to improve the signal-to-noise ratio. A large component of the noise in existing LArTPC experiments is from coherent sources – sources that affect many neighboring wires and/or neighboring readout channels (channels from different planes may be interleaved in the front-end electronics). The contribution from coherent noise to a measured ADC value on a channel can be estimated from the data on nearby channels in the same time slice, and subtracted out. However, this procedure reduces the signal as well as the noise, in a manner that depends on the angle of the track or shower with respect to the drift field.

Procedures that first identify signal hits and protect them from distortion [38] are under study. With software noise filtering, MicroBooNE [39] has achieved excellent noise levels, consistent with expectations, based on the design specification of the cold electronics. In MicroBooNE, various sources of noise have been identified and hardware upgrades are ongoing to eliminate them. Once noise has been removed, signals will be processed to recover the ionization charge.

Hits are identified by seeking deconvoluted signals exceeding thresholds that are adjusted to min-

imize the creation of false noise hits while preserving the true signal hits. The standard LArSoft hit finder fits Gaussian functions to the deconvoluted signals, and saves the times, widths, and amplitudes of the Gaussians. In addition, it saves the sum of the ADC readings in the time windows corresponding to the hits; since a Gaussian function is not always representative of the charge arrival distribution, the resolution of the calorimetry is improved by summing the ADC counts.

The hits are associated with DAQ channels not wire segments, since, due to the wrapping of the induction-plane wires in the APA's, the location of the charge deposition contributing to the hit is ambiguous. Because the wire angle is chosen such that each induction wire intersects each collection-plane wire at most one time, only two views are needed in order to identify hits and resolve ambiguities. A separate LArSoft module compares the hits in the collection and induction views to resolve ambiguities.

Physics analyses are most sensitive with a full 3D reconstruction of the event – the primary vertex (if there is one), the tracks and the showers. ProtoDUNE-SP is implementing several approaches to achieve this. Once hits are identified on wire segments, 2D reconstruction identifies clusters and tracks in each view separately, and 3D hypotheses for the event are constructed by comparing the 2D clusters in the separate planes. The 2D clustering algorithms currently in use are the Blurred Clustering Algorithm [**?**], LineCluster [40], and TrajCluster [41].

3.6.2 Performance

Algorithm performance metrics are efficiency, purity, and completeness. The efficiency of the algorithm is defined as the fraction of true particles that match reconstructed objects within the bounds of pre-specified criteria, such as matching position and length and the type of object expected. The purity of the reconstructed object is defined as the fraction of hits (or charge) included in that object that truly came from the matched particle, divided by the total number of hits (or charge) included in the reconstructed cluster. The completeness is defined as the number of true hits that are found in a cluster, track or shower expressed as a fraction of total true hits in that object.

Particle-level and event-level performance metrics include particle identification and misidentification rates, shower energy resolution, and energy scale offsets.

EMShower

The EMShower package [42] takes the output of the Blurred Clustering Algorithm and produces energies, angles, and start positions for 3D showers, as well as the dE/dx in the initial part of the shower. Identifying events with two showers consistent with $\pi^0 \rightarrow \gamma\gamma$ decays allows for an *in situ* calibration of the electromagnetic energy scale as well as the performance of shower identification and reconstruction for photons that are produced inside the detector. A distribution of reconstructed π^0 masses in Monte Carlo is shown in Figure 3.2.

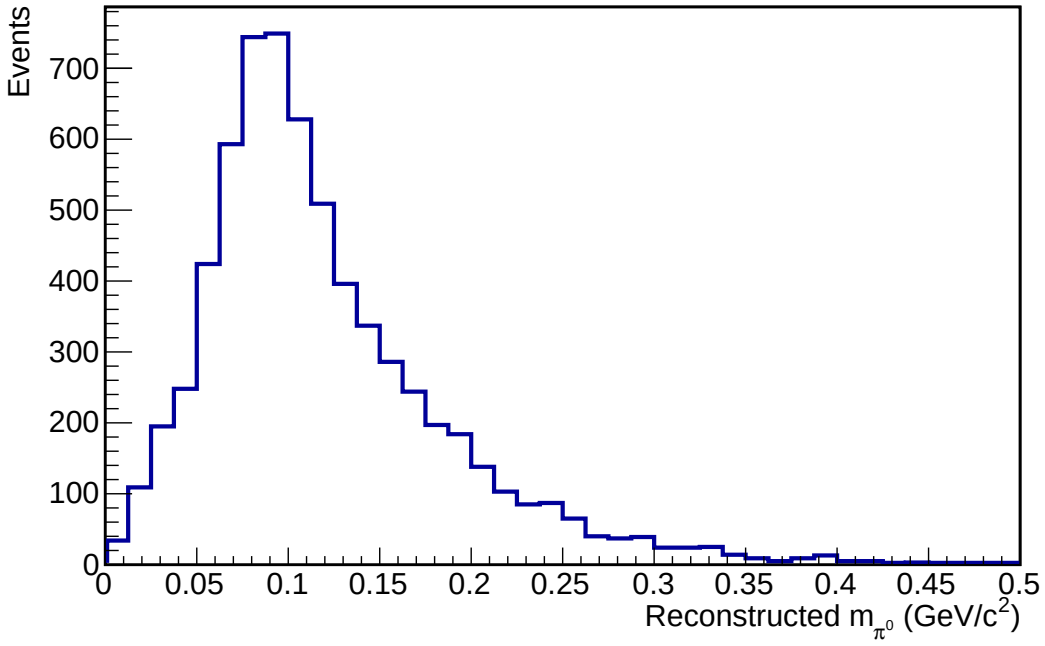

Figure 3.2: The reconstructed invariant masses of π^0 candidates in Monte Carlo using the BlurredCluster and EMShower algorithms. fig:pize

PANDORA

Marshall:2015rfa
The reconstruction framework PANDORA [43] also works by building up a 3D picture from 2D reconstructed objects. PANDORA is a flexible framework developed for ILC detector simulation, and provides a convenient way to develop algorithms for reconstructing particles. In all, more than 80 algorithms, each targeting a specific topology, have been incorporated into PANDORA to date. Multiple passes through reconstructing the data are possible. Different criteria for clustering hits into tracks and showers may be applied when seeking cosmic rays for removal rather than for identifying signal events. PANDORA follows a process that clusters hits in 2D, reconstructs vertices in 3D, reconstructs tracks in 3D, reconstructs showers in 3D, performs a "mop-up" step in 2D and 3D, and finally performs full event-building in 3D.

ILC - int'l linear collider? add to acronyms

Plots of the efficiency, the completeness, and the difference between the true and reconstructed track lengths for single muons with momentum between 300 MeV and 5 GeV in the ProtoDUNE-SP geometry are shown in Figure 3.3. The PANDORA algorithm performs very well, although a small inefficiency occurs in the current algorithm's ability to match track segments from one APA's drift volume to another.
fig:muonpandoraperf

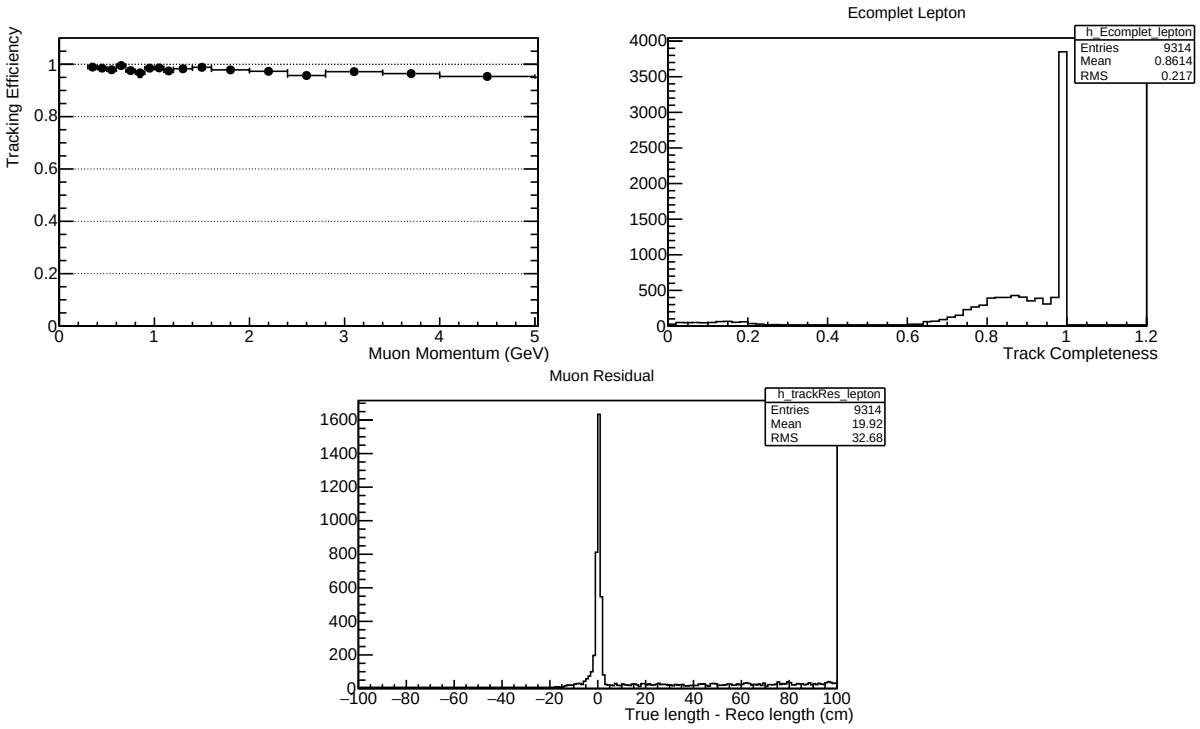

Figure 3.3: Performance of the PANDORA reconstruction algorithm for single muons with momentum between 300 MeV/c and 5 GeV/c. The left-hand figure shows the tracking efficiency as a function of muon momentum, the middle figure shows the distribution of tracking completeness, and the right-hand figure shows the distribution of the difference between the reconstructed muon track length and the true track length. fig:muon

PMA

Another approach to 3D reconstruction in LArTPC detectors is referred to as the *Projection Matching Algorithm (PMA)* [44]. PMA was primarily developed as a technique for 3D reconstruction of individual particle trajectories (trajectory fits) [**?**]. Instead of building up a 3D hypothesis from 2D clusters, it starts with the 3D hypothesis and compares the 2D projection of the predicted trajectory of a particle with the observed data. Association of hits between the 2D planes is not needed in this approach, improving its performance in problematic cases, such as isochronous and short tracks.

PMA can take as input the output from different pattern recognition algorithms, from LineCluster [40] to WireCell (described below). Because these 2D algorithms are run on each 2D projection independently, and because of detector defects, clusters from particles may be broken into several smaller pieces, fractions of 2D clusters may be missing, and clusters obtained from complementary projections are not guaranteed to cover corresponding sections of trajectories. Such behavior is expected since ambiguous trajectories can be resolved only if the information from multiple 2D projections is used. PMA performs higher-level pattern recognition using as input clustering information from all projections in order to search for the best matching combinations of clusters. The algorithm also attempts to correct hit-to-cluster assignments using properties of 3D reconstructed objects.

Plots of the efficiency, the completeness, and the difference between the true and reconstructed track lengths for single muons with momentum between 300 MeV and 5 GeV in the ProtoDUNE-SP geometry are shown in Figure 3.4.

PMA has been used successfully in ProtoDUNE-SP to reconstruct simulated beam particles. In order to illustrate the performance of the entire reconstruction chain, Figure 3.5 shows the spatial resolution of the interaction vertex with neutral pion production appearing in the 2-GeV/c π^+ sample. The resolution is found to be 0.6 cm in this study. A similar resolution is obtained for the reconstruction of inelastic interaction vertices in the 2-GeV/c proton sample.

Figures 3.6 and 3.7 show examples of reconstruction of a 2-GeV/c proton in the test beam and cosmic-ray muons, respectively.

WireCell

WireCell [45] adopts a very different approach from the aforementioned algorithms and is a new reconstruction method under development. Instead of directly doing pattern recognition on each of the 2D views (drift time versus wire number), the first step of the WireCell reconstruction is to perform 3D imaging with time, geometry, and charge information. The algorithm takes advantage of this information in order to suppress the effects of electronic noise. Hits from different wire planes arriving in different time slices cannot be associated with each other. (The definition of *hit* is based on signal strength after charge extraction in a 2-μs time slice.) Hits from wires that do not cross in a region consistent with the charge deposition cannot be associated with each other.

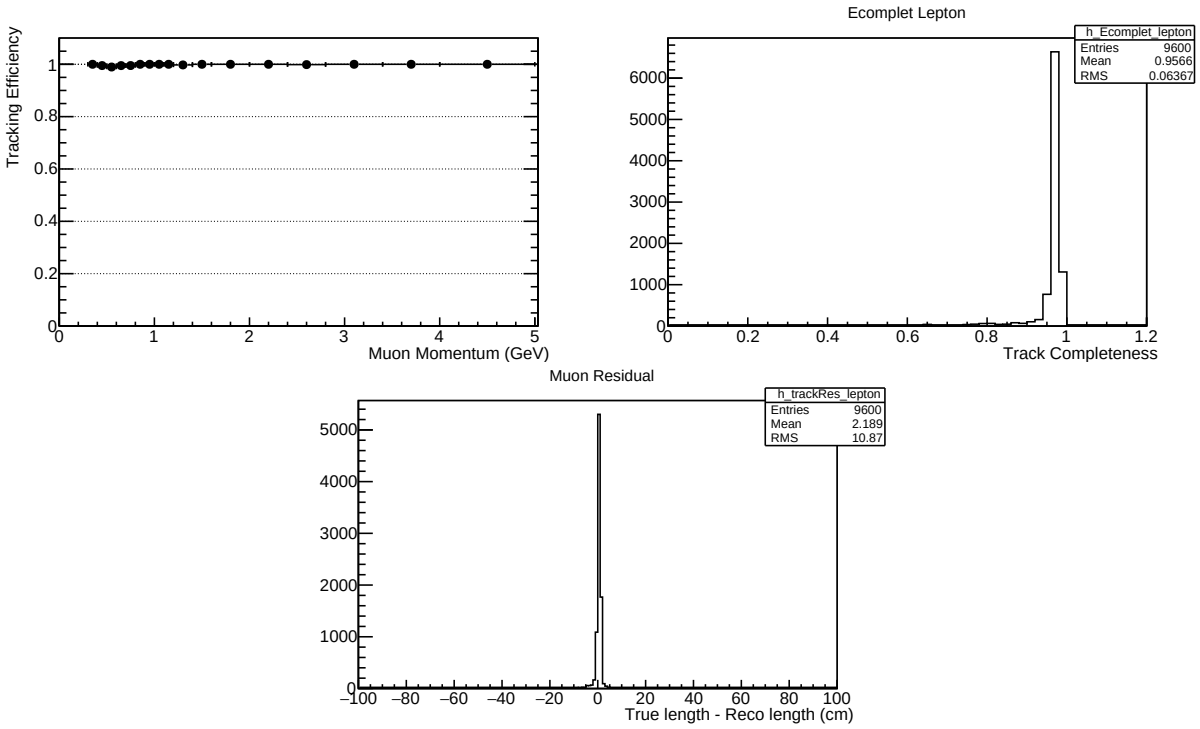

Figure 3.4: Performance of the PMA reconstruction algorithm for single muons with momentum between 300 MeV/c and 5 GeV/c. The left-hand figure shows the tracking efficiency as a function of muon momentum, the middle figure shows the distribution of tracking completeness, and the right-hand figure shows the distribution of the difference between the reconstructed muon track length and the true track length. fig:muon

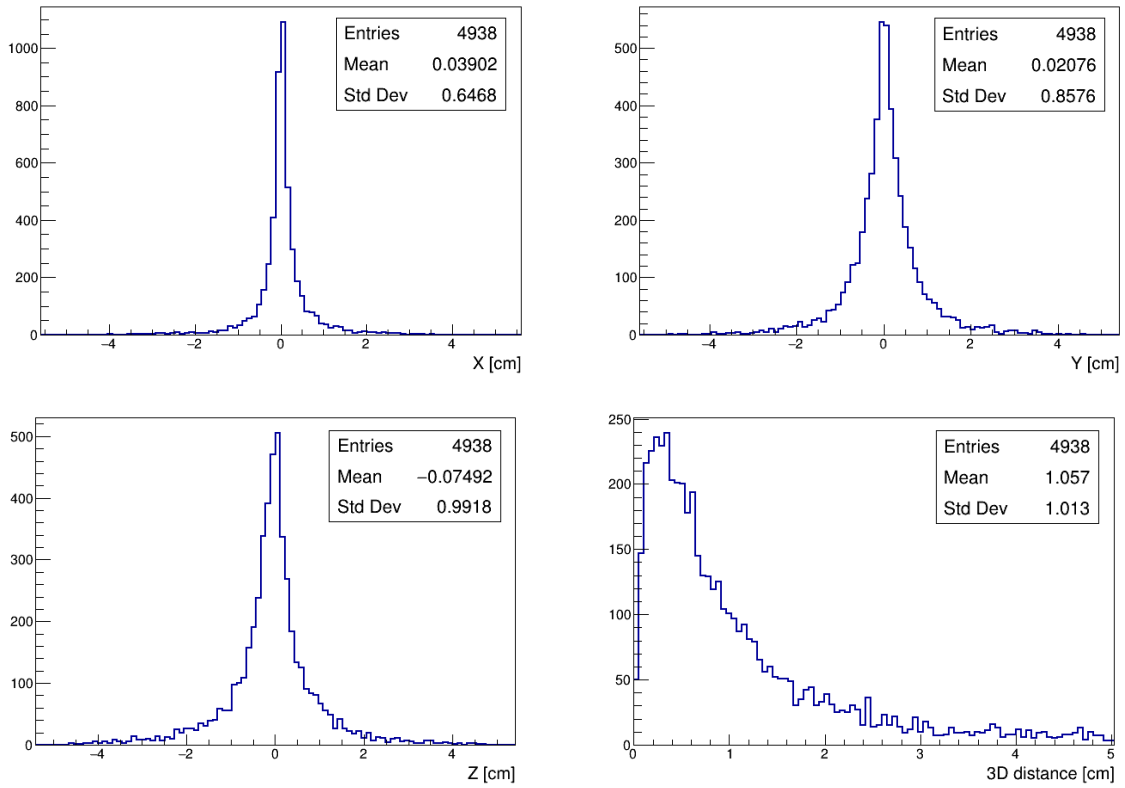

Figure 3.5: Vertex position resolution in cm in x, y, and z and 3D for the inelastic interaction of charged pions on liquid argon nuclei in events in which a π^0 is produced, in ProtoDUNE-SP, using the PMA algorithm.

increase size of stat box entries; if possible remove "temp" header

fig:PMAp

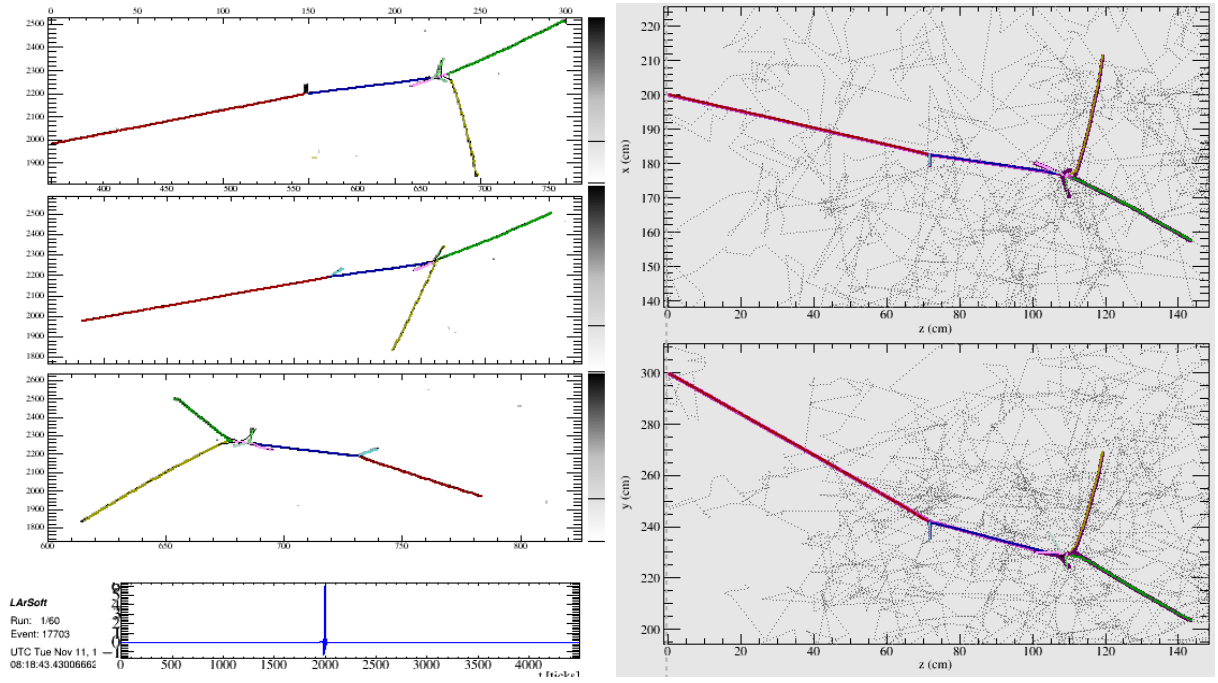

Figure 3.6: Example of reconstructed event of simulated proton with initial momentum 2 GeV/c (reconstruction algorithms: gaushit, Line Cluster and PMA). fig:PMAp

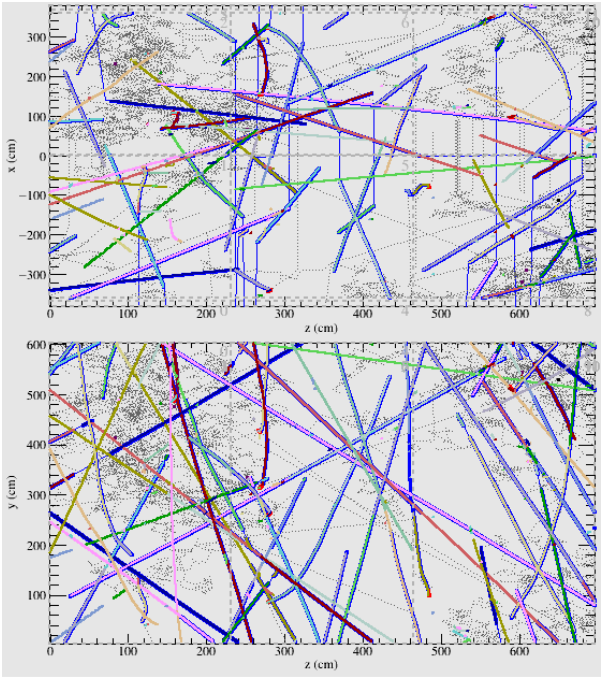

Figure 3.7: Example of reconstructed cosmic muons using gaushit, Line Cluster and PMA. fig:PMAc

Hits from different wire planes with different signal strengths are unlikely to be associated with each other. Use of the charge information takes advantage of the fact that in a LArTPC with induction planes, each of the wire planes, in principle, detects the same ionization electrons as the other planes. Figure 3.8 shows an example of the improvement of WireCell 3D imaging over the more traditional approach.

The suppression of the electronic noise comes at the cost of more sensitivity to hit inefficiencies from dead channels or the signal processing steps. Since the track and shower hypotheses are not used, the 3D imaging works for any event topology. Pattern recognition is needed to identify the content of these 3D images. Figure 3.9 shows the performance of the currently available 3D pattern recognition in WireCell. For the long track going close to parallel to the wire plane, the reconstructed track shows a zig-zag behavior. This is due to the current lack of a fine track-fitting algorithm that is expected to be added in the near future. Further developments of the WireCell pattern recognition algorithms are needed before meaningful physics quantities can be calculated.

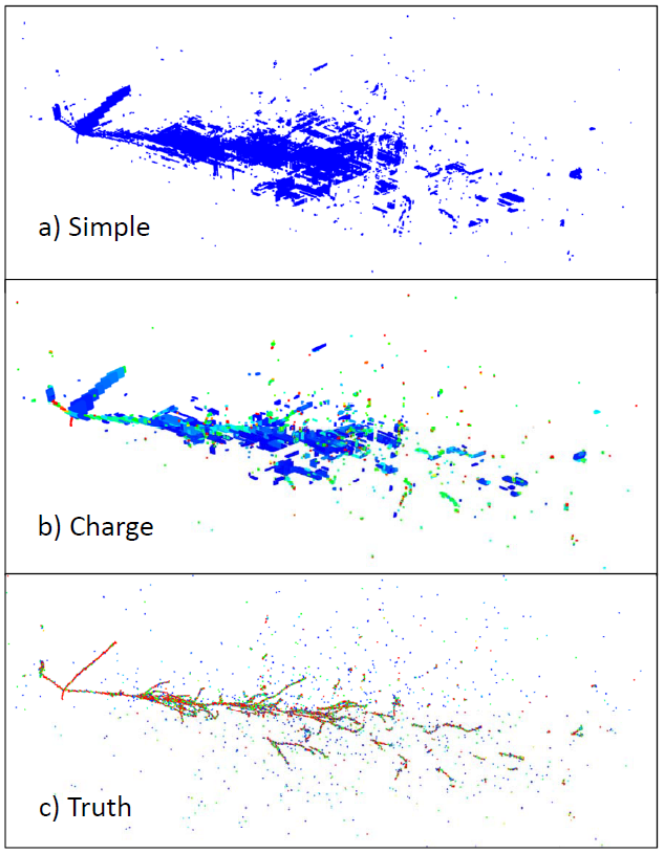

Figure 3.8: Comparison of imaging reconstruction qualities with and without the charge information.

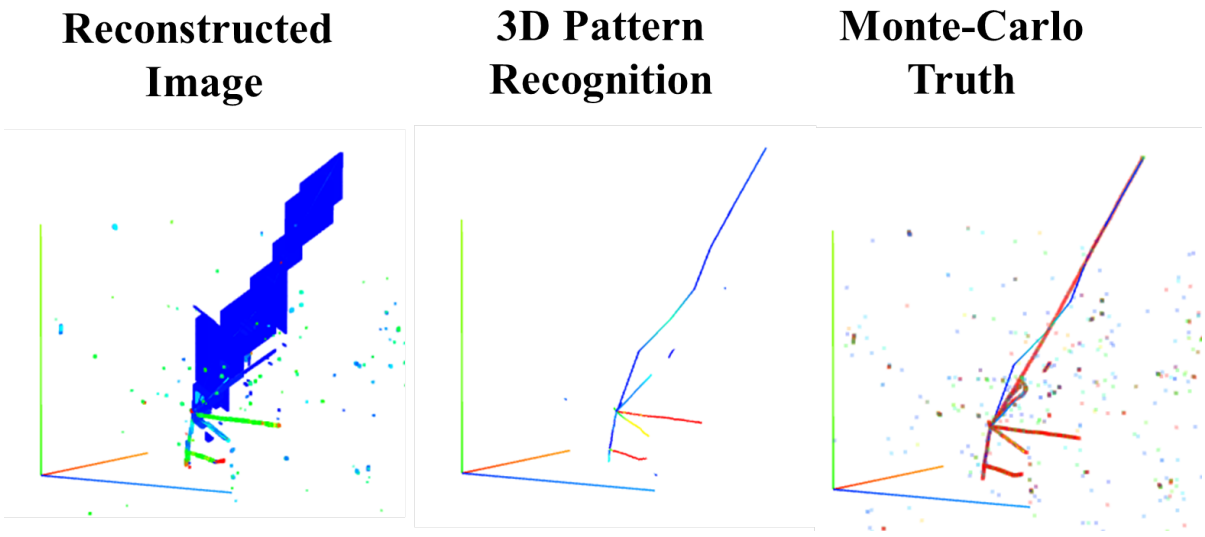

Figure 3.9: The reconstructed image is shown on the left panel for one neutrino interaction event. The image was passed through the 3D pattern recognition program with tracks identified (middle panel). The identified pattern is compared with Monte-Carlo truth in the right panel. The zig-zag line in the right panel is the identified track. More sophisticated track-fitting algorithms, to be added in the future, will improve the track reconstruction. fig:trac

Chapter 4

Space and infrastructure

spacereq

ProtoDUNE-SP is to be housed in an extension to the EHN1 hall in the North Area of the Prévessin site at CERN. The cryostat is constructed in a pit inside the building, surrounded on three sides by the pit walls. On the fourth side of the cryostat, an ISO 8 clean room provides a space to construct, test and assemble the TPC. A material pass-through structure (material SAS) is adjacent to the clean room. Figure 4.1 shows the layout of these structures in EHN1. A naming convention has been established for the four sides of the cryostat, shown in Figure 4.2. The upper side is *Jura*, the lower is *Salève*, the left is *Beam*, and right is *Downstream*.

define SAS

As detector materials are brought into EHN1, they are passed into the SAS through its removable roof, then transported through a set of large doors from the SAS into the clean room, where they are tested and assembled. When ready, each assembled TPC component passes through a temporary construction opening (TCO) in the cryostat for installation. While material is lowered into the SAS from the gallery floor, the doors to the clean room remain closed to reduce contamination of the filtered air in the clean room. Once the roof of the SAS is closed, these doors can be opened to move the material into the clean room.

The lighting inside the clean room and any temporary lighting inside the cryostat is filtered to limit the exposure of the PDS components to UV light. Wavelengths below 450 nm are filtered out.

Figure 4.3 shows an elevation section view of the cryostat indicating the position of the TCO and the location of the integrated cold testing stand (described in Section **??**).

Inside the clean room, a series of rails facilitate the movement of the TPC components during the test and installation processes. The conceptual layout of these rails is shown in Figure 4.4. The rails are positioned vertically at the same height as the detector support structure (DSS) rails inside the cryostat. A temporary rail is installed through the TCO to bridge the DSS rails and clean room rails. All the large components of the cryogenics piping and TPC are supported from these rails on movable trolleys as they are transported to the interior of the cryostat. Figure 4.4

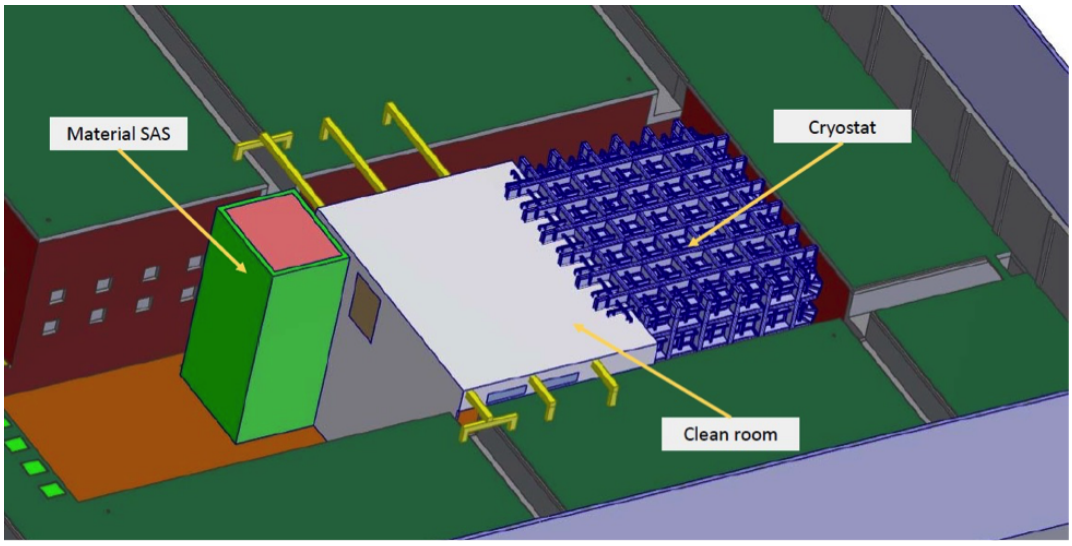

Figure 4.1: Layout of ProtoDUNE-SP cryostat, clean room and material SAS in EHN1 fig:cryo

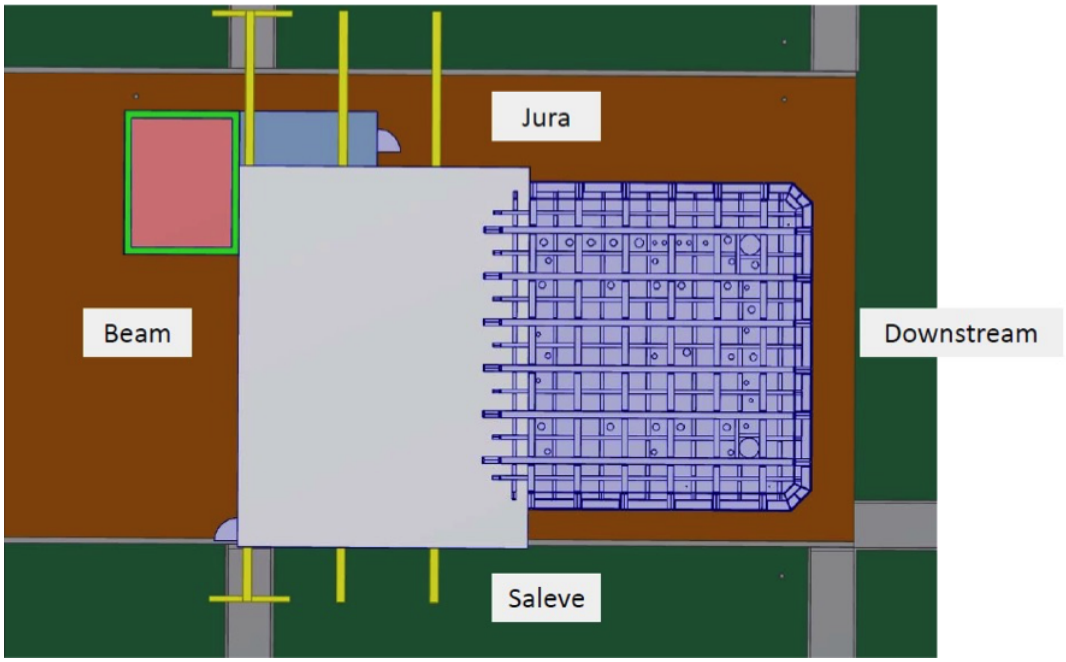

Figure 4.2: Conventions for labeling the four sides of the cryostat fig:cryo

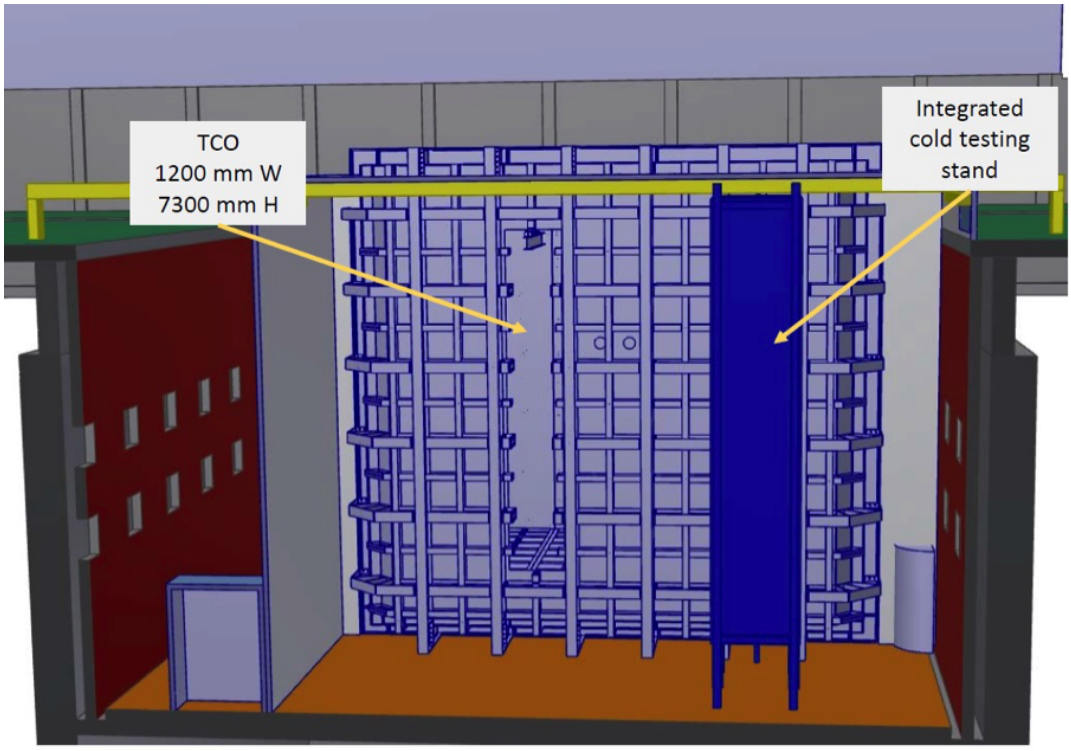

Figure 4.3: Elevation section view of the cryostat

fig:elev

also shows the approximate dimensions for the SAS and the footprint of the clean room space. These spaces are limited by the pit walls on two sides (top and bottom of figure), and by the supports for the beam and beam instrumentation on the other (see left side of figure). Figure 4.5 shows the planned locations for all of the activities that will be performed inside the clean room.

fig:sas-locati

The activities that will take place in the clean room include:

- Assembly of the CPA panels into CPA modules (on a large horizontal surface);
- Rotation of CPA modules from horizontal to vertical, and placement on the clean room rails;
- Attachment of FC assemblies to CPA modules;
- Unpacking and testing of the PDS elements, and installation on the APA frames;
- Unpacking and testing of the CE elements, and mounting onto the APAs; and
- Integrated testing of APA with PDS and CE.

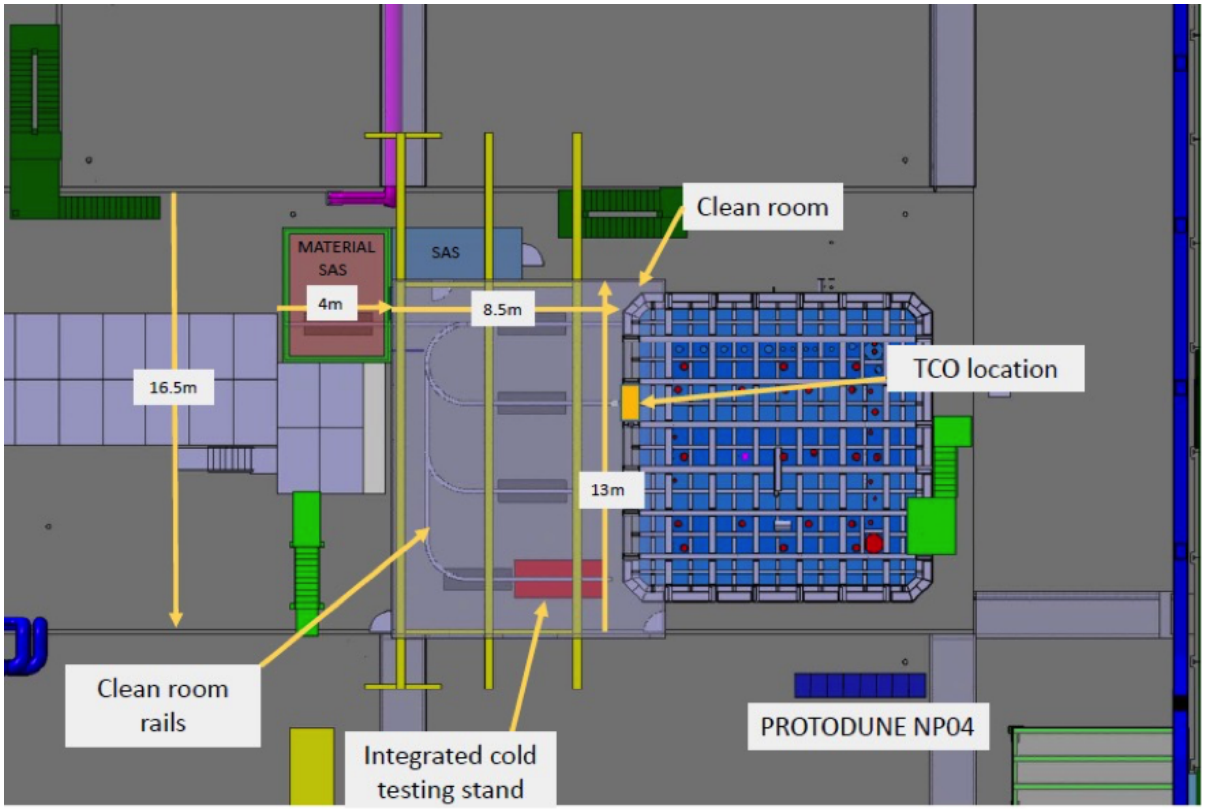

Figure 4.4: Conceptual layout of rails in clean room to facilitate movement of TPC components; approximate dimensions for the material SAS and the footprint of the clean room space are shown. fig:rail

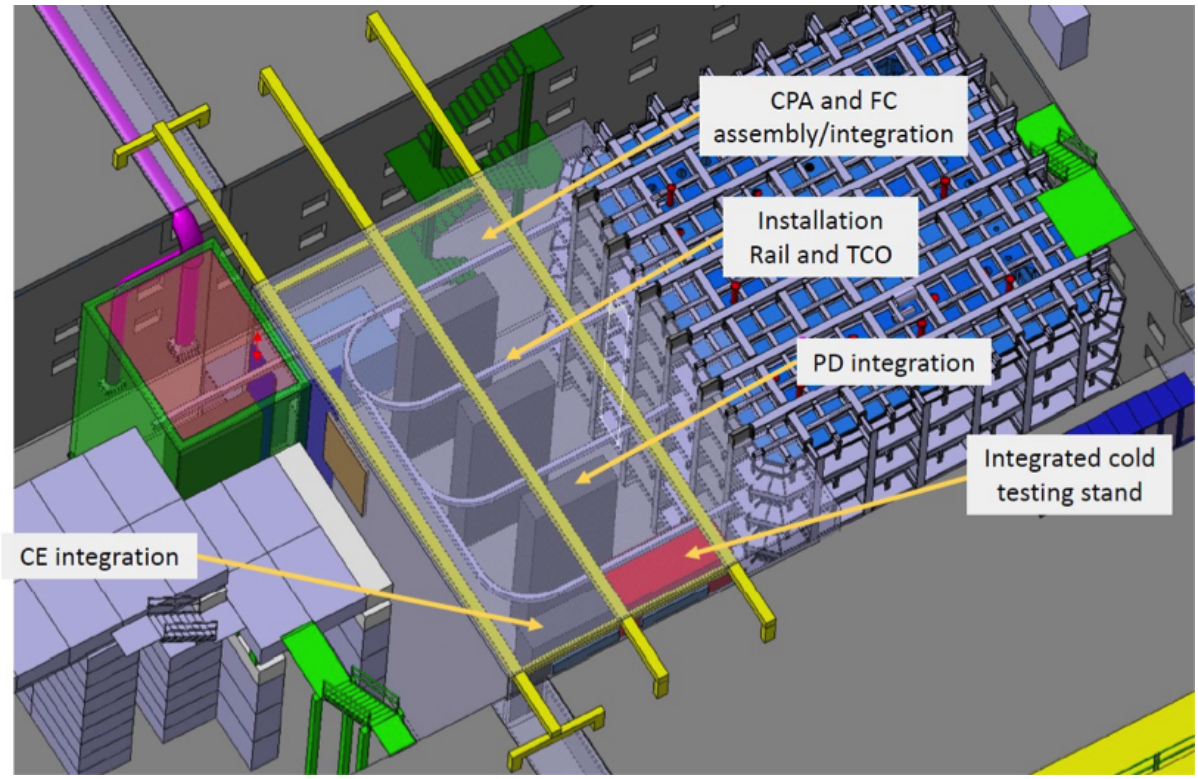

Figure 4.5: Locations of activities to be performed in the clean room fig:sas-

Chapter 5

Test beam specifications

The ProtoDUNE-SP (NP04) experiment will be housed in the EHN1 building at CERN. The detector is situated at the end of the H4 beamline in the newly constructed extension of EHN1. The H4 beamline is also extended and configured to deliver either a hadron or a pure electron beam to the experiment. To produce particles in the momentum range of interest, the secondary beam from the T2 primary target is sent onto a secondary target to generate a tertiary beam. Particles in this tertiary beam are momentum- and charge-selected and transported down the H4 beamline extension to the ProtoDUNE-SP detector. In this Chapter, we discuss the beam requirements, H4 tertiary beamline design and instrumentations, DAQ/trigger, and the physics run plans.

5.1 Beam requirements

irements

The CERN test beam results from ProtoDUNE-SP will be used to evaluate the detector performance, understand the various physics systematic effects, and provide data for event reconstruction studies that are representative of neutrino interactions. The parameters defining the test beam are primarily driven by the requirement that these test beam results be directly applicable to DUNE's future large underground single-phase detector module(s) with minimal extrapolation. To match the charged-particle spectrum and topologies that are expected in the DUNE far detector, the H4 tertiary beam must span a broad range of particle momenta, be composed of electrons, muons, and hadrons, and charge-selectable. The expected momentum distributions for secondary particles from neutrino interactions in the far detector has a large spread that ranges from a few hundred MeV/c to a few GeV/c. The desirable range for ProtoDUNE-SP is in the low-momentum region. Based on the feedback and constraints from the CERN accelerator group, the design of the beamline extension has been developed to allow the transport of beam particles from about 0.5 GeV/c up to 7 GeV/c.

The maximum electron drift time in the ProtoDUNE-SP TPC is about 2.25 ms. In order to keep the pile-up in the TPC at the percent level, the planned beam particle rate should be below 100 Hz. The ProtoDUNE-SP TPC has two drift volumes separated by a cathode plane. It is desirable to

aim the particle beam such that a large fraction of the lower-energy hadronic showers are contained in one drift volume, thus minimizing the uncertainties from particles lost in the inactive detector materials. As shown in Figure 5.1, multiple beam injection points have been explored. Based on inputs from the physics group, the larger angle (beam # 3) w.r.t. the APA plane (Saleve side), which corresponds to about 13°, is preferred. Due to engineering and safety considerations, only beam #3 will be fully instrumented with the beam window system as described in Sections 2.4.5 and 2.10.6. The remaining two beam positions will have partial installation of the beam window system. With this configuration, beam #3 is the primary beam with which most of the physics data will be taken.

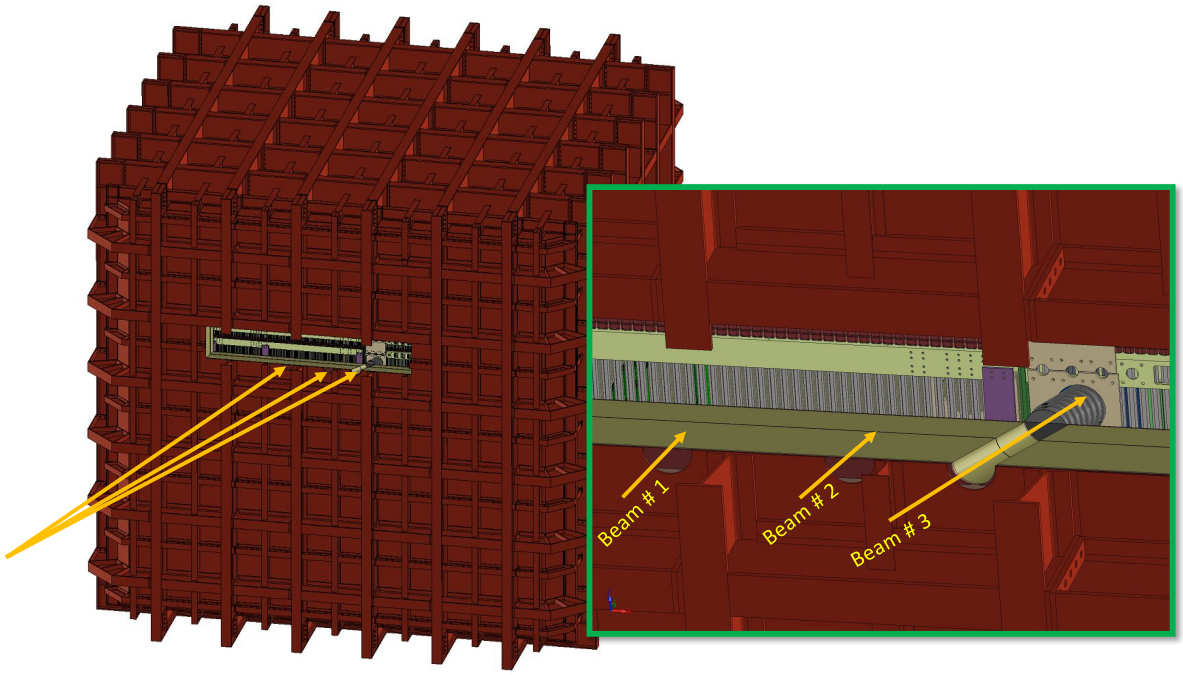

Figure 5.1: Three possible beam injection points. The cryostat support structures near the beam injection points are removed in the Figure to show the interior. Beam window and beam plug are installed only for beam # 3.

A summary of the beam requirements is shown in Table 5.1.

Table 5.1: Particle beam requirements. (Kaon rate is low for beam momentum below 2 GeV/c.)

Parameter	Requirements
Particle Types	$e^{\pm}, \mu^{\pm}, \pi^{\pm}, (K), p$
Momentum Range	0.5 - 7 GeV/c
Momentum Resolution	$\Delta p/p \leq 3$ %
Transverse Beam Size	RMS(x,y) $\approx$ 1 cm (At the entrance face of the LAr cryostat)
Beam Entrance Position	Beam # 3 (Figure 5.1) - Saleve side TPC
Rates	$\sim 25-\sim 100$ Hz

5.2 Beamline

The design of the H4 beamline extension mirrors that of the H2. In this section, we describe the beamline design and the expected beam properties.

5.2.1 H4 beamline layout and optics

The placement of the quadrupole and dipole magnets in the H4 beamline extension is illustrated in Figure 5.2. The distance from the secondary target to the front of the NP04 cryostat is about 37 m. For the hadron beam, either a tungsten or a copper target will be used. For the electron beam, a Pb target of a few radiation lengths will be used. The first two dipole magnets (shown in red) after the secondary target are rotated by about 56° to steer the beam downward towards the cryostat. The third dipole magnet (shown in green) is used for steering the beam horizontally into one of the three beam windows.

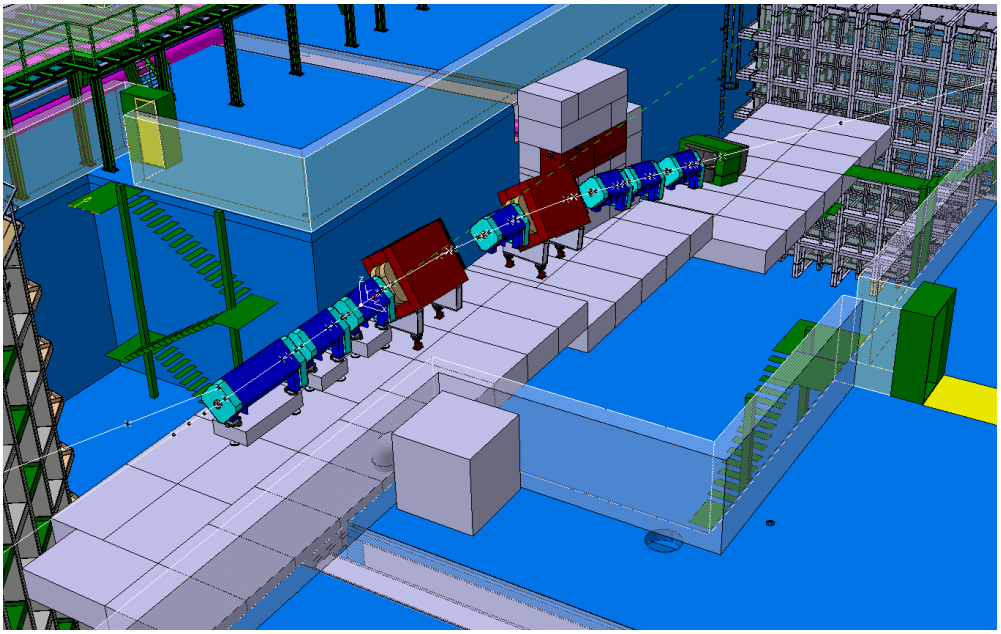

Figure 5.2: Layout of the quadrupole and dipole magnets in the H4 beamline extension. The secondary target (not shown) is upstream of the first quadrupole magnet on the left side of the Figure. Vacuum beam pipe and beam instrumentations are also not shown. (Courtesy of V. Clerc, CERN).

The beamline optics from the target to the cryostat for the horizontal and vertical planes are shown in Figure 5.3. The Figures show the position of the quadrupole magnets (Q17-Q22), dipole magnet (B17 - B19), collimator (C12), Time-of-Flight detectors (TOF1-2), beam profile monitors (BPROF1-4), and the Threshold Cherenkov counters (XCET1-2) relative to the secondary target. For the nominal configuration, the beam is focused at the front of the cryostat to ensure maximum acceptance of beam particles through the beam window penetration and the beam plug inside the cryostat.

The beamline is in vacuum, with a beam pipe extending from the secondary target down to the beam window in the cryostat upstream face.

5.2.2 Beam properties

A full GEANT4 simulation of the H4 beamline including its extension to the ProtoDUNE-SP detector has been performed.The beamline model starts with the H4 secondary beamline and derives the particle properties in the tertiary beamline. Target, magnets, collimators and a preliminary assumption about beam instrumentation are included. The secondary target has been modeled as a Tungsten cylinder (R=30 mm, L=300 mm) for beam momenta $\leq$ 3 GeV/c and as a Copper cylinder of the same dimensions for beam momenta $>$ 3 GeV/c. Optimization of the target dimensions and material is ongoing.

Table 5.2 describes the particle composition of the hadron beam at the entrance of the cryostat. Two features are evident. First, the beam is dominated by positrons at low energies, and secondly, the kaon content, and to a lesser extent the pion content, are depleted at lower energies due to decays of these species along the beam path.

Table 5.2: Beam composition (in percentage) at the cryostat entrance for particles contained in the beam pipe (R= 10 cm).

Momentum (GeV/c)	e^{+-}	K^{+-}	μ^{+-}	p^{+-}	π^{+-}
-7	27.4	3.4	1.0	1.3	66.9
-6	33.5	2.9	1.2	1.3	61.2
-5	43.2	1.9	1.3	1.1	52.5
-4	54.6	1.1	1.4	0.6	42.3
-3	28.4	1.1	2.3	1.4	66.8
-2	48.9	0.3	1.8	0.4	48.6
-1	81.7	0.2	1.1	0.2	16.9
-0.4	98.3	0.0	0.4	0.0	1.3
0.4	99.1	0.0	0.0	0.5	0.5
1	69.3	0.0	0.3	15.3	13.9
2	34.9	0.6	1.7	22.9	39.0
3	19.9	2.8	0.6	18.9	56.6
4	47.1	1.6	1.1	8.8	41.3
5	37.0	2.8	0.9	9.4	49.5
6	28.1	4.0	0.9	10.4	56.2
7	20.6	5.1	1.0	10.7	62.6

Particle rates, assuming a spill intensity of 10^6 particles on the secondary target and a SPS spill length of 4.8 seconds, are reported in Table 5.3. The H4 simulation results are documented in CERN-ACC-NOTE-2016-0052.

At momenta larger than about 4 GeV/c, the particle rates are at the limit or beyond the DAQ

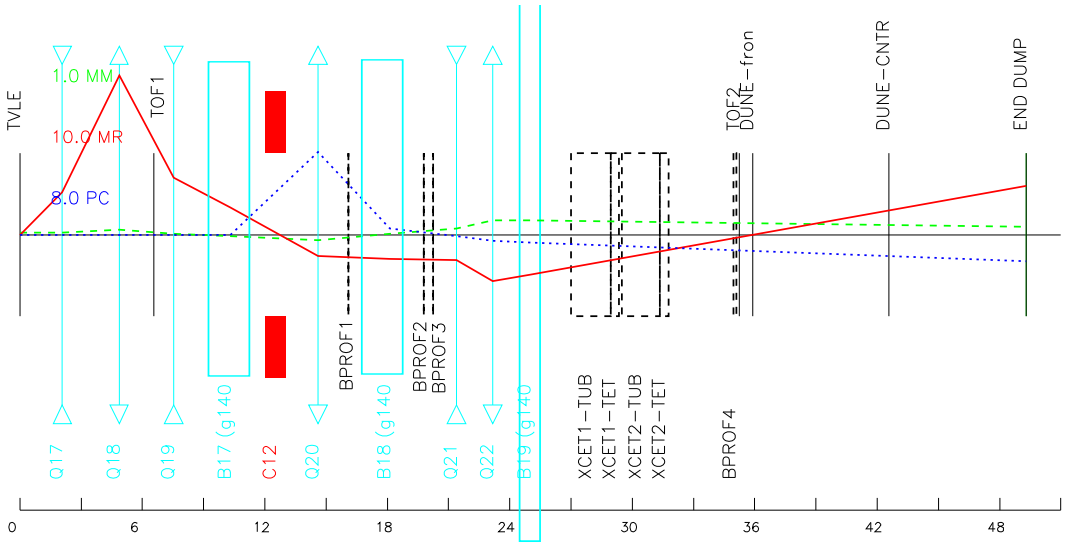

H4-VLE beam to Single Phase ProtoDune

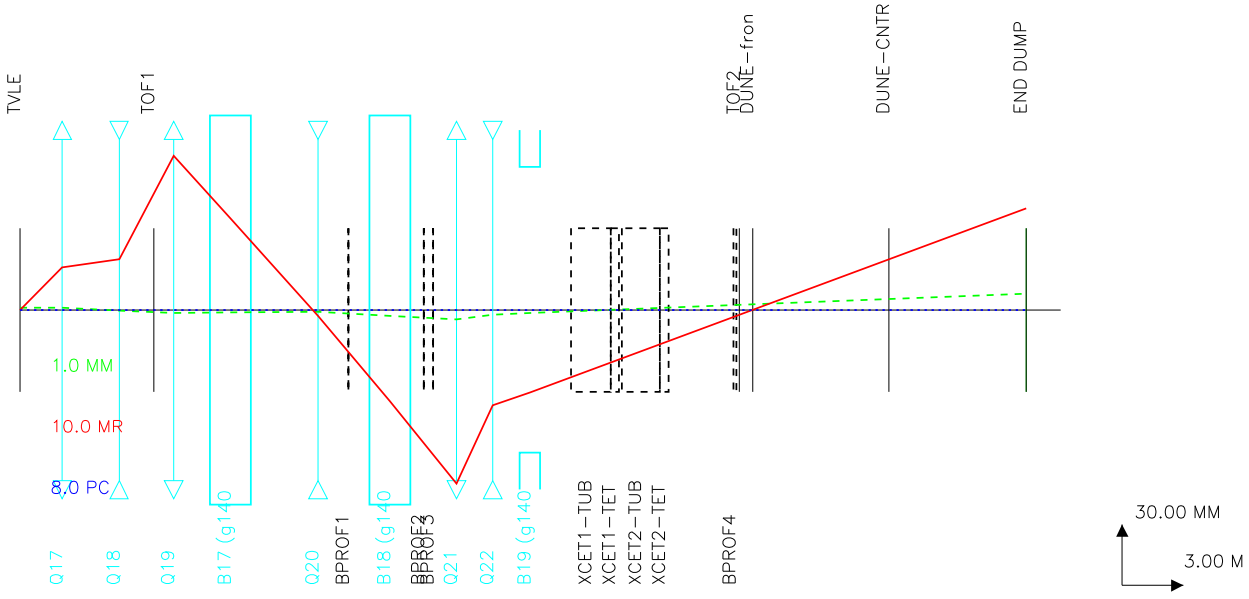

Figure 5.3: H4 beamline extension optics for the horizontal (top) and vertical (bottom) planes. The secondary target is located on the left side of the plots and the front of the ProtoDUNE-SP cryostat is located at the beam focus point, at about 37 m from the secondary target. Q17-Q22 are the quadrupole magnets. B17-B19 are the dipole bending magnets. TOF1-2 are the Time-of-Flight detectors, BPROF1-4 are the beam profile monitors, and XCET1-2 are the threshold Cherenkov counters. fig:beam

Table 5.3: Particle rates (Hz).

Momentum (GeV/c)	e^{+-}	K^{+-}	μ^{+-}	p^{+-}	π^{+-}	total
-7	57	7	2	3	138	207
-6	62	5	2	2	113	185
-5	72	3	2	2	87	166
-4	93	2	2	1	72	170
-3	11	0.5	1	0.5	26	39
-2	13	0	0.5	0.1	16	27
-1	18	0	0.2	0	4	22
-0.4	8	0	0	0	0.1	8
0.4	7	0	0	0	0	7
1	18	0	0	4	4	27
2	13	0.2	0.5	9	15	38
3	11	1	1	11	31	56
4	92	3	2	17	81	196
5	74	6	3	19	99	200
6	63	9	3	24	127	226
7	52	13	2	27	157	252

artrates

capability. At lower energies, the proton and pion rates are much lower, reduced by a factor of 10 at 1 or 2 GeV/c, and are overwhelmed by the positron rate.

The momentum spread of the beam is of the order of 5–7%. At higher energies, where the particle rate is higher, the momentum spread can be narrowed by closing the collimators, at the expense of the beam intensity. For example, Figure 5.4 shows that at $p = 4$ GeV/c the momentum spread can be reduced to $\Delta p/p = 3.6\%$ with a factor of 4 reduction in particle rate.

fig:momcoll

5.2.3 Muon halo

The secondary beam is mainly composed of 80-GeV pions. In the long path (≈ 600 m) between the primary and the secondary target, an intense high-energy muon halo is produced by pion decay. Muons propagate approximately in the direction of the first section of the H4 beamline, that is slightly upward and sidewards of the H4 beamline extension which points at the ProtoDUNE-SP detector. Therefore the most intense part of the muon halo passes about one meter above the left corner of ProtoDUNE-SP cryostat. Figure 5.5 shows the spatial distribution of the muon halo at the face of the cryostat. Only muons with momentum larger than 4 GeV/c have been considered. Despite the low statistics of the simulations, the up-down and left-right asymmetry is clearly visible. The origin of the coordinate system is chosen to coincide with the center of the cryostat face. The color scale shows the muon intensity in μ/m^2/spill for 10^6 particles/spill from the primary target. The muon intensity on the cryostat face, indicated by the black rectangle in Figure 5.5, ranges up to $\sim$400 μ/m^2/spill. However, the rate of halo muons impinging on the front side of the TPC active volume (red rectangle) is expected to be significantly lower, in particular,

fig:muonhalo_HE

fig:muonhalo_HE

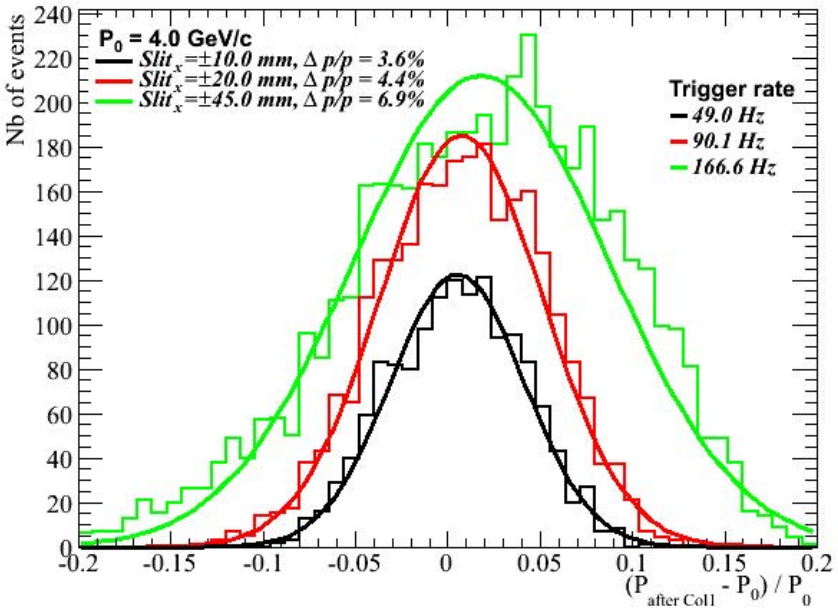

Figure 5.4: Beam momentum spread with different collimator openings at 4 GeV/c.

as low as a few μ/m^2/spill on the Saleve side of the TPC where the H4 beamline points. The rate of beam events with out-of-time halo muon tracks captured in the 2.5 ms time frame of the recorded event is expected to be limited.

Figure 5.5 is very preliminary though, not only because of low statistics, but also because shielding around the low-energy beamline is not included in the simulation, and the muons produced in neighboring beamlines in EHN1, including the H2 beamline that feeds ProtoDUNE-DP, are not considered here. Based on these results, the estimated contribution to the total data volume from beam halo is negligible.

5.3 Beamline instrumentation

The H4 beamline will be instrumented with a number of beamline detectors to provide information about the beam profile, position, momentum, particle identification, and trigger capability. This section discusses the reference design for the beam instrumentation.

5.3.1 Beam profile monitoring, particle tracking and momentum measurements

Operation of the beamline requires at least one beam monitor, able to provide the beam profile in two dimensions (*x,y*) at the entrance point to the NP04 cryostat. The beam monitor can also

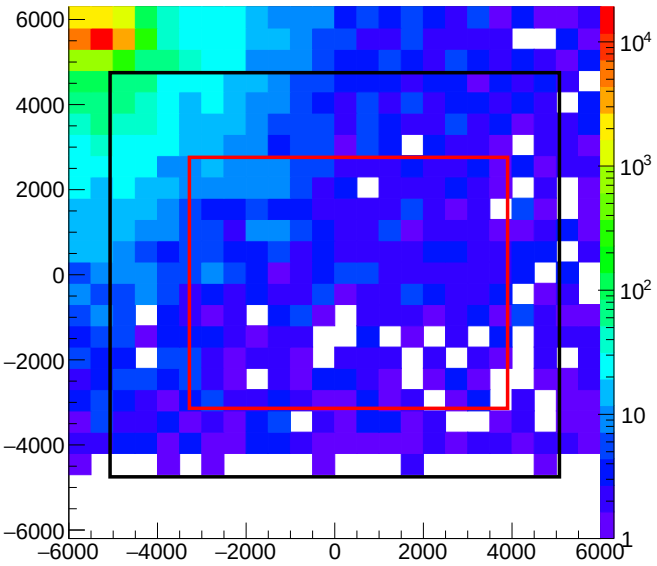

Figure 5.5: Muon halo intensity at the cryostat face for muons originating from the H4 beamline and with $P_\mu \geq 4$ Gev/c. The origin of the $x-y$ coordinate system is centered on the cryostat and dimensions are in mm. Color scale is in units of μ/m^2/spill. The black and red rectangles represent the cryostat face and front face of the active detector volume.

fig:muon

be exploited for data analysis, provided that it delivers data on an event-by-event basis. Another monitor, located immediately downstream of the last bending magnet, is added in the layout in order to determine the incident particle direction and position at the front face of the cryostat, and match it with the reconstructed track in the LAr active volume.

To reduce the uncertainty due to the momentum spread of the beam around the central selected value, the momentum can be measured particle by particle with a set of three detectors placed one upstream and two downstream of the bending magnets B18 (see Figure 5.3). Preliminary results using full simulations indicate that a momentum resolution on the order of 2% is achievable.

fig:beamoptics

Fiber tracker The CERN Beam Instrumentation group will produce the beam monitors using scintillating fiber technology, where the fibers have a polystyrene core surrounded by cladding. Fibers provide a light yield of ∼8000 photons/MeV, deposited with fast rise and decay times of 1–3 ns. The design foresees 1 mm square fibers in two planes to provide x and y coordinates. Fibers will be mirrored on one end to increase light collection. Every monitor consisting of two planes of 1 mm thick fibers adds 0.47% of a radiation length (X_0) to the material budget - the amount of material distributed along the beamline and crossed by the beam particles before entering the TPC active volume. The three devices for momentum measurement will consist of one layer only, oriented perpendicularly to the magnet deflection. A fiber plane is made out of 192 fibers with no space between them. It will cover an area of 192 mm × 192 mm and fits in the beamline. Scintillation light will be read out using SiPMs. These detectors for position and momentum measurement are mounted through special flanges along the beam pipe, without the need to break

the vacuum.

5.3.2 Particle identification

The H4 beamline is capable of delivering two types of beams, electron and hadron. While the electron beam is relatively pure, the hadron beam consists of a mixture of electrons, pions, kaons, and protons. Therefore, for the hadron beam, it is essential to have an efficient particle identification system to cleanly tag particle types on a particle-by-particle basis. To achieve this goal, a particle identification system based on a combination of threshold Cherenkov counters and time-of-flight (ToF) system is planned for ProtoDUNE-SP. Cherenkov counters can be placed in the last segment of the beamline, between the last bending magnet and the cryostat.

Threshold Cherenkov counter Threshold Cherenkov counters have been used extensively in beamlines to discriminate particles. Figure 5.6 shows one of the counters used in the CERN test beam area. It consists of a gas radiator that is contained in a long cylindrical tube, and a detection box in which the Cherenkov light is reflected by a 45° mirror and focused onto a photomultiplier tube (PMT). A variety of gases (e.g., CO_2, nitrogen, argon, Freon 12, air) are available at CERN for filling the Cherenkov counter to optimize particle identification. Two threshold Cherenkov counters will be installed in the beamline, one detecting pions, the other detecting pions and kaons. The combination of the two signals will allow identification of all hadron species. In order to provide signals at low beam momenta, either heavier gases or high pressures are needed. Figure 5.7 shows the gas-pressure threshold for the production of Cherenkov light for various particle types as a function of particle momentum for Freon 12 and CO_2 gases.

Freon 12 has been selected for its heavier mass, however, to avoid liquefaction it cannot be operated at pressures larger than 3 bars. CO_2 can be used more easily at higher pressures.

Figure 5.7 shows that pions can be tagged with a 3-bars Freon counter for momenta larger than 2 GeV/c, and kaons can be tagged with a high-pressure (15-bars) CO_2 counter above 4 GeV/c.

The reference plan for beam instrumentation includes a 2-m-long Cherenkov counter filled with Freon 12 at adjustable pressure up to 3 bars (XCET1), and a 2-m-long Cherenkov counter filled with CO_2 at adjustable pressure up to 15 bars (XCET2).
Existing Cherenkov counters at CERN are designed for pressures lower than 3 bar, therefore a new counter has to be manufactured in order to reach the 15 bars needed to efficiently tag kaons. Drawings for such high-pressure Cherenkov counters do exist, as they have been used in the past. Since it will not be necessary to use both counters at all energies, the CO_2 counter, filled at low pressure, will be used for electron discrimination at beam momenta lower than 4 GeV/c.

A time-of-flight (ToF) system is necessary to distinguish hadrons below the mentioned thresholds. In summary:

- **below 2 GeV/c** : one Cherenkov, filled with CO_2 at low pressure, discriminates electrons; ToF needed for hadrons.

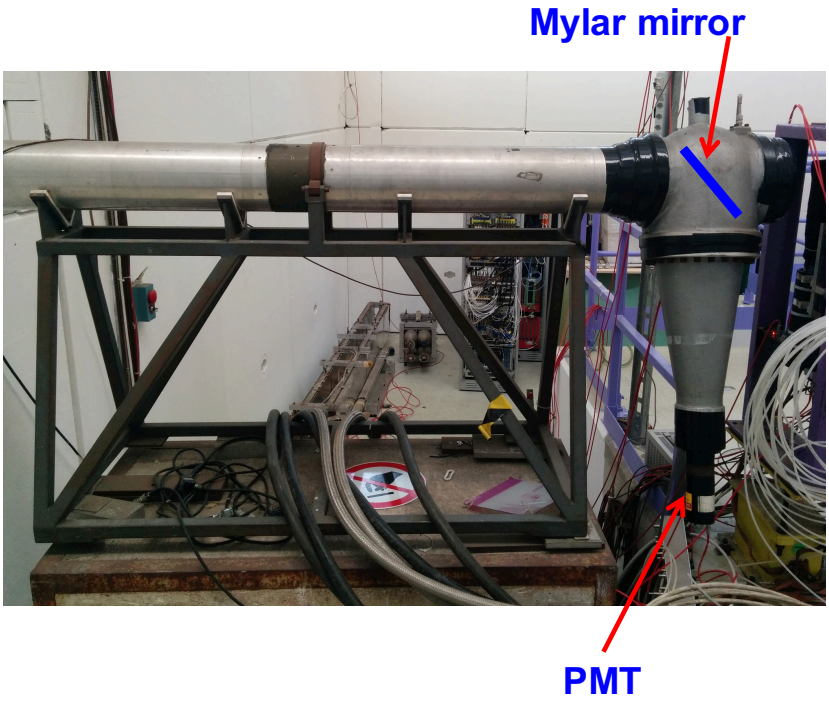

Figure 5.6: CERN threshold Cherenkov counter

fig:ckv

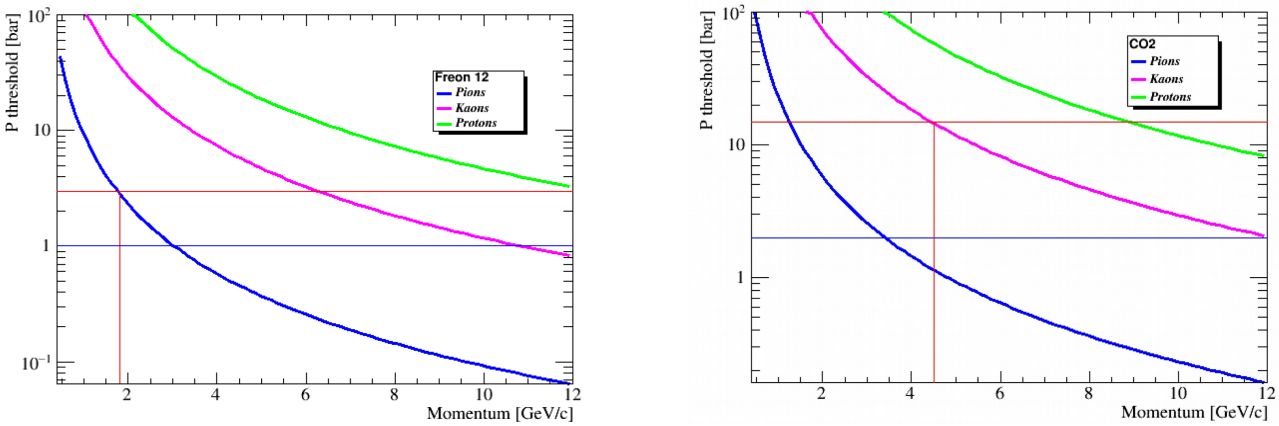

Figure 5.7: Gas pressure threshold for the production of Cherenkov light for various particles as a function of particle momentum for Freon 12 [2] and CO_2 gases.

kv_gases

- **2-3 GeV/c** : one Cherenkov, filled with CO_2 low pressure, discriminates electrons; second Cherenkov, filled with Freon 12, tags pions; kaons content in this range is very low or negligible. ToF is needed to identify protons.

- **3-4 GeV/c** : one Cherenkov, filled with CO_2 at low pressure, discriminates electrons; second Cherenkov, filled with Freon 12, tags pions; ToF is needed for kaon/proton discrimination

- **4-7 GeV/c** : one Cherenkov, filled with CO_2 at high pressure, tags kaons; second Cherenkov, filled with Freon 12, tags pions; electron content of the beam is low and can be discriminated by reconstruction.

tab:beampartcomp
From table 5.2 it is evident that the kaon content of the beam is negligible at least below 2 GeV/c, thus only pion-proton separation is needed at low energies. Figure 5.8 shows the ToF resolution needed to distinguish among particle species at the 4σ level as a function of the particle momentum, assuming a 28-m-long path. To distinguish pions from protons below 2 GeV/c, a 1-ns resolution is enough, while 300 ps are necessary for kaon-proton separation up to 4 GeV/c. It should also be noted that a ToF system with a ∼100-ps resolution would allow identification of protons from other hadrons up to 7 GeV; this would release the need for a high-pressure CO_2 Cherenkov. Conversely, covering the full energy range up to 7 GeV for all hadron types would require a ToF system with a resolution better than 40 ps. In the following, two (possibly complementary) ToF systems are described.
fig:toftau

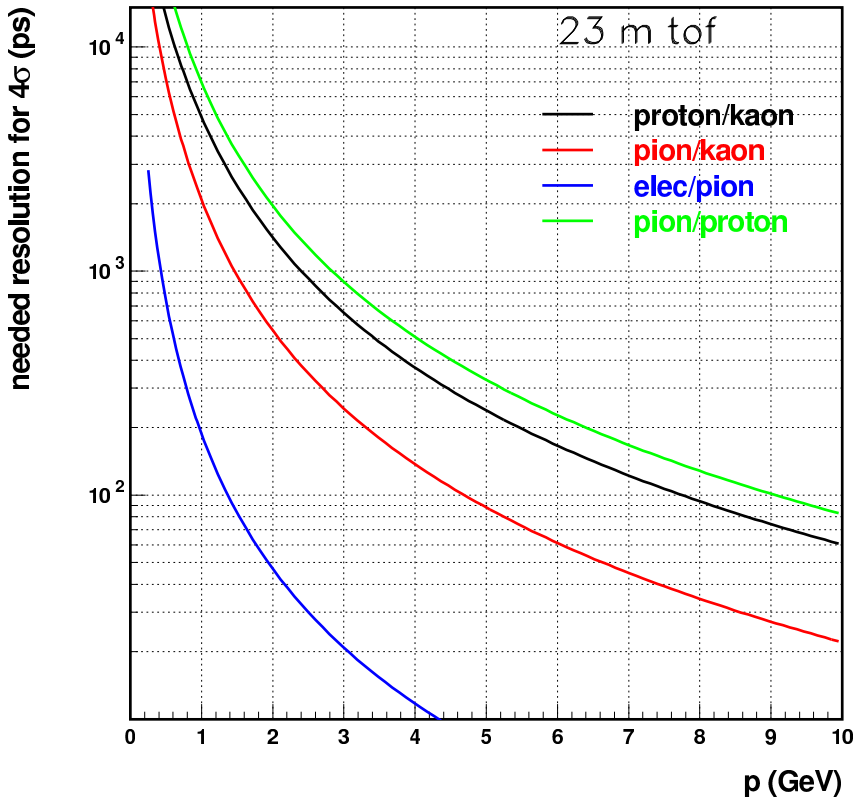

Figure 5.8: Required ToF resolution to distinguish among particle species at the 4σ level as a function of the particle momentum, assuming a 28-m long path. (The figure shows 23 m; it needs to be updated.)
fig:toft

pLAPPD time-of-flight system Fermilab is testing a ToF system from Argonne National Laboratory that would utilize 6×6 cm^2 prototype large-area picosecond photodetectors (pLAPPDs), as shown in Figure 5.9. The microchannel plates based devices are capable of < 50 ps resolution with gains of $10^6 - 10^7$, mm position resolution along one axis, and slightly worse resolution along the other axis. The photodetector is mounted on a readout board, and the relevant exterior dimensions are 165.1 mm $\times$ 109.3 mm and a thickness of 16 mm. The active area is defined by the four squares visible in Figure 5.9, and amounts to about 31 cm^2. Tests of these devices in the Fermilab test beam facility (FTBF) are underway, to precisely assess the efficiency and timing capabilities of such a system. The pulses from the pLAPPDs will be read out by a fast waveform digitizer and the tests at the FTBF include the development of an artDAQ-based DAQ and potentially a ToF trigger module capable of providing a particle trigger to the ProtoDUNE-SP DAQ. Larger area pLAPPD can be made to match the H4 beam profile.

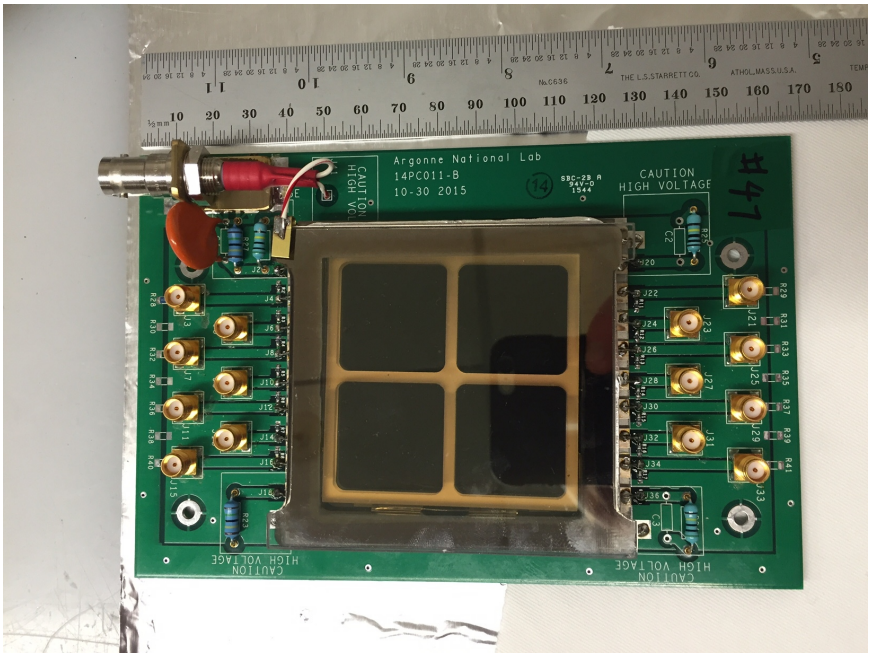

Figure 5.9: Photo of one pLAPPD device as proposed for the H2 and H4 beamlines.

Alternative Time-of-flight system The scintillating-fiber monitors can be used also for ToF purposes with the goal of a 1-ns timing resolution, suitable for low momentum (< 2 GeV/c) beams. The idea is to read out the detectors with the STiC ASIC [46] for SiPM readout.

Is STiC defined?

In this configuration, the time resolution would be dominated by the fiber response. Monte Carlo simulations estimate a resolution better than 1 ns. A small prototype will be built and tested in the next few months to fully validate this solution.

5.3.3 Material budget and discussion

The set of beam detectors considered for instrumenting the H4 tertiary beamline include five beam monitors (two for tracking and three for spectrometry), two ToF devices, and two high density or pressure gas Cherenkov detectors. The selection of the beam detector configuration in the beamline depends on the type of beam (electron of hadron), and on the beam momentum range. For the electron beam and for low momenta hadron beams the amount of detector material along the beamline may result in particle energy degradation and significant reduction of the beam rate delivered at the active detector due to scattering outside the beam pipe. A FLUKA[?, 33] simulation was used to evaluate these effects accounting for the detector materials in the beamline, and materials of the beam window, cryostat and beam plug. Figure 5.10 shows the cumulative increase of the material budget along the tertiary beam line from the target to the TPC, expressed in terms of fraction of radiation length (red line - total $0.6X_0$) and of interaction length (black line - total $0.15\lambda_I$). The average energy loss for a mip is about 28 MeV. The largest contribution to the energy-loss and energy degradation is due to the high pressure Cherenkov detectors and to the pLAPPD. Except for a low-pressure Cherenkov counter for electron discrimination, the high pressure Cherenkov are not necessary at low hadron beam momenta and can be removed or just emptied. Scintillating fiber beam monitors can replace the pLAPPD as ToF devices for the lowest-momentum beam.

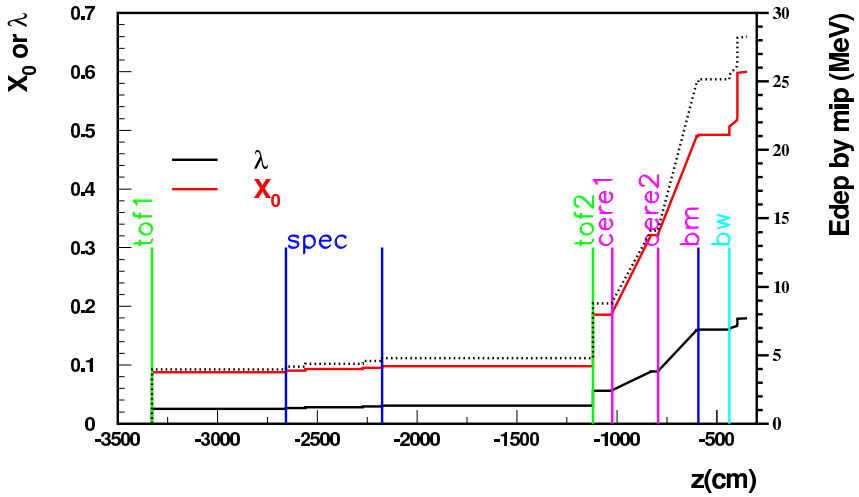

Figure 5.10: Material budget in the beamline, as a function of the distance from the center of the detector (in cm). The red line describes the amount of X_0, the black line the amount of interaction length, both read on the left axis. The black dotted line is the average energy lost by a mip particle, and is read on the right axis (in MeV). Vertical lines show the positions of the various beam monitors (in between the two blue lines are the 3 devices for spectrometry, "bm" is the last beam monitor, "bw" is the starting point of the beam window).

Scattering of low-energy pions and protons in crossing the detector material significantly reduces their content in the low-momenta hadron beam reaching the detector active volume. For example, at 1 GeV/c the rate of pions arriving at the detector is reduced by a factor of 2.5, and the rate of protons is reduced by a factor of 4.

5.3.4 Trigger and data acquisition

The beam instrumentation can provide a trigger signal, built from the coincidence of the two last beam monitors, vetoed by the electron-tagging Cherenkov for low-energy beams. A trigger mask, providing the status of the other counters, can also be provided. Synchronization of the detector data acquisition (DAQ) with the beam instrumentation DAQ will be ensured by a common time stamp through a White Rabbit network.

Beam instrumentation data will be read out independently on a separate DAQ stream. However, the beam data fragments corresponding to events with a valid trigger from both beam and ProtoDUNE-SP will be merged online with the detector data.

References

[1] E.D. Marquardt, J.P. Le, and Ray Radebaugh, "Cryogenic Material Properties Database," tech. rep., 2010. http://www.cryogenics.nist.gov/Papers/Cryo_Materials.pdf.

[2] "Cathode HV Discharge Mitigation Design." http://docs.dunescience.org:8080/cgi-bin/ShowDocument?docid=1320.

[3] A. A. Machado and E. Segreto, "ARAPUCA a new device for liquid argon scintillation light detection," *JINST*, vol. 11, no. 02, p. C02004, 2016.

[4] "Data scenarios spreadsheet." DUNE DocDB 1086.

[5] Silicon Labs, *Si5342/5344/5345/5346/5347 Jitter Attenuating Clocks*, 7 2016. Rev. D.

[6] Avnet, *MicroZed Hardware User's Guide*, 1 2015. v1.6.

[7] R. Herbst, "Design of the slac rce platform: A general purpose atca based data acquisition system," *IEEE*, vol. 978, no. 1-4799-6097-2/14, 2015.

[8] C. Green, J. Kowalkowski, M. Paterno, M. Fischler, L. Garren, and Q. Lu, "The art framework," *J. Phys. Conf. Ser.*, vol. 396, p. 022020, 2012.

[9] Elasticsearch, "Kibana - data analytics and visualisation tool," tech. rep. https://www.elastic.co/products/kibana.

[10] M. Paterno, "artdaq: An event filtering framework for fermilab experiments." http://cd-docdb.fnal.gov/0049/004907/003/artdaq-talk.pdf.

[11] "XRootD, high performance, scalable fault tolerant access to data repositories." http://xrootd.org/.

[12] "Design of the data management system for the protodune experiment." DUNE DocDB 1212.

[13] "GTT Membrane Technologies." http://www.gtt-training.co.uk/gtt-membrane-technologies/.

[14] "EHN1-warm cryostat functional specification." https://edms.cern.ch/document/1531438/3.

[15] "EHN1-warm cryostat current drawings." https://edms.cern.ch/document/1531439/3.

[16] "EHN1-protoDUNE-penetrations." https://edms.cern.ch/document/1543241/3.

[17] "PROTODUNE PENETRATIONS." https://edms.cern.ch/document/1581898/0.

[18] "LBNF-DUNE Requirements (DUNE doc-db 112)." http://docs.dunescience.org

need to get proper link

.

[19] Montanari, D., "LBNE 35 ton proto Talk at LAr1-ND Meeting," tech. rep., 2014. http://lbne2-docdb.fnal.gov/cgi-bin/ShowDocument?docid=8626.

[20] "LAPD Purge and Recirculation Plots." http://lartpc-docdb.fnal.gov:8080/cgi-bin/ShowDocument?docid=706.

[21] "Design of the Data Management System for the protoDUNE Experiment (DUNE doc-db 1212)." http://docs.dunescience.org

need to get proper link

.

[22] "LArSoft Collaboration, Software for LArTPCs." http://larsoft.org.

[23] "The art Event Processing Framework." http://art.fnal.gov.

[24] "Scientific Software for Relocatable UPS ." http://http://scisoft.fnal.gov/.

[25] Chris Hagmann, David Lange, Jerome Verbeke, Doug Wright, "Proton-induced Cosmic-ray Cascades in the Atmosphere," tech. rep. http://nuclear.llnl.gov/simulation/doc_cry_v1.7/cry.pdf.

[26] Chris Hagmann, David Lange, Doug Wright, "Monte Carlo Simulation of Proton-induced Cosmic-ray Cascades in the Atmosphere," tech. rep., 2012. UCRL-TM-229452.

[27] D. Heck, G. Schatz, T. Thouw, J. Knapp, and J. N. Capdevielle, "CORSIKA: A Monte Carlo code to simulate extensive air showers," 1998.

[28] C. Andreopoulos *et al.*, "The GENIE Neutrino Monte Carlo Generator," *Nucl. Instrum. Meth.*,

vol. A614, pp. 87–104, 2010.

[29] S. Agostinelli *et al.*, "GEANT4: A Simulation toolkit," *Nucl. Instrum. Meth.*, vol. A506, pp. 250–303, 2003.

[30] "General Geometry Description (GGD)." `https://github.com/brettviren/gegede`.

[31] J. B. Birks, *The Theory and practice of scintillation counting*. 1964.

[32] M. Szydagis, N. Barry, K. Kazkaz, J. Mock, D. Stolp, M. Sweany, M. Tripathi, S. Uvarov, N. Walsh, and M. Woods, "NEST: A Comprehensive Model for Scintillation Yield in Liquid Xenon," *JINST*, vol. 6, p. P10002, 2011.

[33] G. Battistoni, T. T. Böhlen, F. Cerutti, P. W. Chin, L. S. Esposito, A. Fassò, A. Ferrari, A. Lechner, A. Empl, A. Mairani, A. Mereghetti, P. G. Ortega, J. Ranft, S. Roesler, P. R. Sala, V. Vlachoudis, and G. Smirnov, "Overview of the FLUKA code," *Annals of Nuclear Energy*, vol. 82, p. 10, 2015.

[34] A. Ferrari, P. R. Sala, A. Fasso, and J. Ranft, "FLUKA: A multi-particle transport code (Program version 2005)," 2005.

[35] G. Battistoni, P. R. Sala, M. Lantz, A. Ferrari, and G. Smirnov, "Neutrino interactions with FLUKA," *Acta Phys. Polon.*, vol. B40, pp. 2491–2505, 2009.

[36] M. Mooney, "The MicroBooNE Experiment and the Impact of Space Charge Effects," in *Meeting of the APS Division of Particles and Fields (DPF 2015) Ann Arbor, Michigan, USA, August 4-8, 2015*, 2015.

[37] `http://garfield.web.cern.ch/garfield/`.

[38] "Noise Characterization and Filtering in the MicroBooNE TPC." `http://www-microboone.fnal.gov/publications/publicnotes/MICROBOONE-NOTE-1016-PUB.pdf`.

[39] MicroBooNE noise filtering technot, doc-db:5730 `http://microboone-docdb.fnal.gov:8080/cgi-bin/ShowDocument?docid=5730`.

[40] "The Cluster Crawler Suite Technical Manual." `http://microboone-docdb.fnal.gov/cgi-bin/ShowDocument?docid=2831`.

[41] "TrajCluster: A 2D Cluster Finder ." `https://cdcvs.fnal.gov/redmine/attachments/download/34265/TrajCluster%20Technical%20Note.pdf`.

[42] `http://larsoft.org/single-record/?pdb=113`.

[43] J. S. Marshall and M. A. Thomson, "The Pandora Software Development Kit for Pattern Recognition," *Eur. Phys. J.*, vol. C75, no. 9, p. 439, 2015.

[44] http://larsoft.org/single-record/?pdb=102.

[45] http://www.phy.bnl.gov/wire-cell/.

[46] T. Harion, K. Briggl, H. Chen, P. Fischer, A. Gil, V. Kiworra, M. Ritzert, H. C. Schultz-Coulon, W. Shen, and V. Stankova, "Stic âĂŤ a mixed mode silicon photomultiplier readout asic for time-of-flight applications," *Journal of Instrumentation*, vol. 9, no. 02, p. C02003, 2014.